DISSERTATION

CHARACTERIZATION OF CHANGES IN METABOLIC PATHWAYS DURING DENGUE VIRUS SEROTYPE 2 INFECTION OF THE *AEDES AEGYPTI* MOSQUITO VECTOR TO IDENTIFY CONTROL POINTS FOR INTERRUPTING VIRUS TRANSMISSION

Submitted by

Nunya Chotiwan

Department of Microbiology, Immunology and Pathology

In partial fulfillment of the requirements

For the Degree of Doctor of Philosophy

Colorado State University

Summer 2018

Doctoral Committee:

Advisor: Rushika Perera

Carol Blair
Brian Foy
Claire Huang
Santiago Di Pietro

ABSTRACT

CHARACTERIZATION OF CHANGES IN METABOLIC PATHWAYS DURING DENGUE VIRUS SEROTYPE 2 INFECTION OF THE *AEDES AEGYPTI* MOSQUITO VECTOR TO IDENTIFY CONTROL POINTS FOR INTERRUPTING VIRUS TRANSMISSION

Dengue viruses (DENV) are mosquito-borne viruses that cause a wide range of acute symptoms from mild fever to lethal dengue shock syndrome in humans. DENV are transmitted primarily by *Aedes aegypti* (*Ae. aegypti).* These mosquitoes are widely distributed throughout tropical and subtropical areas around the world. Increasing globalization, urbanization and global warming are factors that enhance the spread of these vectors placing over 2.5 billion people at risk of contracting these viruses.

Transmission of these viruses depends on their ability to infect, replicate and disseminate into several tissues in the mosquito vector. During DENV infection of its human and mosquito hosts, a visible rearrangement of lipid membrane architecture and alterations of the metabolic repertoire is induced. These events occur to facilitate efficient viral replication and virus assembly within the cell and to circumvent antiviral responses from the host. Interference with these virus-induced processes can be detrimental to virus replication and can prevent viral transmission.

In this dissertation, we present the first insight into the metabolic environment induced during DENV serotype 2 (DENV2) replication in *Ae. aegypti*. Using untargeted high-resolution liquid chromatography-mass spectrometry, we explored the temporal metabolic perturbations that occur following dengue virus infection of the midgut, the primary site of the virus infection in the mosquito vector. Temporal changes of metabolites across early-, mid- and late-infection time points were identified. A marked increase in the /content of glycerophospholipids,

sphingolipids and fatty acyls was coincident with the kinetics of viral replication. Elevation of glycerolipid levels and the accumulation of medium-chain acyl-carnitines suggested a diversion of resources during infection from energy storage to synthetic pathways and energy production.

From the observations above, two active pathways, sphingolipid and *de novo* fatty acid synthesis pathways, were further validated to identify metabolic control hubs. Using inhibitor screening of the sphingolipid pathway, we determined that sphingolipid Δ-4 desaturase (DEGS), the enzyme that converts dihydroceramide to ceramide was important for DENV2 infection in cultured *Ae. aegypti* cells (Aag2). Long, double-stranded RNA-mediated knockdown of DEGS expression led to the imbalance of ceramide to dihydroceramide ratios and affected DENV2 infection in cell culture. However, the inhibitory effect to DENV2 replication was not observed during DEGS-knockdown in mosquito vectors.

De novo fatty acid biosynthesis is the pathway that synthesizes the first lipid molecules, fatty acids, required in synthesizing complex lipid molecules, such as glycerophospholipids, glycerolipids and sphingolipids. As a result, this pathway serves as a bottle neck for the control of lipid metabolism. In this study, we annotated and characterized the expression of seven *Ae. aegypti* fatty acid synthase (*Aa*FAS) genes in the different stages of mosquito development and upon exposure to different diets. We found that *Aa*FAS1 shares the highest amino acid similarity to human fatty acid synthase (FAS) and is the dominant *Aa*FAS that expressed in female mosquitoes. Knockdown expression of *Aa*FAS1 expression showed a reduction in DENV2 replication in the Aag2 cells and in the midgut of *Ae. aegypti* mosquitoes during early infection. However, the correlation between viral infection and levels of *Aa*FAS1 expression was difficult to elucidate.

The work in this dissertation has highlighted metabolic pathways that are induced by DENV2 infection and the metabolic control points within these pathways that are critical for DENV2 infection in *Ae. aegypti*. Successful perturbation of metabolic homeostasis can

potentially limit virus replication in the vector, presenting a novel avenue to block the transmission of DENV2 from the mosquitoes to humans.

ACKNOWLEDGEMENTS

First, I would like to thank my advisor, Dr. Rushika Perera, for all the expertise, time, efforts and faith she has put into developing this research project and throughout my graduate studies here at the Colorado State University. Her guidance has pushed me forward beyond the point where I thought I was capable of and helped me grow so much as a scientist. I would also like to thank the members of my graduate committee, Drs. Carol Blair, Brian Foy, Claire Huang and Santiago Di Pietro for their guidance and questions that has shaped this project and their invaluable support throughout the various stages of my studies.

I would also like to thank the members of the extended Arthropod and Infectious Diseases Laboratory group. I was so lucky to be surrounded by so many great minds who have helped me to better as a scientist. Special thanks to Dr. Irma Sanchez-Vargas, who helped me tirelessly with several thousands of mosquitoes used in this study and Barb Andre, the biostatistician, who helped me processing all the mass-spectrometry data and always answer any statistics-related questions. I would also like to thank Drs. Sandra Quackenbush and Joel Rovnak for their infinite support and opportunities that they provided, not only in science but also in life. My life in the laboratory would not be as fun and colorful without the members of the Perera lab. I would like to thank (and give a big hug to) Dr. Becky Gullberg, my Ph.D. partner in crime, for all the help in the lab, her patience to listen to my complaints, the support that she gave me whenever I wanted to give up and her encouragement when I have doubt myself. I would like to also thank Elena Lian, Stephanie Mills, Jenna Read, Kirty Krieger and Caroline Montgomery, brilliant undergraduates, and past members of the Perera lab, especially Dr. Jordan Steel and Kim Anderson for their help throughout my time in this lab.

I would, additionally, like to thank my collaborators at Purdue University who provided useful discussion on my research project. These include Dr. Richard Kuhn, Dr. Catherine Hill,

Dr. Jeffrey Grabowski (now at the Rocky Mountain Laboratories) and Carols Brito. In addition, I would also like to acknowledge the people from the mass-spectrometry facility from the Bindley Bioscience Center, Purdue University, especially Dr. Amber Hopf-Jannasch, who ran all my samples and guided me through the mass-spectrometry data processing.

The work in this dissertation was made possible by funding from the Department of Microbiology, Immunology and Pathology, Colorado State University, Virus Pathogen Resources and Boettcher Foundation.

Lastly, I owe special thanks to my family and friends for their love and encouragement simply helped me get my mind out of stress. I could have not accomplished this without their support. I am grateful to have had all of these people in my life to help me achieve this life goal.

TABLE OF CONTENTS

LIST OF TABLES

LIST OF FIGURES

CHAPTER 1: LITERATURE REVIEW

AEDES AEGYPTI MOSQUITOES

The *Aedes aegypti* (*Ae. aegypti*) mosquito (Diptera: Culicidae) is a primary vector for several arthropod-borne viruses (arboviruses) such as dengue, yellow fever and Zika and chikungunya virus among humans. It is widely distributed throughout tropical and subtropical areas in several continents including Asia, Africa, North America, South America, Europe and Australia [1]. It is hypothesized that *Ae. aegypti* was introduced from Africa to America via the slave trade [2]. Increased globalization due to international trade and travel has escalated the spread of this mosquito globally. *Ae. aegypti* exhibits a strong anthropophilic behavior. For example, it is adapted to breeding in artificial water containers around the house, prefers to stay indoors and feeds almost exclusively on humans [1, 3]. Increased urbanization has helped sustain the vector in these areas. The geographical distribution of the mosquito vector is heavily influenced by temperature [1, 4]. It has been predicted that increases in temperature due to global warming will lead to further expansion of its geographical distribution into temperate regions [5, 6].

DENGUE VIRUSES (DENV)

DENV belong to the family Flaviviridae, genus *Flavivirus*. Other important arbovirus members in this genus are Zika, West Nile, yellow fever, tick-borne encephalitis and Japanese encephalitis viruses. Members of this genus possess a single-stranded, positive sense RNA as genetic material. Following entry of the virus and release of the RNA genome into a new cell, the viral RNA is translated into a single polyprotein which is further proteolytically cleaved into 3

structural proteins (capsid, C, pre-membrane, prM and envelope protein, E) and 7 nonstructural proteins (NS1, NS2A, NS2B, NS3, NS4A, NS4B and NS5) [7]. Both translation and replication of the viral RNA occur within virus-induced membranous structures in the cytoplasm of infected cells [8, 9]. These membranous structures are derived from the endoplasmic reticulum (ER) which is also where virion assembly occurs. Since they are enveloped viruses, they usurp part of the ER membrane as the virion envelope during the assembly process. Newly assembled virions are immature [10]. These immature virions then travel through the secretory pathway and undergo a maturation event in the trans-Golgi network. Specifically, the viral surface glycoproteins (E and prM) rearrange such that the pr peptide of prM is exposed to and cleaved by furin, a cellular protease. Once cleaved the pr-peptide remains associated with the virion (like a cap) until it encounters the neutral pH environment outside the cell. Once the virus particles bud out of the cells, the pr peptide detaches from the particle (cap is released) and the particle becomes mature and primed for infection [7, 10].

DISEASES, VACCINES AND INTERVENTIONS

DENV is the etiologic agent of dengue, also known as break-bone fever [11]. Infections by these viruses are most frequently asymptomatic but can lead to clinical manifestations. Symptomatic dengue ranges from self-limiting dengue fever, to dengue hemorrhagic fever (DHF) to life threatening dengue shock syndrome (DSS) [11]. Over 2.5 billion people are at risk of contracting these diseases with about 390 million infections estimated to occur annually [12]. About 100 million symptomatic cases are reported per year [12].

There are 4 serotypes of DENV, DENV1-4. When humans are infected with DENV, strong neutralizing antibodies are induced against the infecting serotype. This protection is believed to be life-long against the specific serotype [13]. Protection against a secondary infection by another serotype exists only for a few months after the primary infection. After this

period, the neutralizing antibodies generated in the primary infection sometimes enhance the secondary infection, leading to severe and potentially lethal diseases including shock, severe hemorrhaging, plasma leakage and organ impairment. These symptoms were classified as “severe dengue” by World Health Organization in 2009 [11, 13, 14]. This phenomenon is called “antibody-dependent enhancement (ADE)” and has been observed both *in vitro* and in humans [14, 15].

Unfortunately, there is no approved antiviral currently available. Supportive treatment and fluid resuscitation are still the main practices for treating dengue patients [16].To limit the risk of ADE, any vaccine against dengue must induce high neutralizing antibody titers against all 4 serotypes [17]. Only one approved vaccine is currently available, Dengvaxia. It is a live-attenuated tetravalent vaccine which contains the prM and E protein sequences of DENV1-4 in the yellow fever 17D vaccine strain backbone [18]. Dengvaxia can induce high vaccine efficacy to all DENV serotypes except serotype 2 [19]. It was found to increase the risk of developing severe dengue diseases in children and elders who had not had a previous DENV infection, and therefore, was only approved for use in people aged 9-45 years [19]. In addition, recently, it has been shown that Dengvaxia increases the risk of developing severe dengue diseases in the vaccinees who were previously naïve to DENV [19, 20]. As a result, the need to find new interventions for controlling DENV transmission by the mosquito vector, prevention of human infections, and effective treatment of infected patients is extremely urgent.

Mosquito control strategies are still the principal methods to prevent transmission of these viruses. Some examples of these approaches are spraying insecticides, using insect repellent, eliminating potential oviposition sites, improvement of water storage and drainage systems and use of window screens or insecticide-treated bed nets [11]. However, some of these strategies require continuous and long-term administration, a modification of the infrastructure which could be costly or collaboration by the public. As a result, it is usually difficult to implement the strategies in the long run. Moreover, several populations of mosquitoes

around the world have developed resistance to insecticides [21, 22]. As a consequence, the most effective control methods are now failing. Several novel control strategies have been proposed and developed. These strategies involve the use of genomic information, molecular genetic tools and biological controls to reduce the size of the population or modulate the vector competence and/or vectorial capacity for arboviruses [23-27].Therefore, a thorough understanding of the factors that determine vector competence / vectorial capacity of *Ae. aegypti* for arboviruses and the molecular mechanisms of mosquito-pathogen interactions are essential to improve these interventions.

DENV INFECTION OF MOSQUITO VECTORS

Ae. aegypti acquire DENV, as well as other arboviruses, by feeding on the blood of infected patients. The blood meal containing infectious virus particles is deposited in the midgut of the mosquito, and the infection is first established in the midgut epithelium [28]. There are 5 key barriers that the virus is required to overcome for successful infection and transmission of the virus from a mosquito to a human [29, 30].

First, the virus must be able to initiate the infection in the midgut (overcome the midgut infection barrier) and spread throughout the midgut of the mosquitoes. Presence of DENV2 in the midgut tissue can be detected with the 3H5 monoclonal antibody as early as 2 days after the infectious blood meal was taken [28]. Staining at this early stage shows infected foci, indicating that the infection spreads laterally from the initial infected epithelial cells to the neighboring cells and eventually throughout the midgut [28].

Second, the virus must escape the midgut and disseminate to the secondary tissues (overcome the midgut escape barrier). Studies using electron-microscopy have shown that West Nile virus (WNV) and St. Louis encephalitis virus, other flaviviruses, escape from the midgut to the secondary tissues by passing through the basal lamina, the layer of extracellular

matrix surrounding the midgut [9, 31]. Moreover, a study on DENV2 tropism in *Ae. aegypti* detected DENV2 antigen in the trachea from the abdominal areas, suggesting that the trachea may also serve as an escape route of the virus from the midgut [28].

Third, DENV must replicate and amplify the infection in secondary tissues. A study has shown that DENV2 replicates in the fat body, hemocytes, nerve tissues, ommatidia of the compound eyes, esophagus, hindgut, cardia, trachea and Malpighian tubules [28]. Unlike WNV, DENV2 was not found to infect muscles [9, 28].

Fourth, the virus must travel to and infect salivary glands of the mosquito (overcome the salivary gland infection barrier). Infection of DENV2 can be observed in the distal, proximal lateral and median lobes of *Ae. aegypti* salivary glands [28, 32].

Lastly, the virus must be shed from the salivary gland tissues into the salivary ducts (overcome the salivary gland escape barrier). The virus can then be inoculated with the saliva into a new host when the mosquito takes the next blood meal.

CURRENT KNOWLEDGE OF LIPID METABOLISM IN MOSQUITOES

Lipid metabolism in mosquitoes has been studied since the mid-1900s. Due to the lack of advanced technologies, studies on lipid metabolism in mosquitoes focused on the response of mosquito lipids to different diets, the conversion of food to fat, storage of fat in the fat body of the insects, the utilization of fat for energy during flight, metamorphosis, starvation, and the deposition of fat for oogenesis. The recent availability of the genome sequences of certain mosquitoes and the advent of advanced technologies, such as transcriptomics, proteomics and metabolomics, as well as advances in molecular biology have helped us understand lipid metabolism at the molecular level in mosquitoes as well as other insects. The first half of this review will focus on the findings from the late 1900s to the early 2000s, which is on the utilization of lipids in several physiological processes of mosquitoes. The second half of this

review will focus on the discovery (or re-discovery) of mosquito lipids from the molecular biology/omics era.

FAT BODY: THE CENTER OF METABOLISM

The fat body is an organ composed of loose tissues distributed throughout the insect body, lining the underneath of the cuticle and surrounding the gut and reproductive tissues [33]. The majority of the cells in the fat body are adipocytes. These cells contain numerous lipid droplets which serve as the center of cellular lipid storage and energy metabolism [34]. More than 50% of the dry weight of the fat body are lipids [35]. The fat body also stores carbohydrates in the form of glycogen which constitutes about 25% of the dry weight. The rest of the carbohydrate is oxidized or converted to lipids (> 50% of intake glucose in *Ae. aegypti*) [35, 36].

The reserve lipids are required for several physiological processes, such as oogenesis, metamorphosis, diapause, and prolonged flight [37-39]. They also serve as a source for fatty acids which are precursors for synthesizing eicosanoids, pheromones, glycerophospholipids (GPs) and wax [37]. The fat body also serves as a source for synthesizing most of the hemolymph proteins. These proteins are, for example, lipophorin, the protein that is responsible for transporting lipids between cells or tissues, and vitellogenin, the protein that is required for egg maturation during oogenesis [40].

MOBILIZATION OF LIPIDS

The fat body is the central location for lipid synthesis, storage and degradation for energy production [37]. Nutrients that are absorbed in the gut are transported to the fat body and converted to glycogen and lipids [37]. Muscle cells only contain a small amount of energy reserves. As a result, the energy required for prolonged flight is provided by the fat body [41].

Less than 1 % of lipids in eggs are locally synthesized. More than 80% of lipids in eggs are transferred from the fat body [42, 43].

Lipophorin is the main hemolymph lipoprotein. It plays a role as a reusable shuttle transporting lipids between tissues [40]. Similar to human high-density lipoprotein (HDL) and low-density lipoprotein (LDL), there are high- and low- density lipophorins (HDLp and LDLp) in insects. LDLp contains up to 63% of the lipids, while HDLp contains 30-50% of the lipids [44]. Apolipophorin I to III are proteins that associate with the lipophorin particles. Lipophorins in most insects are enriched in diacylglycerol (DAG). However, lipophorins in mosquitoes and some other dipterans, but not *Drosophila melanogaster* (*D. melanogaster*) are enriched in triacylglycerol (TAG) [45, 46]. The mechanism of lipid uptake from lipophorins into the oocytes are still unclear. Both receptor-mediated endocytosis of the intact lipoprotein particles and extracellular hydrolysis of lipids from the lipoprotein core have been observed [40].

ACQUISITION OF LIPIDS DURING MOSQUITO DEVELOPMENT

Neonate larvae acquire lipids from the mother through the maternal deposition of lipids in eggs [42, 43, 47]. Using fluorescently-labeled fatty acids and GPs, Atella and Shahabuddin were able to track the distribution of maternal lipids in eggs and larvae [47]. They found that fatty acid distributed along the sides of the larval body especially where the muscles are located, while GPs aggregated along the intestinal gastric caeca. Larvae further acquire lipids, especially the essential polyunsaturated fatty acids, from aquatic food sources, such as diatoms and algae [39]. They are required for the proper function of innate immunity, developmental processes and the ability to fly in their adult stage [48-50]. Fatty acids that are acquired during larval stages are transferred to the adult stages. However, the distribution of the fatty acid components in the storage lipids (in TAG) and GPs are changed during metamorphosis [39].

Adult mosquitoes are able to synthesize lipids from carbohydrate (sugar) meals [43]. Both males and females possess *de novo* fatty acid biosynthesis machinery, such as fatty acid synthesis and Δ-9 fatty acid desaturase enzymes [39, 51]. By feeding on sugar meals alone, the females are capable of increasing their lipid content up to 300% within 5 days [43]

Blood meals can also serve as an indirect source for lipids. In blood, lipids compose only about 4% of the nutrients [52]. Although no direct evidence has shown that the mosquito midgut epithelium can directly absorb lipids from the blood meal, increases in the expression of the genes that encode the proteins that absorb lipids from food, fatty acid binding protein and long chain fatty acid transport protein, have been reported [53]. The other 95% of nutrients in the blood meal are protein [52]. Using [^{14}C]-labeled protein meals, Zhou et. al., have shown that the majority of the proteins were oxidized to CO_2 or excreted as waste. However, 16% of the meal was converted to TAG, the storage lipid [54]. The expression of several genes involved in lipid synthesis also increased after the blood meal was taken [53]. This finding provides more evidence that the blood meal can serve as a source of lipid reserves in mosquitoes.

Lipids that are synthesized in the fat body are transported and deposited in eggs. These lipids contribute to about 35% of the weight of *Ae. aegypti* oocytes [55]. It should be noted that lipids that are synthesized from carbohydrate meals are not sufficient to trigger the maturation of oocytes. Blood meals, or to be specific, amino acids in the meal, are needed to trigger the release of vitellogenin stimulating hormone in the ovaries to initiate the maturation process of the oocytes [56]. Accumulation of lipids in the oocytes starts only after a blood meal is taken [55]. Although ovaries are capable of synthesizing complex lipids, especially GPs, less than 1% of locally synthesized lipids were found in the egg [40]. Using radioactively labeled lipids, Ziegler et. al., found that the majority of the lipids in eggs were TAG that was transferred from the fat body [42, 43, 57]. *Ae. aegypti* possess a mechanism to maintain metabolic homeostasis during the gonotrophic cycle. Zhou et. al., did not observe differences in lipid and protein content and the number of eggs laid from females that underwent starvation before blood meal [36].

However, they observed significantly lower lipid and glycogen content in the mother after the eggs were laid. This indicates a trade-off between fecundity of the mother and the survival of the eggs. Although a significant portion of lipids accumulating in the oocytes from the first gonotrophic cycle (the first egg production cycle) comes from larval food and pre-existing maternal stores [36], the ability to *de novo* synthesize fatty acids is still important to produce viable eggs. Transient knockdown (KD) of two key enzymes in the *de novo* fatty acid biosynthesis pathway, acetyl-CoA carboxylase (ACC) and fatty acid synthase (FAS), caused a significantly fewer number of eggs in the first gonotrophic cycle [57]. Eggs that were produced from ACC-deficient mosquitoes also lacked eggshells and were nonviable.

LIPIDOMICS STUDIES IN MOSQUITOES AND *DROSOPHILA*

Collective data from several lipidomics studies in *Ae. aegypti, Ae. albopictus* and *D. melanogaster* revealed that insects contain similar lipids species to humans [39, 51, 58-64]. These lipids include GPs: phosphatidic acids (PA), phosphatidylcholine (PC), phosphatidylethanolamine (PE), phosphatidylinositol (PI), phosphatidylglycerol (PG), cardiolipins, phosphatidylserine (PS), and lysophospholipids (LysoGPs); sphingolipids (SPs): ceramide (Cer), ceramide-phosphorylethanolamine (Cer-PE) and sphingomyelin (SM); glycerolipids (GLs): monoacylglycerol (MAG), DAG and TAG; free fatty acids, and sterols. Fatty acid components (fatty acyl chains) of these lipids varied from 12 to 26 carbons (C12 to C26) [51, 58-61]. Several monounsaturated and polyunsaturated fatty acids were profiled in mosquitoes [39]. Similar to humans, mosquitoes possess Δ9 desaturase enzymes to produce monounsaturated fatty acids such as oleic acid, but they cannot produce n-3 polyunsaturated fatty acids. Instead, they acquire these essential fatty acids from aquatic food sources, such as algae, diatoms and dinoflagellates during their larval stages [39, 48]. Essential polyunsaturated fatty acids, such as arachidonic acids (C20 fatty acids), are critical for development of

mosquitoes [65]. *Culex* mosquitoes that were reared with a diet that lacked essential polyunsaturated fatty acids were unable to fly [48].

Aging and metamorphosis also affects the fatty acid profiles in mosquitoes. In *Ae. aegypti* and *Ae. albopictus* cell lines, fatty acid of aged cells (measured during the stationary phase of growth) were more elongated and more unsaturated as compared to those from cells during the logarithmic phase of growth [51, 60]. In mosquitoes, distribution of C20 polyunsaturated fatty acids in the adults was significantly different from larvae. Moreover, there was significantly higher total fatty acid content per wet weight in adults compared to larvae indicating the increase of *de novo* fatty acid synthesis activity in adults [39]. This finding is in agreement with our findings shown in chapter 4 (Figure 4.5).

Odd-chain fatty acids (such as C15:0, C17:0 fatty acids) can also be found in *Anopheles, Ochlerotatus* and *Aedes* mosquitoes and *D. melanogaster* [39, 61, 64]. There is no evidence whether insects possess the enzymes to synthesize odd-chain fatty acids. However, Scheitz et al., have found a positive correlation between the density of *Wolbachia pipientis*, an endosymbiont bacterium that is present in several insect species, and the abundance of odd-chain fatty acids in *D. melanogaster* [64]. This evidence suggests that mosquitoes might acquire odd-chain fatty acids from symbionts. Interestingly, *Ae. aegypti* mosquitoes do not naturally carry *Wolbachia*. It is suspected that the mosquitoes may acquire odd-chain fatty acids from other symbionts.

While PC is the main species of GPs in humans, several studies have shown that PE is the predominant GP species in both *Ae. aegypti, Aedes albopictus* (*Ae. albopictus*) and *D. melanogaster* [51, 58, 59, 62]. The abundance of PE in dipterans ranges from ~ 42-60%, while the abundance of PC ranges from ~ 20-25%. Spatial distribution of GP and SP species in the mosquitoes was studied in *Anopheles stephensi* using atmospheric-pressure scanning microprobe matrix-assisted laser desorption/ionization mass spectrometry imaging (AP-SMALDI

MSI) [63]. This study revealed that some lipid species do not distribute evenly in the mosquitoes. Several PCs, PA, and PEs were found abundantly throughout the whole body, while SM and Cer-PE were found concentrated in the head and antennal lobe, and lysoGPs were found more concentrated in the head-thorax areas [63]. This study suggested that specific lipid species might have unique roles and thus concentrate in certain tissues in mosquitoes.

Another interesting observation from lipidomic studies is a discrepancy between SPs in *D. melanogaster and* mosquitoes. Several studies were unable to detect SM in *D. melanogaster* [59, 62]. A similar SP molecule that is thought to be a substitute of SM is Cer-PE. Cer-PE was found abundantly in both *D. melanogaster* and *Aedes* mosquitoes [51, 59, 62]. Previously, it was assumed that mosquitoes were also unable to synthesize SM. However, several recent studies including our study were able to detect SM by tandem mass spectrometry [51, 58, 61, 63]. Moreover, the transcripts of enzymes that are responsible for synthesizing or catalyzing SMs were putatively annotated in the *Ae. aegypti* genome assembly [66].

UTILIZATION OF STEROLS BY MOSQUITOES

Insects including mosquitoes are incapable of synthesizing sterols [67, 68]. However, sterols play several critical roles in insect physiology. For example, cholesterol can be used directly by inserting into the cellular membrane to maintain membrane fluidity [69]. Cholesterol can also be metabolized to produce ecdysone, an important insect hormone that promotes molting and maturation of eggs [70, 71]. Insects acquire sterols from at least two different sources, from diet and symbionts [72, 73]. A review by Clayton indicated that insects from several orders require cholesterol and other sterol derivatives from their diet as growth factors. *Ae. aegypti* requires cholesterol, sitosterol, coprostanol and ergosterol from the diet [73]. Dietary cholesterol can be absorbed into the midgut [74, 75]. Then it is transferred between tissues by hemolymph lipoproteins [75]. Sterol carrier protein-2 (SCP-2) is responsible for intracellular

transport of cholesterol. This gene family is found in insects as well as in vertebrates [76]. *Ae. aegypti* encode this protein, AeSCP-2, which has 46% identity and 69% similarity to the SCP-2 in mammals [76, 77]. AeSCP-2 was found to be a host factor supporting DENV infection in Aag2 cells [78]. This issue is discussed later in this chapter.

EICOSANOIDS, INSECT IMMUNITY AND SIGNALING MOLECULES.

Eicosanoids are oxygenated metabolites of three C20 polyunsaturated fatty acids including arachidonic acid (20:4n-6), 20:3n-6 and 20:5n-3. Eicosanoids are composed of 3 major groups of metabolites: prostaglandins, lipoxygenase metabolites, and epoxyeicosatrienoic acids [79]. In insects, eicosanoids are known to mediate phagocytosis, microaggregation, nodulation and encapsulation of invading microbes and metazoans [50, 80].

Mosquitoes are unable to synthesize C20 polyunsaturated fatty acids, and therefore, require these fatty acids from diets [39, 81]. All three groups of eicosanoid metabolites are found in mosquitoes [82-84]. They play roles in both basic physiological functions and innate immune responses against infection. In *Ae. aegypti*, prostaglandins but not lipoxins, facilitate fluid excretion in the Malpighian tubules [84]. In *Anopheles gambiae* lipoxin A_4 was found to be induced against the invasion of *Plasmodium* ookinetes in the midgut [83]. The role of eicosanoids in mosquitoes against virus infection has only been reported in C6/36 cells. Prostaglandin A_1 was found to inhibit the replication of vesicular stomatitis virus in a dose-dependent manner [85]. The role of eicosanoid metabolites in DENV infection of mosquitoes is still unknown. Interestingly, DENV infection in human Huh7 and dendritic cells induced the expression of cyclooxygenase-2 (COX-2), the enzyme that produces prostaglandin E_2 [86, 87]. The production prostaglandin E_2 in infected cells was also enhanced and promoted migration of DENV infected dendritic cells from the upper to the lower chamber in culture [87]. Mice that

were treated with COX-2 inhibitor were protected from DENV infection [86]. These findings suggested that prostaglandins might play a role in DENV infection in the mosquito as well.

CURRENT KNOWLEDGE OF LIPID METABOLISM AND FLAVIVIRUS INFECTION IN MOSQUITO CELLS AND MOSQUITO VECTORS

Metabolomic studies of flavivirus infection in mosquito cells

There were only two metabolomic studies of flavivirus infection in mosquito cells prior to the publication by Chotiwan et. al., 2018 (Chapter 2) [61]. As a result, knowledge of altered metabolism in mosquitoes in response to flavivirus infection has been limited. However, the metabolomic study carried out on mosquito cells upon DENV2 infection performed by Perera et. al., provided insight into the metabolic landscape altered by infection [58]. Briefly, DENV2 infected *Ae. albopictus* C6/36 cells (whole cells or extracted replication complex membranes) were subjected to untargeted liquid chromatography-mass spectrometry (LC-MS) analysis. Compared to uninfected cells or cells that were infected with replication-defective virus (UV-inactivated virus), the abundance of several complex lipids such as GPs and SPs and intermediates such as fatty acids and DAG were increased in DENV2 infected cells. Unsaturated fatty acid composition of these lipids was enriched in response to infection, indicating the requirement for membranes that had more fluidity. These membranes are thought to support membrane bending and curvature, required for the assembly of viral replication complexes (described in the next section). These replication complex membranes had a different lipid profile to the rest of the cellular fractions, suggesting enrichment of specific lipids in them. This study also investigated the lipid profile of mosquito cells following treatment with a *de novo* fatty acid synthesis inhibitor, C75. Treatment with C75 showed that fewer lipids (both fatty acids and complex lipids) accumulated in infected cells and virus replication was impaired.

Therefore, these studies suggested that DENV2 altered host lipid metabolism to facilitate its efficient replication in mosquito cells.

Another lipidomics study was performed in ZIKV-infected C6/36 cells by Melo et. al. [88]. In this study, 13 lipids were found to significantly accumulate in ZIKV-infected C6/36 cells. These lipids included 11 GPs, 1 SP and 1 DAG. This result was similar to the finding from Perera et. al. in DENV2-infected C6/36 cells, suggesting that similar repertoires of lipids were induced in response to infections by both DENV and ZIKV. It also further implies that these two viruses may have similar mechanisms to hijack host machinery to facilitate their infection.

Membrane rearrangement upon flavivirus infection was observed in mosquito cells and mosquito tissues.

Flaviviruses infect and rearrange membrane architecture in mosquitoes similarly to the membrane architecture observed in infected human cells [8, 9, 89]. DENV infection in C6/36 cells induced rearrangement of the endoplasmic reticulum (ER) membrane into vesicular structures. These structures are i) vesicles (Ve), the circular vesicular structures that houses the replication complex, ii) vesicle packet (Vp), the larger vesicles that surround Ve and newly assembled virus particles and iii) tubular structures (T), elongated vesicles. In contrast to the ultrastructure observed in DENV2 infected human, Huh7 cells, convoluted membranes (CM) were not found in infected C6/36 cells [8, 89].

Similar vesicular structures were observed in mosquito cell lines infected with other flaviviruses. Electron micrographs revealed the same induction of vesicular structures in *Ae. albopictus* cells infected with Kunjin virus and *Ae. aegypti* cells infected with yellow fever virus [90, 91]. These membrane-rearrangements can also be observed in infected mosquito tissues. This observation has been reported by Girard et. al., in *Culex quinquefasciatus* mosquitoes infected with WNV [9, 92]. Similar structures were seen in the midgut epithelium, midgut muscle

and salivary gland tissues indicating that this specific membrane architecture was universally induced in both human and mosquito hosts in response to infection with most flaviviruses.

These studies on membrane architecture, together with the studies on lipid composition of infected cells discussed above, suggest that in addition to rearranging cellular membrane architecture during infection, additional lipids (such as GPs and SPs) are synthesized and incorporated into these membranes to promote expansion of membrane mass. Lipids with unsaturated fatty acyl chains and cone-shaped lipids such as PE, lysoGPs and Cer are also likelyincreased to provide curvature and membrane-bending capabilities to facilitate the specific architecture required. Essentially, there is a concerted effort (by viral gene products) to alter both lipid metabolism and cellular membrane architecture to acquire an intracellular environment conducive to viral replication [93, 94].

DENV and cholesterol in *Aedes* cells and vectors.

Cholesterol was shown to be essential for flavivirus entry, replication and assembly in human cells [95-98]. Manipulation of cholesterol biosynthesis either by RNA interference (RNAi)-mediated gene silencing of cholesterol biosynthesis genes or using inhibitors of cholesterol biosynthesis enzymes such as lovastatin reduced DENV and WNV replication in human cells [95, 96]

Intracellular availability of cholesterol was also shown to facilitate successful DENV replication in mosquito cells and mosquito vectors. Mosquitoes cannot synthesize cholesterol *de novo* and need to acquire cholesterol exogenously such as from the microbiome or from food [99]. As a result, mosquitoes have to rely on the processes for cellular absorption, trafficking and metabolism of cholesterol. Transcription and protein expression of host factors that are involved in cholesterol trafficking and homeostasis were found increased upon DENV infection, indicating that these cellular factors were DENV agonists [78]. Sterol carrier protein-2 (SCP-2) is a cytosolic protein involved in cholesterol binding and transport in the mammalian cells [76,

77]. Studies by Fu et. al., found that inhibition of SCP-2 using RNAi mediated gene silencing or the SCP-2 inhibitor (*N*-(4-{[4-(3,4-dichlorophenyl)-1,3-thiazol-2-yl]amino}phenyl)acetamide hydrobromide) altered the cellular distribution of free cholesterol and also significantly reduced DENV titer in *Ae. aegypti* Aag2 cells [78, 100]. A similar observation was made in *Ae. aegypti*. Genome-wide transcriptomic analyses of *Ae. aegypti* (Liverpool strain) revealed that the transcripts of members in the lipid-binding protein gene families, the myeloid differentiation 2-related lipid recognition protein (ML) and Niemann Pick type C1 (NPC1) families, were increased upon DENV infection [100, 101]. These proteins function in cholesterol absorption, trafficking and metabolism in mosquitoes [100]. Loss-of-function studies using RNAi mediated gene silencing of these genes also reduced DENV infection in the midgut of both lab-adapted and field-derived strains of *Ae. aegypti* [100]. Lastly, Geoghegan et. al., have shown that *Wolbachia*, an intracellular endosymbiotic bacterium, inhibited DENV in *Ae. aegypti* cells by perturbing cholesterol trafficking and caused accumulation of cholesterol in lipid droplets [102]. A compound, 2-hydroxyorioyl-β-cyclodextrin, that restores lysosomal cholesterol accumulation in Niemann-Pick type C disease can rescue DENV replication in *Wolbachia*-infected mosquito cells [102, 103]. In summary, these studies have shown the importance of cholesterol metabolism and intracellular trafficking, which play agonistic roles facilitating DENV infection and replication in mosquito vectors.

Lipid storage and energy homeostasis

Lipid droplets (LD) are composed of neutral lipids (such as TAG, DAG and cholesterol esters) as a hydrophobic core and surrounded by a monolayer of amphipathic lipids (such as phospholipids, glycolipids and sterols) and variable protein content [104]. LD maintain lipid homeostasis by serving as a source of cellular fatty acids for biosynthesis of complex lipids or a

source for energy via β-oxidation. Moreover, studies have also demonstrated the role of LD in inflammation and in response to immune challenges [104, 105].

In DENV infected cells, studies have reported increased numbers of LDs in response to the virus. This observation was seen in both mammalian cells (BHK, HepG2) and mosquito cells (C6/36 and Aag2) [106, 107]. Moreover, Samsa et. al., have demonstrated that capsid protein of DENV localized to the LD. A mutation in the capsid protein which could no longer associate with LDs impaired DENV replication [106]. In contrast, work by Heaton et. al., observed a reduction of the size but not the numbers of LDs in DENV infected human hepatoma (Huh7.5) cells [108]. This phenomenon was suggested to occur via autophagy. They demonstrated that TAG, the major component of the hydrophobic core of LDs, was depleted during DENV infection. Hydrolysis of TAG gives rise to fatty acids, which can enter the mitochondria and can be catabolized for energy production (ATP) via β-oxidation. An increased rate of β-oxidation was also observed and shown to facilitate DENV infection in Huh7.5 cells [108].

A balance between lipid storage and energy production is important for the physiology of mosquitoes, as well as for the successful replication of virus in the host [108-110]. None of the studies have shown whether DENV infection elevates β-oxidation in mosquito cells or mosquito vectors. In mammalian cells, studies have shown that DENV requires both lipid biosynthesis and lipid catabolism to facilitate its successful replication in the host [108, 111, 112]. These results seem to contradict each other. However, it is possible that different spatial and temporal requirements modulate the need for both these pathways during DENV infection. More comprehensive studies will need to tease out these timelines and metabolic compartments that support DENV replication within human and mosquito hosts.

THE HYPOTHESIS OF THIS STUDY

Several knowledge gaps on lipid metabolic processes and their role in the physiological function of mosquitoes still need to be explored. Even fewer studies have addressed the relationships between lipid metabolism in mosquito cells or mosquito vectors and their roles in supporting or antagonizing DENV infection. In this study, we aimed to expand our understanding of the interaction between DENV2 and their mosquito vectors, focusing on lipid metabolism. Since metabolites are the ultimate effectors of biochemical pathways and contribute to a change in phenotype, we hypothesized that lipid metabolism (either biosynthesis or catabolism) influences outcome of DENV2 infection in the mosquito vector. If our hypothesis is true, identifying metabolites that are altered during the course of DENV2 replication in the mosquito vector may lead to recognizing metabolic control points. Relatedly, alteration of these metabolic control points will lead to avenues to interrupt DENV2 infection in the vector, thus preventing transmission of the virus to humans.

In brief, in chapter 2, we describe our studies using untargeted liquid chromatography mass spectrometry as a tool to identify lipids and other metabolites that were altered during DENV2 infection in midguts (the initial site of virus replication in the mosquito vector) of *Ae. aegypti* mosquitoes. Several key lipid species, including GPs, SPs and acyl-carnitines were altered upon DENV2 infection. These observations indicated that synthesis of complex lipids, energy production and recycling of precursors of biosynthesis pathways were activated by infection. In chapter 3, we describe studies that used loss-of-function approaches to further identify specific control points in the SP pathway critical to control infection. We found that the ratio of Cer to dihydroceramide was important for DENV2 infection *in vitro*. The complex lipids studied thus far are all composed of fatty acids, which are also intermediates of energy production processes. The availability of fatty acids in cells thus is potentially critical for DENV2 infection. Therefore, in chapter 4, we describe the characterization of fatty acid synthase

(*Aa*FAS), the enzyme that synthesizes fatty acids *de novo* from non-lipid precursors. The expression of seven putative *Aa*FAS genes was characterized in different larva, pupa and adult stages of the mosquito following feeding on different food sources. We then extended these studies to explore the relationship between *Aa*FAS and arbovirus infection in both *in vitro* and *in vivo* models. Lastly in chapter 5, we summarize our findings and discuss how to use the knowledge gained in these studies to improve vector control practices.

CHAPTER 2: TEMPORAL METABOLIC RESPONSE PROFILES IN MIDGUTS AND SALIVARY GLANDS OF THE *AEDES AEGYPTI* MOSQUITO VECTOR UPON DENGUE VIRUS INFECTION[1]

INTRODUCTION

The transmission cycle of dengue viruses (DENV) requires a human host and mosquito vector. Mosquitoes acquire DENV via feeding on the blood of an infected human. The blood meal is deposited in the midgut of the mosquito and infection is first established in the midgut epithelium [113]. While digestion of the blood meal is complete within 48 hours [113], viral replication in the midgut tissue reaches its peak only at 7-8 days post-blood meal (pbm) ingestion [114]. Subsequently, the virus disseminates from the midgut and infects other tissues including the fat body and salivary glands. Approximately 10-14 days pbm the salivary glands become infected and the virus can be transmitted in the saliva to a human when the mosquito acquires another blood meal. Since the successful transmission of this virus depends greatly upon its ability to replicate efficiently in several mosquito tissues, the local biochemical and physical environment of each tissue plays a critical role in virus propagation.

In both human and mosquito cells, lipids play an integral role in the life cycle of DENV [8, 58, 89, 111, 114]. Host-derived membranes are incorporated into a lipid envelope that surrounds the capsid protein and genomic RNA of DENV particles [10]. This membranous structure facilitates virus release from infected cells by budding into the endoplasmic reticulum and re-entry into new cells through fusion of virus-host membranes [8, 10, 115]. Additionally,

[1] Adapted from Chotiwan N, Andre BG, Sanchez-Vargas I, Islam MN, Grabowski JM, Hopf-Jannasch A, et al. Dynamic remodeling of lipids coincides with dengue virus replication in the midgut of Aedes aegypti mosquitoes. PLoS Pathog. 2018;14(2):e1006853.

electron tomography has revealed that significant rearrangements of host cell membrane architecture occurs upon DENV infection [8, 89, 116-118]. Virus-induced membrane structures are required as platforms for virus replication and assembly and protect replicating genomes from antiviral defense mechanisms of the host. They have been identified in DENV-infected human and mosquito cells and the midgut epithelium and salivary glands of *Culex* mosquitoes infected with another flavivirus, West Nile virus [9]. This intracellular membrane reorganization imposes a significant metabolic cost to the host cell. It requires activation of biosynthetic processes, and the trafficking and degradation of lipids and other related molecules. Our previous studies investigated the perturbation of lipid homeostasis in C6/36 mosquito cells following infection with DENV2 [58]. We identified lipids involved in maintaining the stability, permeability and curvature of membranes, as well as bioactive lipid molecules that were significantly changed upon infection. Specifically, a burst of glycerophospholipids was observed coincident with viral replication kinetics. This burst of lipids was attributed to the activity of fatty acid synthase (FAS), a key enzyme in glycerophospholipid biosynthesis. Inhibition of this enzyme was detrimental for DENV2 replication in both human and mosquito cells [58, 111]. Collectively, these data demonstrate that lipids play critical roles in DENV infection in cell culture models.

Although lipid biochemistry has been studied in mosquitoes for several years, very little is known about the relationship between virus and mosquito host and the alteration of intracellular lipids that underpins infection capacity. In this study, we used high-resolution mass spectrometry to explore metabolic changes in the midgut of *Ae. aegypti* exposed to DENV-containing blood meals as this tissue represents the crucial site of initial viral replication. Using a time course study, we compared metabolic profiles of infected and uninfected midguts and salivary glands at early-, mid- (peak viral replication) and late time points post-infection. Our results demonstrate significant fluctuations in molecules that function as membrane building blocks, bioactive messengers, energy storage molecules and intermediates in lipid biosynthesis

and lipolysis pathways. Presumably these changes represent both manipulation of cellular resources for viral replication as well as the cellular response to infection. They may result from either *de novo* biosynthesis or the consumption/conversion of metabolites. Additionally, import/export may contribute to the perturbation of metabolite pools. Import pathways are specifically important in the mosquito for molecules such as cholesterol and its derivatives since they cannot be synthesized *de novo* [68, 73, 77]. Many unidentified metabolites (not found in currently available databases that include animal, plant, fungal and bacterial metabolites and synthetic compounds) were also significantly perturbed during virus infection and may represent mosquito-specific metabolites that have not yet been annotated. Identifying metabolic bottlenecks that condition vector competence and transmission of these pathogens could be exploited for novel transmission-blocking interventions for control of globally important diseases.

MATERIALS AND METHODS

Virus

DENV serotype-2 (DENV2) strain Jamaica 1409 (JAM-1409) was obtained from the Centers for Disease Controls and Prevention (CDC), Fort Collins, CO, USA [119]. The virus was passaged in C6/36 cells cultured in L15 medium supplemented with 3% fetal bovine serum (FBS), 50 µg/ml penicillin-streptomycin, and 2 mM L-glutamine by infecting the cells at a multiplicity of infection (MOI) of 0.01. Fresh medium was replaced at 7 days post-infection. At 12-14 days post-infection, virus-containing supernatant and infected cells were harvested to prepare the infectious blood meal.

Mosquito rearing

Ae. aegypti strain Chetumal was originally collected from Yucatan Peninsula, Mexico [120]. Adult mosquitoes were fed on raisins and water, with uninfected blood meals to stimulate

oogenesis, and were maintained at 28ºC, 80% relative humidity with 12-12 hours light-dark periods. Male mosquitoes (20-25 males) were placed in one-pint cartons with 200-250 female mosquitoes to maintain the colony.

Mosquito infection with DENV2

Mosquitoes were orally exposed to a DENV2-infectious blood meal using an artificial membrane feeder as described previously but raisins and water were only removed at 24 and 4 hours prior to blood feeding [121]. For the uninfected control group, we mixed uninfected C6/36 cells suspended in cell culture medium with blood meal at 1:1 to maintain as similar a metabolic input to the DENV2-infected group as possible. Mosquitoes were allowed to feed for 45-60 minutes. Blood-engorged mosquitoes were reared up to 11 days and fed on sucrose and water.

Plaque titration from whole mosquitoes

Thirty mosquitoes were collected on day 11 pbm to test for infectious viral titers. Individual mosquitoes were put in the tube containing 500 µl of 1x Minimum Essential Media (MEM). Mosquitoes were ground using plastic pestle and the homogenates were filtered through 0.22 µm acrodisc filters (13mm diameter; VWR) in to a new tube and used for plaque titration.

Plaque titration was performed on confluent BHK-15 cells. Virus supernatant was serially diluted 10-fold in 1x PBS containing 0.5 mM $CaCl_2$ and 1.2 mM $MgCl_2$ for 3 to 6 dilutions and was inoculated at 150 µl onto a cell layer grown in 24-well plate. Absorption was allowed for 1 hour at room temperature. During absorption, 2x LE Quick Dissolve Agarose (Genemate) was heated to dissolve in miliQ water and was placed in a 55ºC water bath. At the same time, 2x Minimum Essential Media (MEM), supplemented with 2.5% FBS, 50 µg/ml Penicillin/Streptomycin, 50 µg/ml Gentamycin, and 2.5 µg/ml Amphotericin B) was made and placed in a 37ºC water bath. After absorption for 45 minutes, 2x agar and 2x media were mix at

equal volumes to make 1x medium-agar overlay. The overlay was placed in a 42°C water bath for at least 15 minutes before being added to the cell layer (1 ml). The overlay was allowed to set, and the cells were incubated at 37°C with 5% CO_2. On day 2 post infection, 0.5 ml of 1X MEM supplemented with 10% FBS was added onto the agar overlay to prevent cells from drying. Cells were stained with 0.033% neutral red (Sigma) in 1x PBS on day 5 post infection. Viral titers were calculated to plaque forming units per milliliter.

Sample preparation for metabolomics analysis

Mosquito dissection

On days 3, 7 and 11 pbm, midguts and salivary glands were dissected from 200 uninfected and 300 DENV2-infected mosquitoes. Individual midguts were ground in 100 µl phosphate buffered saline (PBS). Two microliters of each individual DENV2-exposed midgut (n= 799) homogenates were collected in a separate tube for quantitative reverse transcription polymerase chain reaction (qRT-PCR) analysis. The rest of the homogenate was immediately frozen on dry ice and stored at -80°C for metabolite extraction.

Quantitative RT-PCR detection of infection in mosquitoes

To determine the presence of DENV2 RNA in the midgut of mosquitoes following an infectious blood meal, 2 µl of midgut homogenate was heated at 95°C for 5 minutes and chilled on ice prior to performing a one-step qRT-PCR reaction without RNA extraction. Presence of viral RNA was quantified using Brilliant III Ultra-Fast SYBR qRT-PCR Master Mix (Aligent Technologies, CA) and with the primer pairs for DENV2 RNA as described previously [122]. Quantitative RT-PCR was performed using an iQ5 real-time PCR detection system using the following cycles: RT at 50°C, 20 minutes; 95 °C, 5 minutes for RT inactivation and 40 cycles of 95 °C, 5 s and 60 °C, 1 minutes. The results were analyzed with the iQ5 optical system software version 2.0 (Bio-Rad, CA).

Metabolite extraction

Two equal pools of 75-100 midguts or salivary glands homogenates for DENV2-infected and mock infected treatment groups were subjected to metabolite extraction. Internal standards (10 µg alanine-leucine-alanine-leucine and 10 µg Ceramide d17:1, Avanti, AL) were added to the pools for normalization of the variation introduced during tissue extraction. To extract metabolites, one volume of methanol and chloroform and 0.01% butylated hydroxyl toluene were added to an equal volume of homogenized tissue in PBS [123]. Samples were vortexed thoroughly prior to separation of the aqueous phase from the organic phase by centrifugation at 1,250 g for 10 minutes. To prevent degradation of metabolites, samples were processed on ice or at 4^{o}C throughout the process. Metabolites from aqueous and organic phases were dried separately by speed-vacuum centrifugation and were stored at -80^{o}C for further metabolomics analysis.

Liquid chromatography - mass spectrometry (LC-MS) profiling analysis of metabolites

Two technical replicates of each pool of midguts or salivary glands were analyzed by a LTQ Orbitrap XL instrument (Thermo Scientific, Waltham, MA). It was coupled to an Agilent 1100 series LC (Agilent Technologies, Santa Clara, CA) equipped with a refrigerated well plate auto sampler and binary pumping device.

For polar metabolite analysis, reverse phase liquid chromatography (LC) was used to analyze the samples. An Atlantis T3 column (Waters Corp., Milford, MA) with 1.0 x 150 mm, 5.0 µm dimensions was used for the separation. Solvent A consisted of water + 0.1 % formic acid. Solvent B consisted of acetonitrile + 0.1 % formic acid. The flow rate was 140 µl/minute. A volume of 5 µl was loaded onto the column. The gradient was as follows: time 0 minutes, 0% B; time 1 minutes, 0% B; time 41 minutes, 95% B; time 46 minutes, 95% B; time 50 minutes, 0% B; time 60 minutes 0% B. The LC-MS analysis was run twice, using positive and negative polarity electrospray ionization (ESI). Data were acquired using data dependent scanning

mode. Fourier transform mass spectrometry (FTMS) resolution of 60,000 with a mass range of 50-1100 was used for full scan analysis and the FTMS was used for tandem MS (MS/MS) data acquisition with a resolution of 7500 and collision induced dissociation (CID) mode.

For non-polar metabolite analysis, reverse phase liquid chromatography was also used to analyze the samples. An Xterra C18 column (Waters Corp., Milford, MA) with 2.1 x 150 mm, 5.0 µm dimensions was used for the separation. Solvent A consisted of water + 10mM ammonium acetate + 0.1 % formic acid. Solvent B consisted of acetonitrile/isopropyl alcohol (50/ 50 v/v) + 10mM ammonium acetate + 0.1 % formic acid. The flow rate was 300 µL/minute. A volume of 10 µL was loaded onto the column. The gradient was as follows: time 0 minutes, 35% B; time 10 minutes, 80% B; time 20 minutes, 100% B; time 32 minutes, 100% B; time 35 minutes, 35% B; time 40 minutes 35% B. The LC-MS analysis was run twice, using positive and negative polarity in ESI. For MS/MS experiments, data were acquired using a data dependent scanning mode. FTMS resolution of 60,000 with a mass range of 100-1200 was used for full scan analysis and the FTMS was used for MS/MS data acquisition with a resolution of 7500 and higher-energy collisional dissociation (HCD) mode. The top five most intense ions were acquired with a minimum signal of 500, isolation width of 2, normalized collision energy of 35 eV, default charge state of 1, activation Q of 0.250, and an activation time of 30.0. The acquired data were evaluated with Thermo XCalibur software (version 2.1.0).

MS data processing and statistical methods

Raw data were converted to .mzXML in centroid form using msConvert [124]. Downstream analyses were conducted in the open source R program [125]. The xcms package was used with the centWave [125-127] algorithm and a Gaussian fit for peak-picking, and the OBI-Warp method for retention time correction and alignment [128]. Features that had retention times outside of limits determined by the gradient of solutions used were not included in further analysis (2 - 33 minutes for nonpolar modes and 0 - 47 minutes for polar modes). Intensities for

technical replicates were averaged to provide a single value for each biological replicate and then normalized using median ratio scaling described by Wang, et al. [129]. One was added to intensity values prior to transformation to $\log_2$ because of the presence of zeroes. Statistical analysis was conducted in the R package limma [130], which fits linear models to the data using an empirical Bayes approach, allowing for information across all features to be used to develop inference about individual features [131]. P-values were based on a moderated t-statistic with a Bayesian adjusted denominator and adjusted for false discovery rate [132]. Each mode (negative / positive + polar / nonpolar) was processed and analyzed separately. Features were designated as significantly different when the absolute $\log_2$ fold change was greater than or equal to one, and the adjusted p-value was less than 0.05. Where results from all modes are included in one table or graph, the significance is based on the analysis in single modes alone.

Metabolite identification and pathway mapping

Putative molecular names of features were identified by searching *m/z* against the Human Metabolome Database (HMDB), LIPID Metabolites and Pathways Strategy (LIPID MAPS), Metabolite, Tandem MS Database (Metlin) and Kyoto Encyclopedia of Genes and Genomes (KEGG) [131]. $[M+H]^+$, $[M+Na]^+$ and $[M+NH_4]^+$ adducts were accounted for in the neutral mass calculation in the positive ionization mode nonpolar phase data and $[M+H]^+$, $[M+Na]^+$ for the polar phase data. $[M-H]^-$ was the only adduct accounted for in the calculation of negative ionization mode data. The identifiable molecules with mass accuracy of <6 ppm error were further classified into metabolic classes. Features with MS/MS data were further validated by searching against the Tandem Mass Spectral Library (NIST MS/MS) (2014) (Agilent Technologies) and LipidBlast (2012) libraries using MS PepSearch (2013) and manually inspected using NIST MS Search (v2.0)[133-135]. Identified putative metabolite IDs were manually mapped to the pathways based on KEGG or reported human metabolic pathways.

RESULTS

DENV2 infection of the *Ae. aegypti* mosquito vector

To profile the alterations in the metabolic environment of mosquito midguts and salivary glands over time post-blood feeding and during the course of DENV2 infection in the mosquito vector, *Ae. aegypti* Chetumal strain mosquitoes were fed an infectious blood meal containing DENV2 strain Jamaica-1409 (JAM-1409; blood titer $1x10^7$ PFU/ml) or exposed to a noninfectious blood meal as a negative control (Figure 2.1). Midguts and salivary glands were dissected from the mosquitoes on days 3, 7 and 11 pbm representing early viral infection in the midgut (day 3), high replication activity in the midgut with early dissemination to the salivary glands (day 7), and high replication activity in salivary glands and other tissues with virus being cleared from the midgut (day 11). Immediately after dissection, individual midguts were tested for DENV2 RNA by qRT-PCR (Figure 2.2A). To ensure that the metabolic profile of the midguts and salivary glands accurately represented the infected environment, every individual midgut was evaluated by qRT-PCR for DENV2 RNA and only infected tissues were pooled. On day 3 pbm, viral genomes were detected in 55% of the dissected midguts, and on days 7 and 11 pbm, detection increased to 73% and 76% respectively. Plaque assays of whole mosquito homogenates harvested on day 11 pbm (n = 30) indicated that 60% of mosquitoes showed detectable infectious virus averaging $8.5x10^3$ PFU/ml (Figure 2.2B). These were similar infection rates to those reported previously by Salazar et. al., [28]. Two independent pools of ~100 tissues were included for each treatment group and time point representing a total of 200 biological samples. The metabolic profiles observed in the infected tissues represent true biological deviations corresponding to the infected state. It should be noted however, that estimation of variance and statistical power are compromised by the small sample sizes since the maximum limit of samples acquirable in order to maintain metabolite integrity at a given time point is limited.

LC-MS data analysis of mosquito midguts following DENV2 infection

Mosquito metabolites in both polar and non-polar phase extracts were analyzed by LC-MS in both positive and negative ionization modes to obtain the most comprehensive coverage possible. Experimental data from each extract in each mode were analyzed separately by the workflow described in materials and methods and shown in Figure 2.1. Only features (molecular identities defined by a unique mass to charge ratio, *m/z,* and retention time) detected in both pools (representing 200 biological replicates) were considered 'present' in the samples. For the midguts, a total of 6,103 molecular features from all modes, treatments and time-points pbm were detected. These features were subjected to statistical analysis to compare the differences in metabolite abundance between DENV2-infected and uninfected midguts at each time point pbm. The features that showed statistically significant differences in abundance ($|\log_2$ fold change$|$) ≥ 1 and p-value < 0.05; total of 936 features) were identified using LIPID MAPS, HMDB, and Metlin databases. Approximately 39% of the significantly different features (363 molecules) were identifiable to an accuracy of < 6 parts per million (ppm) (Table 1 and Supplemental Table S1). About 93% of identified and significantly different features (341 molecules) have recognizable biological relevance. The metabolites detected in the non-polar phase from both negative and positive

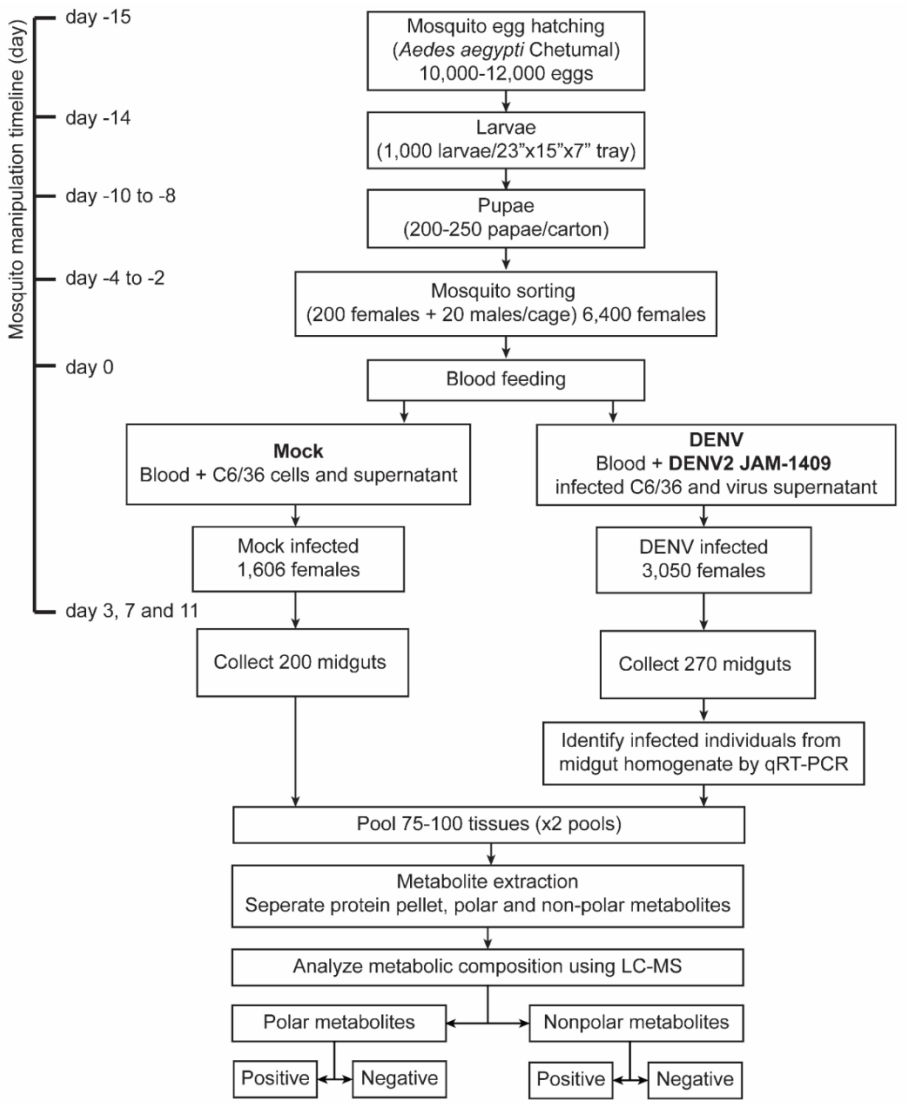

Figure 2.1 *Ae. aegypti* sample preparation for LC-MS analysis. Flow chart shows timeline, numbers of samples and procedures used for mosquito rearing, infection, sample collection and sample processing.

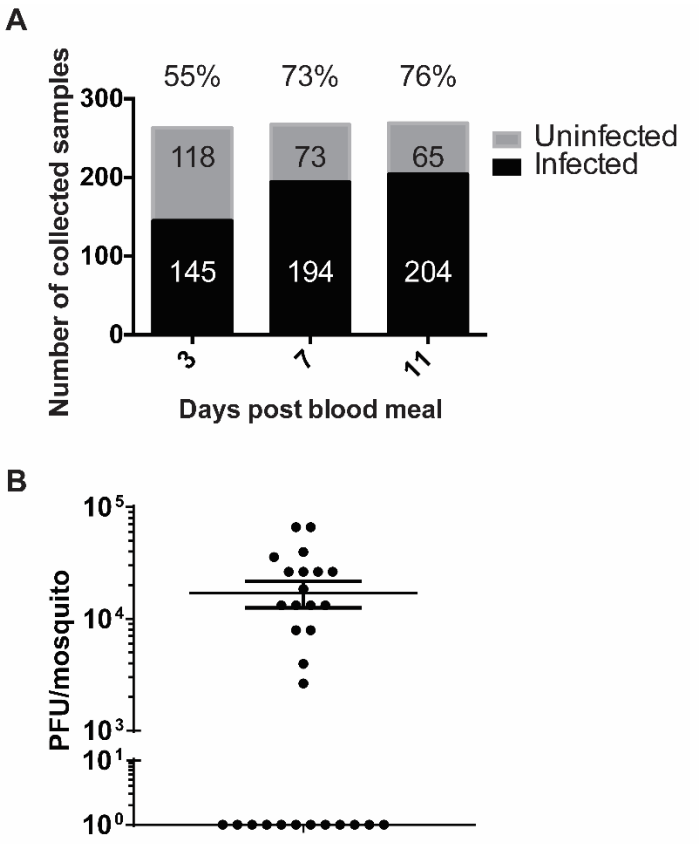

Figure 2.2 DENV2 infection in mosquitoes. Individual midguts dissected from DENV2-fed mosquitoes (n = 799) were tested for the presence of viral RNA by qRT-PCR. (A) Percent of virus-RNA positive midguts are shown above the bar graphs. (B) Infectious viral titers of a representative subset (n = 30) of whole mosquitoes harvested on day 11 pbm were determined to evaluate the range of titers observed in the experiment following dissemination.

ionization modes comprised glycerophospholipids (GPs), sphingolipids (SPs), glycerolipids (GLs),sterols, fatty acyls, acyl-carnitines, prenols, polyketides, amino acids and peptides and other organic compounds. The metabolites detected in polar phases from both detection modes also contained the above molecular species with the exception of GLs and contained nucleosides instead**.** All nomenclatures and categories for lipids are based on the LIPID MAPS comprehensive classification system [136].

Table 2.1 Summary of metabolites from mosquito midguts detected across all time points and treatments

Modes of detection	Nonpolar - Negative	Nonpolar - Positive	Polar - Negative	Polar - Positive	Total
Detected features	1,403	1,864	313	2,523	6,103
Features with differential abundance*	106	557	66	207	936
Identifiable features**	450	787	110	785	2,132
Identifiable features with differential abundance**	28	226	29	80	363

* Features that showed significant differences ($|\log_2$ fold change$| \geq 1$ and $p < 0.05$) in abundance between DENV2-infected and uninfected midguts
** Identification classified as parts per million (ppm) < 6

For the salivary glands, we were able to detect a total of 3,288 molecular features from all modes, treatments and time-points (Table 2.2). About 21% (701 features) showed statistically significant differences in abundance at least one of any statistical comparison: infected vs. uninfected, comparison between days pbm of uninfected and infected midguts and interaction analysis (analysis of temporal trends). However, only 4 features were both identifiable and showed statistically significant differences in metabolite abundance between DENV2-infected and uninfected salivary glands (Table 2.2 and Supplemental Table S2). Two of these molecules do not have known function in animals, while the other two molecules, C17 sphinganine and PC(O-5:0), contain odd numbers of carbons which is thought to be rare in the biological samples.

The small changes observed in the salivary glands might be due to these following reasons. Firstly, DENV2 takes several days to disseminate the infection to the salivary glands. Therefore, the majority of the changes may not occur early during infection. Secondly, we observed a large variation between biological replicates of salivary gland samples. This might be due to the size of the tissues, which are very small, and hence, the overall amount of material provided metabolite abundances near the limits of detection. Since there were only a

few molecules that were significantly changed upon DENV2 infection, we did not include the results from the salivary glands in the publication.

Table 2.2 Summary of metabolites from mosquito salivary glands detected across all time points and treatments

Modes of detection	Nonpolar - Negative	Nonpolar - Positive	Polar - Negative	Polar - Positive	Total
Detected features	115	1,127	233	1,813	3,288
Differentially expressed features*	37	243	70	351	701
Identifiable features**	8	14	22	548	592
Differentially expressed and identifiable features**, ***	0	2	0	2	4

* Features that showed significant differences ($|\log_2$ fold change$| \geq 1$ and $p < 0.05$) in intensity in at least one of any statistical comparison: infected vs. uninfected, comparison between days pbm of uninfected and infected midguts and interaction analysis (analysis of temporal trends).
** Identification classified as parts per million (ppm) < 6
*** Features that showed significant differences ($|\log_2$ fold change$| \geq 1$ and $p < 0.05$) in abundance between DENV2-infected and uninfected midguts

Specific lipids levels are elevated during DENV2 replication in the midgut of *Ae. aegypti*

To explore the metabolic environment in the mosquito midgut during DENV2 infection, we compared the metabolite repertoire of DENV2-infected midguts to uninfected controls. A summary of the data is shown in Figure 2.3 and Supplemental Table S1. Of 6,103 features detected, 936 features (15%) have differential abundance in DENV2-infected midguts compared to uninfected controls in at least one time point (Figure 2.3A and B). The Venn diagram shows the numbers of molecular features with differential abundance in the midgut ($|\log_2$ fold change$| \geq 1$ and adjusted p-value < 0.05) upon DENV2 infection on days 3, 7, and 11 pbm. The profiles of 5,167 features were unaltered at any day post-infection (Figure 2.3A and B). Among the features with altered levels, 274, 283 and 114 features showed differential abundance only on day 3, 7 or 11 pbm, respectively, whereas 98 features showed differential abundance in all 3 days (Figure 2.3B).

Identified metabolites

About 39% of features (363 out of 936) with differential abundance were identifiable through use of three metabolite databases and the putative identifications were categorized into different metabolite classes. The metabolic relationships between the lipid classes are mapped in figure 2.3C. Fatty acyl-CoA can be synthesized *de novo*. It is a precursor that can be modified and incorporated into more complex lipid molecules such as glycerophospholipids, sphingolipids, glycerolipids and sterols. On the other hand, fatty acyl-CoA can be degraded through β-oxidation when cells require energy. The overall trend of changes in lipid molecular levels that changed upon DENV2 infection is summarized in Figure 2.3D. A majority of the metabolites were unchanged (had intensity changes that are less than 2-fold upon infection or $p \geq 0.05$), while a majority of those that showed greater than 2-fold changes in intensity had higher abundances upon DENV2 infection (Figure 2.3D and Supplemental Table S1). Only 61 out of 363 features (~17%) decreased in abundance during DENV2 infection.

Unidentified metabolites

Interestingly, a large number (~61%) of metabolites that were differentially altered in abundance during DENV2 infection were unidentified. A majority of these unidentified metabolites had elevated abundance in the DENV2-infected samples compared to uninfected controls at all three time points post-infection. These metabolites represent a potential resource since they highlight molecules that are not found in currently available databases that include animal, plant, bacterial and fungal metabolites as well as synthetic compounds. Therefore, they could be compounds unique to Diptera, mosquitoes or *Aedes* species that are yet to be annotated. Given their importance to DENV2 infection, they should be exploited in the future as possible transmission-blocking control points.

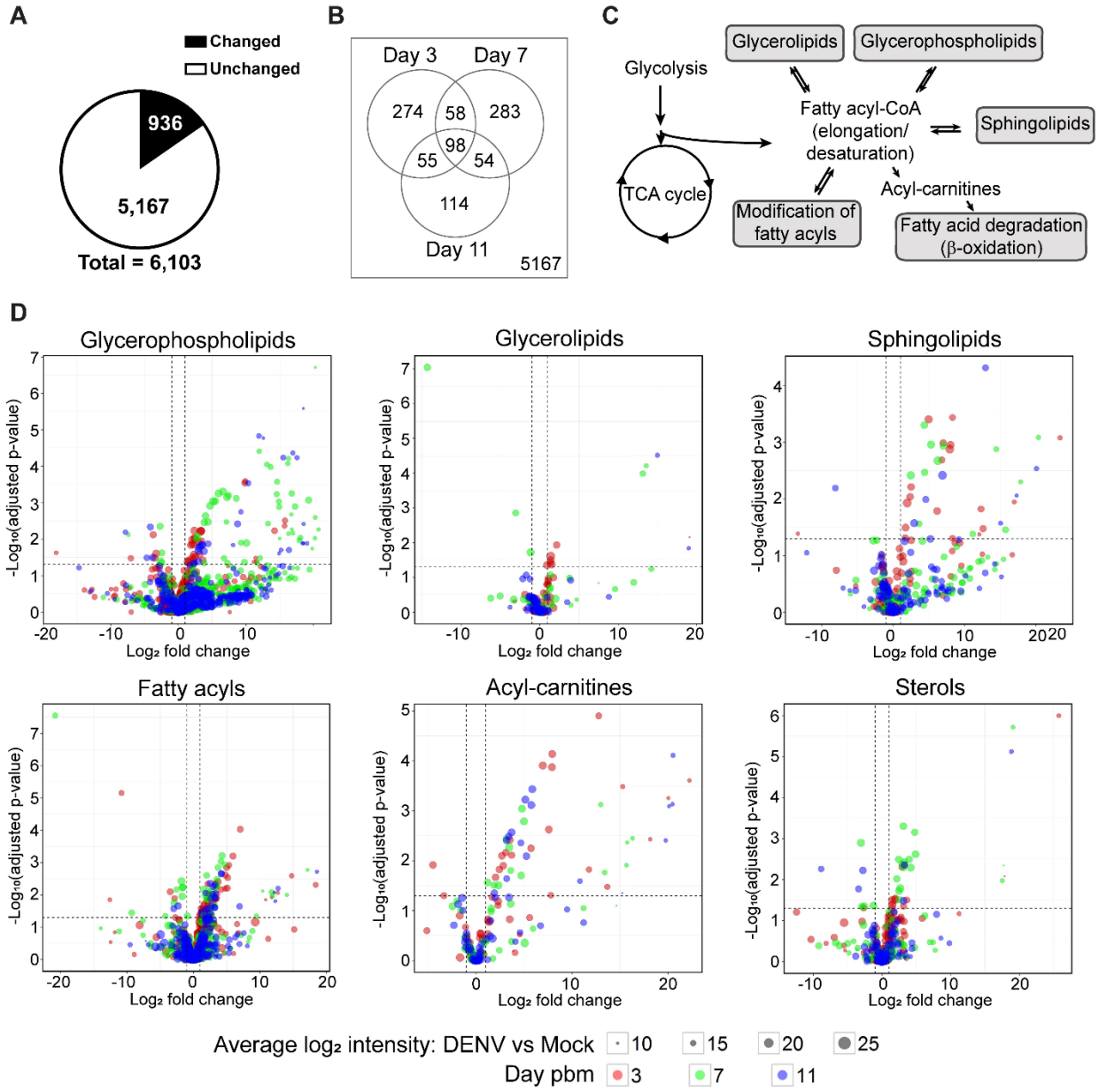

Figure 2.3 Metabolic profile of the mosquito midgut during the course of DENV2 infection. Significant changes were observed in the metabolic profile of the midgut upon infection. (A) The pie chart shows numbers of features in the midgut detected on days 3, 7 and 11 following a DENV2-infectious blood meal compared to a noninfectious blood meal with significantly altered levels of abundance ($|\log_2$ fold change$| \geq 1$ and p-value < 0.05) in black and nonsignificantly altered levels of abundance ($|\log_2$ fold change$| < 1$ or p-value ≥ 0.05) in white. (B) Venn diagram shows numbers of features that were altered in abundance in DENV2-infected midguts compared to uninfected midguts on days 3, 7, and 11 pbm. (C) Overview of lipid classes observed in this study and their relationship to each other within metabolic pathways. Fatty acyl-CoAs can be *de novo* synthesized from intermediates in central carbon metabolism. They can be further modified or incorporated into several classes of more complex lipids or converted to acyl-carnitine for energy production. (D) Volcano plots show the

abundances of metabolites from different classes of lipids detected on days 3, 7 and 11 pbm in DENV2-infected versus uninfected midguts. The vertical dashed lines indicate a 2-fold change in abundance and the horizontal dashed line indicates a p-value = 0.05.

Glycerophospholipids (GPs)

GPs are major components of cellular membranes. GPs are composed of a polar head group, a phosphate group and two fatty acyl chains. The specific composition of GPs in a membrane influences membrane fluidity, leakiness, nutrient exchange, assembly and function of signaling protein complexes and vesicular traffic [62, 137-139]. In insects, the GP composition of membranes also affects tolerance to changing environmental conditions [62]. Pathogenic or endosymbiont infections also drive changes in the intracellular environment and could influence the regulation of GP content in membranes [58, 140-143]. As a point of reference, the metabolic pathways of the major classes of GPs are shown in Figure 2.4A. Our study identified 565 species of GPs in *Ae. aegypti* midguts with 87 species that were altered upon DENV2-infection. The alteration landscape and distribution of the different GPs are shown in Figure 2.4B and 2.4C.

Minimal enrichment of GP species and levels can be observed on day 3 pbm, during the initial establishment of viral infection in the midgut (Figure 2.4B). This enrichment was significantly enhanced on days 7 and 11 pbm. These observations were coincident with known viral infection dynamics (peak viral replication in the midgut on day 7 and viral dissemination to other tissues and clearance from the midgut by day 11) [28]. The signaling GPs, phosphatidylinositols (PIs), were the most diverse (Figure 2.4C) closely followed by PGs, important as surfactants and precursors of cardiolipins in mitochondrial membranes. Phosphatidylcholines (PCs), Phosphatidylethanolamines (PEs) and phosphatidylserines (PSs), which are primary components of most cellular membranes were also increased during infection, especially at the peak of viral replication (day 7 pbm). Interestingly, levels of most of the lyso- or short chain GPs were decreased during infection.

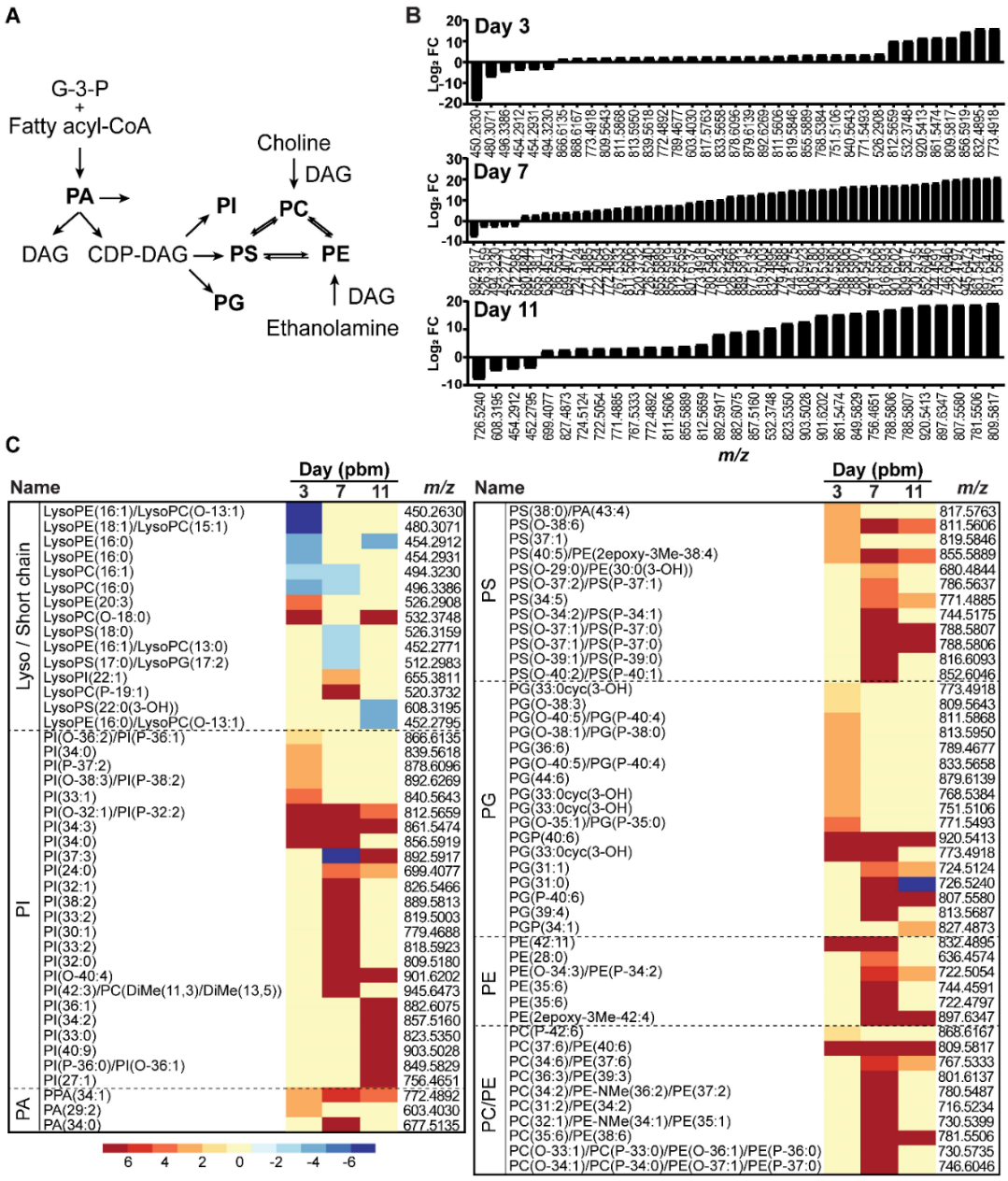

Figure 2.4. GP fluctuation following DENV2 infection of mosquito midguts. (A) The metabolic pathways linking GP classes. Highlighted in bold are the GPs observed in this study. (B) GP landscape altered upon DENV2 infection in midguts. GP species that were altered on days 3, 7, and 11 pbm are listed by *m/z* and arranged by $\log_2$ fold changes from lowest to highest. A significant burst of GP abundance was observed at day 7 post-infection coinciding with increased viral replication in the midgut. (C) Heatmap of $\log_2$ fold changes of GP species on days 3, 7 and 11 arranged by putative ID subclasses. Abbreviations: CDP-DAG, cytidine diphosphate diacylglycerol; DAG, diacylglycerol; G-3-P, glyceraldehyde-3-phosphate; PA, phosphatidic acid; PC, phosphatidylcholine; PE, phosphatidylethanolamine; PG, phosphatidylglycerol; PI, phosphatidylinositol; PS, phosphatidylserine.

Glycerolipids (GLs)

GLs, including mono-, di- and triacylglycerols (MAG, DAG and TAG), are critical effectors of energy metabolism in insects and mammals. Fatty acids absorbed from a digested blood meal or synthesized *de novo* from a sugar meal can be converted into DAG and TAG that can be transported to the fat body for energy storage or the ovaries for vitellogenesis (Figure 2.5) [40, 47, 54, 144-146]. DAG is also an important intermediate in GP synthesis and a critical second messenger regulating cell proliferation, survival, mitochondrial physiology, gene expression and apoptosis [137, 146-148]. Seventy species of GLs were identified in our study, of which eight GLs were significantly changed in abundance upon infection. Most of the MAG, DAG and TAG levels were higher during early time points (day 3 and 7 pbm) in DENV2-infected midguts (Figure 2.5). This might be a result of transportation of these lipids from storage tissues to support the demand for lipids during infection [45, 149]. Interestingly, the level of cytidinediphosphate (CDP-DAG (37:1)) waselevated only during the later phases of infection (days 7 and 11 pbm). CDP-DAG is a precursor for GP synthesis (Figure 2.4A). As a result, increased CDP-DAG (37:1) might support the high demand for GP synthesis on days 7 and 11 pbm during virus infection.

SPs are bioactive molecules that play important roles in the structural composition of cellular membranes and numerous cell-signaling pathways and are critical in microbial pathogenesis [62, 150-154]. *De novo* synthesis of SPs occurs in the endoplasmic reticulum through the condensation of L-serine and palmitoyl-CoA to form Cer via several intermediates [155, 156]. Cer is a precursor for the biosynthesis of several complex SPs such as sphingomyelin (SM) and glycosylceramides or the production of fatty acids and sphingosines through its hydrolysis [157-159]. The SP pathway has been highlighted in many studies in mammalian cells and in mosquito cells as a lipid metabolic pathway altered by flavivirus infection [58, 150].

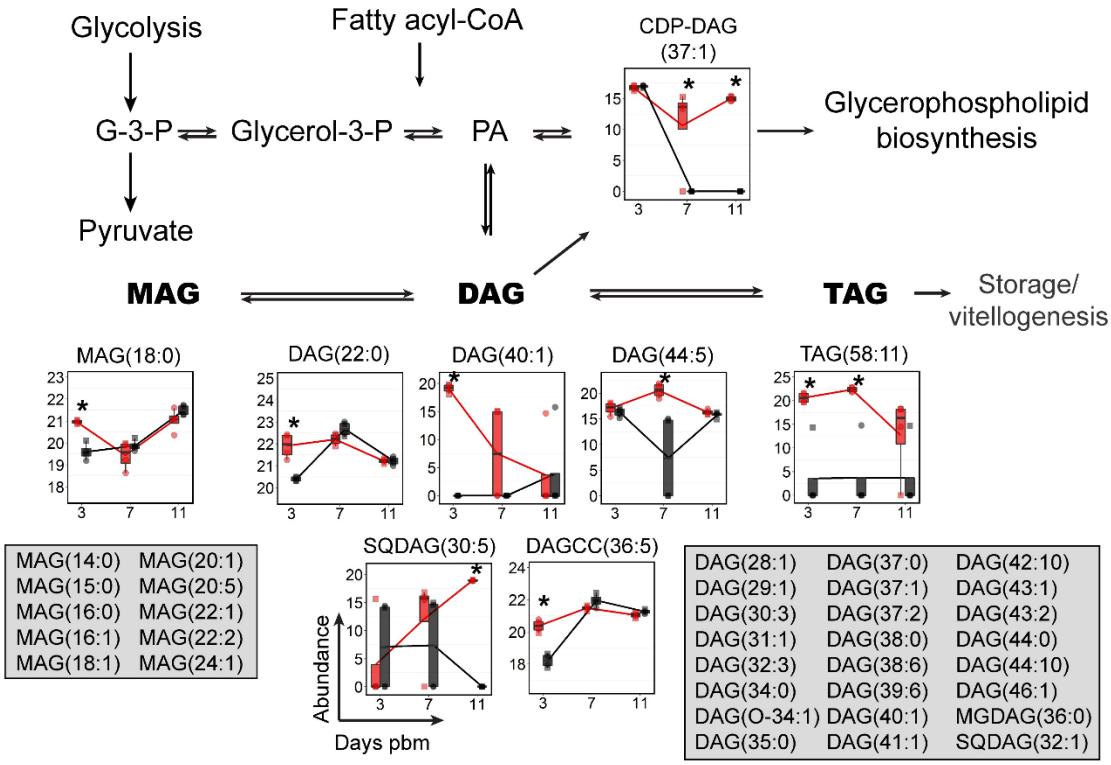

Figure 2.5. GL levels were dynamically altered upon DENV2 infection of mosquito midguts. The abundances of GL species detected in mosquito midguts were mapped to the GL biosynthesis pathway. GL molecules that were significantly altered in abundance are shown in boxplots. Features that were detected but did not change in abundance are listed in the grey boxes. The abundance of metabolites detected in DENV2-infected samples is shown in red and uninfected samples in black. Individual sample pools are represented by circles and squares and technical replicates are dots with the same symbol. Asterisk (*) indicates significantly different levels of abundance between DENV2-infected and uninfected samples ($|\log_2$ fold change$| \geq 1$, $p < 0.05$) Abbreviations: DAG, diacylglycerol; CDP-DAG, cytidine diphosphate diacylglycerol; G-3-P, glyceraldehyde-3-phosphate; glycerol-3-P, glycerol-3-phosphate; MAG, monoacylglycerol; PA, phosphatidic acid; TAG, triacylglycerol; SQDAG, Sulfoquinovosyldiacylglycerol and DAGCC, diacylglycerylcarboxy-N-hydroxymethyl-choline.

Sphingolipids (SPs)

In this study, using the identified SPs from both infected and uninfected mosquito tissues we reconstructed a significant proportion of the SP metabolic pathway for *Ae. aegypti* (Figure 2.6). Several members of the pathway were identified at all three time points in both biological replicates of the infected and uninfected tissues. We observed accumulations of several SPs such as sphinganine, sphinganine-1-PC, sphingosine, Cer and hexosylceramide that were

elevated in DENV2-infected midguts on days 3, 7 and/or 11 pbm. GP-Cers, especially PE-Cers, are sphingomyelin analogues. They function as the principal membrane sphingolipids in *D. melanogaster,* which lacks sphingomyelin synthase [160]. In mosquito midguts, we found decreased abundance of PE-Cer (d32:2(2OH)) upon DENV2 infection on day 3 pbm but an increase in the levels of PE-Cer(d33:2(2OH)), PE-Cer(d36:1), PE-Cer(d36:3(2OH)) and PE-Cer(d36:2(2OH)) on day 7 and/or 11 pbm. Interestingly, SM was found in *Ae. aegypti* mosquito midguts and in cells in culture (Figure 2.6 and Figure 3.4-3.6 in chapter 3); however, the levels of SM were not changed upon DENV2 infection at any of the time points tested. Glycosylated ceramides (hexosylceramide and hexosylceramidesulfate) play critical roles in modulating cellular signaling and gene expression resulting in changes in processes such as proliferation, apoptosis, autophagy and endocytosis [161]. The abundance of the neutral glycosphingolipid, FMC-6(d40:1(2-OH)), was increased on all days and HexCer(d40:1(2OH) sulfate was increased on day 3 following DENV2 infection (Figure 2.6).

Fatty acids and derivatives (Fatty acyls)

Fatty acyls can be acquired from midgut digestion and absorption of a blood meal or can be *de novo* synthesized from central carbon metabolism precursors [54, 162]. Fatty acids that are covalently linked to coenzyme A, fatty acyl-CoAs, can be incorporated into complex lipids such as GPs, SPs and GLs that have structural roles in membranes. In addition, free fatty acids or fatty acyls that are linked to other functional groups can have critical roles in signaling, energy homeostasis and the immune response in insects and mammals (e.g.: fatty amides and eicosanoids) [37, 50, 163]. In this study, at least nine subclasses of fatty acyls were detected and many of these had higher abundances in DENV2-infected midguts compared to uninfected controls in at least one time point pbm (Figure 2.7A and Supplemental Table S1). The molecules observed were fatty amides, hydroxy fatty acids, free fatty acids, eicosanoids and

leukotriene (i.e. immunomodulators), fatty-amines, glycosides, dicarboxylic acids, and keto-fatty acids.

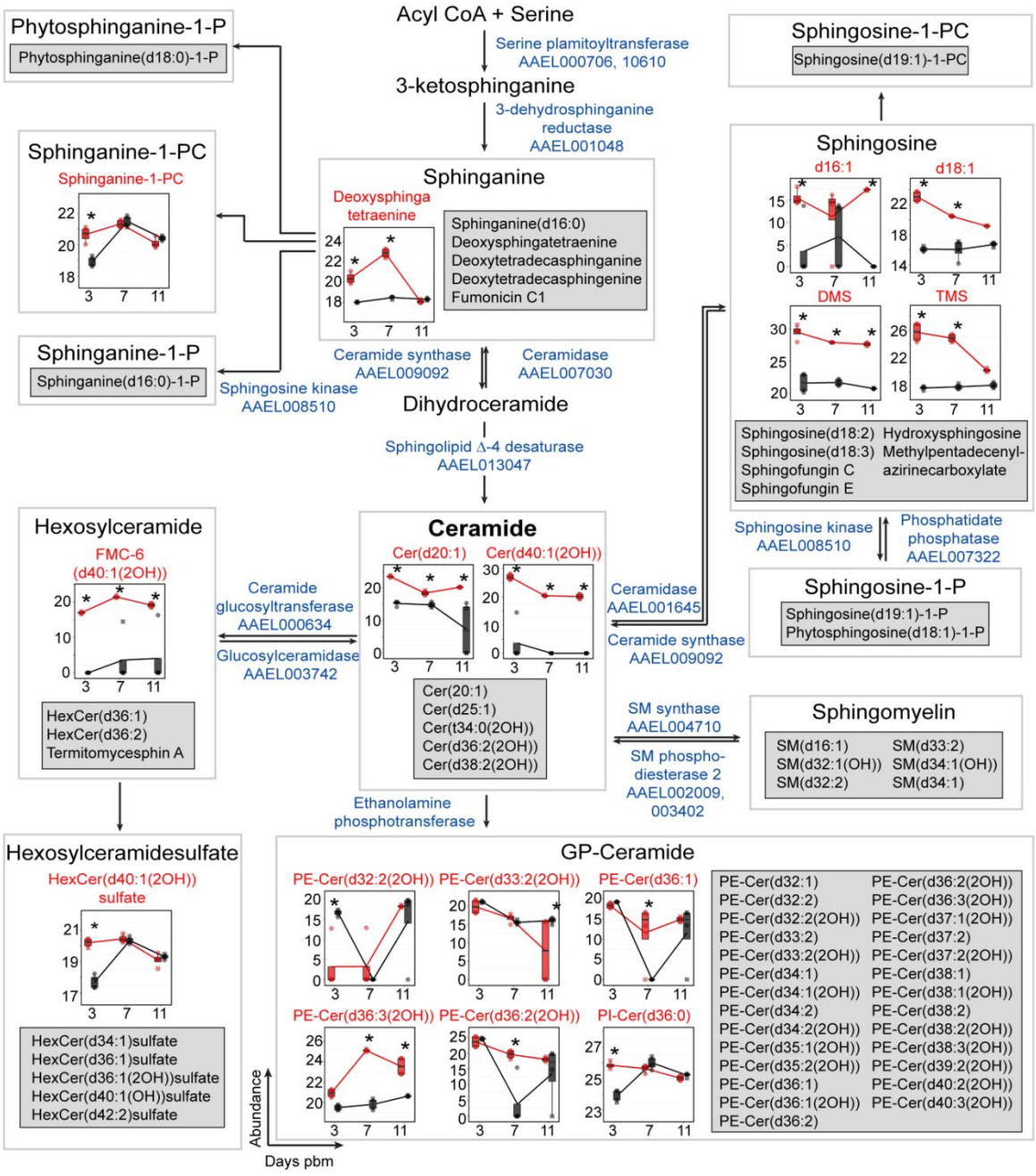

Figure 2.6. Accumulation of SPs during DENV2 infection. The SP pathway for *Ae. aegypti* was reconstructed for the first time in this study. This SP metabolic pathway (modified from Hannun et. al., 2008 [151]) is shown overlaid with box plots with SPs that exhibited significantly altered levels during infection. Features that were detected but unchanged in abundance upon DENV2 infection are listed in the grey boxes. The abundance of metabolites detected in DENV2-infected samples is shown in red and uninfected samples in black. Individual sample

pools are represented by circles and squares and technical replicates are dots with the same symbol. Asterisks (*) indicate significantly different levels of abundance between DENV2-infected and uninfected samples ($|\log_2$ fold change$| \geq 1$, $p < 0.05$). The enzymes predicted to catalyze the reactions in the SP pathway and their VectorBase accession numbers (AAELXXXXXX) according to AaegEL5 assembly and as annotated in the KEGG pathway are given in blue text. Where enzymes are not given it indicates an absence of annotation for *Ae. aegypti* of names via the KEGG database and VectorBase. Abbreviations: Cer, ceramide; GP-Cer, glycerophospholipid-ceramide; HexCer, hexosylceramide; FMC-6, acetyl-sphingosine-tetraacetyl-GalCer(d40:1(2OH)); PE-Cer, phosphatidylethanolamine-ceramide; Phytosphinganine-1-P, phytosphinganine-1-phosphate; PI-Cer, phosphatidylinositol-ceramide; Sphingosine-1-P, sphingosine-1-phosphate; Sphingosince-1-PC, sphingosine-1-phosphatidylcholine and SM, sphingomyelin.

Figure 2.7B and C shows molecules with significantly increased or decreased levels at least at one time point following DENV2 infection that have known functions in immunomodulation (Figure 2.7B) and N-acylamides and other fatty acyls whose accumulation is a marker for malfunction of fatty acid oxidation (Figure 2.7C). Prostaglandins, leukotrienes, thromboxanes and lipoxins are eicosanoids that are synthesized in various tissues. Eicosanoids are inflammatory mediator molecules that have been found to play several important roles in insect immunity [50]. In this study, three prostaglandins (prostaglandin a2, prostaglandin d2, and PGD2-dihydroxypropanylamine) and one thromboxane (dehydrodinor-TXB2) showed increased levels during DENV2 infection and one leukotriene (leukotriene e4) decreased during DENV2 infection. Anti-inflammatory molecules (resolvin d5 and epoxy-DHA) increased during DENV2 infection [164, 165]. Metabolites of linoleic acid that may regulate prostaglandin synthesis (HEPE, HpOTrE and TriHOME) also increased upon DENV2 infection [86, 87, 165]. N-acylamides play important roles in endocannabinoid signaling systems in mammals and have been detected and reported as potentially important signaling molecules in *Drosophila* [166]. Elevated levels of these molecules are also observed in the urine and blood of human patients with fatty acid oxidation disorders [167]. In our study, we found that five N-acylamide molecules (e.g. N-arachidonoylglycine, myristoylglycine, N-stearoylarginine, N-decanoylglycine, and N-undecanoylglycine) had increased levels and N-heptanoylglycine displayed a decreased level in midguts during DENV2 infection (Figure 2.7C).

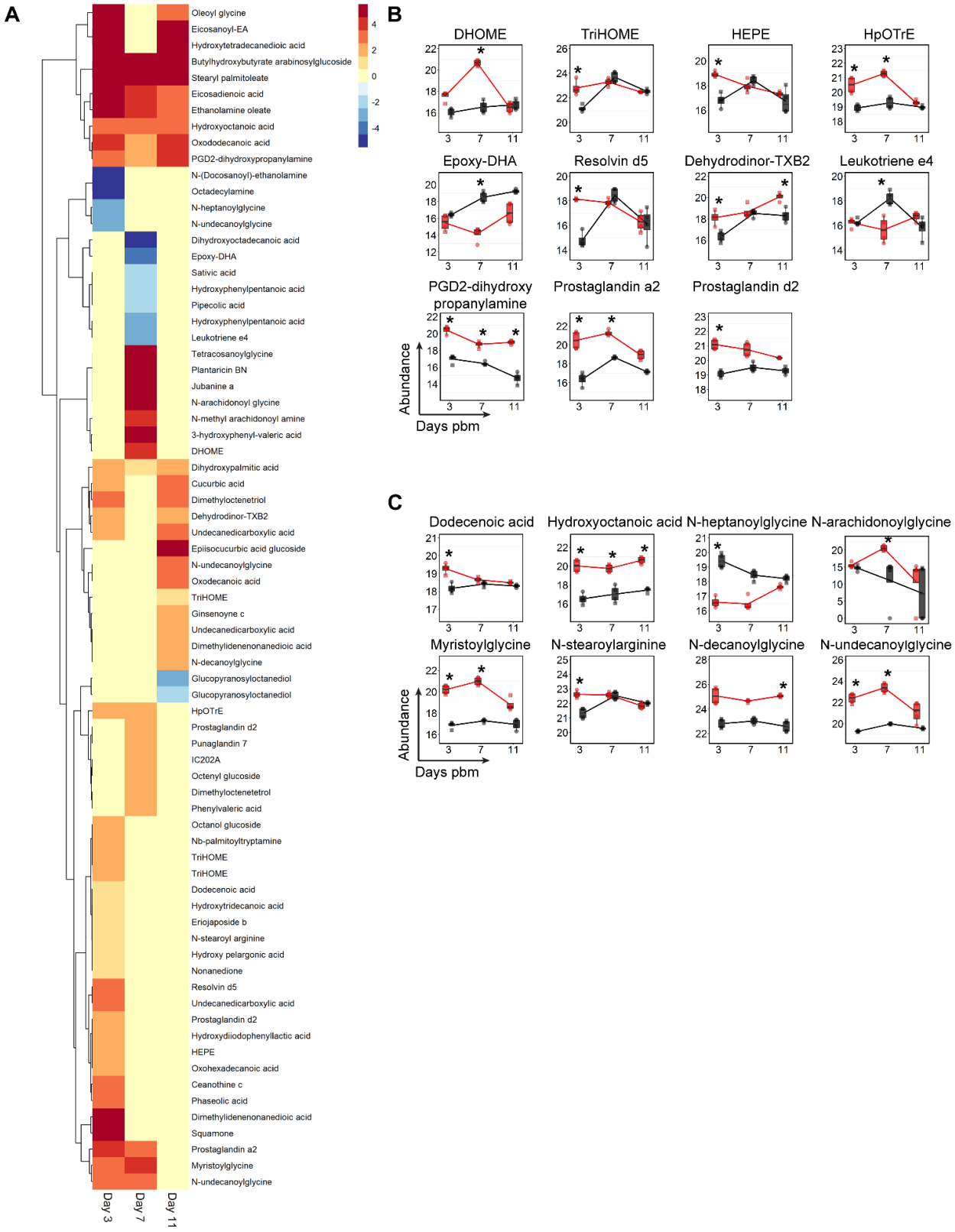
A
Oleoyl glycine
Eicosanoyl-EA
Hydroxytetradecanedioic acid
Butylhydroxybutyrate arabinosylglucoside
Stearyl palmitoleate
Eicosadienoic acid
Ethanolamine oleate
Hydroxyoctanoic acid
Oxododecanoic acid
PGD2-dihydroxypropanylamine
N-(Docosanoyl)-ethanolamine
Octadecylamine
N-heptanoylglycine
N-undecanoylglycine
Dihydroxyoctadecanoic acid
Epoxy-DHA
Sativic acid
Hydroxyphenylpentanoic acid
Pipecolic acid
Hydroxyphenylpentanoic acid
Leukotriene e4
Tetracosanoylglycine
Plantaricin BN
Jubanine a
N-arachidonoyl glycine
N-methyl arachidonoyl amine
3-hydroxyphenyl-valeric acid
DHOME
Dihydroxypalmitic acid
Cucurbic acid
Dimethyloctenetriol
Dehydrodinor-TXB2
Undecanedicarboxylic acid
Epiisocucurbic acid glucoside
N-undecanoylglycine
Oxodecanoic acid
TriHOME
Ginsenoyne c
Undecanedicarboxylic acid
Dimethylidenenonanedioic acid
N-decanoylglycine
Glucopyranosyloctanediol
Glucopyranosyloctanediol
HpOTrE
Prostaglandin d2
Punaglandin 7
IC202A
Octenyl glucoside
Dimethyloctenetetrol
Phenylvaleric acid
Octanol glucoside
Nb-palmitoyltryptamine
TriHOME
TriHOME
Dodecenoic acid
Hydroxytridecanoic acid
Eriojaposide b
N-stearoyl arginine
Hydroxy pelargonic acid
Nonanedione
Resolvin d5
Undecanedicarboxylic acid
Prostaglandin d2
Hydroxydiiodophenyllactic acid
HEPE
Oxohexadecanoic acid
Ceanothine c
Phaseolic acid
Dimethylidenenonanedioic acid
Squamone
Prostaglandin a2
Myristoylglycine
N-undecanoylglycine
Day 3
Day 7
Day 11
4
2
0
-2
-4
B
DHOME
TriHOME
HEPE
HpOTrE
Epoxy-DHA
Resolvin d5
Dehydrodinor-TXB2
Leukotriene e4
PGD2-dihydroxy propanylamine
Prostaglandin a2
Prostaglandin d2
Abundance
Days pbm
C
Dodecenoic acid
Hydroxyoctanoic acid
N-heptanoylglycine
N-arachidonoylglycine
Myristoylglycine
N-stearoylarginine
N-decanoylglycine
N-undecanoylglycine
Abundance
Days pbm

Figure 2.7. Temporal fluctuations in levels of fatty acyl molecules following DENV2 infection of mosquito midguts. (A) Comparative analysis of fatty acyls in mosquito midguts following DENV2 infection. Average abundance of fatty acyl molecules in DENV2 infected midguts was compared with uninfected midguts and represented as log_2 fold change. Each row shows a different fatty acyl molecule, grouped based on the classification of molecular structure. Columns represent 3, 7, and 11 day pbm. Log_2 fold changes that are zero represent the changes that were not significantly different in DENV2 infected versus uninfected tissues. Log_2 fold changes shown in dark red or dark blue represent log_2 fold changes that are greater than 5 or lower than -5. (B) The abundances of fatty acyls that have known functions in immunomodulation. (C) The abundances of free fatty acids and N-acylamides that have known functions in signaling and/or that are markers of malfunction in fatty acid oxidation are shown. The abundances of metabolites detected in DENV2-infected samples are shown in red and uninfected samples in black. Individual sample pools are represented by circles and squares and technical replicates are dots with the same symbol. Asterisks (*) indicate a significantly different abundance between DENV2-infected and uninfected samples ($|log_2$ fold change$| \geq 1$, $p < 0.05$). Abbreviations: DHOME, dihydroxyoctadecenoic acid; Dehydrodinor-TXB2, dehydrodinor-oxothromboxadienoic acid; Epoxy-DHA, epoxydocosahexaenoic acid; HEPE, hydroxyeicosapentaenoate; HpOTrE, hydroperoxyoctadecatrienoic acid; PGD2-dihydroxypropanylamine, Prostaglandin D2-dihydroxypropanylamine and TriHOME, trihydroxyoctadecenoic acid.

Acyl-carnitines

One of the most prominent observations in this study is the change in abundance of acyl-carnitines in midgut tissue after DENV2 infection (Figure 2.8). These molecules are intermediates that shuttle fatty acyl-CoA from the cytoplasm into the mitochondria for β-oxidation and resultant energy (ATP) production. A total of 54 acyl-carnitine molecules were detected in the midgut metabolome. Following DENV2 infection, 26 acyl-carnitines had a significant increase in abundance and only one had decreased abundance (Figure 2.8A). Interestingly, of those that increased in abundance, 25 out of 26 molecules contained medium chain-length fatty acyls of 4-12 carbons. The accumulation of acyl-carnitines with medium-length carbon chains was reported to be a result of incomplete β-oxidation [168].

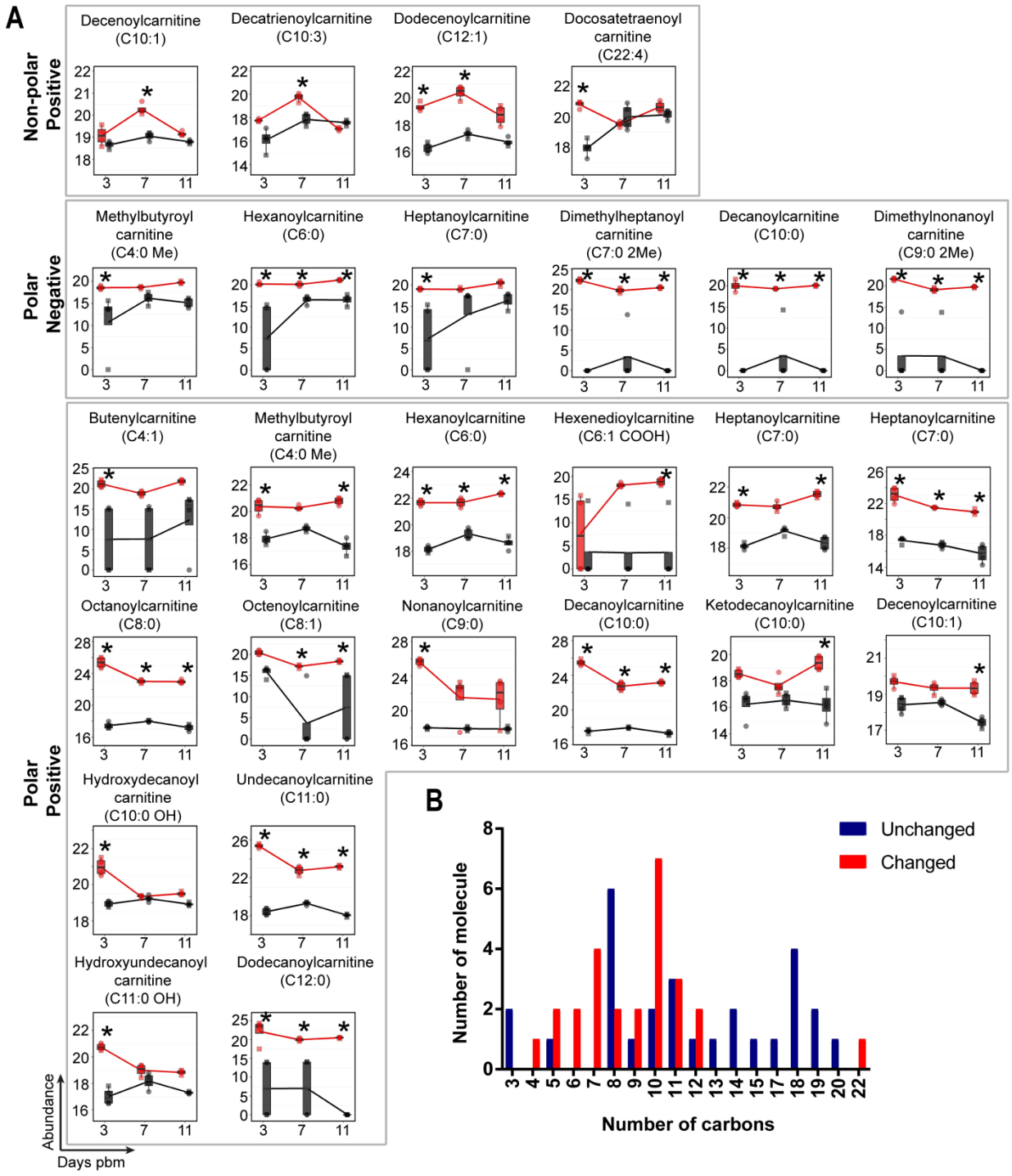

Figure 2.8 Acyl-carnitines accumulate in mosquito midguts during DENV2 infection. (A) Molecules showing differential abundance after DENV2 infection. Numbers of carbons in the fatty acyl chains are indicated in parentheses. The abundance of metabolites detected in DENV2-infected samples is shown in red and uninfected samples in black. Individual sample pools are represented by circles and squares and technical replicates are dots with the same symbol. Asterisks (*) indicate significantly different abundance between DENV2-infected and

uninfected samples ($|\log_2$ fold change$| \geq 1$, $p < 0.05$). (B) Bar graph showing numbers of detected acyl-carnitine molecules corresponding to the numbers of carbons in the acyl-chains. Red bars indicate molecules with significantly altered abundances while blue bars indicate molecules that remained unaltered during DENV2 infection.

Sterol lipids

Sterol lipids are a group of cyclic organic compounds composed of 17 carbon atoms arranged in a four-ring structure. In insects, cholesterol is a component of cellular membranes and a precursor of the ecdysone hormone [73, 169-171]. However, insects cannot synthesize cholesterol *de novo* but must absorb it from dietary sources and/or microflora [67, 68]. During infection of mammalian cells, cholesterol in the flavivirus envelope seems to be critical for viral entry and fusion [97, 98]. It has also been shown that flaviviruses can manipulate cellular cholesterol homeostasis to facilitate genome replication [95]. However, the role of cholesterol in flavivirus replication in the mosquito vector has not been determined. In this study, we detected 111 sterol lipid molecules. Many of these have no reported function in insects. Since sterols in the mosquito are acquired from dietary sources (in this case, raisins, sucrose, sheep blood and cell culture medium), we did not exclude sterol lipids identified as plant or other animal from our analyses. Of the 111 molecules, 25 showed different levels of abundance during DENV2 infection compared to controls (Supplemental Table S1). Twenty-one molecules increased during infection while only four molecules decreased during infection. A majority of the changes occurred on day 3 (10 molecules) and day 7 (14 molecules) pbm. Only one molecule showed significant changes (decreased) on day 14 pbm.

DISCUSSION

The dynamic metabolic environment of an organism is an indicator of physiological changes that occur following exposure to varying environmental conditions. When arboviruses such as DENV infect a mosquito vector, they must strike a delicate balance between metabolic

commensalism and competition to achieve persistent replication in mosquito tissues to allow transmission to a new host. Here, we have explored the metabolic landscape of *Ae. aegypti,* the primary vector of DENV, ZIKV, YFV and CHIKV, during infection with DENV. Our study focused on the midgut, the site of initial viral replication prior to viral dissemination to other tissues and transmission to the vertebrate host [28]. The observed biochemical changes highlight specific metabolites that may be markers of infection. They may be required for viral replication or produced as part of the defensive response of the vector to the invading pathogen. We have consistently observed a link between DENV2 infection and an increased abundance of GPs; our previous work on DENV2-infected human cells showed that fatty acid synthase (FAS), a key enzyme required for fatty acid synthesis (essential pre-cursors of GP synthesis), is activated by the expression of virus-encoded nonstructural protein NS3 and relocates to sites of viral RNA replication through interaction with NS3 [111]. Inhibition of FAS activity using C75 caused a reduction in viral replication and we observed this in both cultured human and mosquito cells [58, 111]. We profiled the metabolic changes upon C75 inhibition of FAS in mosquito cells and demonstrated that the GP repertoire was directly reduced coincident with the reduction in viral replication. Therefore, in cell culture models an abundance of GPs is required for viral replication. The current study supports these observations and reveals that DENV2 infection also significantly alters the abundance of GPs and other lipid-related molecules in the midgut of the mosquito vector during infection (summarized in Figure 2.9). While our previous studies showed that *de novo* synthesis of lipids plays an important role in DENV2 replication, other processes such as lipolysis, lipid conversion/consumption or import/export may also critically shape the metabolite pool observed in these infected tissues [108, 172].

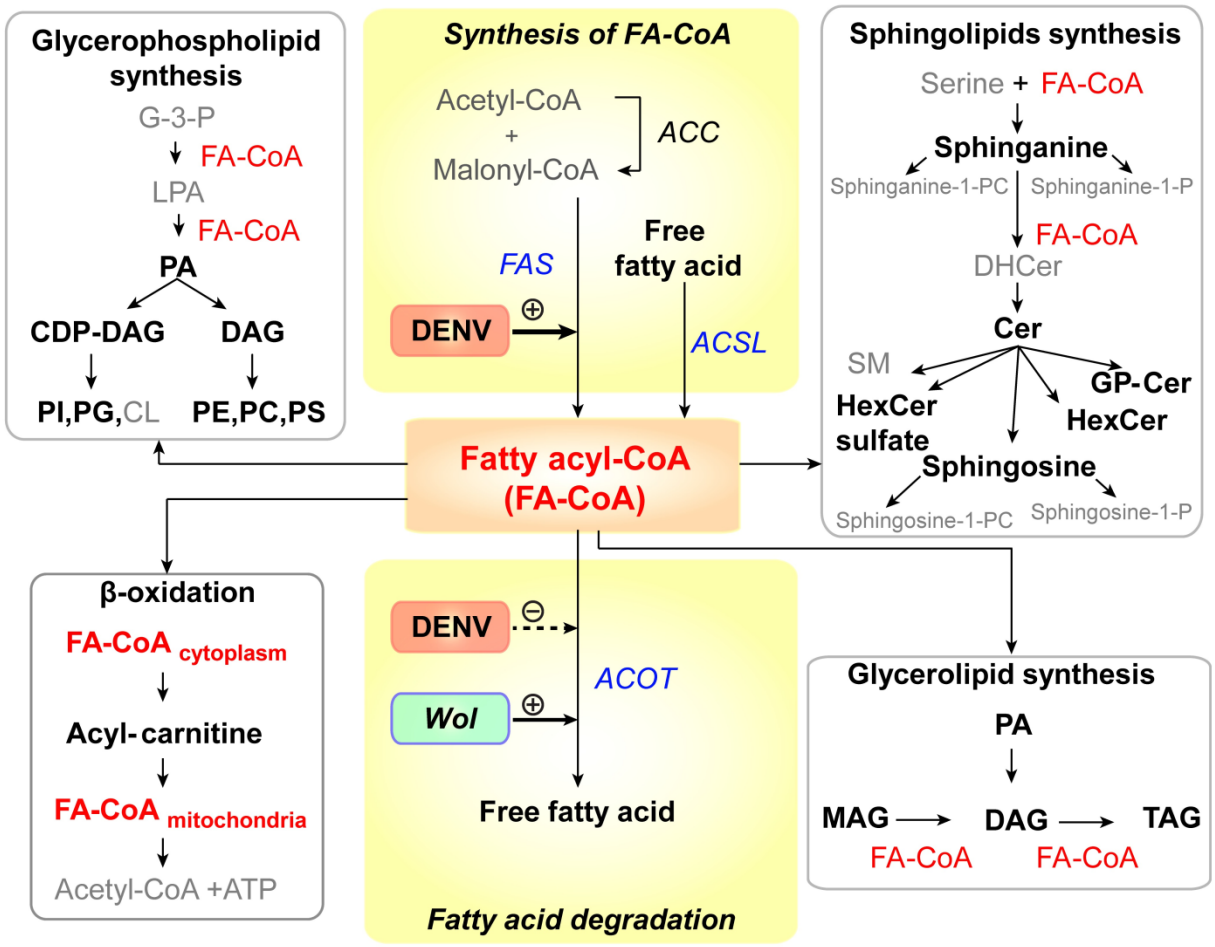

Figure 2.9. DENV2 infection results in alteration of lipid homeostasis in infected *Ae. aegypti*. This study revealed that the abundance of lipids in six main lipid metabolic pathways [173] was altered following DENV2 infection of the mosquito midgut (names of lipids that were altered in abundance during infection are in black (bold) and lipids that remained unchanged are in grey). All of these pathways require fatty acyl-CoA (FA-CoA), activated fatty acids, as a precursor for the synthesis of complex lipids (red). Names of enzymes involved in FA-CoA homeostasis are italicized (*FAS, ACOT* and *ACSL*). Previous studies by Heaton et al, 2010 [111] and Perera et al, 2012 [58] have shown that DENV2 infection requires and can enhance the activity of FAS in human and mosquito cells. Ye et al, 2013 [174] have shown that *Wolbachia*, the insect endosymbiont used to control DENV2 transmission by *Ae. aegypti* mosquitoes can increase FA-CoA catabolism by increasing the expression of ACOT enzymes. Therefore, FA-CoA metabolism represents a 'hub' that may control lipid metabolic competition in the midgut that mediates the success of DENV2 replication. Abbreviations: ACC, acetyl-CoA carboxylase; ACSL, long-chain acyl-CoA synthetase; ACOT, acyl-CoA thioesterase; CDP-DAG, cytidine diphosphate diacylglycerol; Cer, ceramide; ; CL, cardiolipin; DAG, diacylglycerol; DHCer, dihydroceramide; G-3-P, glycerol -3-phosphate; GP-Cer, glycerophospholipid-ceramide; FAS, fatty acid synthase; HexCer, hexosyl ceramide; LPA, lysophosphatidic acid; MAG, monoacylglycerol; PA, phosphatidic acid; PC, phosphatidylcholine; PE, phosphatidylethanolamine; PI, phosphatidylinositol; PG, phosphatidylglycerol; PS, phosphatidylserine; SM, sphingomyelin; sphinganine-1-P, sphinganine-1-phosphate; sphinganine-1-PC, sphinganine-1-phosphatidylcholine; sphingosine-1-P, sphingosine-1-

phosphate; sphingosine-1-PC, sphingosine-1-phosphatidylcholine; TAG, triacylglycerol and *Wol*, *Wolbachia*.

Glycerophospholipids (GPs)

One of our most striking observations was the marked elevation of GP levels coincident with the kinetics of viral replication in the midgut [28]. Digestion of the blood meal is completed within ~48 hours post-ingestion, and provides a major source of amino acids and fatty acids used for the biosynthesis of macromolecules [53, 175]. These macromolecules are required for vitellogenesis (yolk formation) and energy storage [40, 43, 176, 177]. In DENV2-infected mosquitoes, the rapid increase in GP content is observed at day 7 pbm when viral replication reaches its peak in the midgut. While it is currently unknown if biosynthesis alone contributes to this burst in GP content, the increase is consistent with requirements for DENV2 replication within human and mosquito cells in culture [58, 111]. Specifically, DENV2 infection induces a massive expansion of intracellular membranes required for the assembly and function of viral replication complexes and assembly and release of enveloped progeny virions [8, 89]. This membrane expansion is coincident with increased GP biosynthesis through the co-opted functions of FAS, a key enzyme in the pathway. Electron microscopic studies have revealed similar membrane expansions associated with the midgut of WNV-infected *Culex* mosquitoes, but equivalent studies have not been performed in *Ae. aegypti* infected with DENV [9].

Sphingolipids (SPs)

Reconstruction of the SP pathway in *Ae. aegypti* revealed significant conservation with that of *Homo sapiens*, allowing us to identify a majority of orthologous metabolites in the pathway. Importantly, most metabolites were identified in both pools of 100 midguts, at all time points and in both infected and uninfected tissues, confirming a significant presence in the midgut metabolome. Additionally, we were able to identify orthologous effector enzymes for a majority of the SP metabolic pathways in our study using annotations in the AaegEL5 assembly

of the *Ae. aegypti* genome on VectorBase [66]. SPs are important components of lipid rafts in membranes that in mammalian systems, together with cholesterol, support the assembly and function of various protein signaling complexes [178]. Metabolites of SPs are well-studied signaling molecules [155]. These lipids have been studied in *D. melanogaster* [64, 140, 179] and it has been demonstrated that these lipids are critical for development, reproduction and maintenance of tissue integrity in the fruit fly [180]. SPs have also been identified in *Anopheles stephensi* by spatial mapping and in *Aedes* and *Culex* cells in culture [58, 63, 181]. However, the specific functionality of these lipids has not been extensively studied either *in vitro* or *in vivo* in mosquitoes. All viruses and most bacteria are incapable of SP synthesis and rely on the host to provide these lipids. The specific species of SPs that are increased in abundance during infection could influence the balance between commensalism, competition and/or host damage [150, 182].

Mitochondrial β-oxidation and metabolite trapping

During mitochondrial β-oxidation activated fatty acids (FA-CoAs) in the cytoplasm are esterified with carnitine to produce acyl-carnitines that are then shuttled to the mitochondrial matrix for energy production [183-185]. In this study, we observed a temporal accumulation of medium-length carbon chain-containing acyl-carnitines in DENV2-infected midguts compared to uninfected midguts. The accumulation of medium-length carbon chain acyl-carnitines was reported to be indicative of incomplete β-oxidation [186]. Given that DENV2 replication requires FA-CoAs, for lipid biosynthesis and subsequent membrane expansion, it is possible that acyl-carnitine accumulation results from a manipulation of β-oxidation (an increase or decrease) in order to provide for viral replicative needs [58, 108, 150].

There are two possible hypotheses to explain the accumulation of medium-chain length acyl-carnitines during DENV2 infection (Figure 2.10). In hypothesis I, accumulation of acyl-

carnitines might be caused by inhibition or blockage of β-oxidation in the mitochondria, reducing the production of ATP (Fig 2.10, *I*). This phenomenon has been observed in cells exposed to hypoxic conditions [187-189]. Similar effects were observed during DENV infection of human cells; in infected HepG2 cells, mitochondrial membrane damage appeared to lead to a reduction in ATP levels [190]. To maintain energy homeostasis, energy consumption is diverted towards increasing glucose uptake and glycolysis [187]. This response has also been observed in DENV-infected primary human cells [191]. Due to the stalling of acyl-carnitine transport and a blockage of β-oxidation, FA-CoA lipid partitioning may occur to divert FA-CoAs towards synthesis of complex lipids and membrane expansion at the expense of fatty acid oxidation [188, 191, 192].

Alternatively, in hypothesis II, an accumulation of medium-length carbon chain acyl-carnitines could occur because of mitochondrial overload (Fig 10, *II*). In this scenario, due to increased energetic demands during infection, a large proportion of FA-CoAs enter mitochondria but are only partially broken down by β-oxidation, which serves as a bottle neck for this reaction. This phenomenon was observed in human skeletal muscle insulin resistance [168]. The ATP that is produced by β-oxidation is sufficient to supply the energetic needs for producing more virions, and acetyl-CoA (2-carbon product) can be recycled for *de novo* synthesis of new longer-chain FA-CoA molecules directly at the site of virus replication [111]. This hypothesis is supported by Heaton et al. during DENV2 infection of Huh7.5 human liver cells, where they observed an increase in autophagosome processing of cellular lipid droplets and TAGs to produce free fatty acids and a stimulation of mitochondrial β-oxidation [108]. The molecular mechanisms of how mitochondrial energetics are diverted to benefit DENV replication in the mosquito midgut are still unclear and the observations in this study present the first insight into the possibilities.

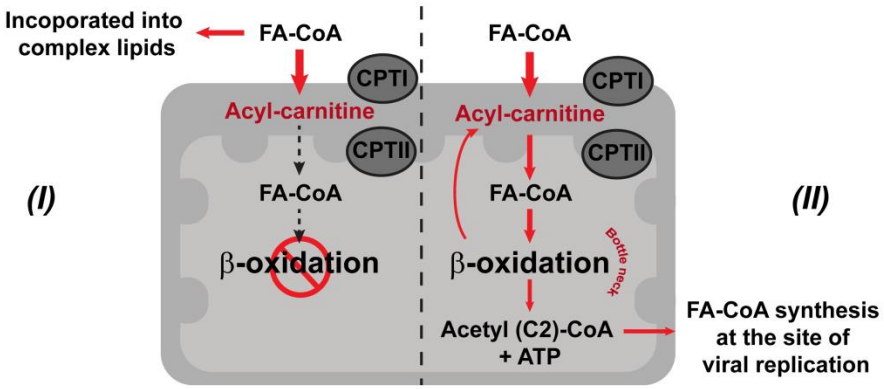

Figure 2.10. DENV2 infection perturbs cellular energy production from lipids. The schematic shows the carnitine shuttle translocating fatty acyl-CoA from the cytosol into the mitochondrial matrix for fatty acid degradation (β-oxidation) and two hypotheses (*I and II*) to explain the accumulation of medium-chain length acyl-carnitines and the diversion of FA-CoAs during DENV2 infection. Hypothesis *I* represents a pathway where an accumulation of acyl-carnitines is observed because β-oxidation in the mitochondria is inhibited or blocked by infection. Hypothesis *II* represents a pathway that leads to mitochondrial overload during infection due to increased energetic demands. Abbreviations: CPTI, carnitine palmitoyl transferase I; CPTII, carnitine palmitoyl transferase II; and FA-CoA, fatty acyl-CoA. Red arrows represent the hypothesized flow of intermediates occurring during infection.

Metabolic competition versus commensalism

FA-CoAs (activated fatty acids) form a primary hub that integrates multiple lipid metabolic pathways, some of which were found to be perturbed in this study during DENV2 infection (Figure 2.9). These molecules are key to the synthesis of more complex lipids, which are important for DENV2 replication in both human and mosquito cells [8, 58, 89, 111]. FA-CoAs are also important for activating several signaling pathways in the cell [193, 194]. Interestingly, there is evidence that *Wolbachia*, the endosymbiotic bacterium used to control DENV2 infection in *Ae. aegypti*, might drive this metabolic balance in the opposite direction (FA-CoA to free fatty acid) suggesting opposing metabolic driving forces resulting in a competition between virus and endosymbiont [174]. Recent studies in *Wolbachia*-infected *Ae. albopictus* (Aa23) cells have supported this hypothesis and indicated that several lipid groups such as SP, PC, and DAG previously shown to be elevated in DENV-infected C6/36 cells were depleted upon *Wolbachia* infection of the cells [58, 140, 141].

The hypothesis that metabolic challenge rather than immune pathways form the basis for pathogen-blocking capabilities of *Wolbachia is* further supported by observations by Caragata et al, 2013 [195] who showed that cholesterol might also be a limiting factor that drives metabolic competition between virus and endosymbiont. Specifically, increasing cholesterol availability via an enriched diet increases virus replication in the insect and reduces the impact of *Wolbachia*-mediated pathogen suppression. Mosquitoes are incapable of *de novo* synthesis of sterols, and must sequester these molecules from the blood meal or from microbiota that are capable of synthesizing these lipids [68, 99]. In the presence of *Wolbachia*, it is possible that cholesterol "stealing" from the vertebrate blood meal may make cholesterol unavailable for DENV infection/replication. In mammalian systems, it has been shown that cholesterol is critical for DENV replication [97, 98], and therefore, it is interesting to contemplate what might happen in the mosquito where these lipids are limited. Alternately, other species of lipids could substitute for the function(s) of cholesterol during DENV replication in mosquitoes. In this study, we detected over one hundred cholesterol molecules with one fourth of the molecules showing alterations during early phases of DENV replication in the midgut. The specific role these molecules might play in virus-vector interactions yet remain to be explored.

Comparison to cell culture models

These *in vivo* studies are the obvious next step to previous studies that have evaluated metabolic changes induced by DENV infection in cell culture models. Interestingly, in both human [111] and mosquito cell cultures models [58] we observed a significant increase in GP expression during DENV2 infection. We determined that this burst of GP abundance is due to the activity of FAS that seems to be stimulated and re-localized to sites of viral RNA replication by DENV2 nonstructural protein 3 (NS3) [111]. We anticipated that this might also be true *in vivo*. Accordingly, we saw a significant increase in GPs in *Ae. aegypti* midguts that directly coincides with the peak of viral replication (similar to that observed in both human hepatoma

and C6/36 cells) indicating that it could be a key modulator of DENV2 infection. In mosquitoes, we did not see significant PG and PI involvement during infection *in vitro* (C6/36 cells) studied by Perera et. al., but we observed the changes in PG and PI abundance *in vivo* following infection in this study [58]. PGs are important lipids in prokaryotes and abundance is higher in bacterial membranes than that in eukaryote membranes. [196]. Therefore, the presence of higher PG abundance we observed in mosquitoes could be caused by elevation of the microbiome in the midguts post infection, which is absent in the cell culture system. However, to accurately compare the specific GP landscape with respect to true concentrations of head groups, extensive targeted analyses will need to be carried out in the future. Lysophospholipids (LysoGPs), a derivative of GP with one of the acyl chain removed by phospholipase A2, was also more heavily perturbed in C6/36 cells compared to mosquito midguts. This observation was in concordant with an evidence that phospholipase A2 have increased activity during DENV2 and WNV infection [58, 197]. In this study, we observed that the abundance of lysoGPs were prominently decreased in infected midguts but were increased in infected C6/36 cells. These lipids are known to be stress-related as well as to function as precursors and signaling molecules that also play important roles in influencing membrane architecture [198, 199]. These different response patterns *in vitro* and *in vivo* indicate a more complex situation in the whole animal and is evidence that *in vitro* observations are not always translatable to the *in vivo* environment.

In summary, we present the first comprehensive analysis of the metabolome of *Ae. aegypti,* the primary mosquito vector of dengue, Zika, chikungunya and yellow fever viruses, during DENV infection. Alterations in the metabolome are quantitative indicators of the outcome of arbovirus-host interactions that facilitate virus replication or may result from host responses to infection. Our study provides evidence that DENV2 infection specifically alters the lipid repertoire at the initial site of viral replication, the midgut of the mosquito. Since this study was carried out using a highly susceptible mosquito strain with a laboratory-adapted virus, it

highlights metabolic pathways that may be critical for achieving optimal levels of replication in the midgut required for successful dissemination and ultimately transmission. Given that vector competence for infection and transmission is dependent on the specific virus-vector pairing, it will be critical to evaluate the metabolic environment under conditions where the virus has a less robust infection rate, and/or the vector presents infection and transmission barriers. This is particularly important in field settings where vector competence is also influenced by environmental conditions, co-infecting pathogens and the microbiome of the vector. In addition, there is a growing body of evidence that metabolic competition between arboviruses and endosymbionts such as *Wolbachia* may form the basis of endosymbiont-mediated control of viral transmission. Therefore, exploring vector metabolism is a powerful and integrative means to identify metabolic control points that could be exploited to interfere with pathogen transmission or to implement vector control.

CHAPTER 3: VALIDATION OF A METABOLIC CONTROL HUB THAT CAN POTENTIALLY BE USED FOR INTERRUPTING DENGUE VIRUS SEROTYPE 2 INFECTION IN MOSQUITO CELLS[2]

INTRODUCTION

Sphingolipid (SP) is a class of eukaryotic lipids. Their molecular structure is composed of two key building blocks: (i) a long chain base that uses serine (or to a lesser extent alanine or glycine) as a backbone and (ii) a fatty acid chain [137]. The unique characteristic of this core feature, the variety of fatty acid chains that attach to the core and the modifiable head-group give rise to the diversity of SP molecular shapes and functions.

SPs play critical roles as both structural components of membranes and signaling molecules. Due to their unique chemical features, SPs can impact physical properties such as the curvature and the thickness of a membrane [200-202]. At the plasma membrane, SPs that associate with sterols can form lipid rafts which can control several membrane-associated processes such as membrane invagination, endocytosis and signal transduction [201-203]. SPs also serve important roles as signaling molecules for both intra- and extra-cellular signaling events. Homeostasis of SPs is critical for controlling cell proliferation, senescence, cell death, cell differentiation, cell migration and inflammation [151, 152]. SPs that are located on the extracellular surface of the plasma membrane can contribute to cell-cell communication and can also play a role in host-pathogen interactions [202, 204, 205].

Metabolism of SPs involves about 40 enzymes [151]. A simplified metabolic pathway is shown in Figure 3.1. Briefly, SPs are *de novo* synthesized from serine (or in some cases,

[2] Some parts of this chapter were published in Chotiwan N, Andre BG, Sanchez-Vargas I, Islam MN, Grabowski JM, Hopf-Jannasch A, et al. Dynamic remodeling of lipids coincides with dengue virus replication in the midgut of Aedes aegypti mosquitoes. PLoS Pathog. 2018;14(2):e1006853.

alanine or glycine) and palmitic acid (C16 fatty acid) by serine palmitoyltransferase (SPT). The product, 3-Ketosphinganine, is further converted to sphinganine and then dihydroceramide (DHCer). Saturated DHCer is then converted to ceramide (Cer) by sphingolipid Δ-4 desaturase (DEGS) enzyme. Cer is considered an important metabolite that acts as a hub of the SP pathway because it can be i) converted into sphingomyelin, an important SP for membrane composition, especially in lipid rafts, ii) attached to hexose sugars to form hexosylceramide, which is exported to the extracellular surface to function in cell-cell communication, iii) phosphorylated to function as a cell signaling molecule, Cer-1-P, and iv) converted to another important signaling molecule, sphingosine [152].

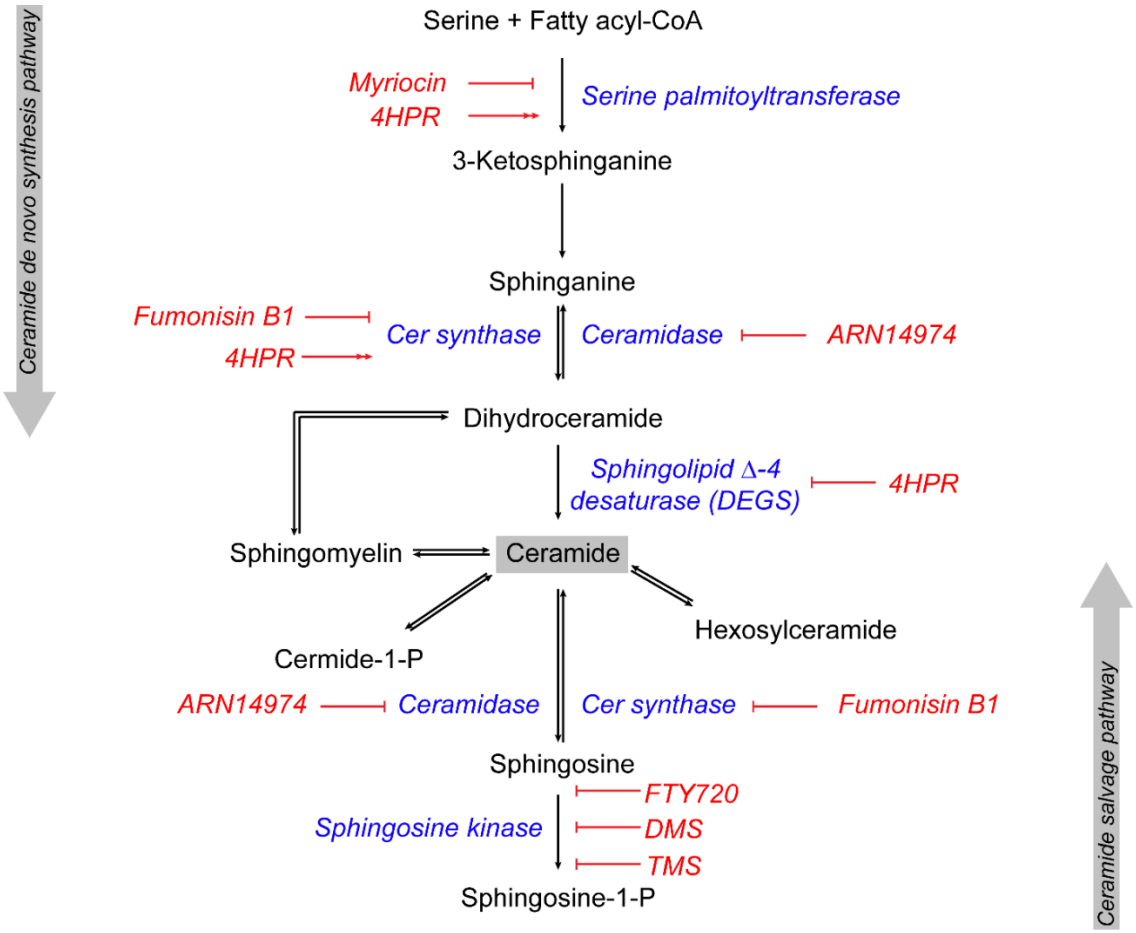

Figure 3.1. SP pathway and inhibitors. The schematic shows a simplified SP pathway. Lipids in the SP pathway are shown in black. Inhibitors used in this study are shown in red. Only enzymes that are involved in the steps affected by the inhibitors are listed in this schematic (blue). Activation of the enzymes by the drug is indicated as red double arrows and inhibition is

indicated as a red perpendicular line. Note that Cer *de novo* synthesis includes the steps from the conversion of serine and palmitic acid to the production of Cer via the DEGS enzyme. The Cer salvage pathway is involved in the production of Cer from sphingosine-1-P. Abbreviations: 4HPR, 4-Hydroxyphenyl retinamide; Cer synthase, ceramide synthase; DEGS, sphingolipid Δ-4 desaturase; DMS, *N, N*-dimethylsphingosine; SPT, serine palmitoyltransferase and TMS, *N, N, N*-trimethylsphingosine.

Our previous metabolomic study of *Aedes aegypti* (*Ae. aegypti*) mosquito midguts showed alterations of several SPs upon dengue virus serotype 2 (DENV2) infection (chapter 2, [61]). This includes sphinganine, sphingosine, Cer, glycerophospholipid-Cer, hexosylceramide and hexosylceramidesulfate. Most SPs were elevated in abundance during DENV2 infection. Sphinganine, sphingosine and Cer are the major SP metabolites in the Cer *de novo* synthesis and salvage pathways (Figure 3.1). Previous studies have shown that DENV replication was affected by the inhibition of Cer synthesis in mammalian cells [182, 206]. In this study, we investigated the role of SP metabolism, especially the metabolites in the Cer *de novo* synthesis and salvage pathways, in DENV2 replication in mosquito cells and mosquito vectors. Screening with SP inhibitors showed that DENV2 infection and replication are sensitive to the inhibition of DHCer to Cer conversion. Transient knockdown (KD) of DEGS using long double stranded RNA (dsRNA) caused an imbalance in the ratio of Cer to DHCer and reduced DENV2 replication in the cell. However, systemic DEGS-KD did not affect DENV2 infection or transmission in *Ae. aegypti* mosquitoes.

MATERIALS AND METHODS

Cells and viruses

Ae. aegypti (Aag2) cells were cultured in Schneider's insect medium (Sigma-Aldrich). *Ae. albopictus* (C6/36) cells were cultured in Minimum Essential Media (MEM). Both media were supplemented with 10% fetal bovine serum (FBS), 2 mM L-glutamine (GE Healthcare), and non-essential amino acids (GE Healthcare). Aag2 cells were maintained at 28^{o}C without CO_2 while

C6/36 cells were cultured at 28ºC with 5% CO_2. All FBS used in these studies were heat inactivated at 60ºC for 1 hour.

DENV2 strain Jamaica 1409 was used for infections in cell culture [119]. The virus was passaged by infecting C6/36 cells at multiplicity of infection (MOI) of 0.01. The infected cells were cultured in MEM supplemented with 2% FBS, 2 mM L-glutamine and non-essential amino acids for 8-10 days. DENV2 strain BC-17 (Merida, Mexico, GenBank #AY449677) gifted by Dr. William Black IV, was used for the infection in the *Ae. aegypti* mosquitoes [207]. The stock virus was passaged in Vero cells by infection at MOI of 0.01. The infected cells were cultured in Dulbecco's modified Eagle's medium (DMEM) supplemented with 2% FBS, 2 mM L-glutamine and non-essential amino acids. The infected cells were maintained at 37ºC with 5% CO_2.

Inhibitor studies in Aag2 and C6/36 cells

N-(4-hydroxyphenyl) retinamide (4HPR; Sigma-Aldrich), *N, N*-dimethylsphingosine (DMS; Enzo Life), *N, N, N*-trimethylsphingosine (TMS; Enzo Life), FTY720 (Sigma-Aldrich) and ARN14974 (Cayman Chemical) were solubilized in dimethyl sulfoxide (DMSO). Fumonisin B1 (Cayman Chemical) and Myriocin (Sigma Aldrich) were solubilized in methanol (MeOH) at the recommended concentration by the manufacturer. The inhibitors were diluted in the solvent to 100x concentration and were further diluted to 1x concentration in cell culture media. The final concentration of the solvent in all cell culture media was 1%.

Cells were pre-treated with inhibitors at the concentration designated in the figures for 24 hours prior to DENV2 infection. At 24 hours post treatment, cells were infected with DENV2. Medium was removed and virus inoculum (virus diluted in 1x phosphate buffered saline (PBS) containing 0.5 mM calcium chloride ($CaCl_2$) and1.2 mM magnesium chloride ($MgCl_2$)) was added to the cells at MOI of 0.3 for Aag2 and 0.1 for C6/36 cells. Absorption was allowed for 1 hour at room temperature. Following absorption, cells were overlaid with MEM containing 2%

FBS and fresh inhibitors or vehicle (control). Virus-containing supernatant was harvested at 24 hours post infection and titrated by plaque assay. Cell viability assays were performed on treated cells without DENV2 infection. Cell Titer-Glo Luminescent Cell Viability Assay (Promega) was used for the assay in Aag2 and Resazurin (Sigma Aldrich) was used for the assay in C6/36 cells.

Plaque assay

Plaque titration was performed on confluent BHK-15 cells. Virus supernatant was serially diluted 10-fold in 1x PBS containing 0.5 mM $CaCl_2$ and 1.2 mM $MgCl_2$ for 3 to 6 dilutions and was inoculated at 250 µl onto a cell layer grown in 6-well plate. Absorption was allowed for 1 hour at room temperature. During absorption, 2x LE Quick Dissolve Agarose (Genemate) was heated to dissolve in miliQ water and was placed in a 55^{o}C water bath. At the same time, 2x Minimum Essential Media (MEM), supplemented with 2.5% FBS, 50 µg/ml Penicillin/Streptomycin, 50 µg/ml Gentamycin, and 2.5 µg/ml Amphotericin B) was made and placed in a 37^{o}C water bath. After absorption for 45 minutes, 2x agar and 2x media were mix at an equal volumes to make 1x medium-agar overlay. The overlay was placed in a 42^{o}C water bath for at least 15 minutes before being added to the cell layer (3 ml). The overlay was allowed to set, and the cells were incubated at 37^{o}C with 5% CO_2. On day 2 post infection, 1 ml of 1X MEM supplemented with 10% FBS was added onto the agar overlay to prevent cells from drying. Cells were stained with 0.033% neutral red (Sigma) in 1x PBS on day 5 post infection. Viral titers were calculated to plaque forming units per milliliter.

Quantitative RT-PCR detection of intracellular DENV2 RNA in infected cells

At 24 hours post infection, medium was removed, cells were washed with 1x PBS extensively and TRIzol reagent (Life Technologies) was added to the infected cells. Total RNA was extracted according to the manufacturer's protocol. Quantitative reverse transcription

polymerase chain reaction (q RT-PCR) was performed in LightCycler 96 (Roche) and analyzed in LightCycler96 software. The detailed protocol for qRT-PCR was described in the materials and methods section in Chapter 2.

Quantification of SPs in Aag2 cells by multiple reaction monitoring (MRM)

SPs were extracted from Aag2 cells following the protocol published by Merrill et. al., [208]. Briefly, cells were trypsinized and washed twice in PBS. Equal cell numbers between treated and control samples were collected. Cer/Sph mixture I Internal standard (Avanti Polar Lipids) was premixed with chloroform used for extraction. The final concentration of the internal standard was at 2 nM. Metabolite extraction was performed as described below. Extracted metabolites were dried using nitrogen gas.

An Agilent 1200 Rapid Resolution liquid chromatography (LC) system coupled to an Agilent 6460 series QQQ mass spectrometer (MS) was used to analyze SPs in each sample according to Merrill et al., 2005 with some modifications [208]. A Waters Xbridge C18 2.1mm x 100mm, 3.5 µm column was used for all LC separations (Waters Corp. Milford, MA). The buffers were (A) MeOH/water/formic acid (74/25/1 v/v) + 5mM ammonium formate and (B) MeOH/formic acid (99/1 v/v) + 5mM ammonium formate for all analyses. All extracted, dried samples were reconstituted in 200 µl of 80/20 buffer A/B just prior to analysis and 10 µl was injected for each analysis. All data were analyzed with Agilent MassHunter Quantitative Analysis (Version B.06.00).

Analysis of free sphingoid bases and 1-phosphate species

The linear LC gradient was as follows: time 0 minutes, 0 % B; time 1 minute, 0 % B; time 10 minutes, 100 % B; time 10.5 minutes, 100 % B; time 11 minutes, 0 % B; time 15 minutes, 0 % B. The flow rate was 0.3 mL/min. MRM was used for MS analysis. The data were acquired in positive electrospray ionization (ESI) mode according to Table 3.1. The jet stream ESI

interface had a gas temperature of 325°C, gas flow rate of 8 L/minute, nebulizer pressure of 45 psi, sheath gas temperature of 250°C, sheath gas flow rate of 7 L/minute, capillary voltage of 4000 V in positive mode, and nozzle voltage of 1000 V. The ΔEMV voltage was 500.

Table 3.1. MRM table for data acquisition of free sphingoid bases and 1-phosphates (according to Merrill et al., 2005 [208])

Compound	Precursor (*m/z*)	Product (*m/z*)	Collision Energy (V)
d17:0	288.3	252.3	12
d18:1	300.3	264.3	12
d18:0	302.3	266.3	12
t18:0	318.3	282.3	12
d20:1	328.4	292.3	12
d20:0	330.3	294.3	12
d17:1-P	366.4	250.3	12
d17:0-P	368.4	252.3	12
d18:1-P	380.4	264.3	12
d18:0-P	382.4	266.3	12
d20:1-P	408.4	292.3	12
d20:0-P	410.4	294.3	12
d17:1	286.3	250.3	12
DMS	328.4	310.3	15
TMS	342.4	60.2	20

Analysis of ceramide (16 and 18 carbon sphingoid-backbone) species

Isocratic conditions of 100% B buffer for 30 minutes were used for the analysis. The flow rate was 0.3 mL/minute. MRM was used for MS analysis. The data were acquired in positive ESI mode according to Table 3.2. The jet stream ESI interface had a gas temperature of 325°C, gas flow rate of 8 L/minute, nebulizer pressure of 45 psi, sheath gas temperature of 250°C, sheath gas flow rate of 7 L/minute, capillary voltage of 4000 V in positive mode, and nozzle voltage of 1000 V. The ΔEMV voltage was 400.

Table 3.2. MRM table for data acquisition of Cer and DHCer ([208]) and 16 carbon sphingoid-backbone Cer and DHCer (modified from Merrill et al., 2005 [208])

Compound	Precursor (*m/z*)	Product (*m/z*)	Collision Energy (V)
d16:0/16:0	512.5	238.3	20
d16:0/16:1	510.5	238.3	20
d16:0/18:0	540.5	238.3	20
d16:0/18:1	538.5	238.3	20
d16:0/18:2	536.5	238.3	20
d16:0/20:0	568.6	238.3	20
d16:0/22:0	596.6	238.3	20
d16:0/24:0	624.6	238.3	20
d16:0/24:1	622.6	238.3	20
d16:0/26:0	652.7	238.3	20
d16:0/26:1	650.6	238.3	20
d16:1/16:0	510.5	236.3	20
d16:1/16:1	508.5	236.3	20
d16:1/18:0	538.5	236.3	20
d16:1/18:1	536.5	236.3	20
d16:1/18:2	534.5	236.3	20
d16:1/20:0	566.5	236.3	20
d16:1/22:0	594.5	236.3	20
d16:1/24:0	622.6	236.3	20
d16:1/24:1	620.6	236.3	20
d16:1/26:0	650.6	236.3	20
d16:1/26:1	648.6	236.3	20
d18:0/12:0	482.6	264.3	20
d18:0/16:0	540.7	266.3	20
d18:0/18:0	568.7	266.3	20
d18:0/20:0	596.7	266.3	20
d18:0/22:0	624.8	266.3	20
d18:0/24:0	652.9	266.3	20
d18:0/24:1	650.9	266.3	20
d18:0/26:0	678.9	264.3	20
d18:0/26:0	680.9	266.3	20
d18:0/26:1	678.9	266.3	20
d18:1/16:0	538.7	264.3	20
d18:1/18:0	566.7	264.3	20
d18:1/20:0	594.7	264.3	20

(cont.)

Compound	Precursor (*m/z*)	Product (*m/z*)	Collision Energy (V)
d18:1/22:0	622.8	264.3	20
d18:1/24:0	650.9	264.3	20
d18:1/24:1	648.9	264.3	20
d18:1/25:0	664.7	264.3	20
d18:1/25:0	664.7	264.3	20
d18:1/26:1	676.9	264.3	20

Analysis of sphingomyelin species

The linear LC gradient was as follows: time 0 minutes, 20 % B; time 1 minute, 20 % B; time 10 minutes, 100 % B; time 20 minutes, 100 % B; time 22 minutes, 20 % B; time 30 minutes, 20 % B. The flow rate was 0.3 mL/minute. MRM was used for MS analysis. The data were acquired in positive ESI mode according to Table 3.3. The jet stream ESI interface had a gas temperature of 325°C, gas flow rate of 8 L/minute, nebulizer pressure of 45 psi, sheath gas temperature of 250°C, sheath gas flow rate of 7 L/minute, capillary voltage of 4000 V in positive mode, and nozzle voltage of 1000 V. The ΔEMV voltage was 400.

Table 3.3. MRM table for data acquisition of sphingomyelins (according to Merrill et al., 2005 [208])

Compound	Precursor (*m/z*)	Product (*m/z*)	Collision Energy (V)
d18:1/16:0	703.8	184.4	20
d18:0/16:0	705.8	184.4	20
d18:1/18:0	731.8	184.4	20
d18:0/18:0	733.8	184.4	20
d18:1/20:0	759.8	184.4	20
d18:0/20:0	761.8	184.4	20
d18:1/22:0	787.9	184.4	20
d18:0/22:0	789.9	184.4	20
d18:1/24:1	813.9	184.4	20
d18:0/24:1	815.9	184.4	20
d18:1/24:0	815.9	184.4	20
d18:0/24:0	817.9	184.4	20

(cont.)

Compound	Precursor (*m/z*)	Product (*m/z*)	Collision Energy (V)
d18:1/26:1	841.9	184.4	20
d18:0/26:1	843.9	184.4	20
d18:1/26:0	843.9	184.4	20
d18:0/26:0	845.9	184.4	20
d18:1/12:0	647.7	184.4	20

Generating long double-stranded RNA for mosquito gene expression knockdown by RNA interference

Long double-stranded RNA (dsRNA) was reverse transcribed and amplified from *Ae aegypti* mosquito total RNA. Briefly, total RNA was extracted from a whole mosquito homogenized in TRIzol reagent (Ambion). Primers were designed to amplify a region of ~ 500 base pairs of the gene of interest and a T7 promotor sequence was added to the 5' end of both forward and reverse primers (Table 3.4). Reverse transcription reaction (RT) and polymerase chain reaction (PCR) were performed in two-steps using SuperScript III Reverse Transcriptase (Invitrogen) and *Taq* polymerase (NEB) respectively. PCR products were purified using the GeneJET PCR Purification kit (Thermo Scientific) and subjected to *in vitro* transcription using the MEGAscript T7 kit (Invitrogen) according to the manufacturer's protocol. The reactions were incubated at 37^{o}C for 12 hours. The transcribed products were then heated to 75^{o}C for 5 minutes and cooled down at room temperature for 4 hours to allow dsRNA to anneal. The products were then treated with DNase to get rid of the DNA template and purified by phenol-chloroform followed by ethanol precipitation. The purified dsRNAs were stored at -80^{o}C for future use.

Table 3.4. Gene-specific primers for dsRNA transcript against DEGS gene

Primer name	Sequence (5' to 3')*	Target gene
DEGS-dsRNA_F	ATACAGATTTGCCAACGCTG	*Ae aegypti* DEGS (VB: AAEL012801)
DEGS-dsRNA_R	GCTTCGGATTTACGATCAGC	*Ae aegypti* DEGS (VB: AAEL012801)
GFP-dsRNA_F	GACCACATGAAGCAGCACGA	eGFP
GFP-dsRNA_R	CGCTTCTCGTTGGGGTCTTT	eGFP
DENV2-dsRNA_F	ACGGAGAACCACACATGATCG	DENV2 (NCBI: U87411.1)
DENV2-dsRNA_R	CTCCTGAAACCCCTTCCACAA	DENV2 (NCBI: U87411.1)

* T7 promotor sequence (5' GAATTAATACGACTCACTATAGGGAGA 3') was added to the 5' end of all primers to make dsRNA
VB, VectorBase accession number; NCBI, NCBI accession number

Double stranded RNA knockdown of genes in Aag2 cells

Aag2 cells were cultured in Schneider's insect medium (Sigma-Aldrich) supplemented with 2 mM L-glutamine, non-essential amino acids, and 10% FBS. To perform dsRNA KD in Aag2 cells, the cells were seeded in a 48-well plate at 50,000 cells/well. Twenty-four hours later, the cells were transfected with 260 ng of dsRNA mixed with TransIT-2020 Reagent (Mirus) following the manufacturer's protocol. New medium with 2% FBS was replaced at 6 hours post transfection. Cell viability assays were performed at 2 days post transfection using the CellTiter-Glo Luminescent Cell Viability Assay (Promega). KD cells were infected with DENV2 at MOI of 0.3 using the same methods as described in the "Inhibitor studies in Aag2 and C6/36 cells" section above. Quantification of infectious DENV2 by plaque assay and absolute quantification of intracellular DENV2 genome replication was described in the "Inhibitor studies in Aag2 and C6/36 cells" and "Quantitative RT-PCR detection of intracellular DENV2 RNA in the infected cells" sections above.

Quantifying mosquito gene expression upon dsRNA knockdown

Cells were collected in 200 µl TRIzol reagent at two days post dsRNA transfection. RNA extraction was performed following the manufacture's protocol. Total RNA (500 ng) was subjected to RT using random primers (Invitrogen). The cDNA was amplified by specific primers and quantified by quantitative PCR (qPCR) using PowerUp SYBR Green Master Mix (Applied biosystems). Primer sequences designed to quantify DEGS and actin (internal control) genes are shown in Table 3.5. Comparative Ct method ($\Delta\Delta$Ct) was used for calculating percent gene expression of the target gene compared to the GFP KD control [209].

Table 3.5. Primers for detecting gene expression levels following RNAi knockdown

Primer name	Sequence (5' to 3')
DEGS-qPCR_F	ATACAGATTTGCCAACGCTG
DEGS-qPCR_R	GCTTCGGATTTACGATCAGC
Actin-qPCR_F	GAATGTGCAAGGCCGGATTC
Actin-qPCR_R	GCTCGATCGGGTACTTCAGG

Intrathoracic injection of dsRNA into mosquitoes

Ae. aegypti were collected from the field in Poza Rica, Mexico [210]. Adult females were subjected to intrathoracic (IT) injection at the age of 3 to 4-days post eclosion as described previously [211]. Briefly, mosquitoes were cold anesthetized and were kept on ice during injection. Glass needles were prepared with a vertical pipette puller (P-30, Sutter Instrument Co., Novato, CA). Mosquitoes were IT injected with 3 µg/µl of dsRNA at an injection volume of 69 nl twice (total of ~400 ng of dsRNA) using a Nanoject II (Drummond Scientific Company, Broomall, PA). Injected mosquitoes were fed on 10% sucrose solution or blood and reared at 28°C, 80% relative humidity up to 17 days post injection.

Mosquito dissection and plaque titration

Mosquito saliva and tissues were collected on different days as indicated in the figure legends. As described by Rückert et. al. [212], dissected midguts or the rest of the body without midgut ('carcass') were placed individually in 2 ml safe-lock Eppendorf tubes (Eppendorf) that contain 250 µl of mosquito diluent (1 × PBS supplemented with 20% FBS, 50 µg/ml Penicillin/Streptomycin (Gibco), 50 µg/ml Gentamycin (Gibco), and 2.5 µg/ml Amphotericin B (Gibco)) and a stainless-steel bead. Tissues were homogenized using a Retsch Mixer Mill MM400 at 24 cycles per second for 1 minute and centrifuged at 15,000g for 5 minutes at 4°C. Supernatant was transferred to a new tube and used for plaque titration.

To collect saliva, mosquitoes were cold-anesthetized. Wings and legs were removed from the mosquito and the proboscis of the mosquito was inserted into a capillary tube filled with immersion oil. Salivation was allowed for 20 minutes. Capillary tubes were checked under the microscope for the presence of the saliva. The end of the capillary tubes containing saliva were broken off into a microcentrifuge tube containing 100 µl of mosquito diluent. The tubes were then centrifuged at 15,000g for 5 minutes [212]. Supernatant was used for plaque titration.

RESULTS

DENV2 infection and RNA genome replication were affected by treatment with SP inhibitors

To determine which steps in the SP pathway may play important roles in DENV2 infection, we performed a screen for the effect of several inhibitors of various steps in the SP pathway on DENV2 infection in Aag2 and C6/36 cell lines (Figure 3.2). The results were similar between treatments in both cell lines (Figure 3.2, upper panels). Treatment with these inhibitors using the designated concentrations had more than 80% cell viability compared to the vehicle control (Figure 3.2, lower panels). 4-Hydroxyphenyl retinamide (4HPR) or fenretinide is a

synthetic retinoid that alters ceramide homeostasis [206]. It activates SPT and Cer synthase but inhibits DEGS enzyme in the Cer *de novo* synthesis pathway (Figure 1). 4HPR treatment showed the most significant inhibitory effect on DENV2 infection in both C6/36 and Aag2 cells without causing cytotoxicity, especially in C6/36 cells at 3.75 µM (Figure 3.2A-B). DMS and TMS are sphingosine analogues. DMS is a naturally occurring metabolite that inhibits sphingosine kinase and increases the level of ceramide via the ceramide salvage pathway (Figure 3.1) [213]. DMS had minimal inhibitory effects on DENV2 infection in C6/36 and Aag2 cells, while TMS also had minimal inhibitory effect on DENV2 infection in C6/36 cells (Figure 3.2C-F). FTY720 is a fungal metabolite that is also a sphingosine analogue. It is an FDA approved immunosuppressive drug for treating multiple sclerosis [214]. FTY720 functions in inhibiting sphingosine kinase and is also a potent antagonist of the sphigosine-1-phosphate (S1P) receptors (Figure 3.1) [215]. FTY720 showed only small inhibitory effects on DENV2 infection in Aag2 cells (Figure 3.2G-H). Fumonisin B1 is also a fungal metabolite. It functions as an inhibitor of Cer synthase which causes the accumulation of both sphinganine (ceramide *de novo* synthesis pathway) and sphingosine (a conversion of sphingosine to ceramide in the salvage pathway) (Figure 3.1) [216]. Interestingly, Fumonisin B1 slightly inhibited DENV2 infection at a low concentration (6.25 µM) but the inhibitory effect was dampened at higher concentrations (12.5 and 25 µM) in C6/36 cells (Figure 3.2I). ARN14974 is a benzoxazolone carboxamide compound that is a ceramidase inhibitor (Figure 3.1) [217]. In mosquito cells, ARN14974 showed no effects to DENV2 infection in both cell types (Figure 3.2K and L).

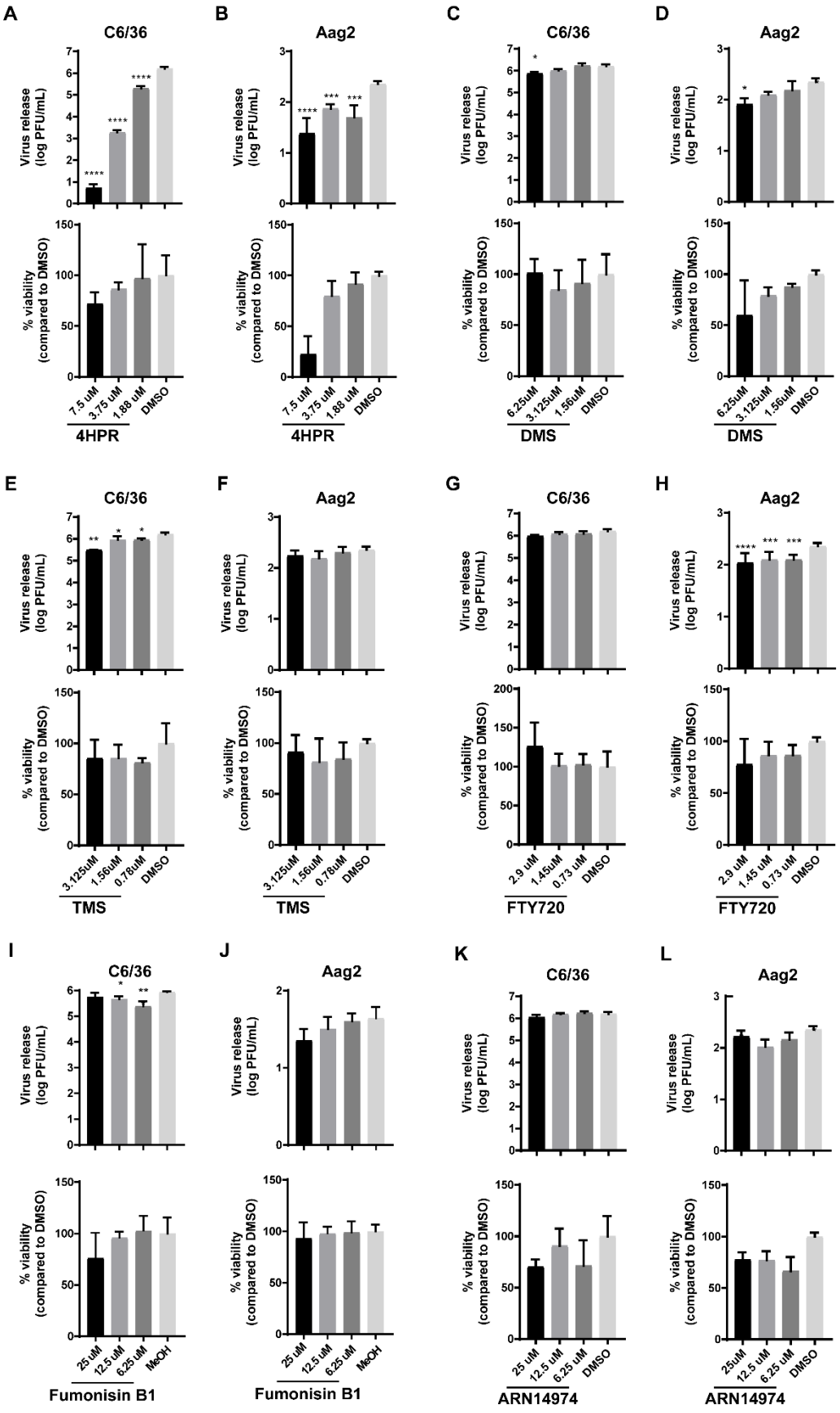
A
C6/36
Virus release (log PFU/mL)
% viability (compared to DMSO)
7.5 uM
3.75 uM
1.88 uM
DMSO
4HPR
B
Aag2
Virus release (log PFU/mL)
% viability (compared to DMSO)
7.5 uM
3.75 uM
1.88 uM
DMSO
4HPR
C
C6/36
Virus release (log PFU/mL)
% viability (compared to DMSO)
6.25uM
3.125uM
1.56uM
DMSO
DMS
D
Aag2
Virus release (log PFU/mL)
% viability (compared to DMSO)
6.25uM
3.125uM
1.56uM
DMSO
DMS
E
C6/36
Virus release (log PFU/mL)
% viability (compared to DMSO)
3.125uM
1.56uM
0.78uM
DMSO
TMS
F
Aag2
Virus release (log PFU/mL)
% viability (compared to DMSO)
3.125uM
1.56uM
0.78uM
DMSO
TMS
G
C6/36
Virus release (log PFU/mL)
% viability (compared to DMSO)
2.9 uM
1.45uM
0.73 uM
DMSO
FTY720
H
Aag2
Virus release (log PFU/mL)
% viability (compared to DMSO)
2.9 uM
1.45 uM
0.73 uM
DMSO
FTY720
I
C6/36
Virus release (log PFU/mL)
% viability (compared to DMSO)
25 uM
12.5 uM
6.25 uM
MeOH
Fumonisin B1
J
Aag2
Virus release (log PFU/mL)
% viability (compared to DMSO)
25 uM
12.5 uM
6.25 uM
MeOH
Fumonisin B1
K
C6/36
Virus release (log PFU/mL)
% viability (compared to DMSO)
25 uM
12.5 uM
6.25 uM
DMSO
ARN14974
L
Aag2
Virus release (log PFU/mL)
% viability (compared to DMSO)
25uM
12.5 uM
6.25 uM
DMSO
ARN14974

Figure 3.2. The effect of SP inhibitors on DENV2 infection in mosquito cells. (A-L upper panels) C6/36 and Aag2 Cells were pre-treated with inhibitors for 24 hours prior to virus infection. The inhibitors were dissolved in the solvent (DMSO or MeOH) and diluted in the cell culture medium at the final concentration indicated in the graphs. All treatments contain a final concentration of 1% solvent. After 24 hours of pre-treatment, cells were infected with DENV2 at MOI of 0.1 and 0.3 for C6/36 and Aag2 cells, respectively. Fresh inhibitors were added to the medium overlay. The virus was allowed to replicate for 24 hours before the supernatant was harvested and the titer was measured by plaque assay. (A-L lower panels) Cell viability was measured upon inhibitor treatments. Cells were treated with the inhibitors the same ways as the upper panel, but cells were not infected with DENV2. Cell viability was measured using Resazurin in C6/36 cells (A, C, E, G, I and K lower panels) and Cell Titer Glo in Aag2 cells (B, D, F, H, J and L lower panels). Viability of the vehicle control (DMSO or MeOH) was set at 100%.

Next, we wanted to investigate if the inhibitors reduced virus release by inhibiting viral genome replication. Intracellular DENV2 RNA genome copy numbers from the inhibitor treated cells were compared to the vehicle-only treated cells (Figure 3.3). In C6/36 cells (Figure 3.3A and B), we observed a reduction of intracellular DENV2 genome copies upon 4HPR (3.125 µM), DMS (6.25 µM) and TMS (3.125 µM) treatment. This was consistent with the reduction of infectious virus release observed by plaque titration in Figures 3.2A, C and E. The decreased in DENV2 genome replication was not observed in C6/36 cells treated with Fumonisin B1, suggesting that the inhibitory effect of Fumonisin B1 may act on DENV2 at steps post RNA genome replication.

In Aag2 cells, we only observed a reduction in DENV2 genome replication when cells were treated with 4HPR with about a log reduction (Figure 3.3 C). Slight, but not significant reduction in genome replication was observed in DMS treated Aag2 cells (Figure 3.3C). Interestingly, we did not observe a reduction of DENV2 replication in C6/36 or Aag2 cells treated with myriocin suggesting SPT, the rate limiting step of the Cer *de novo* synthesis pathway, may not play an important role in DENV2 infection in mosquito cells (Figure 3.3D).

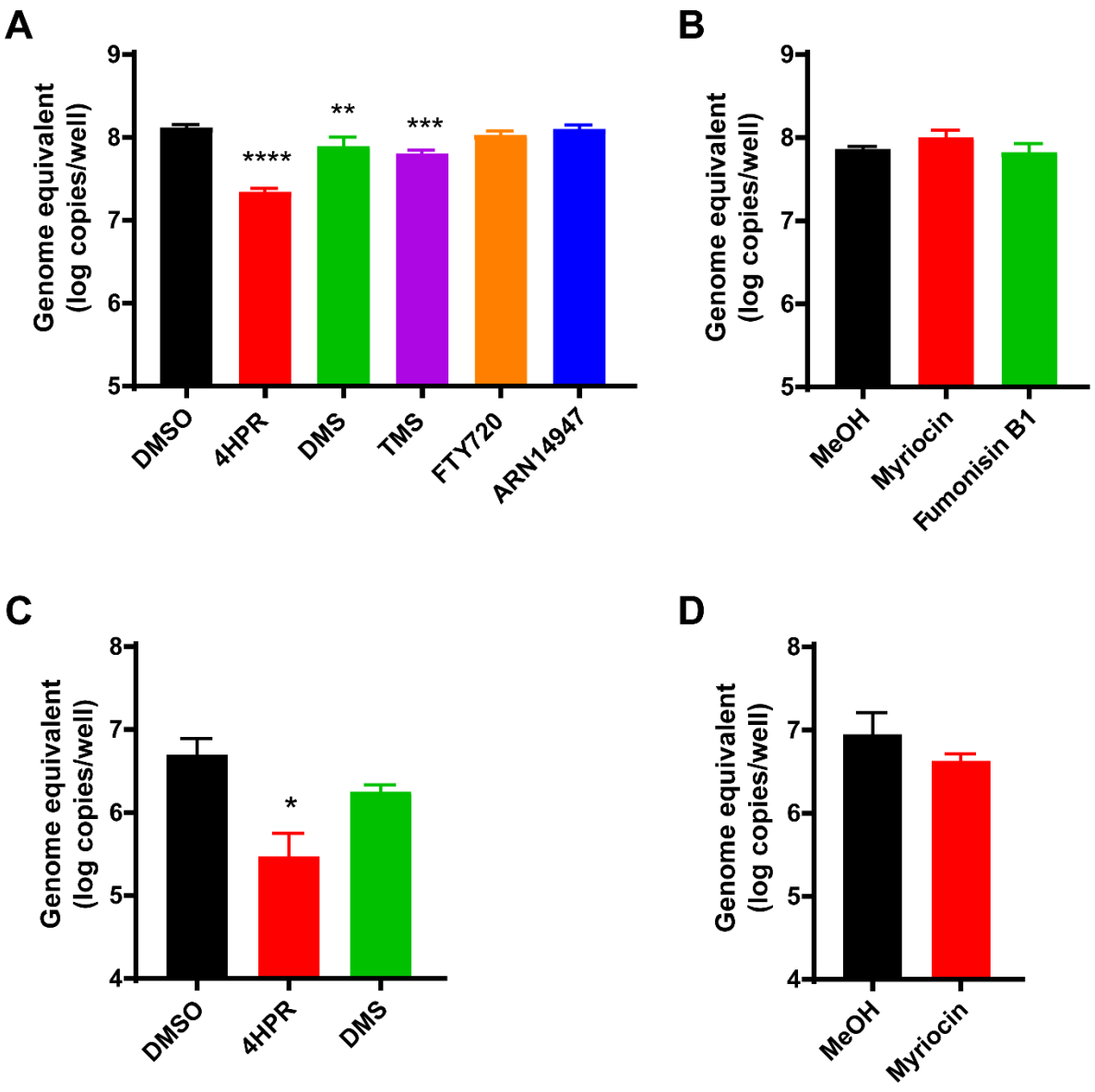

Figure 3.3. **DENV2 RNA genome replication was affected by treatment with SP pathway inhibitors.** (A-B) C6/36 and (C-D) Aag2 cells were pretreated with the inhibitors for 24 hours followed by DENV2 infection at MOI of 0.1 and 0.3, respectively. The infected cells were harvested at 24 hours post infection. Total RNA was extracted and DENV2 genome copy numbers were measured by qRT-PCR. The final concentration of inhibitors in cell culture media are listed accordingly: A. 4HPR 3.125 µM, DMS 6.25 µM, TMS 3.125 µM, FTY720 3.125 µM and ARN14974 12.5 µM; B. Myriocin 12.5 µM and Fumonisin B1 12.5 µM; C. 4HPR 3.125 µM and DMS 3.125 µM; D. Myriocin 12.5 µM. Statistical analysis was performed using one-way ANOVA followed by Dunnet's multiple comparison test. *, $p < 0.05$; **, $p < 0.01$; ***, $p < 0.005$ and ****, $p < 0.001$

Changes in the Cer-DHCer ratio impair DENV2 infection in mosquito cells

Since we observed the most pronounced inhibition of DENV2 genome replication and infectious particle release from 4HPR treated cells (Figure 3.2A-B and 3.3), we further investigated the inhibitory mechanism of this control point. The metabolic impact of 4HPR on sphingolipid metabolism was validated using MRM LC-MS/MS (Figure 3.4). We observed accumulation of Cer(d18:1/16:0), Cer(d18:1/18:0), Cer(d18:1/24:1), and Cer(d18:1/26:1) and DHCer(d18:0/18:0) in cells following 4HPR treatment (Figure 3.4A, lower). However, their accumulation did not alter the Cer/DHCer ratios (Figure 3.4A, upper). None of the levels of the long chain sphingoid bases, Cer and DHCer with 16-carbon backbones were affected (Figure 3.4B). We also did not see changes in sphingosine (d18:1), sphingosine-1-P (d18:1-P), sphinganine (d18:0) or SM levels following 4HPR treatment. This is expected as the enzymes that produce these molecules are not the primary targets of 4HPR (Figure 3.4 C and D). In addition, this result also seemed to indicate that there is no compensation of Cer and DHCer through the conversion from sphingomyelin by sphingomyelinase (Figure 3.1)

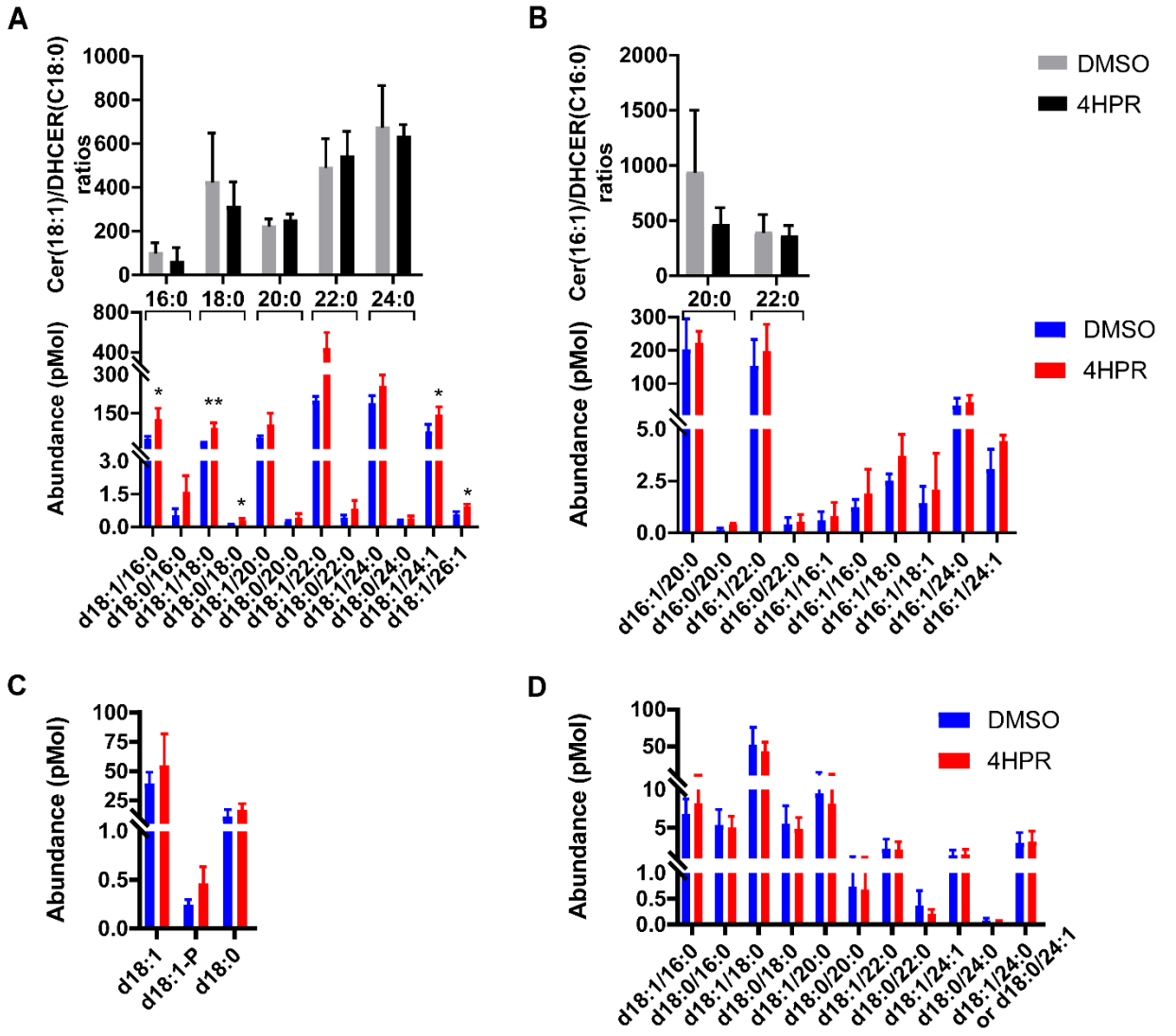

Figure 3.4. 4HPR treatment resulted in increased accumulation of both Cer and DHCer but did not alter the Cer/DHCer ratios. MRM profiling of SPs in 4HPR or DMSO treated Aag2 cells (N=3). The cells were treated with 3.75 µM 4HPR or DMSO. Medium with fresh 4HPR or DMSO was replaced at 24 hours after treatment (to mimic the 4HPR treatment of DENV2-infected cells) and cells were harvested at 24 hours post medium changed. SPs that were profiled are as follows: (A, lower panel) Cer(d18:1/xx:x) and DHCer(d18:0/xx:x) with 18-carbon long chain sphingoid bases, (B, lower panel) Cer(d16:1/xx:x) and DHCer(d16:0/xx:x) with 16-carbon long chain sphingoid bases, (C) sphingosine (d18:1), sphingosine-1-phosphate (d18:1-P) and sphinganine (d18:0), (D) sphingomyelin. (A and B, upper panel) show Cer/DHCer ratios of Cer and DHCer species with the same fatty acyl chain length. These ratios demonstrated that Cer/DHCer ratios were not altered by 4HPR treatment. Student's t-test was applied to compare the differences upon 4HPR treatment to DMSO control. *, $p < 0.05$; **, $p < 0.01$

To validate that the reduction of DENV2 genome replication was caused by the loss of SP metabolites or Cer/DHCer imbalance and not due to off-target effects of the inhibitor, the expression of DEGS, the target enzyme of 4HPR, in Aag2 cells was transiently knocked down by RNA interference, using long dsRNA (Figure 3.5A-D). In DEGS KD (DEGS-KD) cells, DENV2 titer and genome replication were significantly reduced compared to the GFP dsRNA (GFP-KD) negative control but were similar to the DENV2 dsRNA (DENV-KD) positive control (Figure 3.5A and B). SP metabolic profiling of the DEGS-KD cells compared to GFP-KD cells revealed striking reduction of Cer(d18:1/18:0), DHCer(d18:0/20:0) and DHCer(d18:0/22:0) after DEGS-KD (Figure 3.5E and F, lower panel). Interestingly, DEGS-KD also greatly altered the Cer/DHCer ratio for molecules with 18- and 16-carbon long chain sphingoid bases, especially those with very long fatty acyl chain lengths (20:0 – 24:0) (Figure 3.5E and F, upper panel). These results indicated that perturbation of the Cer-DHCer balance reduced both DENV2 genome replication and infectious virus formation. As expected we did not see changes in sphingosine (d18:1), sphingosine-1-P (d18:1-P), sphinganine (d18:0) or SM levels during dsRNA treatment (Figure 3.5G and H).

When DENV2-infected and uninfected Aag2 cells were compared for alterations in the SP pathway, we observed a significant increase in the abundance of Cer(d18:1/20:0) and Cer(d18:1/24:1) and DHCer(d18:0/22:0) in infected cells, but a decrease in Cer(d16:1/16:1) in infected cells (Figure 3.6A and B, lower). These changes did not, however, affect the Cer/DHCer ratios for very long fatty acyl chain containing molecules (Figure 3.6A and B, upper). We did not see changes in sphingosine (d18:1), sphingosine-1-P (d18:1-P), sphinganine (d18:0) or SM levels during dsRNA treatment (Figure 3.6C and D).

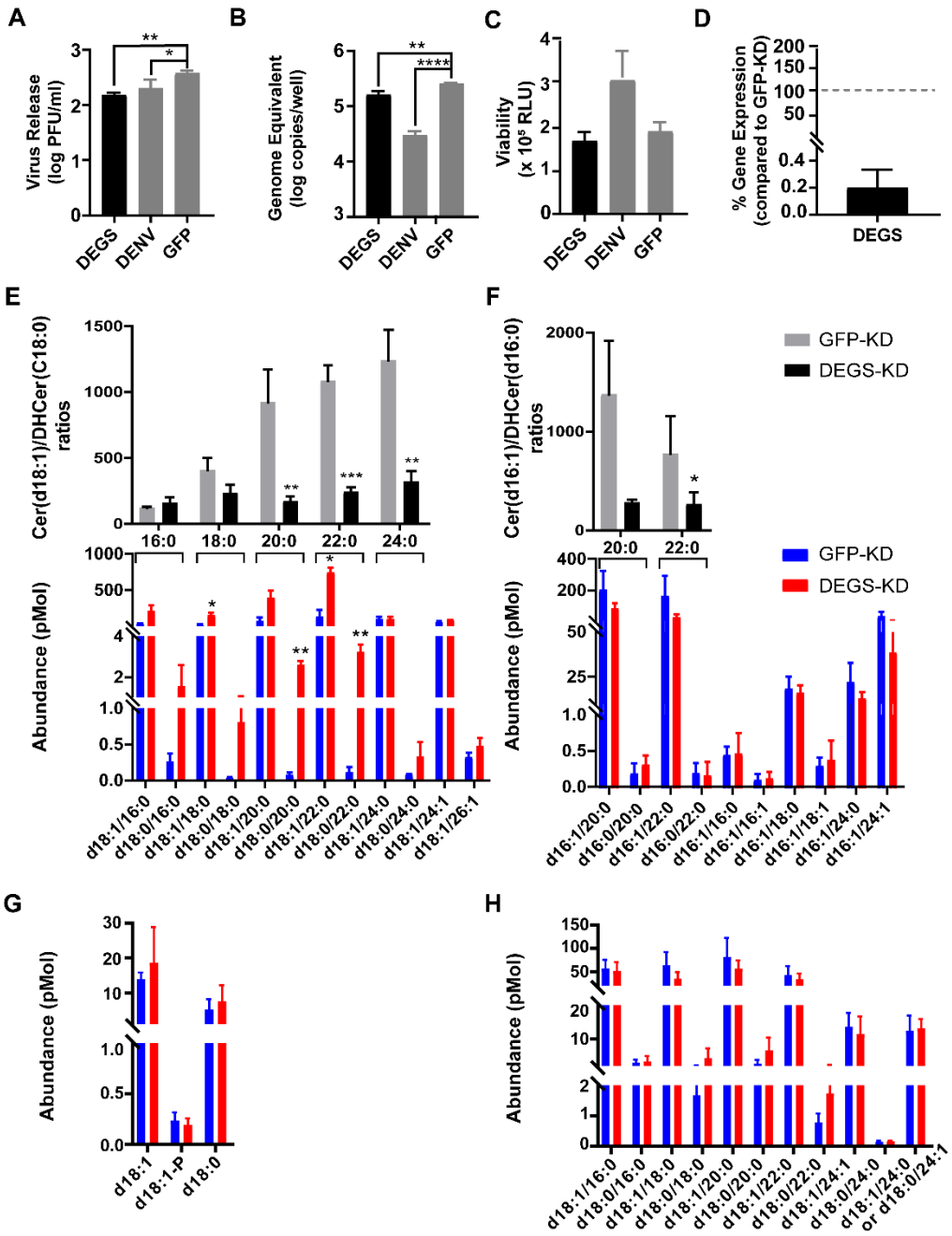

Figure 3.5. **Changes in the Cer-DHCer balance impair DENV2 infection in Aag2 cells.** (A and B) Aag2 cells were transfected with dsRNA derived from DEGS gene (VectorBase: AAEL013047, NCBI:LOC5577178), DENV2 RNA (positive control) or GFP (negative control) genes. Two days post transfection, cells were infected with DENV2 at 0.3 MOI. Cell culture supernatant (A) or intracellular total RNA (B) were collected at 24 hours post infection (hpi) and analyzed for infectious virus in medium and intracellular DENV2 RNA, respectively. One-way ANOVA followed by Dunnett's multiple comparisons test were used for statistical analysis. (C) Viability of Aag2 cells after dsRNA treatments at 48 hours post dsRNA transfection. (D) DEGS mRNA expression in DEGS-KD cells compared to the expression of the DEGS mRNA in GFP-KD cells (set at a 100%). (E and F) Analysis of Cer and DHCer species in DEGS-KD (red) and

GFP-KD cells (blue) using LC-MS/MS MRM (N=3). (E) and (F) show Cer and DHCer molecules with 18- and 16-carbon long chain sphingoid bases, respectively. Lower panels show the abundance of individual species of Cer(d18:1/xx:x or d16:1/xx:x) or DHCer(d18:0/xx:x or d16:0/xx:x) where xx:x refers to the fatty acyl chain attached to each sphingoid head group. The upper panels show the ratio of Cer/DHCer species with the same fatty acyl chain lengths. These ratios highlight the Cer-DHCer imbalance caused by manipulation of DEGS gene expression. (G) Abundance of sphingosine (d18:1), sphingosine-1-phosphate (d18:1-P) and sphinganine (d18:0) and (H) sphingomyelins upon DEGS-KD was compared to GFP-KD control. Student's t-test was applied for statistical analysis. *, $p < 0.05$; **, $p < 0.01$; ***, $p < 0.005$ and ****, $p < 0.001$

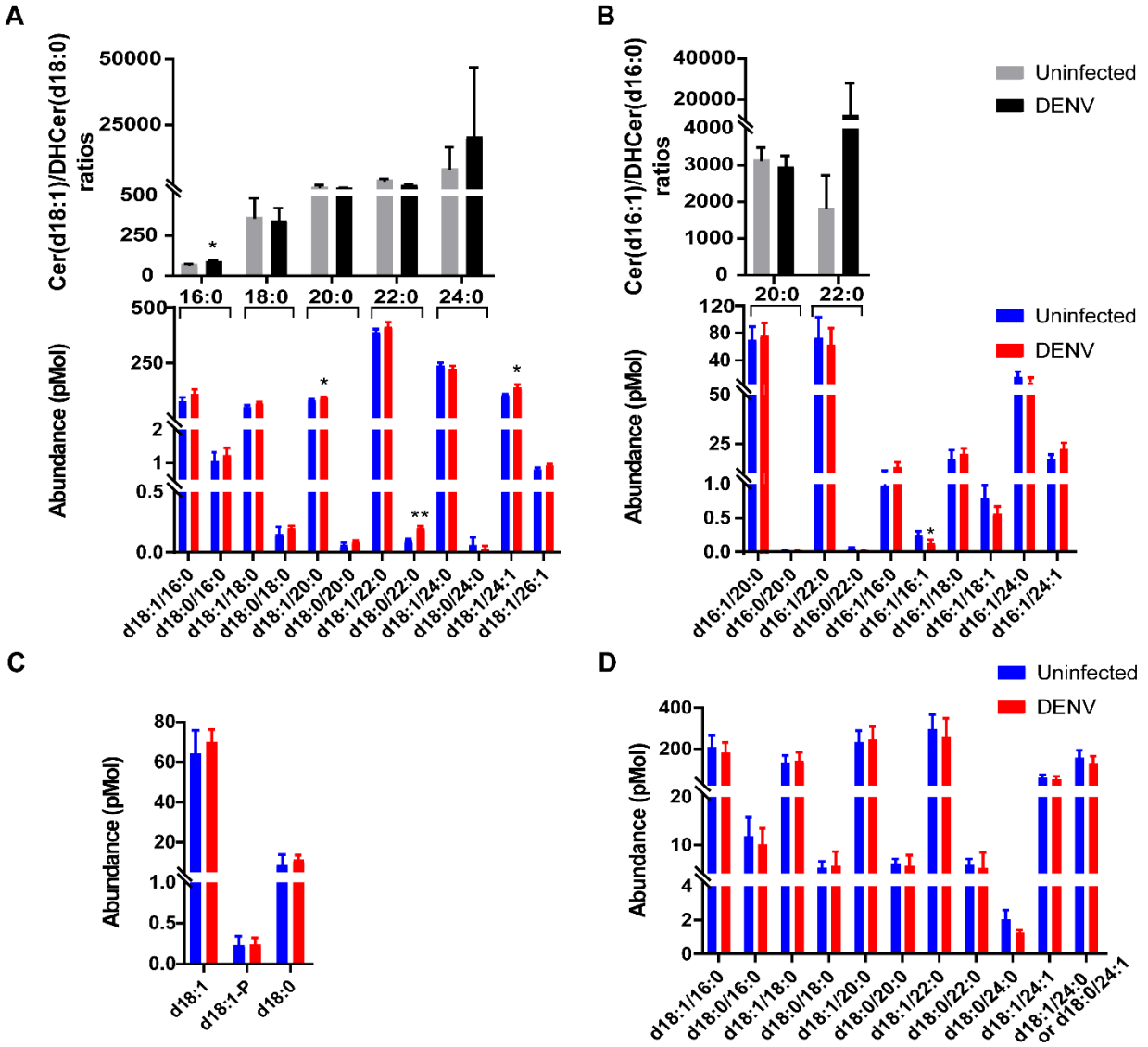

Figure 3.6. MRM profiling of SPs in Aag2 cells during DENV2 infection. DENV2 infected (MOI of 3) or mock infected Aag2 cells were harvested at 24 hpi and processed for SP profiling by MRM (N=3). (A, lower panel) Cer(d18:1/xx:x) and DHCer(d18:0/xx:x) with 18-carbon long chain sphingoid bases, and (B, lower panel) Cer(d16:1/xx:x) and DHCer(16:0/xx:x) with 16-

carbon long chain sphingoid bases. Cer/DHCer ratios of the species that have the same fatty acyl chain length (e.g. Cer(d18:1/16:0) and DHCer(d18:0/16:0)) were calculated and shown in (A) and (B) upper panels. (C) Sphingosine (d18:1), sphingosine -1-phosphate (d18:1-P) and sphinganine (d18:0), (D) sphingomyelin, Student's t-test was applied for statistical analysis. *, $p < 0.05$ and **, $p < 0.01$.

Knockdown of DEGS did not reduce DENV2 infection and transmission in *Ae. aegypti* mosquitoes

To further investigate if the balance of DHCer and Cer controlled by the DEGS gene is critical in DENV2 infection and transmission, we performed a dsRNA KD in *Ae. aegypti* mosquitoes. Mosquitoes were IT injected with dsRNA against DEGS or GFP (control) two days prior to DENV2 oral infection. Blood engorged mosquitoes were reared and were collected for dissections on days 3, 7 and 14 post blood feeding (days 5, 9 and 16 post dsRNA injection) (Figure 3.7). Five mosquitoes were collected to examine the levels of DEGS expression post dsRNA injection (Figure 3.7A). On the day of the infectious blood meal infection (day 2 post injection), the KD of DEGS expression was very effective. The levels of DEGS expression upon dsRNA KD was at 2.22 ± 1.98% compared to DEGS expression in GFP-KD mosquitoes (Figure 3.7A). However, the KD effect only temporary. The expression of DEGS in most of the DEGS-KD mosquitoes was still less than the expression of DEGS in the GFP-KD control on day 3 post blood meal (day 5 post injection). However, the expression of DEGS in the majority of the mosquitoes DEGS-KD was higher than the levels in GFP-KD control on day 7 post blood meal (day 9 post infection).

To determine the effect of DEGS-KD on DENV2 infection in mosquitoes, midguts, bodies and saliva were collected and titered for levels of DENV2 (Figure 3.7B-E). However, we did not observe a reduction in DENV2 infection in terms of both percent of mosquitoes that were infected and the titer of virus in the infected tissues from the DEGS-KD compared to the GFP-KD groups. These measurements were performed during the establishment of infection in the midgut (midgut day 3 post blood meal; Figure 3.7B), peak infection in the midgut (midgut day 7

post blood meal; Figure 3.7C), dissemination of virus to other tissues (body day 7 post blood meal; Figure 3.7D), and transmission of the virus into saliva (saliva day 14 post blood meal; Figure 3.7E). These results indicated that transient KD of DEGS transcript did not affect DENV2 infection and transmission in mosquitoes.

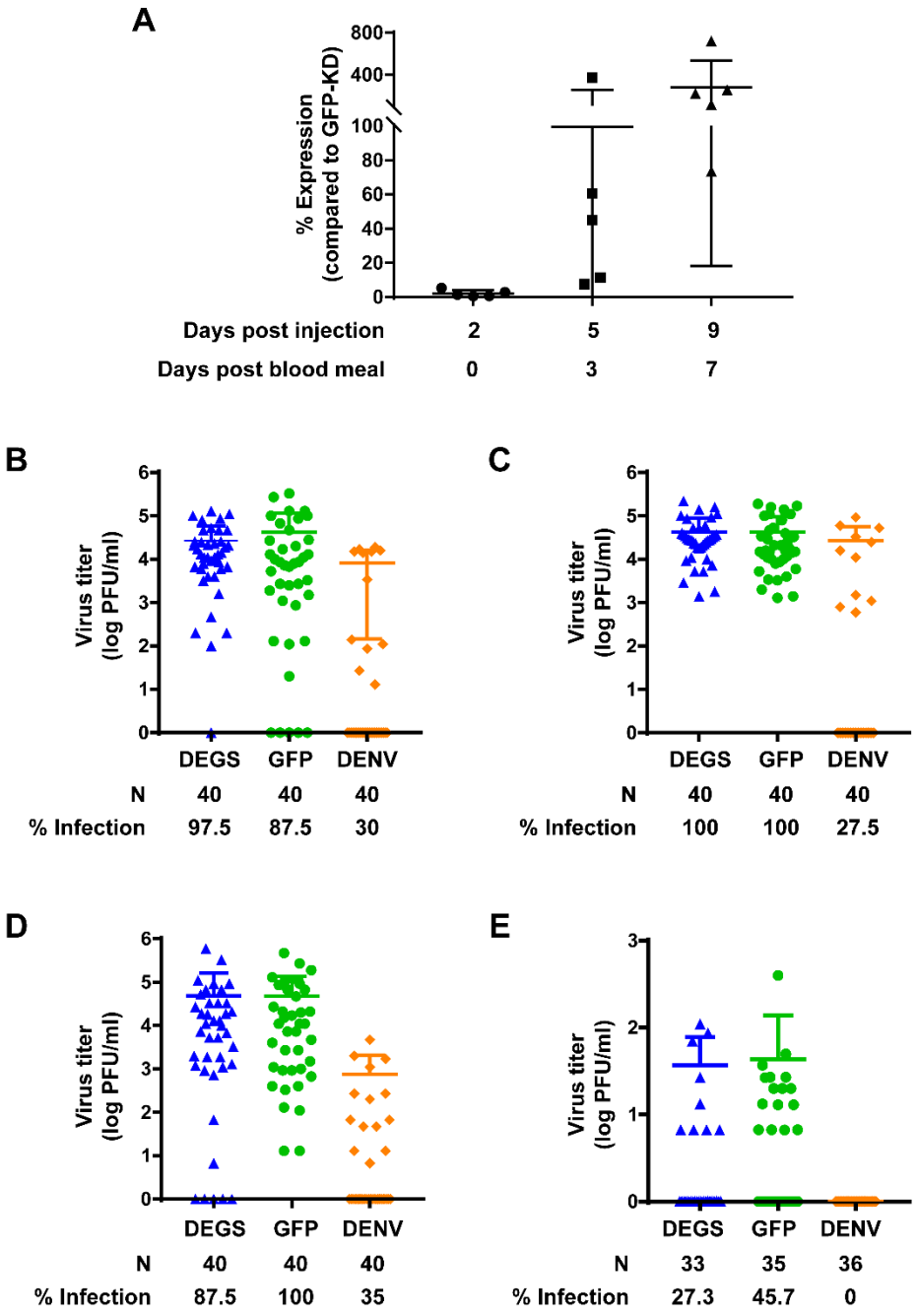

Figure 3.7. Transient knockdown of DEGS did not reduce DENV2 infection and transmission in *Ae. aegypti*. *Ae. aegypti* mosquitoes were IT injected with dsRNA against DEGS, GFP (KD negative control) and DENV2 (KD positive control) two days prior to DENV2-infectious blood feeding. Injected and blood engorged mosquitoes were reared up to 16 days post injection. (A) Whole mosquitoes (N=5) were collected on days 2, 5 and 9 post injection to test for the levels of DEGS transcript expression post DEGS-KD. The expression in the DEGS-

KD mosquitoes was compared to the expression in GFP-KD control. (B-E) mosquito tissue or saliva were collected and the level of virus replication was determined by plaque assay. (B) Midgut day 3 represents the early establishment of virus infection at the first site of infection in the mosquitoes. (C) Midgut day 7 represents the peak virus replication in the midgut of the mosquitoes. (D) Body (without midgut) day 7 represents the ability of the virus to disseminate infection to other tissues of the mosquito and (E) saliva day 14 represents the ability of the mosquitoes to transmit the virus to new human host.

DISCUSSION

Several studies have elucidated the presence of SPs and their physiological roles in mosquitoes or other insects [63, 179, 181, 218]. However, only a few have shown the link between SPs and DENV2 infection in mosquito cells and the mosquito vector [58, 61, 141]. In our previous study (Chapter 2), the most striking observation is that several SP metabolites that are precursors or derivatives of Cer showed increased abundance in DENV2-infected midguts compared to controls [61]. This result indicated that SPs might play important roles in DENV2 infection in mosquitoes as well. To investigate this hypothesis, mosquito cells were used to validate the SP metabolic control points upon DENV2 infection using SP inhibitors of SP metabolic pathway enzymes and RNAi methods.

Several SP inhibitors were used against enzymes that controls critical steps in the SP pathway in mammalian cells. Inhibitor screening on DENV2 infected mosquito cells in Figure 3.2 showed that DENV2 infection in both C6/36 and Aag2cells was the most effectively inhibited by 4HPR. This inhibition reduced DENV2 at the genome replication step or prior to it (Figure 3.3). Other SP inhibitors, such as DMS, TMS and FTY720 can statistically reduce DENV2 infection, but these reductions were subtle and might not be biologically relevant.

The SP profiling of Aag2 cells treated with 4HPR showed accumulation of 4 different 18-carbon long chain sphingoid bases Cer and 1 DHCer, but no 16-carbon long chain sphingoid bases. This is surprising to us because we expected to see the accumulation of DHCer upon 4HPR treatment [219]. However, it is possible that upon DEGS inhibition by 4HPR, cells have

other mechanisms to compensate for the loss of Cer by increasing the conversion of other SPs to Cer. For example, Cer levels can be compensated via the salvage pathway (through ceramide synthase) or the hydrolysis of sphingomyelin (through sphingomyelinase) (Figure 3.1). In this experiment, we also did not observe alterations of sphingomyelin, sphingosine and sphinganine upon 4HPR treatment (Figure 3.4C and D). This indicated that the effect of 4HPR is specific to DHCer and Cer but not other SPs.

Another experiment to further confirm the importance of DHCer and Cer on DENV2 replication is shown in Figure 3.5. DEGS gene expression in Aag2 cells was transient KD using dsRNA followed by DENV2 infection (Figure 3.5A-D). Upon DEGS-KD, we observed a significant reduction of both virus release and genome copy numbers. The most striking observation was seen in the SP profiling (Figure 3.5E and F). We observed accumulations of several DHCer and Cer species and a remarkable reduction of the ratios of the long chain base Cer to DHCer (Figure 3.5E and F). Important biological roles of the SP pathway are determined by conversion from DHCer to Cer. The balance between Cer and DHCer concentrations plays critical roles in regulating both membrane physical function and homeostasis that determines the fates (proliferation or death) of cells [151, 152, 220]. As a result, this observation has proven the point that we were able to KD the expression of DEGS at the transcriptional level as well as alter not only the abundance but also the balance of the metabolites in this pathway. In addition, these alterations affected DENV2 replication in mosquito cells highlighting the importance of this hub for infection.

Since perturbation of SP homeostasis caused a reduction in DENV2 replication, we asked the question whether DENV2 infection alters the balance of SPs. SP profiling revealed slight accumulation of some Cer and DHCer species, but not sphinganine, sphingosine or sphingomyelin (Figure 3.6). In our previous studies, we observed elevated levels of Cer and sphingomyelin during DENV2 infection in C6/36 cells [58] but only Cer during the infection in *Ae.aegypti* mosquito midgut (Chapter 2) [61].

Transient KD of DEGS in *Ae. aegypti* mosquitoes showed no effect on DENV2 infection, dissemination and transmission (Figure 3.7). These results suggested the complexity of the organism level which might have more compensatory mechanism to atone for the loss of the enzymes and metabolites. Firstly, although the KD of DEGS gene expression was greatly successful (~98% KD), the effect was only temporary (2-5 days; Figure 3.7A). After the KD effect waned, levels of the transcript seemed to bounce back higher than the normal level of expression which could possibly boost DENV2 infection. Secondly, we do not know whether KD of DEGS transcript reduced the protein or activity levels of DEGS. Thirdly, levels of Cer also can be compensated for via hydrolysis of sphingomyelin and salvage pathways. Lastly, transport of SP from exogenous sources such as from blood meal could potentially be the mechanism to compensate for the loss of DEGS function. Intracellular SP transportation has been reported, yet very few SP metabolites were reported to enter the cells [221-223]. However, MRM profiling of SPs in the mosquito upon DEGS-KD will result in a better understanding of SP regulation in the mosquito vector.

An important observation from the three systems studied thus far (*Ae. aegypti* mosquito midgut tissue, *Ae. aegypti*-derived Aag2 cells and *Ae. albopictus*-derived C6/36 cells) showed that the SP biosynthetic pathway is significantly activated during infection, with Cer concentration being a focal point [58, 61]. However, discrepancies of the SPs activated or required for infection may indicate the differences of species, stages of development and complexity between cell and organism levels. Therefore, the SP synthetic pathway requires further investigation to determine how the Cer hub and other intermediates in the SP metabolic pathway might support or limit infection.

CHAPTER 4: EXPRESSION OF FATTY ACID SYNTHASE GENES AND THEIR ROLE IN DIFFERENT STAGES OF DEVELOPMENT AND DURING ARBOVIRAL INFECTION IN *AEDES AEGYPTI*

INTRODUCTION

Several enzymes that control metabolism of the host have been shown to facilitate the replication of dengue viruses (DENV) in human and mosquito cells [58, 96, 108, 111, 191]. Fatty acid synthase (FAS) is one of these enzymes that has been demonstrated to play a critical role for DENV replication in both human and mosquito cells [58, 111]. FAS is a key enzyme that catalyzes over 40 steps in the *de novo* fatty acid biosynthesis pathway in mammals [224]. While fatty acid biosynthesis of bacteria and plants is accomplished by a series of monofunctional enzymes, fatty acid synthesis of fungi and vertebrates is accomplished by multifunctional FAS enzymes [225]. Fungal FAS contains seven catalytic domains which spread between two peptides and the enzyme functions as heterododecamers [226, 227]. In contrast, vertebrate FAS contains 7 catalytic and 3 non-catalytic domains in one peptide and functions as homodimers [224].

During mammalian *de novo* fatty acid biosynthesis process, acetyl-CoA carboxylase (ACC), the first enzyme and a rate limiting enzyme of the pathway, converts acetyl-CoA (which derives from hexose sugar and ketogenic amino acids) into malonyl-CoA. The malonyl group of malonyl-CoA is transferred to the acyl carrier protein (ACP) on one monomer of FAS by the malonyl-CoA/acetyl-CoA-ACP transacylase (MAT) domain. Another monomer of FAS is attached to the acetyl group of acetyl-CoA at the ACP site. β-ketoacylsynthase (KS) domain condenses an acyl intermediate (or acetyl group in the first cycle) with malonyl-ACP to a β-ketoacyl-ACP intermediate (or an acetoacetyl-ACP in the first cycle). This elongated product is

further reduced, dehydrated, and reduced again by a β-ketoacyl reductase (KR), dehydratase (DH) and a β-enoyl reductase (ER) domains. These reduction steps require nicotinamide adenine dinucleotide phosphate (NADPH) as a reducing factor. The acyl-chain is further elongated by cycling through these reactions and two-carbon units derived from malonyl-CoA are added to the chain per cycle. Once the length of the chain reaches 16-18 carbons, thioesterase (TE) cleaves the product from ACP and releases palmitoyl-CoA (C16:0) or stearic-CoA (C18:0) from the FAS enzyme. These newly produced fatty-acyl-CoA can used for incorporating into complex lipids, such as phosphoglycerolipids (GPs), sphingolipids (SPs) and glycerolipids (GLs) for assembly of cellular membranes, signaling molecules, and storage lipids, respectively.

FAS has been shown to serve as an important host factor in several arbovirus infections in mammalian and mosquito cells in culture [58, 111, 228, 229]. FAS activity, *de novo* synthesizes of fatty acids, is thought to support the expansion and rearrangement of endoplasmic reticulum (ER) membranes that occur to house viral replication machinery and assist in viral assembly [8, 89]. These molecules were shown to increase in abundance upon dengue virus serotype 2 (DENV2) infection in *Aedes albopictus* (Ae. albopictus) C6/36 cells as well as in the mosquito midgut [58, 61].

During DENV2 infection, DENV2 nonstructural protein 3 (NS3) was found to recruit FAS enzyme from the cytoplasm to sites of viral RNA replication on the ER membrane. Additionally, NS3 was shown to enhance FAS enzymatic activity [111]. In human hepatoma cells (Huh7), inhibition of FAS gene expression using siRNAs and FAS activity using inhibitors resulted in a reduction in DENV2 replication and infectious particle production [111]. Similar inhibition of DENV2 replication was also observed in C6/36 cells treated with C75, a potent FAS inhibitor [58].

In this study, we determined if FAS played role in supporting the infection of *Aedes aegypti* (*Ae. aegypti*) mosquitoes with DENV2. We identified seven different putative *Aa*FAS genes (*Aa*FAS 1-6 and *Aa*FAS-like) annotated in the AaegL5 genome assembly and characterized the expression profile in different stages of development. *Aa*FAS1 has the closest amino acid similarity to human FAS. In addition, *Aa*FAS1 is the dominant FAS in female mosquitoes. Knockdown (KD) of *Aa*FAS1 showed no significant compensation from other *Aa*FAS genes, indicating that these other *Aa*FAS genes cannot serve as backups for *Aa*FAS1. Significant reduction of DENV2 replication was observed following *Aa*FAS1-KD in *Ae. aegypti* cells. However, only transient reduction of DENV2 infection was found in *Ae. aegypti* midguts at early time points post DENV2 and CHIKV but not ZIKV infections by blood meal. In addition, an FAS inhibitor did not seem to effectively inhibit DENV2 replication in mosquitoes. Lastly, expression of *Aa*FAS1 in cell culture infected with DENV2 and in mosquito vectors IT injected or orally fed with DENV2 was profiled. We observed elevation of *Aa*FAS1 expression coincidently with increased DENV2 replication in cell culture. However, the induction of *Aa*FAS1 expression upon DENV2 infection was inconclusive.

MATERIALS AND METHODS

Alignments, conserved motifs and phylogenetic tree

Sequences from the AaegL3 genome assembly were retrieved from VectorBase and were blasted against the AaegL5 genome assembly using tBLASTn [66, 101, 230]. Sequences of all FAS genes from *Anopheles gambiae, Drosophila melanogaster* (*D. melanogaster*)*, Apis mellifera, Ixodes scapularis, Homo sapiens*, *Mus musculus* and *Saccharomyces cerevisiae* were obtained from NCBI and aligned using ClustalW along with FAS-AaegL3 in order to identify the analogues in the AaegL5 assembly [231]. Individual amino acid alignments between FAS-AaegL3 and FAS-AaegL5 were used to identify improvements in the AaegL5 models.

Conserved motifs were identified by global alignment of vertebrate, invertebrate and yeast proteins in MultAlin online software (accession numbers are shown in Table 4.1) [232]. Conserved amino acids were verified in the literature to determine catalytic domains of functional FAS. mRNA sequences were retrieved from NCBI and were manually curated to confirm the intron/exon boundaries.

Table 4.1. Organisms, gene names and NCBI accession numbers of vertebrate, invertebrate and yeast FAS proteins.

Organisms	Gene names	Accession numbers
Homo sapiens	Hm_FASN	NP_004095.4
Mus musculus	Mm_FASN	NP_032014.3
D. melanogaster	Dm_FASN1_A	NP_608748.1
	Dm_FASN1_C	NP_001137778.2
	Dm_FASN2_A	NP_647613.1
	Dm_FASN2_B	NP_001259986.1
	Dm_FASN3	NP_001015405.3
Apis mellifera	Am_FAS	XP_006567467.1
	Am_FAS-like	XP_395426.4
Anopheles gambiae	AgaP_AGAP001899	XP_321166.4
	AgaP_AGAP009176	XP_319941.4
	AgaP_AGAP008468	XP_316979.4
Ixodes scapularis	IscW_ISCW009053	XP_002403503.1
	IscW_ISCW005148	XP_002434035.1
	IscW_ISCW018177	XP_002433745.1
	IscW_ISCW018176	XP_002433744.1
	IscW_ISCW014149	XP_002415859.1
	IscW_ISCW014346	XP_002415657.1
	IscW_ISCW014347	XP_002415658.1
	IscW_ISCW014350	XP_002415661.1
	IscW_ISCW014349	XP_002415660.1
	IscW_ISCW024925	XP_002415410.1
	IscW_ISCW014534	XP_002400721.1
	IscW_ISCW014535	XP_002400722.1
	IscW_ISCW010398	XP_002403522.1
	IscW_ISCW010397	XP_002403521.1
	IscW_ISCW010399	XP_002403523.1
	IscW_ISCW010394	XP_002403184.1
	IscW_ISCW011309	XP_002411956.1

(cont.)

Organisms	Gene names	Accession numbers
	IscW_ISCW011310	XP_002411957.1
	IscW_ISCW009844	XP_002411379.1
	IscW_ISCW009052	XP_002405259.1
	IscW_ISCW008122	XP_002408143.1
	IscW_ISCW004392	XP_002409541.1
	IscW_ISCW001913	XP_002409867.1
	IscW_ISCW000257	XP_002408321.1
	IscW_ISCW001566	XP_002406467.1
	IscW_ISCW001073	XP_002403028.1
Saccharomyces cerevisiae	Sc_FAS1	NP_012739.1
	Sc_FAS2	NP_015093.1
	Sc_CEM1	NP_010983.2

Annotation of protein domains in *Ae. aegypti* FAS genes

To investigate if *Ae. aegypti* FAS (*Aa*FAS) proteins contain seven catalytic and three noncatalytic domains similar to mammalian FAS, amino acid sequences of *Aa*FAS genes were aligned against full-length human FAS (NP_004095.4) or the ten domains of FAS using Clustal Omega [233]. The alignment results were viewed using MView tool [234]. The annotation of conserved domains or motifs in human FAS and all *Aa*FAS genes was performed using Pfam 31.0 tool [235].

Mosquito rearing

Ae. aegypti strain Chetumal was originally collected from the Yucatan Peninsula, Mexico, in 2002 and established as a laboratory colony [120]. Eggs which were collected and dried on paper were placed in water to hatch. Within 24 hours, the larvae that hatched from the eggs were fed with ground fish food (Tetra). Once they molted into the pupal stage, pupae were collected in a plastic cup (~200 pupae in 2 oz. cup) and placed into 1-pint paper cartons covered with organdy. The adults that emerged were fed on 10% sucrose solution and water and maintained at 28°C, 80% relative humidity with 12–12 hours light-dark period.

Blood feeding

Mosquitoes were starved for food (10% sucrose solution) for 24 hours and water for 4 hours prior to blood feeding. Defibrinated sheep blood (Colorado Veterinarian Product) was mixed with 1mM ATP and placed in an artificial membrane feeder warmed by a 37°C water jacket. Mosquitoes were allowed to feed for 45-60 minutes. Fully engorged mosquitoes were sorted and reared on 10% sucrose solution and water.

Generating long double-stranded RNA

Long double-stranded RNA (dsRNA) was generated from *Ae. aegypti* mosquito total RNA. Primers were designed to amplify a region of ~ 500 base pairs (bp) of the gene of interest (Table 4.2). First, cDNA was obtained by reverse transcription (RT) reactions using specific reverse primers. The region of interest was then amplified by polymerase chain reaction (PCR) using specific primers that contained a T7 promotor sequence at the 5' end of both forward and reverse primers. RT and PCR were carried out using SuperScript III Reverse Transcriptase (Invitrogen) and *Taq* polymerase (NEB), respectively. The PCR product was then purified using the GeneJET PCR Purification kit (Thermo Scientific) and subjected to *in vitro* transcription using the MEGAscript T7 kit (Invitrogen). The reaction was incubated at 37^{o}C for 12 hours. Following incubation, the product was heated to 75^{o}C for 5 minutes and slowly cooled to room temperature for 4 hours to allow dsRNA to anneal. The dsRNA product was treated with DNase (NEB) and purified by phenol-chloroform followed by ethanol precipitation. The purified dsRNAs were stored at -80°C.

Table 4.2. Gene-specific primers for generating dsRNA transcript against *Aa*FAS1 gene

Target genes	Primers	References
*Aa*FAS1 (AAEL001194)	F- 5' GTCCCGTGTGTCTACTCAACAGT 3' R- 5' GCTTGTTCCACCTGTTGGTC 3'	[57]
eGFP	F- 5' GACCACATGAAGCAGCACGA 3' R- 5' CGCTTCTCGTTGGGGTCTTT 3'	[61]

* * T7 promotor sequence (5' GAATTAATACGACTCACTATAGGGAGA 3') was added to the 5' end of all primers to make dsRNA

Intrathoracic injection of dsRNA into mosquitoes

Adult females were subjected to intrathoracic (IT) injection at 3 to 4 days post eclosion. The detailed protocol was described in the materials and methods in Chapter 3.

dsRNA knockdown of *Aa*FAS1 gene followed by DENV2 infection in Aag2 cells

dsRNA KD was performed in RNA interference-competent *Ae. aegypti* (Aag2) cells. Detailed dsRNA KD protocol was described in the materials and methods section in Chapter 3.

KD cells were infected with infectious DENV2 expressing a luciferase reporter (DEN-Luc) gifted by Dr. Charles Rice from the Rockefeller University. At 48 hours post dsRNA transfection, cell culture medium was replaced with 300 µl of DEN-Luc supernatant and incubated at 28^{o}C without CO_2. At 24 hours post infection, virus supernatant was removed. Cells were lysed, and luciferase activity was read using Luciferase Assay System (Promega) by following the manufacture protocol.

Analysis of gene expression

Total RNA was extracted from either midgut or whole mosquito by TRIzol (Life Tech). Total RNA was reverse transcribed into cDNA with random primers (Life Tech) using SuperScript III Reverse Transcriptase (Invitrogen). About 400 ng of total cDNA was used in a quantitative PCR (qPCR). Specific primers for each gene are listed in Table 4.3. Actin was used as a reference gene. Relative *Aa*FAS gene expression was compared to the levels of the actin gene (100%). The comparative Ct ($\Delta\Delta$Ct) method was used for calculating percent *Aa*FAS gene expression upon treatment (dsRNA KD or virus infection) compared to the control [209].

Table 4.3. Gene-specific primers for detecting levels of *Aa*FAS expression

Target gene	Primers	References
*Aa*FAS1 (VB: AAEL001194)	F- 5' GAGGTCGTCCGATTGGTTTC 3' R- 5' AGGACAACCTTGCCGATGTG 3'	[57]
*Aa*FAS2 (VB: AAEL008160)	F- 5' CATTTCAAGCAGGCCCACAC 3' R- 5' TCTCAGACTCGGCAAAGCAG 3'	
*Aa*FAS3 (VB: AAEL002204)	F- 5' GTGCAGCTTCGAGATGCCATA 3' R- 5' GCTCCATCACAGAGTTTGCC 3'	
*Aa*FAS4 (VB: AAEL002237)	F- 5' GCTATGCTGGGATGTGCCAA 3' R- 5' TTCCTACGAGCTACATCCATAGC 3'	
*Aa*FAS5 (VB: AAEL002228)	F- 5' GGGACTGCAAGCCTTCAACA 3' R- 5' ATCCTTGGACAACACACCCA 3'	
*Aa*FAS-like (VB: LOC110675236)	F- 5' CTTGGTTTGTTGGGGTGTGC 3' R- 5' GTTACAATTGCCGCATCGCA 3'	
Actin (VB: AAEL004616)	F- 5' GAATGTGCAAGGCCGGATTC 3' R- 5' GCTCGATCGGGTACTTCAGG 3'	[61]
CHIKV (strain LR2006_OPY1, GB: DQ443544.2)	F- 5' GTACGGAAGGTAAACTGGTATGG 3' R- 5' TCCACCTCCCACTCCTTAAT 3'	[236]
DENV2 (strain 16681, NCBI: BC_001474.2)	F- 5' ACAAGTCGAACAACCTGGTCCAT 3' R- 5' GCCGCACCATTGGTCTTCTC 3'	[122]
ZIKV (strain PRVABC59, NCBI: KU501215.1)	F- 5' CCGCTGCCCAACACAAG 3' R- 5' CCACTAACGTTCTTTTGCAGACAT 3'	[237]

VB, VectorBase accession number; NCBI, NCBI accession number

Virus infection in mosquitoes by delivered of infectious bloodmeal

Viruses were cultured in cell culture prior to infectious bloodmeal feeding in mosquitoes as follows:

Dengue virus serotype 2

DENV2 serotype 2 strain Jamaica-1409 [119] was cultured in C6/36 cells. Briefly, C6/36 cells were infected with DENV2 at a multiplicity of infection (MOI) of 0.01. Absorption was allowed at room temperature for 1 hour. Virus supernatant was removed, and infected cells were cultured in 5 ml total volume of L15 medium supplemented with 3% fetal bovine serum (FBS), 50 µg/mL penicillin-streptomycin, and 2 mM L-glutamine. Fresh medium was replaced at

7 days post-infection. Virus supernatant was harvested on days 12-14 post-infection. Fresh supernatant (unfrozen) was directly used to prepare the infectious blood meal.

Zika virus

ZIKV strain PRVABC59 was cultured in Vero cells at a MOI of 0.1 [238]. Absorption was allowed for 1 hour at room temperature. Infected cells were cultured in Dulbecco Modified Eagle Medium (DMEM) supplemented with 2% FBS, 2 mM L-glutamine and non-essential amino acids. Virus supernatant was harvested on day 5 post infection and used directly to prepare the infectious blood meal.

Chikungunya virus

CHIKV strain R99659 was cultured in Vero cells at a MOI of 0.1 [239]. The infection was performed as for infection with ZIKV. Virus supernatant was harvested at 24 hours post infection and used for preparing the infectious blood meal.

To prepare infectious blood meals, virus supernatant and sheep defibrinated blood were mixed in equal volumes. Supernatant from uninfected cells was used to prepare the mock infectious blood meal. Feeding with the infectious blood was performed as described previously in the “blood feeding” section above.

Midgut dissection and plaque titration

Midguts from dsRNA injected mosquitoes were dissected as described in the “mosquito dissection and plaque titration” section in materials and methods section of Chapter 3**.** Plaque titration was performed on confluent BHK-15 cells for DENV2 and Vero cells for ZIKV and CHIKV. Detailed methods were also described in Chapter 3.

Inhibitor treatment

Mosquitoes were treated with C75 (Cayman Chemicals), the inhibitor for *de novo* fatty acid biosynthesis enzyme, FAS. C75 was diluted in DMSO, which was also used as a vehicle control. C75 or DMSO was added to the blood or sucrose solution at the final concentration designated in figures. The final concentration of DMSO in the solution was 0.1%.

RESULTS

Analysis of FAS genes and amino acid sequences in the AaegL5 assembly of *Ae. aegypti* genome

AaegL5 assembly is a full genomic sequence assembly and annotation of *Ae. aegypti* strain Liverpool [240, 241]. It was released in 2017 from the *Aedes aegypti* Genome Working Group (AGWG) at Rockefeller University in an attempt to improve the assembly and the annotation of the *Ae. aegypti* genome which was previously released as the AaegL3 by the Broad Institute and the Institute of Genomic Research (TIGR) [242]. Seven putative FAS genes were identified in the AaegL5 assembly, and the sequence of the gene models was confirmed via manual annotation [243]. Only two candidate FAS genes were identified in the gene models derived from the AaegL3 assembly, *Aa*FAS1 and *Aa*FAS2. In the current annotation, we named five additional genes *Aa*FAS3-6 and *Aa*FAS-like.

*Aa*FAS1 had the greatest number of exons (11 exons), whereas *Aa*FAS2 had 5 exons, *Aa*FAS3-5 had 6 exons and *Aa*FAS-like and *Aa*FAS6 had only 2 and 3 exons, respectively (Figure 4.1, Table 4.4).

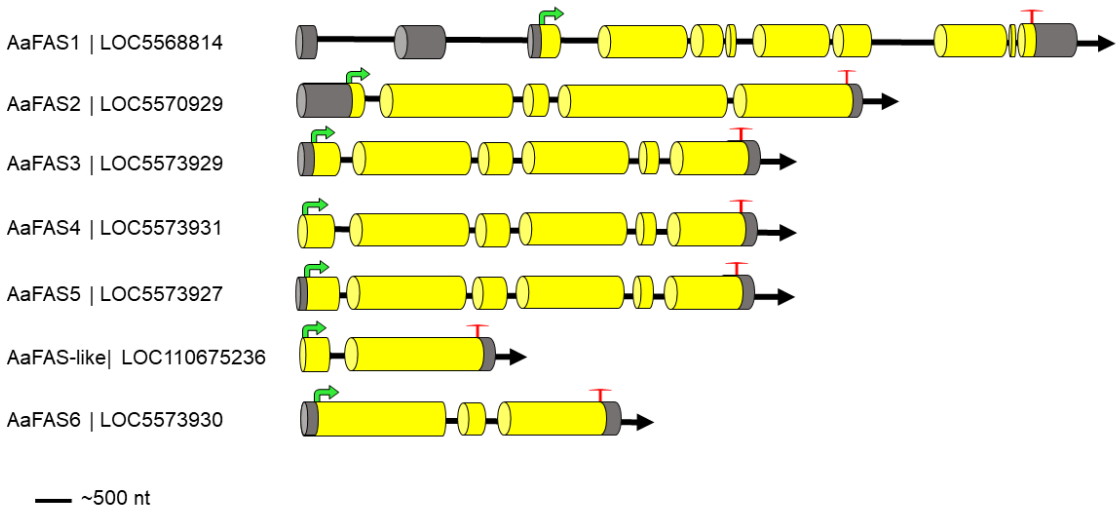

Figure 4.1. Schematic showing the predicted gene structure of the *Aa*FAS genes. Exons are indicated by yellow cylindrical bars, 5' and 3' non-coding exons by dark grey shading, introns by black line, start codon by green arrow and stop codon by red T.

Five of the *Aa*FAS genes were full length (*Aa*FAS1-5) and the average length of the gene product was 2360 amino acids (Table 4.4). The predicted *Aa*FAS1-5 proteins possessed features associated with functional FAS, including an initiation methionine, a stop codon and functional catalytic motifs (DTACSS, EAH and GSVKS) important for ketoacyl synthesis as described by Beedessee *et al*. 2015 [244]. Additionally, *Aa*FAS1-5 contained the YKELRLRGY motif conserved among the FAS genes of vertebrates, invertebrates and yeast. *Aa*FAS3 lacked 6 amino acid residues in the 3' terminus of exon 6 and a total count of 127 non-synonymous substitutions as compared to the AaegL3 ortholog.

*Aa*FAS-like and *Aa*FAS6 are likely incomplete gene models: the *Aa*FAS-like gene model was 800 amino acids in length and contained all functional catalytic motifs, whereas *Aa*FAS6 was 1386 amino acids in length, lacked catalytic motifs but contained the conserved motif YKELRLRGY typically located in the 3' end of FAS genes. Interestingly, *Aa*FAS3, *Aa*FAS-like and *Aa*FAS6

Table 4.4. List of *Aa*FAS genes

Name	AaegL3	AaegL5	% identity (AaegL3 & AaegL5)	Max # of exons	Chromosome	Location	% Identity with human FAS	Length (nucleotides)	Length (amino acids)	No. Splice variants/isoforms	Notes on the revised annotation
*Aa*FAS1	AAEL001194	LOC5568814	99.9	11	2	NC_035108.1 (307544012..307601765, complement)	45.3	9732	2422	1	1 SNP in exon_4
*Aa*FAS2	AAEL008160	LOC5570229	100	5	3	NC_035109.1 (9993811..10002427, complement)	36.7	8368	2385	1	1 SNP in exon_5
*Aa*FAS3	AAEL002204	LOC5573929	94.6	6	2	NC_035108.1 (429256663..429264110, complement)	32.9	7144	2334	1	18 SNPs exon_1, 31 SNPs exon_2, 11 SNPs exon_3, 52 SNPs exon_4, 3 SNPs exon_5, and 12 SNPs exon_6. Deletion of six amino acid residues when compared with the AaegL3 orthologue
*Aa*FAS4	AAEL002237	LOC5573931	99.1	6	2	NC_035108.1 (429327062..429334421, complement)	34.6	7068	2333	1	4 SNPs exon_2, 10 SNPs exon_4, 6 SNPs exon_6
*Aa*FAS5	AAEL002228	LOC5573927	99.5	6	2	NC_035108.1 (429228612..429236010, complement)	32.9	7097	2324	1	5 SNPs exon_2, 2 SNPs exon_3, 3 SNPs exon_4, 1 SNP exon_6
-	AAEL002227	-	-	-	-	-	-	-	-	-	-
-	AAEL002200	-	-	-	-	-	-	-	-	-	-

(cont.)

Name	AaegL3	AaegL5	% identity (AaegL3 & AaegL5)	Max # of exons	Chromosome	Location	% Identity with human FAS	Length (nucleotides)	Length (amino acids)	No. Splice variants/isoforms	Notes on the revised annotation
*Aa*FAS-like	-	LOC110675236	-	2	2	NC_035108.1 (429280401..429282870, complement)	36.1	2409	800	1	-
*Aa*FAS6	-	LOC5573930	-	3	2	NC_035108.1 (429275401..429279876, complement)	36.8	4353	1386	1	-

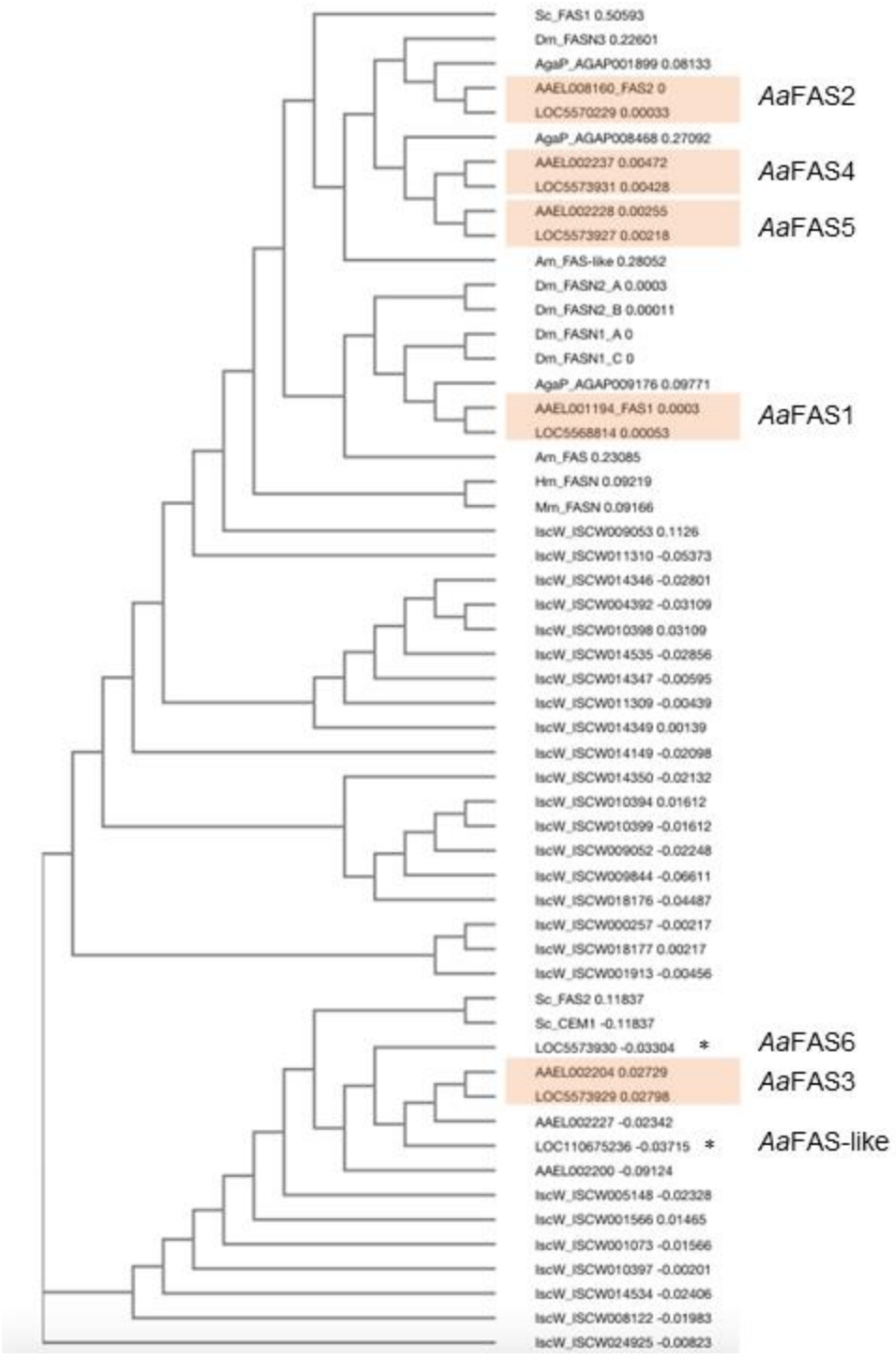

Figure 4.2. Sequence analysis of AaFAS genes. Analysis of AaFAS genes was performed using neighbor-joining from AaegL3 and AaegL5 genome assemblies and representative FAS from *Anopheles gambiae* (Agap), *D. melanogaster* (Dm), *Apis mellifera* (Am), *Ixodes scapularis* (IscW), human (Hm), mouse (Mm) and yeast (Sc). Orange boxes indicate gene pairing of the FAS from AaegL3 (AAEL) and AaegL5 (LOC). Asterisks indicate “un-paired” FAS genes from AaegL5 to FAS genes from AaegL3.

clustered at the base of the tree with the FAS of yeast and ticks. Phylogenetic analyses suggest *Aa*FAS1-5 as the orthologs of the AaegL3 genome assembly-derived gene models as follows: LOC5568814-AAEL001194; LOC5570229-AAEL008160; LOC5573929-AAEL002204; LOC5573931-AAEL002237 & LOC5573927-AAEL002228 (Figure 4.2, Table 4.4). Orthologues of *Aa*FAS-like and *Aa*FAS6 (LOC110675236 & LOC5573930) were not identified from the AaegL3 gene models suggesting these models are unique to AaegL5.

To further investigate the potential function of *Ae. aegypti* FAS, amino acid sequences of all 7 *Aa*FAS genes were aligned with human FAS using Clustal Omega [233]. Human FAS contains 7 catalytic domains and 3 noncatalytic domains [224]. The alignment results (Table 4.5) showed all *Aa*FAS genes had less than 50% amino acid identity to human FAS. *Aa*FAS1 had the highest amino acid identity to the human FAS (Table 4.4 and 4.5). Alignment of FAS domain sequences also showed low to medium sequence identity between human and *Aa*FAS (23.03-63.56%) while *Aa*FAS1 contained the highest similarity score for most of the domains (Table 4.5). Linear organization of mammalian FAS domains annotated by Maier et. al., is shown in Figure 4.3A [224, 245]. Functional domains or motifs recognized by searching protein databases using Pfam 31.0 software are shown in Figure 4.3B. Dotted lines between figures 4.3A and B superimpose the region of mammalian FAS domains (Figure 4.3A) on the *Aa*FAS domains annotation by Pfam on figure 4.3B. Analysis from Pfam revealed that *Aa*FAS genes do not contain methyltransferase domains (Figure 4.3B). Protein sequence alignment using Clustal Omega also showed low sequence homology of the *Aa*FAS proteins to human FAS within pseudo-methyltransferase (ΨME) domains across all *Aa*FAS (16.20-23.03% identity; Table 4.5). This result reflects about 75-90 amino acid deletions in *Aa*FAS proteins when aligned with human FAS (Figure 4.4).

Table 4.1. Percent amino acid sequence identity between *Aa*FAS to full-length or individual domains of human FAS

Domains	Percent identity to human FAS (NP_004095.4)						
	***Aa*FAS1**	***Aa*FAS2**	***Aa*FAS3**	***Aa*FAS4**	***Aa*FAS5**	***Aa*FAS-like**	***Aa*FAS6**
Human FAS (full-length)	**45.3**	36.7	35.7	32.9	34.6	36.1	36.8
KS	**55.5**	47.6	44.9	47.6	43.7	44.9	N/A
Linker	**31.2**	27.2	23.5	24.7	23.5	23.5	N/A
MAT	**48.1**	38.8	21.2	22.7	21.2	20.1	N/A
DH	**47.5**	35.3	32.1	32.8	32.1	N/A	26.3
ΨME	**23.0**	23.3	21.9	19.0	16.2	N/A	21.2
ΨKR	27.0	30.2	34.4	32.3	34.4	N/A	**36.5**
ER	**59.3**	45.7	44.2	47.9	47.2	N/A	43.3
KR	**63.6**	54.7	51.3	55.5	50.0	N/A	50.4
ACP	49.1	43.9	48.2	48.2	**50.0**	N/A	48.2
TE	**34.5**	21.6	21.4	18.2	20.8	N/A	20.6

Note: Bold numbers highlight the highest amino acid identity among all *AaFAS.* Abbreviations: KS, β-ketoacyl synthase; MAT, malonyl-acetyl transferase; DH, dehydratase; ΨME, pseudo-methyltransferase; ΨKR, pseudo β-ketoacyl synthase; ER, enoyl reductase; KR, β-ketoacyl synthase; ACP; acyl carrier protein and TE, thioesterase.

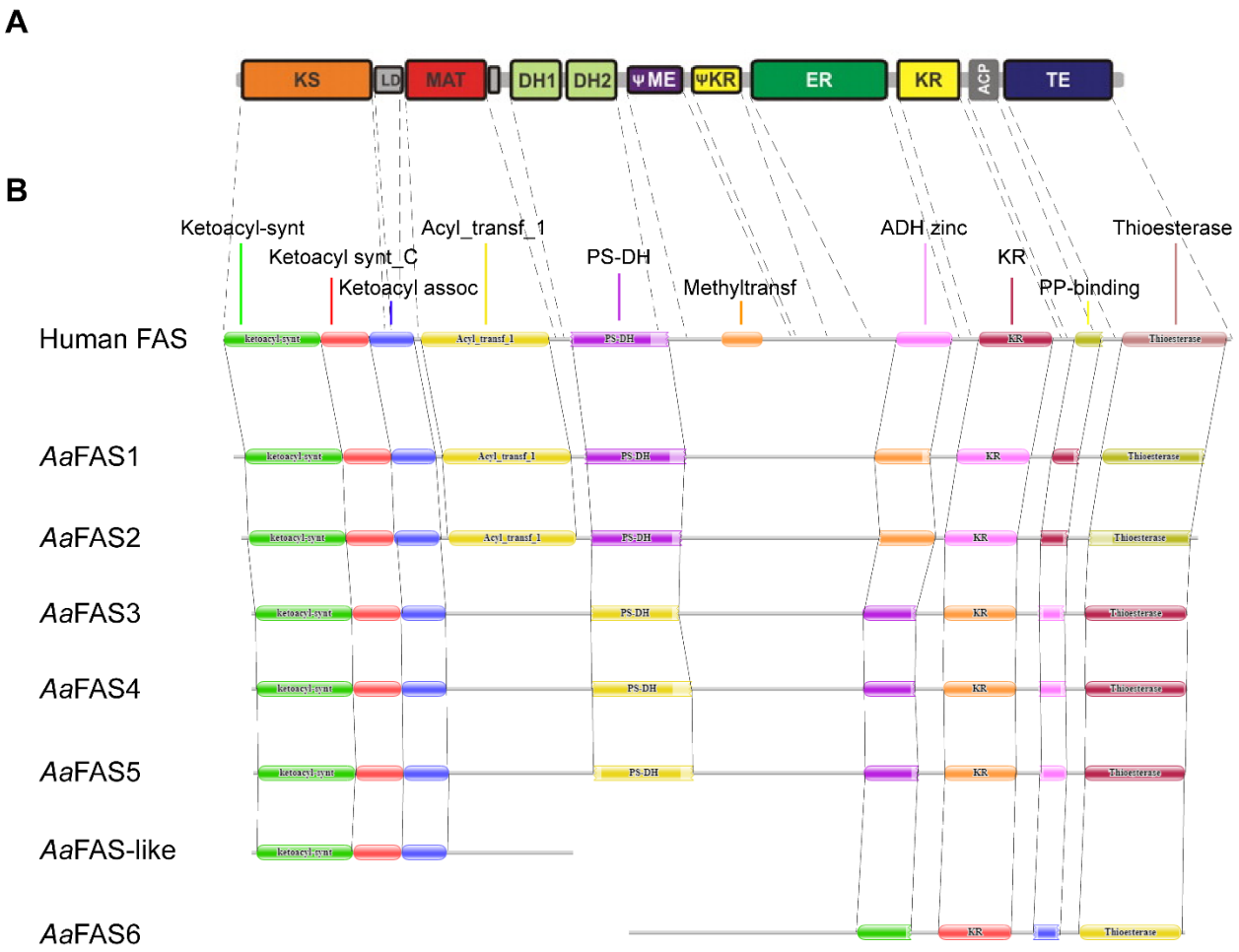

Figure 4.3. FAS domain organization. (A) Schematic shows linear organization of 7 catalytic and 3 noncatalytic domains of mammalian FAS annotated by Maier et. al. [224]. Seven catalytic domains are shown in big squares and 3 non-catalytic domains are shown in smaller squares. Abbreviations: KS, β-ketoacyl synthase; LD, linker; MAT, malonyl-acetyl transferase; DH, dehydratase; ΨME, pseudo-methyltransferase; ΨKR, pseudo β-ketoacyl synthase; ER, enoyl reductase; KR, β-ketoacyl synthase; ACP; acyl carrier protein and TE, thioesterase. (B) Schematics show conserved domains or motifs of FAS genes and their organization annotated using Pfam 31.0 software. Abbreviations are as follows: ketoacyl_synt, β-ketoacyl synthase; ketoacyl_synt_C, β-ketoacyl-acyl carrier protein synthase; ketoacyl_assoc, ketoacyl-synthase C-terminal extension; acyl_transf_1, acyl transferase domain; PS-DH, polyketide synthase; methyltransf, methyltransferase domain; ADH-zinc, zinc binding dehydrogenase; KR, β-ketoreductase domain; PP-binding, phosphopantetheine attachment site; thioesterase, thioesterase domain.

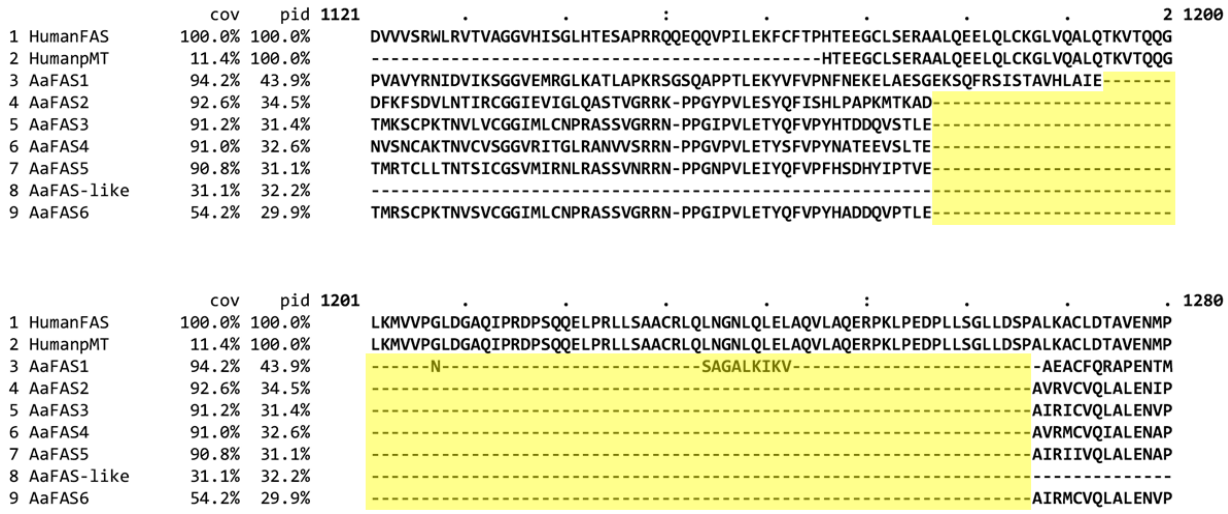

Figure 4.4. Alignment of ΨME domains of human and *Ae. aegypti* FAS proteins. Amino acid sequence alignment was performed using Clustal Omega followed by viewing in mView. The alignment of human FAS, ΨME domain of human FAS and 7 *Aa*FAS proteins revealed the deletion of ~75-90 amino acids in *Aa*FAS (shown in yellow).

Another important observation was seen in the *Aa*FAS-like and *Aa*FAS6 in Figure 4.3B. *Aa*FAS-like contains ketoacyl synthase, ketoacyl synthase_C and ketoacyl-synthase C-terminal extension domains which are the first 3 domains of *Aa*FAS1-5 and human FAS (Figure 4.3B). On the other hand, *Aa*FAS6 contains ADH zinc, β-ketoreductase, PP binding and thioesterase domains, which are the last 4 domains of *Aa*FAS1-5 and human FAS (Figure 4.3B). This result further supports our speculation that that the *Aa*FAS-like and *Aa*FAS 6 are a split gene model.

Expression of fatty acid synthase genes at different stages of mosquito development

Mosquitoes undergo 4 distinct developmental stages in their life cycle: egg, larva, pupa and adult. Expression patterns of different *AaFAS* genes might be distinct among these stages. To investigate this hypothesis, 5 individual mosquito samples were collected at 4th instar larval, pupal and adult stages. At the adult stage, males and females that were fed exclusively on sugar and females that were fed with one blood meal were collected (all adults were collected at

the same age, on day 3 post blood-feeding). *Aa*FAS gene expression was normalized to the average expression of the actin gene ($2^{-\Delta Ct}$) (Figure 4.5).

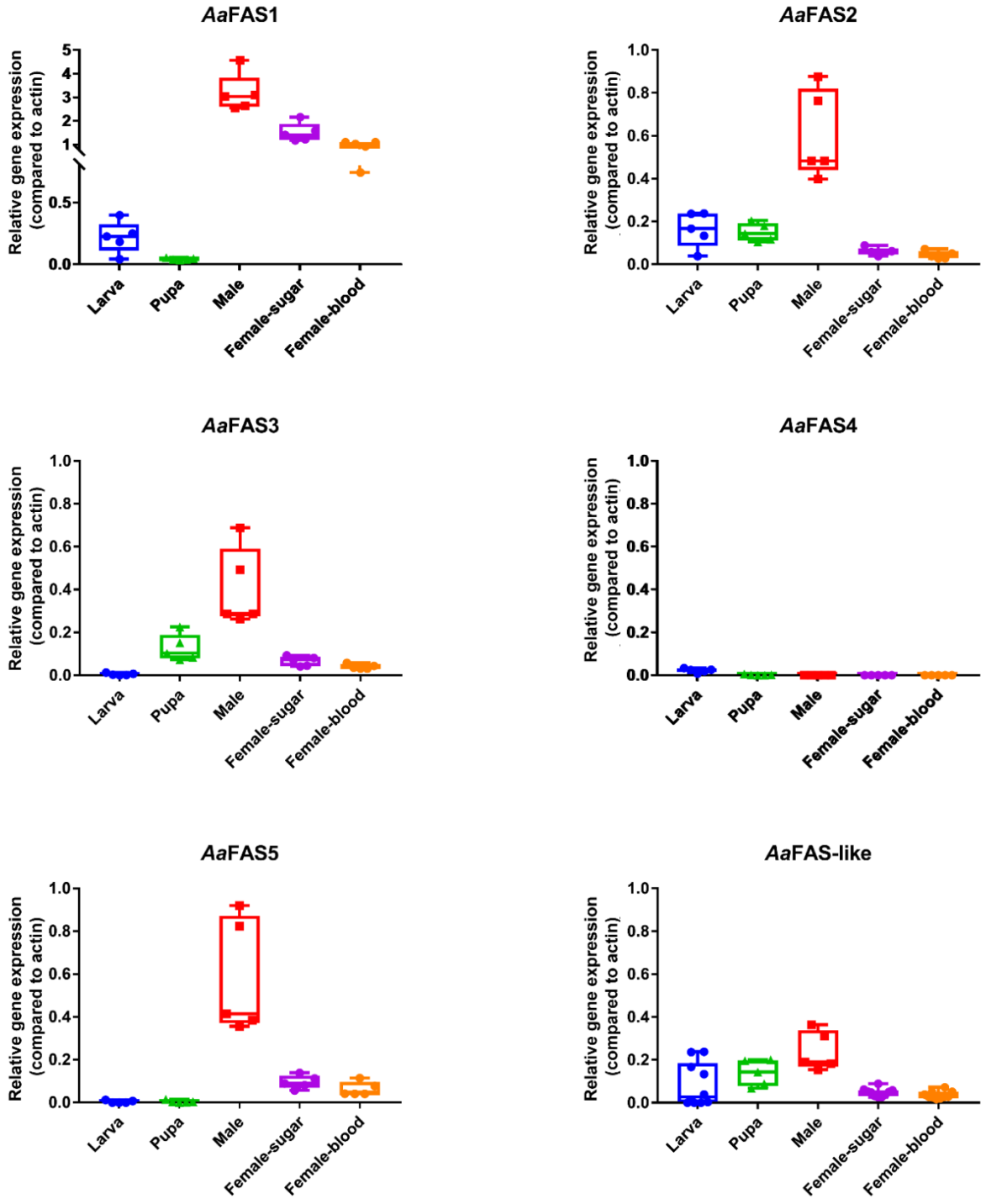

Figure 4.5. *Aa*FAS gene expression at various stages of mosquito development. Five individual mosquitoes at different stages of development were subjected to RNA extraction followed by two-step RT-qPCR. *Aa*FAS1-5 and *Aa*FAS-like expression was measured. The abundance of RNA in the samples was normalized to the actin gene using $2^{-\Delta Ct}$ method. Boxes show the 25th and 75th percentiles, whiskers show the minimum and maximum values and midline shows median.

Minimal expression of *AaFAS* genes were detected in larval and pupal stages (Figure 4.5). *Aa*FAS1, 2 and *Aa*FAS-like were expressed at the low levels in larval while *Aa*FAS2, 3 and *Aa*FAS-like were expressed at low level in pupae. Interestingly, we were able to detect the highest level of *Aa*FAS1, 2, 3, 5 and *Aa*FAS-like expression in adult males compared to other stages or adult females. In females, *Aa*FAS1 was expressed at a high level and almost exclusively regardless of food sources. *Aa*FAS4 was minimally detectable in any stages of development (Figure 4.5).

Blood meal ingestion inhibits the expression of *Aa*FAS1 in adult females.

The blood meal is rich in nutrients, especially proteins. The intake of lipids in the blood meal possibly triggers lipolysis instead of biosynthesis. Our analyses from Figure 4.5A showed slightly lower *Aa*FAS1 expression in blood-fed females compared to sugar fed-females. To test this hypothesis, *Aa*FAS1 from mosquitoes that were fed sugar meals only were compared with mosquitoes that were fed one blood meal or two blood meals (Figure 4.6). These mosquitoes had access to sugar meals at all times. However, blood meals were only given as shown in Figure 4.6A. Expression of *Aa*FAS1 was profiled as ratios normalized to the actin gene. The comparative expression ($2^{-\Delta\Delta Ct}$) showed reduction of *Aa*FAS1 expression in the blood-fed group compared to the sugar-fed group on days 1, 3 and 4 post-blood meal (pbm) (Figure 4.6B: F vs. B, G vs. C and H vs. D). These results showed that blood meal reduces *Aa*FAS1 expression for at least 4 days, but the inhibitory effect was no longer observed on day 6 post first blood meal (Figure 4.6B: I vs E). The inhibitory effect was also observed on day 1 post second blood meal (Figure 4.6B: J vs. D). Interestingly, on day 3 post 2nd blood meal, the expression of *Aa*FAS1

was upregulated compared to the group fed on sugar meals (Figure 4.6B: K vs.E).This might indicate the active requirement of AaFAS1 that is needed for egg production [36].

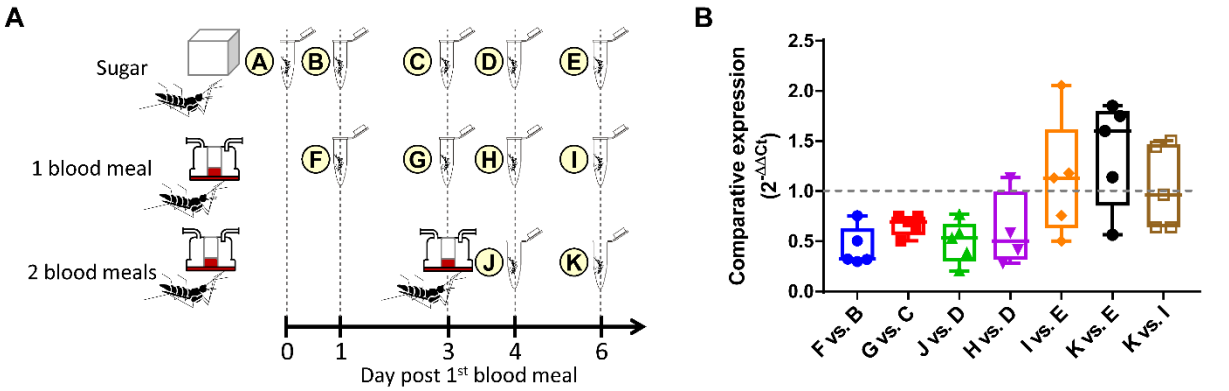

Figure 4.6. *Aa*FAS1 expression was reduced upon blood meal ingestion. (A) A schematic of the experimental design. Two groups of mosquitoes were fed on blood meals as indicated in the figure. Mosquitoes in all groups had access to sugar meals and water at all times. (B) Expression of *Aa*FAS1 was measured by the comparative expression method. The samples used for comparisons are indicated in the X- axis. Boxes show the 25th and 75th percentiles, whiskers show the minimum and maximum values and midline shows median.

Redundancy of *Aa*FAS genes contributes to minimal but not significant compensation during the loss of *Aa*FAS1 in adult females

We investigated if other *Aa*FAS could act as backups for *Aa*FAS1 during loss of function studies. Female mosquitoes were IT injected with dsRNA derived from *Aa*FAS1 or GFP (an irrelevant KD control). On day 2 post dsRNA injection, 5 mosquitoes were collected to test for *Aa*FAS gene expression levels (Figure 4.7). The expression of *Aa*FAS1 was reduced to ~39.3±13.9% compared to the GFP-KD control in the *Aa*FAS1-KD mosquitoes (Figure 4.7A). Expression levels of *Aa*FAS2, 3, 5 and *Aa*FAS-like were increased to 191.7±38.6%, 161.4±21.8%, 191.1±38.9% and 230.1±36.2%, respectively, indicating some compensation occurred to atone for the loss of the *Aa*FAS1 transcript. On the other hand, the expression of *Aa*FAS4 was slightly reduced to 87.71±74.0% compared to *Aa*FAS4 expression in GFP-KD.

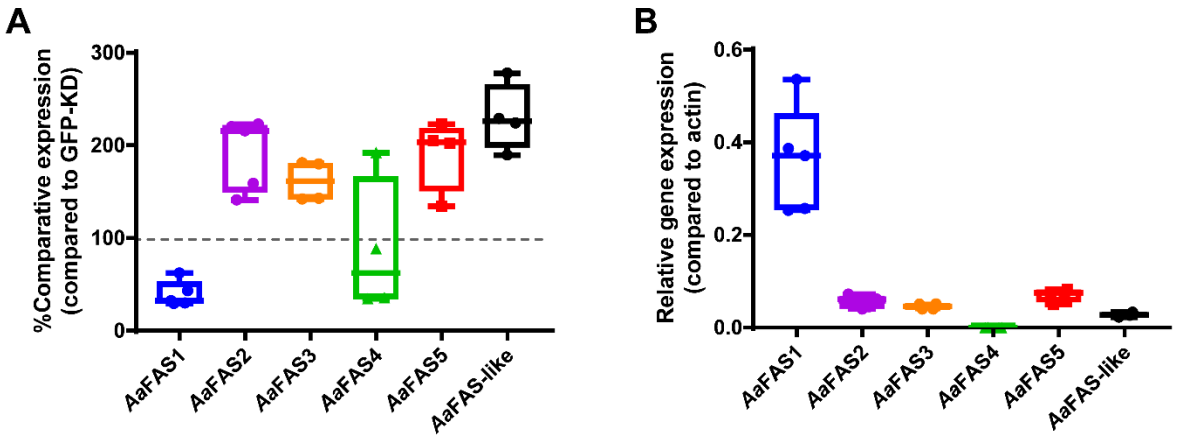

Figure 4.7. Comparisons of *Aa*FAS gene expression when *Aa*FAS1 expression is knocked down. Three-day-old adult female mosquitoes were intrathoracically injected with dsRNA derived from *Aa*FAS1 or GFP mRNA sequence (an irrelevant dsRNA control). Injected mosquitoes were reared on sugar solution for two more days and were collected for *Aa*FAS gene expression measurements. (A) Gene expression (%) of *Aa*FAS genes in *Aa*FAS1-KD mosquito was compared to and GFP-KD using the comparative Ct ($2^{-\Delta\Delta Ct}$) method. Relative *Aa*FAS gene expression to *Aa*FAS1 in *Aa*FAS1-KD is reported. (B) Gene expression profiles of *Aa*FAS were measured as normalized to actin gene expression ($2^{-\Delta Ct}$). Boxes show the 25th and 75th percentiles, whiskers show the minimum and maximum values and midline shows median.

To compare if the expression level changes among these *Aa*FAS after *Aa*FAS1-KD, expression levels of each *Aa*FAS gene was normalized to levels of actin expression (Figure 4.7B). We found that, upon *Aa*FAS1-KD, increases of other *Aa*FAS transcripts (5.6±1.44% for *Aa*FAS2, 4.6±0.00% for *Aa*FAS3, 7.07±0.62% for *Aa*FAS5 and 2.76±0.43% for *Aa*FAS-like) were incomparable to the remaining expression level of *Aa*FAS1 upon *Aa*FAS1-KD (36.1±11.6% remained expression). Overall, there appeared to be some low levels of compensation of *Aa*FAS gene expression. However, without measurement of the activity of each *Aa*FAS, it is unclear whether the limited increase of other *Aa*FAS transcripts would be sufficient to compensate for the potential loss *Aa*FAS1 function.

Inhibition of *Aa*FAS1 expression can reduce DENV2 replication in *Ae. aegypti* cells

Since *Aa*FAS1 is the main FAS expressed in female mosquitoes and the most similar to human FAS, we investigated if the KD of *Aa*FAS1 gene expression would affect DENV2 replication in *Ae. aegypti* (Aag2) cells. First, *Aa*FAS1 expression in the Aag2 cells that has functional RNAi machinery was transiently knocked down using dsRNA derived from *Aa*FAS1 or GFP control (Figure 4.8) [246]. At 48 hours post-*Aa*FAS1-KD (time zero of DENV2 infection), the expression level of *Aa*FAS1 in Aag2 cells was reduced to 5.15 ± 6.33 % compared to *Aa*FAS1 expression in GFP-KD control cells (Figure 4.8A). This KD did not cause detrimental effects to the cells (Figure 4.8B). At 24 hours post DENV2 infection, significant reduction of DENV2 RNA replication was observed in *Aa*FAS1-KD cells as compared to the GFP-KD controls. This level was comparable to DENV2-KD, the KD positive control (Figure 4.8C).

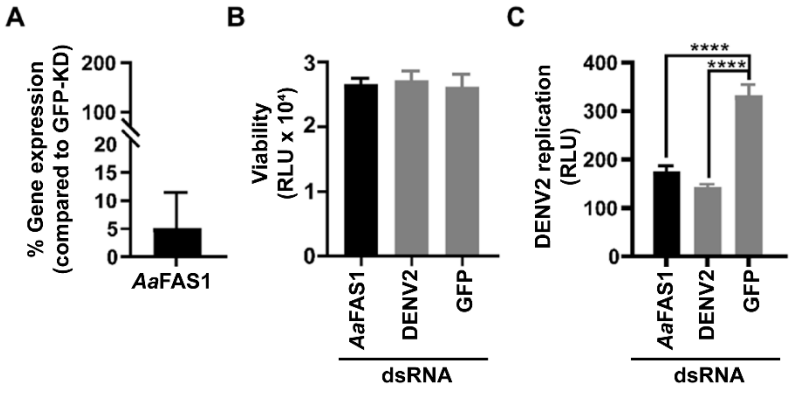

Figure 4.8. AaFAS1 gene expression knockdown reduced DENV2 replication in Aag2 cells. (A) Percent *Aa*FAS1 expression in *Aa*FAS1-KD Aag2 cells compared to the *Aa*FAS1 expression in GFP-KD cells. Expression was measured at two days post dsRNA transfection. (B) Viability of Aag2 cells treated with dsRNA derived from FAS, DENV2 (positive DENV2 KD control) and GFP (negative DENV2 KD control) genes. (C) RNA replication of luciferase-expressing DENV2 in Aag2 cells treated with dsRNA derived from *Aa*FAS1, DENV2 and GFP. Cells were transfected with dsRNA for two days prior to infection with luciferase-tagged DENV2. At 24 hpi, cells were lysed and were assayed for luciferase activity (RLU). One-way ANOVA followed by Tukey's multiple comparison test were applied for statistical analysis. ****, $p < 0.001$.

Transient inhibition of *Aa*FAS1 expression reduced infection of DENV2 and CHIKV but not ZIKV at early time points in the midgut tissues of *Ae. aegypti*

To further investigate if FAS could serve as a metabolic control point that can be manipulated to limit DENV2 replication and dissemination in the mosquito vector, mosquitoes were IT injected with dsRNA derived from *Aa*FAS1 or GFP genes two days prior to DENV2 infection by blood meal. On days 0, 3 and 7 pbm (corresponding to 2, 5 and 9 days post dsRNA injection), whole mosquitoes were collected and analyzed for *Aa*FAS1 gene expression (Figure 4.9A). On the day of DENV2 infection by blood meal (2 days post dsRNA injection), the level of *Aa*FAS1 expression was reduced to 53.73 ± 27.13%. However, *Aa*FAS1 gene expression rapidly recovered to 119.82 ± 49.43 % by day 3 pbm and was comparable to the *Aa*FAS1 expression level in the GFP control. On day 7 pbm, *Aa*FAS1 was overexpressed to 191.69 ± 50.17 %, suggesting a possible over-compensation post KD effect (Figure 4.9A). Upon *Aa*FAS1 KD, although the level of *Aa*FAS1 gene expression had recovered to control levels by day 3 pbm, the percent of DENV2 infected midguts was reduced significantly compared to the GFP-KD control (Figure 4.9B). The odds ratio for *Aa*FAS1 in *Aa*FAS1-KD compared to GFP-KD on day 3 pbm was 0.20 (95% confidence interval (CI): 0.06 - 0.60) and for DENV2 compared to GFP-KD was 0.03 (CI: 0.01 – 0.13). This indicated significantly less mosquitoes were infected with DENV2 in the *Aa*FAS1-KD group as compared to the GFP-KD group on day 3 pbm. However, there were no differences in percent infection on days 7 and 14 pbm. Infectious particles produced from midguts (virus titer) from *Aa*FAS1-KD and DENV2-KD groups were significantly different from GFP-KD group when the uninfected samples were included in the analysis using the nonparametric Kruskal-Wallis test followed by Dunn's test, with p-values adjusted with the Bonferroni method ($p = 0.0002$ and $p < 0.0001$, respectively). However, if the titers of uninfected midguts were excluded, differences in virus titer among different dsRNA treatments were not detected (tested by one-way ANOVA followed by Dunn's test; virus titer

*Aa*FAS1-KD: $2.40x10^2$, GFP-KD: $2.18x10^3$, and DENV2-KD: $6.43x10^2$ plaque forming unit (PFU)/midgut).

We found that the inhibitory effect of *Aa*FAS1-KD on DENV2 infection did not last in the midgut. The titer and percent infection in the *Aa*FAS1-KD mosquitoes were comparable to the GFP-KD mosquitoes on day 7 pbm (*Aa*FAS1-KD: $2.70x10^3$, GFP-KD: $2.95x10^4$ and DENV2-KD: $5.88x10^3$ PFU/midgut; Figure 4.9C). No differences in viral titer and percent infection wereobserved in midgut on day 7pbm. To investigate if the transient *Aa*FAS1-KD could interfere with virus dissemination, mosquito carcasses (whole body without midgut) were tested on day 14 pbm for virus infection (*Aa*FAS1-KD: $6.57x10^4$, GFP-KD: $8.47x10^4$ and DENV2-KD: 0.00 PFU/carcass; Figure 4.9D). Although the mean titer in the carcass showed no statistical differences in *Aa*FAS1 compared to GFP-KD control, two distinct populations of mosquitoes with viral titers in *Aa*FAS1-KD carcasses were observed (Figure 4.9D); some with viral titers comparable to GFP-KD control ($5.77x10^4$ PFU/carcass) and some with distinctively lower titers ($2.95x10^1$ PFU/carcass). This observation highlighted that transient KD of *Aa*FAS1 potentially impacted dissemination of DENV2 in mosquitoes.

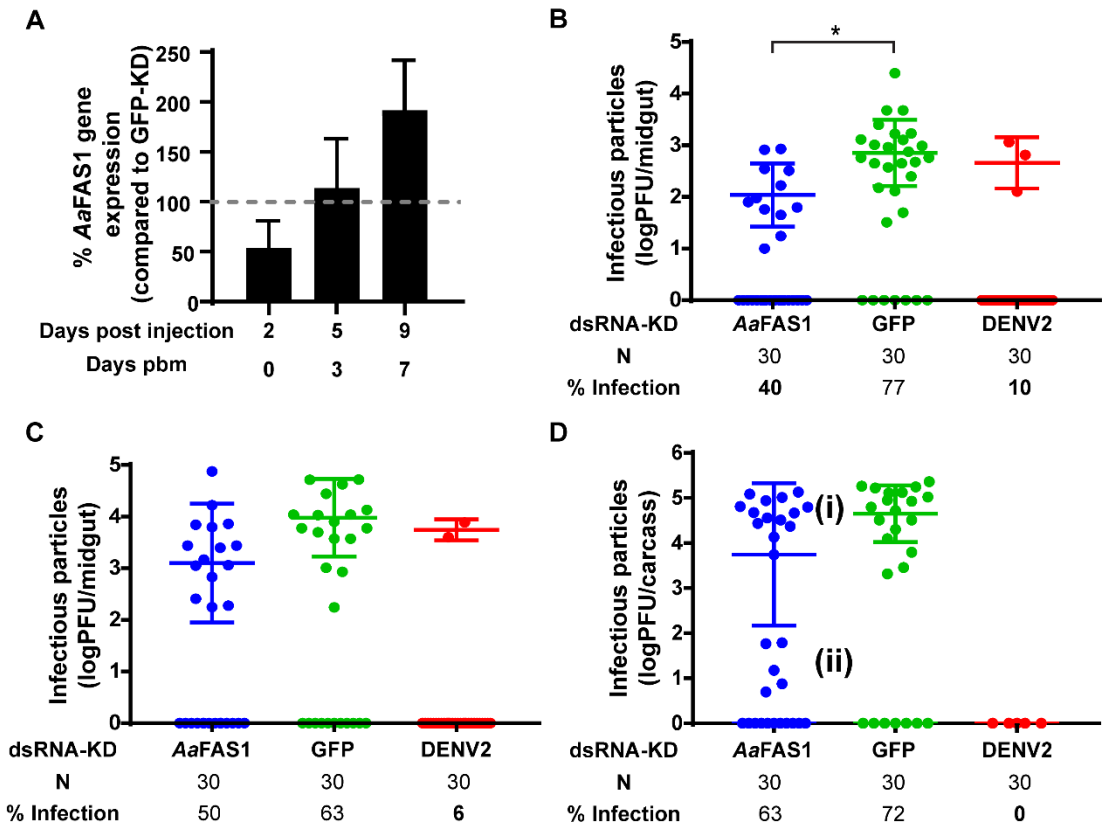

Figure 4.9. Transient KD of AaFAS1 expression by dsRNA temporarily reduced DENV2 infection in midguts and potentially dissemination in *Ae. aegypti* mosquitoes. (A) Percent *Aa*FAS1 expression in FAS-KD mosquitoes. Mosquitoes were IT injected with ~400 ng of dsRNA derived from *Aa*FAS1, DENV2 or GFP two days prior to blood meal infection. On days 0, 3 and 7 pbm (days 2, 5 and 9 days post IT injection), 3 pools of 5 mosquitoes were collected and analyzed for *Aa*FAS1 expression compared to *Aa*FAS1 expression in GFP-KD mosquitoes. (B-D) Mosquitoes were IT injected with dsRNAs and infected with DENV2 by infectious blood meal at 2 days post injection. Plaque assay was performed on midguts dissected on (B) day 3 and (C) day 7 and (D) carcasses (whole body without midgut) collected on day 14 pbm. (i) and (ii) indicate the separation of DENV2 titers in the carcass that were produced from the *Aa*FAS1-KD mosquitoes.
Mean virus titer (infectious particles) was calculated for infected samples only. One-way ANOVA followed by Dunn's tests were applied to test the differences in virus titer among samples, *, $p < 0.05$. The odds ratio was applied to test the differences in percent infection. The significant reduction of percent infection in *Aa*FAS1-KD or DENV2-KD compared to GFP-KD are highlighted in bold.

We also investigated if the perturbation of *Aa*FAS1 would affect other arbovirus infections in mosquitoes. *Aa*FAS1-KD mosquitoes were infected with ZIKV and CHIKV by infectious blood feeding at day 2 post dsRNA injection (Figure 4.10). KD of *Aa*FAS1 gene

expression in whole mosquitoes at day 2 post dsRNA injection was confirmed (Figure 4.10A). The level of *Aa*FAS1 expression was reduced to 21.50 ± 12.02% compared to GFP-KD control. On day 3 post virus infection (day 5 post dsRNA injection), midguts were dissected and processed for determining levels of virus infection by plaque assay. The result showed that the titer of infectious CHIKV statistically lower, yet very minimally changed upon *Aa*FAS1-KD compared to the GFP-KD control (*Aa*FAS1-KD: $5.44x10^4$, GFP-KD: $7.94x10^4$ and CHIKV-KD: $2.65x10^4$ PFU/midgut; Figure 4.10B). However, *Aa*FAS1-KD did not affect the percent infection of CHIKV in midguts (100%, same as in GFP-KD control). Interestingly, inhibitory effects upon *Aa*FAS1-KD were not observed in ZIKV infected mosquito midguts, suggesting ZIKV might possess other mechanisms to fulfill the need for fatty acids (*Aa*FAS1-KD: $7.24x10^5$, GFP-KD: $8.26x10^5$ and ZIKV-KD: $1.74x10^3$ PFU/midgut; Figure 4.10C).

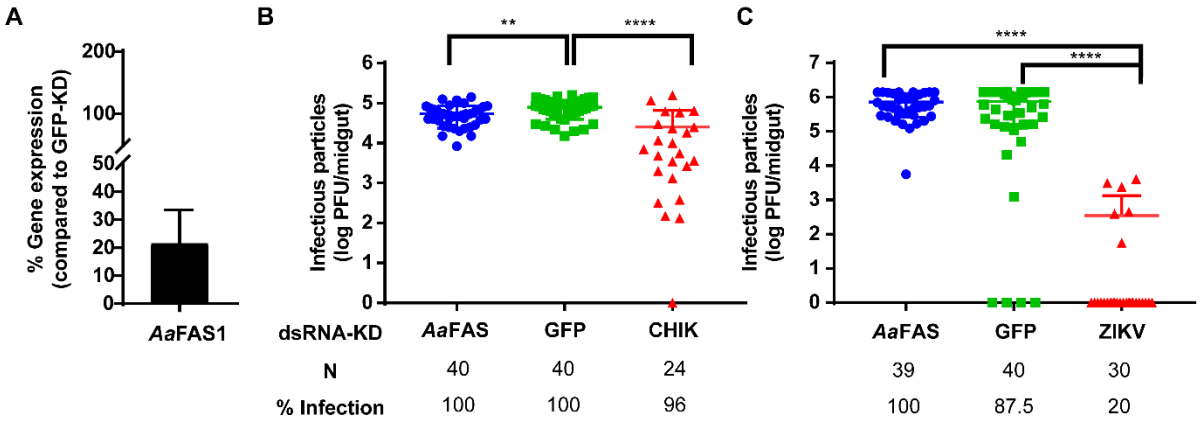

Figure 4.10. Knockdown of AaFAS1 gene expression reduced CHIKV but not ZIKV infection at early time points in mosquito midguts. Mosquitoes were IT injected with dsRNA against *Aa*FAS1, GFP and CHIKV or ZIKV followed by oral feeding of blood meal containing CHIKV and ZIKV. (A) The KD levels of *Aa*FAS1 was confirmed on day 2 post injection. Two days post injection, mosquitoes were fed with blood meal containing (B) CHIKV (1.45×10^6 PFU/ml) or (C) ZIKV (9.9×10^4 PFU/ml). Three days post blood feeding, midguts were dissected and infectious virus particles in the midgut were measured by plaque titration. Blood engorged mosquitoes were reared for 3 additional days. On day 3, midguts were dissected and homogenized in mosquito diluent for analysis of virus titer in the midgut by plaque assay. Mean virus titer (infectious particles) were calculated from infected samples only. One-way ANOVA followed by Dunn's tests were applied to test the differences in virus titer among samples. **, $p < 0.01$; **** $p < 0.001$.

We also tested if treatment with a FAS inhibitor would affect DENV2 replication in the midgut of *Ae. aegypti*. We used C75, the potent FAS inhibitor that effectively inhibits DENV2 replication in both human (Huh7) and *Ae. albopictus* mosquito (C6/36) cells [58, 111]. First, the administrative doses were tested in the mosquitoes. High (1,000 ng/ml) and low (10 ng/ml) doses were given to the mosquitoes in a blood meal on day 0. Dead mosquitoes were counted daily up to 11 days. (Figure 4.11A). We observed a significant death (40%) of mosquitoes by day 11 post treatment with the high dose of C75, but only about 10% died with the low dose of C75.

Since C75 might metabolize rapidly and become less effective in mosquitoes on later days, we administered the inhibitor continuously by adding C75 at the low dose concentration in sugar meals in addition to the first administration with the blood meal. C75 was added to the sucrose solution and was given fresh to the mosquitoes daily. There were the only food and water sources that mosquitoes could access; therefore, the mosquitoes were forced to ingest the inhibitor continuously over the course of the experiment. Similar survival rates in mosquitoes exposed to continuous administration of C75 compared to the single administration were observed (Figure 4.11B). However, because the high dose of C75 caused observable numbers of deaths while the low dose caused minimal deaths, we used low dose of C75 in the following experiments.

To test whether C75 reduced DENV2 replication in mosquito midguts, C75 at the low dose concentration was given to mosquitoes. C75 was administered 2 days prior to virus infection, with the infectious blood meal, and with sugar meals daily throughout the experiment. Midguts of mosquitoes were dissected on days 3 and 7 pbm and viral RNA copies in individual midguts were assessed by qRT-PCR (Figure 4.11C and D). The results showed slight decreases in RNA copies in midguts treated with C75. However, we did not observe statistically significant differences between viral RNA copies and percent infected mosquitoes in DMSO and C75 treatments from days 3 and 7 pbm.

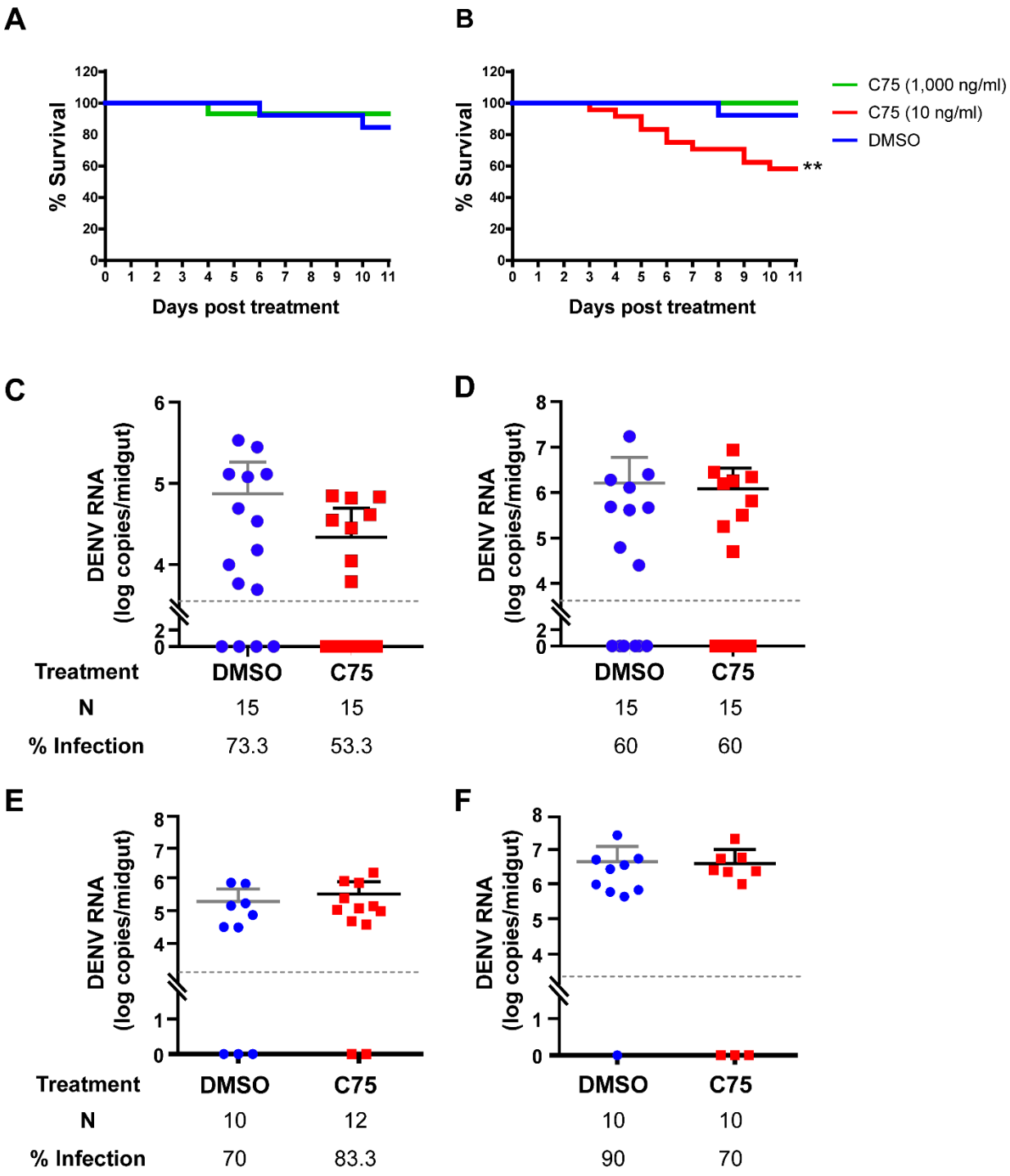

Figure 4.11. C75 caused minimal but not significant reduction of DENV2 infection in midguts of mosquitoes. (A-B) Kaplan-Meier survival curves showed percent survival of *Ae. aegypti* mosquitoes fed with C75 or DMSO (control) at the designated concentration. **, $p < 0.01$ tested by Mantel-Cox test (A) Mosquitoes were fed with C75 once on day 0 with the blood meal. (B) Mosquitoes were fed with C75 with blood meal on day 0 and forced to access sucrose solution that contained C75 (10 ng/ml) over the course of the experiment. (C-D) DENV2 RNA copy numbers measured from midguts of mosquitoes exposed to DENV2 on day 3 (C) and 7

(D) pbm. The mosquitoes were fed with C75 (10 ng/ml) or DMSO 2 days prior to DENV2 infection. During the infection, DENV2 and C75 (10 ng/ml) were mixed with the blood meal, and after infection, the mosquitoes were forced to access sucrose solution that contained C75 over the course of the experiment. A t-test was applied to compare RNA copy numbers of the infected midguts between the C75 and DMSO treatment groups. Minimal but not significant decreases in RNA copies were observed in the C75 treatment group on day 3 pbm.

Expression of *Aa*FAS1 gene upon arboviral infection

Studies in cell culture have shown that flaviviruses require FAS activity for genome replication [111, 228, 247]. Inhibition of FAS activity by pharmaceutical inhibitors reduced dengue virus replication in both human and mosquito cells [58, 111, 229]. To investigate if *Aa*FAS1 gene expression is elevated upon DENV2 infection, *Aa*FAS1 expression in DENV infected Aag2 and C6/36 cells was measured. As expected (from previous work on human cells), we observed an increase in expression of *Aa*FAS1 in both DENV2 infected C6/36 and Aag2 cells (Figure 4.12A). Expression of *Aa*FAS1 was also enhanced as levels of infection which increased with time (Figure 4.12B).

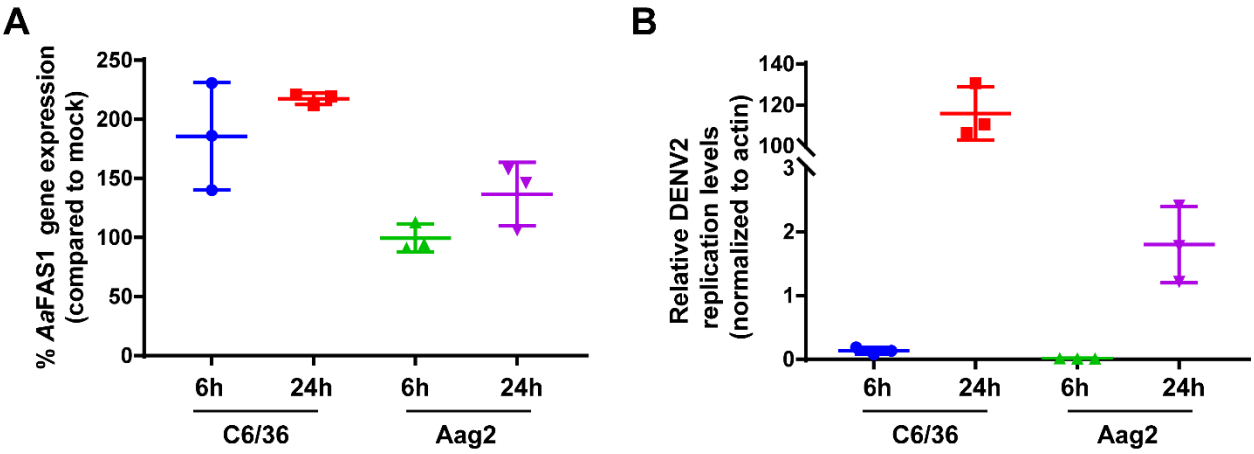

Figure 4.12. DENV2 infection enhanced AaFAS1 expression in mosquito cell culture. C6/36 and Aag2 cells were infected with DENV2 at MOI of 3. (A) Comparative expression (%) of AaFAS1 in C6/36 and Aag2 cells upon DENV2 infection. Expression of AaFAS1 in DENV2 infected samples was compared to that of mock infected samples using the $2^{-\Delta\Delta Ct}$ method. (B) DENV2 infection levels in C6/36 and Aag2 cells compared to levels of actin gene expression. The profile was calculated using the $2^{-\Delta Ct}$ method.

To further investigate if the relationship between DENV2 infection and *Aa*FAS1 expression holds true *in vivo*, *Aa*FAS1 expression levels in response to DENV2 infection in *Ae. aegypti* mosquitoes were measured. First, *Aa*FAS1 levels were measured in mosquitoes that were IT injected with DENV2 to ensure systemic infection (Figure 4.13). The results showed that *Aa*FAS1 expression was enhanced during early time point posts infection (day 3; Figure 4.13 A). Expression of *Aa*FAS1 on day 7 post injection was still higher than the mock infection (~200% expression). Comparing day 3 to day 7 pbm, while the expression of *Aa*FAS1 was not much higher on day 3, the levels of DENV2 RNA on day 3 were much higher than on day 7 (Figure 4.13 A and B). This might be due to the remnants of the injected DENV2 RNA which did not enter the cells but had not been totally degraded. The levels of *Aa*FAS1 seemed to decrease on day 14 post injection (late stage infection), coinciding with the levels of virus replication b in mosquitoes (Figure 4.13 A and B). To determine if *Aa*FAS1 expression levels correlated with levels of DENV2 RNA, a linear regression graph was plotted and correlation between expression of *Aa*FAS1 and levels of DENV2 RNA (Figure 4.13 C). Pearson's correlation coefficient = 0.6894 (p value = 0.006) indicating a positive, yet moderate, correlation between the expression of *Aa*FAS1 and DENV2 RNA.

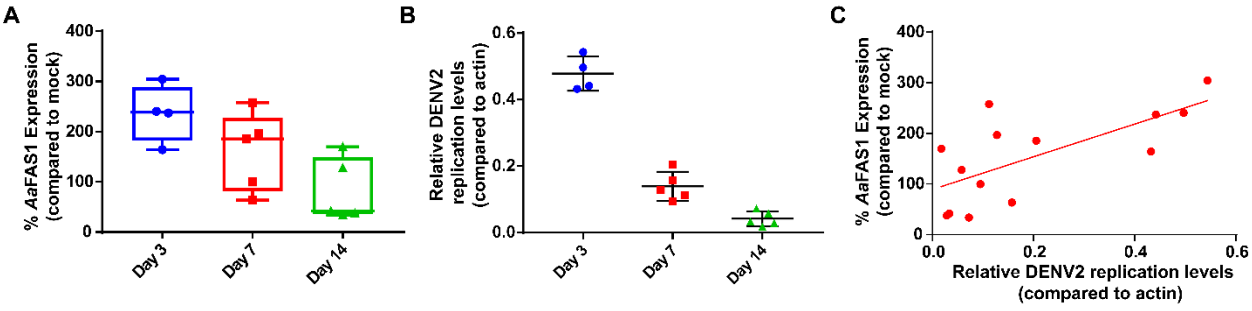

Figure 4.13. AaFAS1 expression levels in mosquitoes intra-thoracically injected with DENV2 showed positive correlations with DENV2 replication. Mosquitoes were IT injected with 69 nl of DENV2 (2,400 PFU). Injected mosquitoes were reared with 10% sucrose solution (no blood meal) up to 3, 7, and 14 days post injection. Whole mosquitoes were collected and *Aa*FAS1 and DENV2 RNA expression levels were measured by two-step RT-qPCR. (A) Percent expression of *Aa*FAS1 from DENV2 injected mosquitoes was compared to expression of *Aa*FAS1 in mock infections by comparative expression $2^{-\Delta\Delta Ct}$ method. (B) Relative levels of DENV2 replication compared to actin ($2^{-\Delta Ct}$) in the same mosquitoes as in (A) were normalized

to the expression of actin gene. (C) Linear regression graph showing the relationship between *Aa*FAS1 expression (y-axis) and levels of DENV2 RNA replication (x-axis) in the same mosquito.

Next, to reflect the natural route of DENV2 infection in mosquitoes, we determined the levels of *Aa*FAS1 expression in mosquitoes that were infected with DENV2 by oral feeding (Figure 4.14). Only mosquitoes that tested positive for DENV2 RNA by qRT-PCR were measured for *Aa*FAS1 levels. In Figure 4.14A-C, expression of *Aa*FAS1 and DENV2 RNA were measured from whole mosquitoes. We observed an increase in *Aa*FAS1 expression compared to mock on day 3, but expression of *Aa*FAS1 was no longer elevated in DENV2 infected mosquitoes on days 7 and 14 (Figure 4.14A). Pearson's correlation coefficient of this data = -0.2649 and p-value = 0.342, indicating no correlation between expression of *Aa*FAS1 and DENV2 RNA in mosquitoes that were fed DENV2-containing infectious blood meal (Figure 4.14C). This lack of correlation is despite the fact that some mosquitoes displayed high levels of DENV2 replication at day 14 (Figure 4.14B). We further investigated whether we could see a correlation of *Aa*FAS1 expression and DENV2 RNA levels in specific tissues. Midguts and carcasses (from the same mosquitoes) were analyzed (Figure 4.14 D-F for midgut and G-I for matched carcass). The result showed that expression of *Aa*FAS1 seemed to increase in midguts but not in the carcasses on day 3 pbm, when the infection has just established in the midgut and dissemination had not occurred. On day 7 pbm, high DENV2 RNA levels were shown in both midguts and carcasses of mosquitoes (Figure 4.14E and H). However, the levels of *Aa*FAS1 expression were surprisingly low, indicating that *Aa*FAS1 might be suppressed during the peak of DENV2 RNA replication (Figure 4.14D and G). On day 14 pbm, a slight inhibition of *Aa*FAS1 expression was seen in both midguts and carcasses while DENV2 RNA levels were not as high as on day 7 pbm. The results of *Aa*FAS1 expression seemed to be opposite to the levels of DENV2 RNA in both tissues. However, the Pearson's correlation coefficient showed no significant correlation between *Aa*FAS1 and DENV2 replication (midgut,

Pearson's correlation coefficient = -0.456, p = 0.088; carcass, Pearson's correlation coefficient = -0.253, p = 0.383)

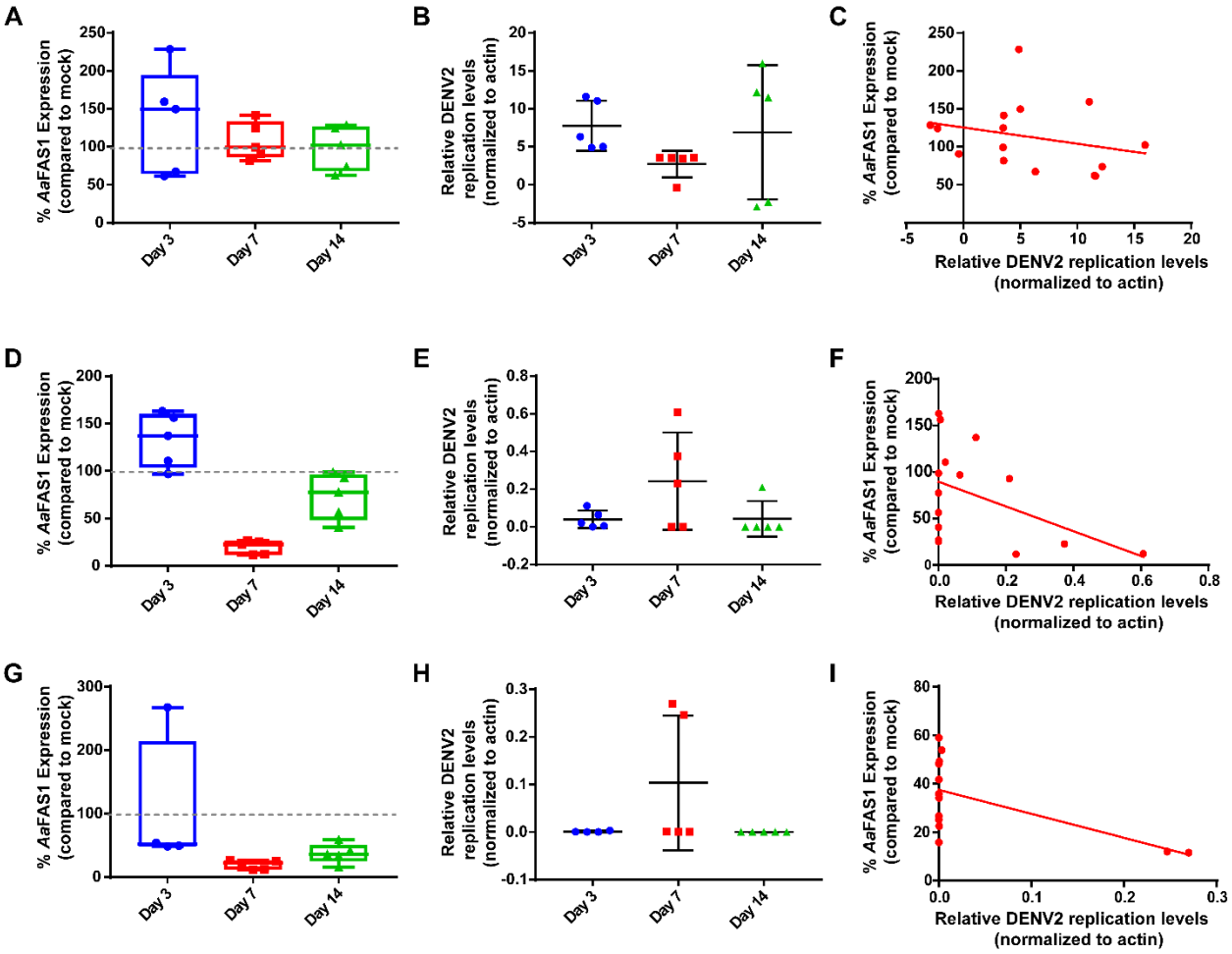

Figure 4.14. *Aa*FAS1 expression levels did not correlate with levels of DENV2 RNA in mosquitoes infected with DENV2 orally infection. Mosquitoes were fed a blood meal containing DENV2 (5.2 x 10^5 PFU/ml). On days 3, 7 and 14 pbm, midguts, carcasses or whole mosquitoes were collected for RNA extraction. Mosquitoes that were DENV2 positive (tested by qRT-PCR) were used for the analysis of AaFAS1 expression. (A, D and G). Analyses of AaFAS1 expression in DENV2 positive mosquitoes or tissues were compared to mock infected mosquitoes calculated by comparative $2^{-\Delta\Delta Ct}$ method. (B, E and H) Levels of DENV2 RNA expression in mosquitoes were compared to levels of actin gene expression using $2^{-\Delta Ct}$. (C, F and I) Linear regression graphs show the relationship between the expression levels of AaFAS1 (x-axis) and DENV2 RNA (y-axis). (A-C) whole mosquitoes, (D-F) midguts and (G-I) carcasses. Note that midgut and carcass samples were from the same mosquitoes.

Lastly, we wanted to determine the response of *Aa*FAS1 expression to infection by other arboviruses. The expression levels of *Aa*FAS1 in mosquitoes infected with DENV2, ZIKV and CHIKV were compared (Figure 4.15). In this experiment, mosquitoes were fed with blood meals containing DENV2, ZIKV or CHIKV. On days 3 and 7, whole mosquitoes were collected. Only the ones that were virus positive (by qRT-PCR) were further analyzed for levels of *Aa*FAS1 expression. The results in Figure 4.15 showed that, unlike the previous experiment in Figure 4.14, the expression of *Aa*FAS1 was suppressed on day 3 pbm (early infection), but the *Aa*FAS1 levels started to increase with time and with higher levels of replication. This trend was seen in all 3 viruses (Figure 4.15 A-B, D-E and G-H). Linear regression graphs showed significant, yet moderate, positive correlation between the levels of *Aa*FAS1 expression and virus infection in DENV2 (Pearson's correlation coefficient = 0.734, p = 0.016; Figure 4.15C) and CHIKV (Pearson's correlation coefficient = 0.729, p = 0.017; Figure 4.15I). The correlation was not significant in ZIKV samples but trended towards the positive correlation (Pearson's correlation coefficient = 0.351, p = 0.320; Figure 4.15F), similar to the other viruses.

In summary, the expression levels of AaFAS1 in infectious blood-fed mosquitoes seem to be responsive to replication of arboviruses. However, the responses were varied (some were enhanced, and some were suppressed) from experiment to experiment. A larger sample size might be needed to clarify the response patterns.

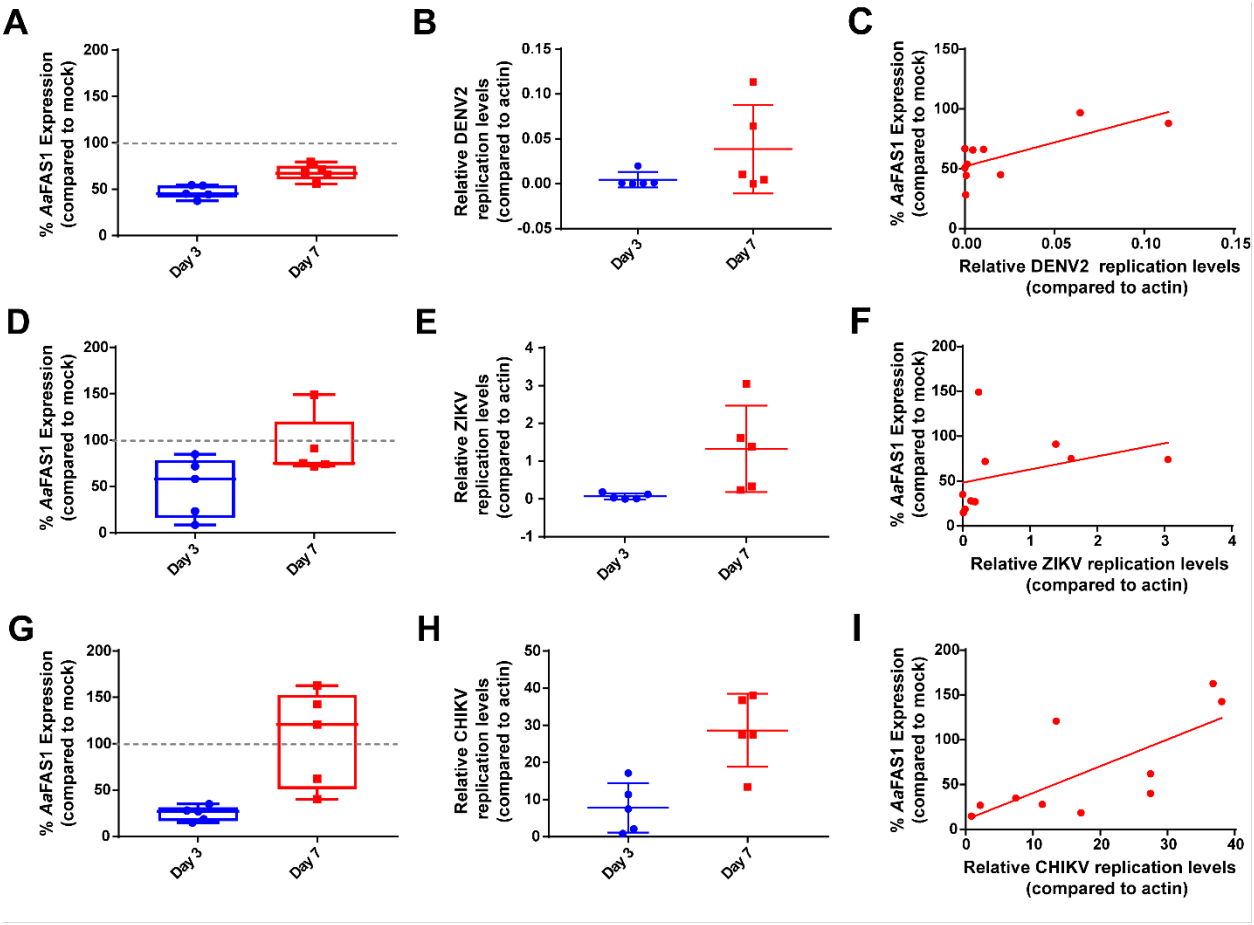

Figure 4.15. AaFAS1 expression was suppressed during early infection time points in response to arbovirus infection but increased with time and levels of replication. Mosquitoes were fed with blood meals containing DENV2 (5.2 x 10^5 PFU/ml), ZIKV (4.6 x 10^5 PFU/ml) and CHIKV (1.45 x 10^6 PFU/ml). On days 3 and 7 and 14 pbm, whole mosquitoes were collected for RNA extraction. Mosquitoes that were virus positive were used for the analysis of *Aa*FAS1 expression. (A-C) DENV2, (D-F) ZIKV and (G-I) CHIKV. (A, D and G) The analyses of *Aa*FAS1 expression in virus positive mosquitoes compared to mock infected mosquitoes calculated by comparative $2^{-\Delta\Delta Ct}$ method. (B, E and H) Levels of viral RNA expression in mosquitoes were compared to levels of actin gene expression using $2^{-\Delta Ct}$. (C, F and I) Linear regression graphs showing the relationship between expression levels of *Aa*FAS1 (x-axis) and viral RNA (y-axis).

DISCUSSION

Lipids are required to fulfill several physiological activities in mosquitoes such as maintaining water balance, depositing in eggs for oogenesis, and providing energy during flight,

diapause, and starvation [36, 37, 54, 57, 248]. Mosquitoes acquire lipids from maternal deposition in eggs and from food. They also have a capability to synthesize lipids from non-lipid materials. In this study, we comprehensively characterized the expression of *Ae. aegypti* FAS (*Aa*FAS) genes, the genes that transcribed one of the two key enzymes in the *de novo* lipid biosynthesis pathway, in different stages of development and upon different food sources. We also characterized the response of *Aa*FAS1 expression during arbovirus infections and the role of *Aa*FAS1 in supporting arboviral replication in the mosquito vector.

First, we identified 7 putative *Aa*FAS genes from the AaegL5 assembly . of the *Ae. aegypti* genome. Amino acid sequence alignment of these proteins showed that although they had low amino acid identity (< 50%) compared to human FAS (Table 4.4). *Aa*FAS genes contain all 7 catalytic and 2 out of 3 noncatalytic domains similar to human FAS (Figure 4.3A) [224, 245]. The potential function of these domains was further confirmed by the annotation of recognizable conserved domains or motifs by Pfam tool (Figure 4.3B) [235]. Result of Pfam annotation revealed that all *Aa*FAS genes lack a methyltransferase domain which lies within the ΨME domain region. The observation by Maier et. al., further reported that the deletion of amino acid sequences within ΨME domain region was also found not only unique to *Ae. aegypti*, but also lost in other insects such as *D. melanogaster* (fruit fly), *Bombyx mori* (silkworm), *Apis mellifera* (honey bee), *Culex pipiens*, and *Anopheles gambiae* [224]. In addition, annotation of the conserved domains by Pfam further confirmed our hypothesis that *Aa*FAS-like and *Aa*FAS6 belong to the same FAS gene but were split during genome assembly and annotation processes (Figure 4.3B).

Gene duplication is thought be a source of the evolutionary features [249]. Duplicated genes that are kept throughout evolutionary processes should lower the fitness cost or give a benefit to the organism [250]. In this study, we tried to answer why *Ae. aegypti* mosquito possesses several different genes in the *Aa*FAS gene family. Since mosquitoes undergo four

distinct developmental stages in their life and these stages possess very distinct habitats and food sources, different *Aa*FAS genes may play roles supporting the unique requirements for FAS in these different life stages.

Transcription profiles of six *Aa*FAS genes revealed the distinct patterns in gene expression at different developmental stages. We observed minimal *Aa*FAS expression in larval and pupal stages (Figure 4.5). During oogenesis, maternal lipids are deposited in eggs and comprise about 35% of dry weight [43]. These lipids are carried over into larval stage to serve as a metabolic and energy source for the larva [47]. Larvae also acquire external fatty acids and other lipids from food. Microorganisms such as algae, diatoms and dinoflagellates are important sources of polyunsaturated fatty acids [39]. Some of these polyunsaturated fatty acids cannot be synthesized by mosquitoes but are essential for mosquito development and muscle development for flight [39, 49]. As a result, *de novo* fatty acid biosynthesis may not be required while lipolysis may play a bigger role in these juvenile stages.

Interesting observations were made in the adult male mosquitoes. Most of the *Aa*FAS except *Aa*FAS4 were observed in males at a prominently higher level than females and other developmental stages. Due to the evolution of their mouth parts, males cannot bite and suck blood. They can only acquire food from natural sources of sugar, such as plant nectar, honeydew or fruits [251]. Since they are not evolutionarily equipped to drink blood, which can serve as an external source of lipids, the high expression levels of *Aa*FAS may reflect the dependency on FAS for *de novo* synthesis lipids for their needs. Similar observations reported elevated expression of genes associated with carbohydrate metabolism in male *Anopheles gambiae* [252].

*Aa*FAS1 is a dominant *Aa*FAS gene expressed in females. Interestingly, *Aa*FAS1 is the closest *Aa*FAS to human and mouse FAS genes (Figure 4.2 and Table 4.4 and 4.5). We found that the expression level of *Aa*FAS1 is influenced by the food source. Slight reduction of *Aa*FAS1 expression was observed upon blood meal ingestion compared to females fed only on

sugar (Figure 4.6). This result suggested that mosquitoes can directly use lipids that are in the blood meal for relevant purposes and decrease fatty acid biosynthesis for a few days after the blood meal is taken.

One issue that we have not investigated in this study is whether the expression of different *Aa*FAS genes is tissue specific. Differential expression of genes within the same gene family in different tissues has been observed in both mosquitoes and other insects [252, 253]. In this study, we only looked at *Aa*FAS expression from the whole mosquitoes. It is possible that other *Aa*FAS genes rather than *Aa*FAS1 might be expressed in specific tissues, but the expression was diluted out by the overall high-abundance of *Aa*FAS1 transcript.

Since mosquitoes possess several *Aa*FAS genes, we asked if other *Aa*FAS genes serve as substitutes when the *Aa*FAS1 malfunctions. In our study, we found a two-fold increase in other *Aa*FAS genes when *Aa*FAS1 expression was knocked down in female mosquitoes (Figure 4.7A). However, these compensations were insufficient to fulfill the loss of *Aa*FAS1 transcript (Figure 4.7B). This minimal compensation observed might be because the KD only caused about 50-70% reduction of levels of the *Aa*FAS1 transcript (Figure 4.7A, 4.9A and 4.10A). The remaining 30-50% of *Aa*FAS1 expression was still about 4-5 times higher than the expression of other *Aa*FAS genes. This level of *Aa*FAS1 expression might also be sufficient for function and thus, does not signal the backup system to compensate for the loss. Improvement of *Aa*FAS1-KD by either improving the KD efficiency (such as changing dsRNA to target other areas of the *Aa*FAS1 sequence) or extending the period of KD (such as using CRISPR-CAS9 knockout of *Aa*FAS1 gene or creating transgenic mosquitoes that express dsRNA against *Aa*FAS1 [27]) may reveal a higher and more robust compensation by other *Aa*FAS.

Alternatively, the different *Aa*FAS genes may be regulated differently and/or have different functionalities and/or activity efficiencies. A few studies have shown a link between insect hormones (such as adipokinetic, ecdysones and juvenile hormones) and their role in controlling lipid metabolism [37, 110, 254]. It is possible that the differences in hormone levels in

different developmental stages may be a major determinant of which *AaFAS* is expressed [255]. Further investigation is needed to better understand the regulation and functionality of different *Aa*FAS genes.

Previous studies have demonstrated the importance of FAS in DENV replication [58, 111, 229]. Heaton et. al., have shown that human FAS is relocalized to sites of DENV2 RNA replication, likely through interaction between the DH domain of FAS and nonstructural protein 3 (NS3) of DENV2 [111]. siRNA KD of FAS in human cells or using C75, a potent inhibitor of FAS activity, reduced DENV2 replication in both human hepatoma (Huh7.5) and C6/36 cells [58, 111]. As a result, in this study, we wanted to investigate if *Aa*FAS, specifically *Aa*FAS1, also played an important role in DENV2 infection in the mosquito vector. KD of *Aa*FAS1 in Aag2 cells showed significant inhibition of DENV2 replication (Figure 4.8). However, the inhibition of DENV2 infection in midguts of *Aa*FAS1-KD mosquitoes was only observed on day 3 pbm (Figure 4.9). This might be because the KD effect was only transient. When the KD effect wore out, *Aa*FAS1 gene expression and the activity became available, and as a result, virus titer reached comparable levels to the GFP-KD samples.

An interesting observation was seen in Figure 4.9A. On day 9 post *Aa*FAS1-KD, we found an overcompensation of *Aa*FAS1 expression, which increased to about 200% compared to the *Aa*FAS1 levels in the GFP-KD control. This is an important observation, especially for studies that intend to deploy transient suppression of host factors as a strategy to suppress pathogens. Transient suppression of host factors may only delay the infectivity of the pathogens, but if overcompensation occurs after suppression has worn out, host factors may become abundantly available and could cause a burst of replication of the pathogens.

Another interesting observation from this experiment is that we observed a separation of the virus titers into two groups: high, (i; 5.77×10^4 PFU/carcass) and low, (ii; 2.95×10^1 PFU/carcass) titers in the carcass of the *Aa*FAS1-KD mosquitoes (Figure 4.9D). Ye et. al., have shown that when mosquitoes were IT injected with DENV at 10^6PFU, they expectorated DENV

into the saliva at about 10^2 PFU, which is about 100 folds less than mosquitoes that were IT injected with DENV at 10^7 PFU (approximate DENV titer in saliva = 10^4 PFU) [256]. This result indicated that the titer of DENV in saliva is highly dependent on the titer of DENV in the body (disseminated titers). As a result, in our observation, it is likely that mosquitoes with low body titers (group ii) would be inefficient to transmit the virus. This result indicated that the KD of *Aa*FAS1 might have an overall effect in some mosquitoes and may result in a reduction of transmission potential.

Similar to DENV2, we expected to see reduction in CHIKV and ZIKV infection in midguts at early time points following *Aa*FAS1-KD since both viruses are also enveloped, positive-strand RNA viruses. However, we observed only minimal reduction of CHIKV infection and no significant reduction in ZIKV infection in the midguts post *Aa*FAS1-KD (Figure 4.10). The replication kinetics of both CHIKV and ZIKV are faster than DENV2. As a result, the inhibitory effect might only appear at the earlier time points, which we didn't measure. This might be because, at earlier time points, digestion of blood meal has not been completed. As a result, it is possible to measure the input virus particles that remain in the blood meal instead of measuring virions that are released from the infected midgut epithelial cells. Moreover, we can only reduce the expression of *Aa*FAS1 to about 50-70%. The remaining 30-50% of *Aa*FAS1 might be sufficient to support the replication of these arboviruses. Knockout of *Aa*FAS1 may improve the inhibition of arboviral infection, but *Aa*FAS1 is an essential gene. Knockout of this gene may cause death of the mosquitoes.

We observed an increase of *Aa*FAS1 expression upon DENV2 infection in cell culture (Figure 4.12). However, the levels of *Aa*FAS1 expression in response to arbovirus infections *in vivo*, especially when the viruses were delivered via infectious blood meal, is equivocal (Figure 4.13-4.15). Several factors can contribute to these inconclusive results. First, viruses were delivered to the mosquito via blood meal. In this study, we have demonstrated that the expression levels of *Aa*FAS1 can be affected by the food sources (Figure 4.5 and 4.6).

Secondly, mosquitoes have an ability to transport lipids between cells or tissues to maintain homeostasis, while this ability is limited in cell culture. Upon infection in mosquitoes, the need for available lipids might be fulfilled not only via *de novo* lipid biosynthesis by *Aa*FAS*,* but by lipolysis of storage lipids in infected cells, or transportation of lipids from fat body to infected cells [40, 45, 108]. As a result, these phenomena might cause variable levels of *Aa*FAS1 expression from mosquito to mosquito. Blocking lipolysis and lipid transport during DENV infection in mosquitoes may give a clearer understanding of the dynamics of lipid metabolism in mosquito vectors. Another possible explanation is that since this study only observed the response of *Aa*FAS to infection at the transcription level we may have missed expression modulation at the translational level. However, attempts to monitor *Aa*FAS protein expression were unsuccessful because antibodies to mammalian FAS do not recognize mosquito *Aa*FAS. An antibody against mosquito *Aa*FAS is unavailable. It is possible that the regulation of arbovirus infections by FAS in the mosquito vectors happen at the protein or the enzymatic activity levels. This observation was previously reported by Heaton et. al., in human cells [111]. As a result, we did not observe a pattern or striking alterations of *Aa*FAS genes in response to infection.

In this study, we have comprehensively studied the response of the key enzyme of *de novo* lipid biosynthesis, *Aa*FAS, at the transcriptional level. We have shown that although the amino acid sequence of *Aa*FAS showed low identity to human FAS, the functionality of these proteins based on domain structure have likely been conserved through evolutionary processes. We have annotated 7 *Aa*FAS genes from the AaegL5 genome assembly. Two of these seven *Aa*FAS genes were hypothesized to be a single *Aa*FAS gene that was split during the assembly of the contigs. Specific *Aa*FAS genes were found to express differently at different stages of development and did not compensate for each other indicating that different gene orthologues might have a different regulation mechanism. Studies of the response of *Aa*FAS1 in the mosquito vector showed equivocal responses to infection, in contrast to the results in cell

culture. These results have re-emphasized that observations in cell culture may not always represent regulatory mechanisms that occur *in vivo*. Primarily, other homeostatic mechanisms that are limited in cell culture such as intercellular/inter-tissue transportation of metabolites may alter the expected phenotypes. In summary, our in-depth analysis of both *in vitro* and *in vivo* systems in *Ae. aegypti* have provided valuable insight into the complexities of studying gene expression patterns in this organism during viral infection.

CHAPTER 5: SUMMARY AND FUTURE DIRECTIONS

SUMMARY

The current lack of vaccines to protect against dengue, unsuccessful attempts to develop a specific antiviral and the rise of insecticide resistant mosquitoes have moved us to explore novel avenues to interfere with the transmission cycle of DENV. However, to rationally design better control and prevention strategies, we need a more detailed understanding of how these pathogens interact with their human and mosquito hosts to achieve a replicative advantage. In this dissertation, I have explored how biochemical processes in *Ae. aegypti* are altered during dengue virus serotype 2 infection and investigated their potential to be choke-points that control viral transmission from the mosquito vector. The work within represents the first, most comprehensive analysis of the mosquito midgut metabolome contributing to the annotation of how biochemical pathways activate within this tissue.

Briefly, we have optimized protocols and workflow for analyzing the lipidome/metabolome of *Ae. aegypti*. We have established capabilities to study the midgut of the mosquito, which is the initial site of invasion and/or replication of several medically important pathogens. We have identified metabolites in the midgut that were altered in expression levels in response to DENV2 infection and mapped these metabolites to biochemical pathways previously annotated for humans, other mammals, plants, fungi and bacteria. Through these studies, we have contributed to the extensive annotation of metabolic pathways in the mosquito vector which will be available to the public through the Virus Pathogen Resource (VIPR) and VectorBase.

In the context of viral infection, we were able to associate specific metabolic signatures with the dynamics of viral replication in the midgut. There was a clear temporal increase in the

abundance of glycerophospholipids (GPs), with the highest changes in abundance and numbers of GP species observed on day 7 pbm, corresponding to the peak of DENV2 replication in the midgut. Metabolites in the sphingolipid (SP) pathway were also significantly and temporally perturbed, providing us the opportunity to identify and reconstruct for the first time, the majority of the SP pathway in the mosquito. Most of the metabolites that were altered in abundance in response to DENV2 infection belonged to the ceramide *de novo* synthesis and salvage pathways. We also observed a distinct accumulation of medium-chain acyl-carnitines during DENV2 infection. This was likely an indication of mitochondrial overload, leading us to the hypothesis that DENV2 infection may alter the balance of energy homeostasis by increasing demand for energy though β-oxidation.

Directed by the above observations, we validated two important metabolic control hubs within the SP and the *de novo* fatty acid biosynthesis pathways. SPs are important bioactive molecules that could play a role in determining the fate of cells that are infected with DENV2. Some SPs when inserted into membranes induce curvature which could be beneficial to assembly of the viral replication complex. Using inhibitor screening, we found that DENV2 replication was sensitive to inhibition of enzymatic activities along the ceramide (Cer) *de novo* synthesis and salvage pathways only at the step that converts dihydroceramide (DHCer) to Cer. This step is controlled by the sphingolipid Δ-4 desaturase (DEGS) enzyme. Using RNA interference-mediated knockdown of DEGS (DEGS-KD), we demonstrated that the ceramide (Cer) to dihydroceramide (DHCer) ratio was critical for DENV2 infection in Aag2 cells. However, we did not observe a reduction of virus infection upon DEGS-KD in the *Ae. aegypti* mosquito vector.

For the *de novo* fatty acid biosynthesis pathway, we discovered significant differences between the human and *Ae. aegypti* pathways with respect to a key enzyme, fatty acid synthase (FAS). Specifically, *Ae. aegypti* had seven FAS genes compared to the single gene in humans.

Therefore, we annotated and characterized the expression of these seven fatty acid synthase genes in *Ae. aegypti* (*Aa*FAS1-6 and *Aa*FAS-like). We observed that *Aa*FAS6 and *Aa*FAS-like likely belonged to the same gene but were split during genome sequencing and assembly. Different *Aa*FAS genes were expressed differently at the distinct stages of mosquito development. *Aa*FAS1 has the highest amino acid similarity to human FAS and expressed predominantly in adult female mosquitoes. Loss-of-function studies showed that there was no compensation from other *Aa*FAS genes when expression of *Aa*FAS1 was knocked down. Transient KD of *Aa*FAS1 expression impaired DENV2 replication *in vitro* and dampened the infection in the midgut at an early time point. However, at later time points, we could not technically sustain the reduction in *Aa*FAS activity, which complicated the analysis of its impact on DENV replication.

CONTRIBUTIONS TO THE FIELD OF VECTOR BIOLOGY: PROBLEMS ENCOUNTERED AND LESSONS LEARNED

In this dissertation, we identified two choke points from two biochemical pathways and showed that these choke points were critical for DENV2 infection *in vitro*. However, we only observed a minimal inhibition of DENV2 infection *in vivo*. There are several explanations for this phenomenon. The first is that limitations in the efficacy or the stability of the dsRNA or chemical inhibitors used to control the specific metabolic hubs within mosquito tissues may have dampened their impacts on the phenotype. These technical issues could be mitigated by improvement of the design of inhibitors or use of more complex technologies such as CRISPR-Cas9 that would provide more sustainable losses in function of enzymes of interest. The second is related to the complexity of the metabolic homeostasis of the vector itself which is harder to manipulate. The heterogeneous cell types in the mosquito and the ability to transport lipids between cells or tissues play a key role in maintaining metabolic homeostasis in mosquitoes.

Therefore, when the *de novo* fatty acid biosynthesis pathway of the mosquitoes was systemically knocked down by dsRNA, the fat body (tissue that stores lipids) could have provided fatty acids through lipolysis of lipid stores and transported these fatty acids to tissues in need, such as the midgut. Therefore, because of this extracellular supply, blocking availability of fatty acids (as well as other important lipids) by inhibiting of *Aa*FAS could have been ineffective, allowing the virus to replicate in the midgut. Therefore, in order to limit infection by targeting metabolic choke points in the mosquito vector, we may also need to eliminate the ability of cells within the midgut to acquire extracellular metabolites that could supply the needs of virus replication. These observations from our study, therefore, shed light into processes such as lipid transport that also need to be investigated in concert with *de novo* fatty acid biosynthesis in order to develop metabolic choke-points to limit viral transmission by the mosquito.

LONG-TERM IMPACT

The overarching goal of these studies was to identify metabolic choke points that are critical for DENV2 infection and replication in the mosquito vectors and interfere with these control points as an avenue to block viral replication and/or transmission. Modulation of mosquito metabolic control points can potentially reduce both vector competence and vectorial capacity. These factors can be manipulated to reduce the chance that the vector can transmit these viruses.

Vector competence is the ability of the vector to acquire, maintain and transmit pathogens [29]. In our studies, we have shown that manipulation of metabolic enzymes, FAS and DEGS, using loss-of-function approaches, resulted in a reduction in DENV2 replication in mosquito cells. However, a strong inhibition of virus replication *in vivo* was not successfully demonstrated, Possibly, better design of delivery methods, improving the stability and the

efficacy of inhibitors or dsRNA treatments can assist in implementing this strategy in transmission control.

Vectorial capacity is an overall transmission of a pathogen by a vector population. According to MacDonald's model, vectorial capacity is influenced by i) the vector density in relation to the host, ii) human biting rate, iii) daily mosquito survival rate, iv) vector competence and v) the extrinsic incubation period [257]. The values of some of these factors can be reduced when the balance of the metabolic environment is perturbed. Manipulation of the host metabolic environment can create unfavorable environments for the virus to replicate and thus can reduce not only vector competence but can also lengthen the time that pathogens require to replicate before they can be transmitted. In addition, changing the metabolic balance within the vector often times can come with a potential reduction of vector fitness. This is, in fact, beneficial because it can shorten the lifespan of the vector (reduce the daily mosquito survival rate) which also shorten the time that the vector carries and can transmit the pathogens. In this study, we only focused on the modulation of metabolic control points and their effects on the vector competence (one out of five components that contribute to vectorial capacity). However, studying the effect of manipulation of metabolic pathways on vectorial capacity (disregarding virus infection) is, in fact, also useful in identifying effective vector control strategies.

Detailed knowledge of vector metabolism can also be used to elucidate the mechanisms behind existing control strategies. *Wolbachia* (*Wol*) is an endosymbiont bacterium that is found in several insects but not in *Ae. aegypti.* However, researchers have generated *Ae. aegypti* lines that are infected by *Wol* and found that it can inhibit DENV replication [23, 256]. Currently, the Global Mosquito Program is employing these mosquitoes to replace the natural *Wol*-free populations as a means to reduce DENV transmission [258-260]. The mechanisms of how *Wol* prevents DENV replication and transmission in these mosquitoes are, however, unknown. It is hypothesized that it may due to metabolic competition between Wol and the virus. We are

currently investigating these options to better understand the metabolic requirements of *Wol* that might overlap or oppose the requirements of DENV replication in *Ae. aegypti*.

REFERENCES

1. Kraemer MU, Sinka ME, Duda KA, Mylne AQ, Shearer FM, Barker CM, et al. The global distribution of the arbovirus vectors Aedes aegypti and Ae. albopictus. Elife. 2015;4:e08347. Epub 2015/07/01. doi: 10.7554/eLife.08347. PubMed PMID: 26126267; PubMed Central PMCID: PMC4493616.

2. Brown JE, Evans BR, Zheng W, Obas V, Barrera-Martinez L, Egizi A, et al. Human impacts have shaped historical and recent evolution in Aedes aegypti, the dengue and yellow fever mosquito. Evolution. 2014;68(2):514-25. Epub 2013/10/12. doi: 10.1111/evo.12281. PubMed PMID: 24111703; PubMed Central PMCID: PMC3946797.

3. Scott TW, Takken W. Feeding strategies of anthropophilic mosquitoes result in increased risk of pathogen transmission. Trends Parasitol. 2012;28(3):114-21. Epub 2012/02/04. doi: 10.1016/j.pt.2012.01.001 S1471-4922(12)00004-9 [pii]. PubMed PMID: 22300806.

4. Brady OJ, Golding N, Pigott DM, Kraemer MU, Messina JP, Reiner RC, Jr., et al. Global temperature constraints on Aedes aegypti and Ae. albopictus persistence and competence for dengue virus transmission. Parasit Vectors. 2014;7:338. Epub 2014/07/24. doi: 10.1186/1756-3305-7-338
1756-3305-7-338 [pii]. PubMed PMID: 25052008; PubMed Central PMCID: PMC4148136.

5. Khormi HM, Kumar L. Climate change and the potential global distribution of Aedes aegypti: spatial modelling using GIS and CLIMEX. Geospat Health. 2014;8(2):405-15. Epub 2014/06/04. doi: 10.4081/gh.2014.29. PubMed PMID: 24893017.

6. Mweya CN, Kimera SI, Stanley G, Misinzo G, Mboera LE. Climate Change Influences Potential Distribution of Infected Aedes aegypti Co-Occurrence with Dengue Epidemics Risk Areas in Tanzania. PLoS One. 2016;11(9):e0162649. Epub 2016/09/30. doi: 10.1371/journal.pone.0162649
PONE-D-16-09436 [pii]. PubMed PMID: 27681327; PubMed Central PMCID: PMC5040426.

7. Perera R, Kuhn RJ. Structural proteomics of dengue virus. Curr Opin Microbiol. 2008;11(4):369-77. Epub 2008/07/23. doi: 10.1016/j.mib.2008.06.004
S1369-5274(08)00089-1 [pii]. PubMed PMID: 18644250; PubMed Central PMCID: PMC2581888.

8. Welsch S, Miller S, Romero-Brey I, Merz A, Bleck CK, Walther P, et al. Composition and three-dimensional architecture of the dengue virus replication and assembly sites. Cell Host Microbe. 2009;5(4):365-75. Epub 2009/04/22. doi: 10.1016/j.chom.2009.03.007
S1931-3128(09)00098-5 [pii]. PubMed PMID: 19380115.

9. Girard YA, Popov V, Wen J, Han V, Higgs S. Ultrastructural Study of West Nile Virus Pathogenesis in Culex pipiens quinquefasciatus (Diptera: Culicidae). Journal of Medical Entomology 2005;42(3). Epub 444.

10. Kuhn RJ, Zhang W, Rossmann MG, Pletnev SV, Corver J, Lenches E, et al. Structure of dengue virus: implications for flavivirus organization, maturation, and fusion. Cell. 2002;108(5):717-25. Epub 2002/03/15. doi: S0092867402006608 [pii]. PubMed PMID: 11893341; PubMed Central PMCID: PMC4152842.

11. Organization WH. Dengue: Guildlines for Diagnosis, Treatment, Prevention and Control.: http://www.who.int/tdr/publications/documents/dengue-diagnosis.pdf; 2009.

12. Bhatt S, Gething PW, Brady OJ, Messina JP, Farlow AW, Moyes CL, et al. The global distribution and burden of dengue. Nature. 2013;496(7446):504-7. Epub 2013/04/09. doi: 10.1038/nature12060

nature12060 [pii]. PubMed PMID: 23563266; PubMed Central PMCID: PMC3651993.
13. Sabin AB. Research on dengue during World War II. Am J Trop Med Hyg. 1952;1(1):30-50. Epub 1952/01/01. PubMed PMID: 14903434.

14. Katzelnick LC, Gresh L, Halloran ME, Mercado JC, Kuan G, Gordon A, et al. Antibody-dependent enhancement of severe dengue disease in humans. Science. 2017;358(6365):929-32. Epub 2017/11/04. doi: 10.1126/science.aan6836
science.aan6836 [pii]. PubMed PMID: 29097492; PubMed Central PMCID: PMC5858873.

15. Halstead SB. Observations related to pathogensis of dengue hemorrhagic fever. VI. Hypotheses and discussion. Yale J Biol Med. 1970;42(5):350-62. Epub 1970/04/01. PubMed PMID: 5419208; PubMed Central PMCID: PMC2591710.

16. Organization WH. Handbook for clinical management of dengue 2012.
17. Whitehead SS, Blaney JE, Durbin AP, Murphy BR. Prospects for a dengue virus vaccine. Nat Rev Microbiol. 2007;5(7):518-28. Epub 2007/06/15. doi: nrmicro1690 [pii]
10.1038/nrmicro1690. PubMed PMID: 17558424.

18. Guy B, Guirakhoo F, Barban V, Higgs S, Monath TP, Lang J. Preclinical and clinical development of YFV 17D-based chimeric vaccines against dengue, West Nile and Japanese encephalitis viruses. Vaccine. 2010;28(3):632-49. Epub 2009/10/08. doi: 10.1016/j.vaccine.2009.09.098
S0264-410X(09)01445-5 [pii]. PubMed PMID: 19808029.

19. Hadinegoro SR, Arredondo-Garcia JL, Capeding MR, Deseda C, Chotpitayasunondh T, Dietze R, et al. Efficacy and Long-Term Safety of a Dengue Vaccine in Regions of Endemic Disease. N Engl J Med. 2015;373(13):1195-206. Epub 2015/07/28. doi: 10.1056/NEJMoa1506223. PubMed PMID: 26214039.

20. Flasche S, Jit M, Rodríguez-Barraquer I, Coudeville L, Recker M, Koelle K, et al. Comparative modelling of dengue vaccine public health impact (CMDVI). 2016.

21. Flores AE, Ponce G, Silva BG, Gutierrez SM, Bobadilla C, Lopez B, et al. Wide spread cross resistance to pyrethroids in Aedes aegypti (Diptera: Culicidae) from Veracruz state Mexico. J Econ Entomol. 2013;106(2):959-69. Epub 2013/06/22. PubMed PMID: 23786088; PubMed Central PMCID: PMC3980443.

22. Francis S, Saavedra-Rodriguez K, Perera R, Paine M, Black WCt, Delgoda R. Insecticide resistance to permethrin and malathion and associated mechanisms in Aedes

aegypti mosquitoes from St. Andrew Jamaica. PLoS One. 2017;12(6):e0179673. Epub 2017/06/27. doi: 10.1371/journal.pone.0179673
PONE-D-17-13148 [pii]. PubMed PMID: 28650966; PubMed Central PMCID: PMC5484480.

23. Moreira LA, Iturbe-Ormaetxe I, Jeffery JA, Lu G, Pyke AT, Hedges LM, et al. A Wolbachia symbiont in Aedes aegypti limits infection with dengue, Chikungunya, and Plasmodium. Cell. 2009;139(7):1268-78. Epub 2010/01/13. doi: 10.1016/j.cell.2009.11.042
S0092-8674(09)01500-1 [pii]. PubMed PMID: 20064373.

24. Hill CA, Kafatos FC, Stansfield SK, Collins FH. Arthropod-borne diseases: vector control in the genomics era. Nat Rev Microbiol. 2005;3(3):262-8. Epub 2005/02/11. doi: nrmicro1101 [pii]
10.1038/nrmicro1101. PubMed PMID: 15703759.

25. von Seidlein L, Kekule AS, Strickman D. Novel Vector Control Approaches: The Future for Prevention of Zika Virus Transmission? PLoS Med. 2017;14(1):e1002219. Epub 2017/01/18. doi: 10.1371/journal.pmed.1002219
PMEDICINE-D-16-03976 [pii]. PubMed PMID: 28095418; PubMed Central PMCID: PMC5240911 stipend as a specialty consulting editor for PLOS Medicine and serves on the journal's editorial board.

26. Alphey L, Benedict M, Bellini R, Clark GG, Dame DA, Service MW, et al. Sterile-insect methods for control of mosquito-borne diseases: an analysis. Vector Borne Zoonotic Dis. 2010;10(3):295-311. Epub 2009/09/04. doi: 10.1089/vbz.2009.0014. PubMed PMID: 19725763; PubMed Central PMCID: PMC2946175.

27. Franz AW, Sanchez-Vargas I, Adelman ZN, Blair CD, Beaty BJ, James AA, et al. Engineering RNA interference-based resistance to dengue virus type 2 in genetically modified Aedes aegypti. Proc Natl Acad Sci U S A. 2006;103(11):4198-203. Epub 2006/03/16. doi: 0600479103 [pii]
10.1073/pnas.0600479103. PubMed PMID: 16537508; PubMed Central PMCID: PMC1449670.

28. Salazar MI, Richardson JH, Sánchez-Vargas I, Olson KE, Beaty BJ. Dengue virus type 2: replication and tropisms in orally infected Aedes aegypti mosquitoes BMC Biology. 2007;7(9).
29. Black WCt, Bennett KE, Gorrochotegui-Escalante N, Barillas-Mury CV, Fernandez-Salas I, de Lourdes Munoz M, et al. Flavivirus susceptibility in Aedes aegypti. Arch Med Res. 2002;33(4):379-88. Epub 2002/09/18. doi: S0188-4409(02)00373-9 [pii]. PubMed PMID: 12234528.

30. Franz AW, Kantor AM, Passarelli AL, Clem RJ. Tissue Barriers to Arbovirus Infection in Mosquitoes. Viruses. 2015;7(7):3741-67. Epub 2015/07/18. doi: 10.3390/v7072795
v7072795 [pii]. PubMed PMID: 26184281; PubMed Central PMCID: PMC4517124.

31. Whitfield SG, Murphy FA, Sudia WD. St. Louis encephalitis virus: an ultrastructural study of infection in a mosquito vector. Virology. 1973;56(1):70-87. Epub 1973/11/01. doi: 0042-6822(73)90288-2 [pii]. PubMed PMID: 4583310.

32. Raquin V, Wannagat M, Zouache K, Legras-Lachuer C, Moro CV, Mavingui P. Detection of dengue group viruses by fluorescence in situ hybridization. Parasit Vectors. 2012;5:243. Epub 2012/11/01. doi: 10.1186/1756-3305-5-243
1756-3305-5-243 [pii]. PubMed PMID: 23110979; PubMed Central PMCID: PMC3507901.

33. Dettloff M, Wittwer D, Weise C, Wiesner A. Lipophorin of lower density is formed during immune responses in the lepidopteran insect Galleria mellonella. Cell Tissue Res. 2001;306(3):449-58. Epub 2001/12/06. doi: 10.1007/s00441-001-0468-9. PubMed PMID: 11735046.

34. Olofsson SO, Bostrom P, Andersson L, Rutberg M, Perman J, Boren J. Lipid droplets as dynamic organelles connecting storage and efflux of lipids. Biochim Biophys Acta. 2009;1791(6):448-58. Epub 2008/09/09. doi: 10.1016/j.bbalip.2008.08.001 S1388-1981(08)00150-9 [pii]. PubMed PMID: 18775796.

35. Ziegler R. Changes in lipid and carbohydrate metabolism during starvation in adult Manduca sexta. J Comp Physiol B. 1991;161(2):125-31. Epub 1991/01/01. PubMed PMID: 1869693.

36. Zhou GL, Pennington JE, Wells MA. Utilization of pre-existing energy stores of female Aedes aegypti mosquitoes during the first gonotrophic cycle. Insect Biochemistry and Molecular Biology. 2004;34(9):919-25. doi: DOI 10.1016/j.ibmb.2004.05.009. PubMed PMID: ISI:000224001200004.

37. Arrese EL, Soulages JL. Insect fat body: energy, metabolism, and regulation. Annu Rev Entomol. 2010;55:207-25. Epub 2009/09/04. doi: 10.1146/annurev-ento-112408-085356. PubMed PMID: 19725772; PubMed Central PMCID: PMC3075550.

38. Zhou G, Miesfeld RL. Energy metabolism during diapause in Culex pipiens mosquitoes. J Insect Physiol. 2009;55(1):40-6. Epub 2008/11/11. doi: 10.1016/j.jinsphys.2008.10.002 S0022-1910(08)00215-1 [pii]. PubMed PMID: 18992753; PubMed Central PMCID: PMC2646908.

39. Sushchik NN, Yurchenko YA, Gladyshev MI, Belevich OE, Kalachova GS, Kolmakova AA. Comparison of fatty acid contents and composition in major lipid classes of larvae and adults of mosquitoes (Diptera: Culicidae) from a steppe region. Insect Sci. 2013;20(5):585-600. Epub 2013/08/21. doi: 10.1111/j.1744-7917.2012.01582.x. PubMed PMID: 23956110.

40. Ziegler R, Van Antwerpen R. Lipid uptake by insect oocytes. Insect Biochem Mol Biol. 2006;36(4):264-72. Epub 2006/03/23. doi: S0965-1748(06)00006-3 [pii] 10.1016/j.ibmb.2006.01.014. PubMed PMID: 16551540.

41. Kaufmann C, Brown MR. Regulation of carbohydrate metabolism and flight performance by a hypertrehalosaemic hormone in the mosquito Anopheles gambiae. J Insect Physiol. 2008;54(2):367-77. Epub 2007/12/08. doi: S0022-1910(07)00240-5 [pii] 10.1016/j.jinsphys.2007.10.007. PubMed PMID: 18062987; PubMed Central PMCID: PMC2267862.

42. Ziegler R. Lipid synthesis by overies and fat body of Aedes aegypti (Diptera: Culicidae). European Journal of Entomology. 1997;94:385-91.

43. Ziegler R, Ibrahim MM. Formation of lipid reserves in fat body and eggs of the yellow fever mosquito, Aedes aegypti. Journal of Insect Physiology. 2001;47(6):623-7. doi: Doi 10.1016/S0022-1910(00)00158-X. PubMed PMID: ISI:000168207100011.

44. Beenakkers AM, Van der Horst DJ, Van Marrewijk WJ. Insect lipids and lipoproteins, and their role in physiological processes. Prog Lipid Res. 1985;24(1):19-67. Epub 1985/01/01. PubMed PMID: 3916237.

45. Pennington JE, Nussenzveig RH, Van Heusden MC. Lipid transfer from insect fat body to lipophorin: comparison between a mosquito triacylglycerol-rich lipophorin and a sphinx moth diacylglycerol-rich lipophorin. J Lipid Res. 1996;37(5):1144-52. Epub 1996/05/01. PubMed PMID: 8725165.

46. Pennington JE, Wells MA. Triacylglycerol-rich lipophorins are found in the dipteran infraorder Culicomorpha, not just in mosquitoes. J Insect Sci. 2002;2:15. Epub 2004/09/30. PubMed PMID: 15455049; PubMed Central PMCID: PMC355915.

47. Atella GC, Shahabuddin M. Differential partitioning of maternal fatty acid and phospholipid in neonate mosquito larvae. J Exp Biol. 2002;205(Pt 23):3623-30. Epub 2002/11/01. PubMed PMID: 12409488.

48. Dadd R, Kleinjan J, Stanley-Samuelson D. Polyunsaturated fatty acids of mosquitos reared with single dietary polyunsaturates. Insect Biochemistry. 1987;17(1):7-16.

49. Dadd RH, Kleinjan JE. Essential fatty acid for the mosquito Culex pipiens: arachidonic acid. J Insect Physiol. 1979;25(6):495-502. Epub 1979/01/01. doi: S0022-1910(79)80008-6 [pii]. PubMed PMID: 489998.

50. Stanley DW, Miller JS. Eicosanoid actions in insect cellular immune functions. Entomologia Experimentalis Et Applicata. 2006;119(1):1-13. doi: DOI 10.1111/j.1570-7458.2006.00406.x. PubMed PMID: ISI:000236022600001.

51. Jenkin HM, McMeans E, Anderson LE, Yang TK. Comparison of phospholipid composition of Aedes aegypti and Aedes albopictus cells obtained from logarithmic and stationary phases of growth. Lipids. 1975;10(11):686-94. Epub 1975/11/01. PubMed PMID: 1196018.

52. Lehane M. Biology of Blood-Sucking Insects: HarperCollins Publisher; 1991.

53. Sanders HR, Evans AM, Ross LS, Gill SS. Blood meal induces global changes in midgut gene expression in the disease vector, Aedes aegypti. Insect Biochem Mol Biol. 2003;33(11):1105-22. Epub 2003/10/18. doi: S0965174803001243 [pii]. PubMed PMID: 14563362.

54. Zhou GL, Flowers M, Friedrich K, Horton J, Pennington J, Wells MA. Metabolic fate of [C-14]-labeled meal protein amino acids in Aedes aegypti mosquitoes. Journal of Insect Physiology. 2004;50(4):337-49. doi: DOI 10.1016/j.jinsphys.2004.02.003. PubMed PMID: ISI:000221212400010.

55. Troy S, Anderson WA, Spielman A. Lipid content of maturing ovaries of Aedes aegypti mosquitoes. Comp Biochem Physiol B. 1975;50(3):457-61. Epub 1975/03/15. PubMed PMID: 1116351.

56. Hagedorn HH, Shapiro JP, Hanaoka K. Ovarian ecdysone secretion is controlled by a brain hormone in an adult mosquito. Nature. 1979;282(5734):92-4. Epub 1979/11/01. PubMed PMID: 503195.

57. Alabaster A, Isoe J, Zhou G, Lee A, Murphy A, Day WA, et al. Deficiencies in acetyl-CoA carboxylase and fatty acid synthase 1 differentially affect eggshell formation and blood meal digestion in Aedes aegypti. Insect Biochem Mol Biol. 2011;41(12):946-55. Epub 2011/10/06. doi: 10.1016/j.ibmb.2011.09.004
S0965-1748(11)00175-5 [pii]. PubMed PMID: 21971482; PubMed Central PMCID: PMC3210400.

58. Perera R, Riley C, Isaac G, Hopf-Jannasch AS, Moore RJ, Weitz KW, et al. Dengue virus infection perturbs lipid homeostasis in infected mosquito cells. PLoS Pathog. 2012;8(3):e1002584. Epub 2012/03/30. doi: 10.1371/journal.ppat.1002584
PPATHOGENS-D-11-02103 [pii]. PubMed PMID: 22457619; PubMed Central PMCID: PMC3310792.

59. Hammad LA, Cooper BS, Fisher NP, Montooth KL, Karty JA. Profiling and quantification of Drosophila melanogaster lipids using liquid chromatography/mass spectrometry. Rapid Commun Mass Spectrom. 2011;25(19):2959-68. Epub 2011/09/14. doi: 10.1002/rcm.5187. PubMed PMID: 21913275.

60. Mcmeans E, Yang TK, Anderson LE, Jenkin HM. Comparison of Lipid-Composition of Aedes-Aegypti and Aedes-Albopictus Cells Obtained from Logarithmic and Stationary Phases of Growth. Lipids. 1975;10(2):99-104. doi: Doi 10.1007/Bf02532163. PubMed PMID: ISI:A1975V714200008.

61. Chotiwan N, Andre BG, Sanchez-Vargas I, Islam MN, Grabowski JM, Hopf-Jannasch A, et al. Dynamic remodeling of lipids coincides with dengue virus replication in the midgut of Aedes aegypti mosquitoes. PLoS Pathog. 2018;14(2):e1006853. Epub 2018/02/16. doi: 10.1371/journal.ppat.1006853
PPATHOGENS-D-16-00829 [pii]. PubMed PMID: 29447265; PubMed Central PMCID: PMC5814098.

62. Guan XL, Cestra G, Shui G, Kuhrs A, Schittenhelm RB, Hafen E, et al. Biochemical membrane lipidomics during Drosophila development. Dev Cell. 2013;24(1):98-111. Epub 2012/12/25. doi: 10.1016/j.devcel.2012.11.012
S1534-5807(12)00532-1 [pii]. PubMed PMID: 23260625.

63. Khalil SM, Rompp A, Pretzel J, Becker K, Spengler B. Phospholipid Topography of Whole-Body Sections of the Anopheles stephensi Mosquito, Characterized by High-Resolution Atmospheric-Pressure Scanning Microprobe Matrix-Assisted Laser Desorption/Ionization Mass Spectrometry Imaging. Anal Chem. 2015;87(22):11309-16. Epub 2015/10/23. doi: 10.1021/acs.analchem.5b02781. PubMed PMID: 26491885.

64. Scheitz CJ, Guo Y, Early AM, Harshman LG, Clark AG. Heritability and inter-population differences in lipid profiles of Drosophila melanogaster. PLoS One. 2013;8(8):e72726. Epub 2013/09/10. doi: 10.1371/journal.pone.0072726
PONE-D-13-02124 [pii]. PubMed PMID: 24013349; PubMed Central PMCID: PMC3754969.

65. Dadd RH. Essential Fatty-Acids for the Mosquito Culex-Pipiens. J Nutr. 1980;110(6):1152-60. PubMed PMID: ISI:A1980JV95800009.

66. Giraldo-Calderon GI, Emrich SJ, MacCallum RM, Maslen G, Dialynas E, Topalis P, et al. VectorBase: an updated bioinformatics resource for invertebrate vectors and other organisms related with human diseases. Nucleic Acids Res. 2015;43(Database issue):D707-13. Epub 2014/12/17. doi: 10.1093/nar/gku1117
gku1117 [pii]. PubMed PMID: 25510499; PubMed Central PMCID: PMC4383932.

67. Clark AJ, Bloch K. Conversion of ergosterol to 22-de-hydrocholesterol in Blattella germanica. J Biol Chem. 1959;234:2589-94. Epub 1959/10/01. PubMed PMID: 13810424.

68. Clayton RB, Edwards AM, Bloch K. Biosynthesis of cholesterol in an insect, silverfish (Ctenolepisma sp.). Nature. 1962;195:1125-6. Epub 1962/09/15. PubMed PMID: 13879846.

69. Cooper RA. Influence of increased membrane cholesterol on membrane fluidity and cell function in human red blood cells. J Supramol Struct. 1978;8(4):413-30. Epub 1978/01/01. doi: 10.1002/jss.400080404. PubMed PMID: 723275.

70. Spielman A, Gwadz RW, Anderson WA. Ecdysone-initiated ovarian development in mosquitoes. J Insect Physiol. 1971;17(10):1807-14. Epub 1971/10/01. doi: 0022-1910(71)90125-9 [pii]. PubMed PMID: 4398560.

71. Yamanaka N, Rewitz KF, O'Connor MB. Ecdysone control of developmental transitions: lessons from Drosophila research. Annual Review of Entomology. 2013;58:497-516. Epub 2012/10/18. doi: 10.1146/annurev-ento-120811-153608. PubMed PMID: 23072462; PubMed Central PMCID: PMC4060523.

72. Douglas AE. The microbial dimension in insect nutritional ecology. Funct Ecol. 2009;23(1):38-47. doi: 10.1111/j.1365-2435.2008.01442.x. PubMed PMID: ISI:000262510400005.

73. Clayton RB. The Utilization of Sterols by Insects. J Lipid Res. 1964;5:3-19. Epub 1964/01/01. PubMed PMID: 14173327.

74. Jouni ZE, Zamora J, Wells MA. Absorption and tissue distribution of cholesterol in Manduca sexta. Arch Insect Biochem Physiol. 2002;49(3):167-75. Epub 2002/02/22. doi: 10.1002/arch.10017 [pii]
10.1002/arch.10017. PubMed PMID: 11857677.

75. Chino H, Gilbert LI. Uptake and Transport of Cholesterol by Haemolymph Lipoproteins. Insect Biochemistry. 1971;1(3):337-&. doi: Doi 10.1016/0020-1790(71)90051-5. PubMed PMID: ISI:A1971K857000011.

76. Vyazunova I, Lan Q. Yellow fever mosquito sterol carrier protein-2 gene structure and transcriptional regulation. Insect Mol Biol. 2010;19(2):205-15. Epub 2009/12/17. doi: 10.1111/j.1365-2583.2009.00959.x
IMB959 [pii]. PubMed PMID: 20002221; PubMed Central PMCID: PMC2862845.

77. Krebs KC, Lan Q. Isolation and expression of a sterol carrier protein-2 gene from the yellow fever mosquito, Aedes aegypti. Insect Mol Biol. 2003;12(1):51-60. Epub 2003/01/25. doi: 386 [pii]. PubMed PMID: 12542635.

78. Fu Q, Inankur B, Yin J, Striker R, Lan Q. Sterol Carrier Protein 2, a Critical Host Factor for Dengue Virus Infection, Alters the Cholesterol Distribution in Mosquito Aag2 Cells. J Med Entomol. 2015;52(5):1124-34. Epub 2015/09/04. doi: 10.1093/jme/tjv101
tjv101 [pii]. PubMed PMID: 26336241.

79. Stillwell W. Bioactive Lipids. Introduction to Biological Membranes: Composition, Structure and Function, 2nd Edition. 2016:453-78. doi: 10.1016/B978-0-444-63772-7.00020-8. PubMed PMID: ISI:000430059800021.

80. Stanley D, Shapiro M. Eicosanoid biosynthesis inhibitors increase the susceptibility of Lymantria dispar to nucleopolyhedrovirus LdMNPV. J Invertebr Pathol. 2007;95(2):119-24. Epub 2007/03/28. doi: S0022-2011(07)00041-9 [pii]
10.1016/j.jip.2007.02.002. PubMed PMID: 17386933.

81. Blomquist GJ, Borgeson CE, Vundla M. Polyunsaturated Fatty-Acids and Eicosanoids in Insects. Insect Biochemistry. 1991;21(1):99-106. doi: Doi 10.1016/0020-1790(91)90069-Q. PubMed PMID: ISI:A1991FD19700013.

82. Xu J, Morisseau C, Yang J, Mamatha DM, Hammock BD. Epoxide hydrolase activities and epoxy fatty acids in the mosquito Culex quinquefasciatus. Insect Biochem Mol Biol. 2015;59:41-9. Epub 2015/02/18. doi: 10.1016/j.ibmb.2015.02.004
S0965-1748(15)00027-2 [pii]. PubMed PMID: 25686802; PubMed Central PMCID: PMC4387068.

83. Ramirez JL, de Almeida Oliveira G, Calvo E, Dalli J, Colas RA, Serhan CN, et al. A mosquito lipoxin/lipocalin complex mediates innate immune priming in Anopheles gambiae. Nat Commun. 2015;6:7403. Epub 2015/06/24. doi: 10.1038/ncomms8403
ncomms8403 [pii]. PubMed PMID: 26100162; PubMed Central PMCID: PMC4542143.

84. Petzel DH, Stanleysamuelson DW. Inhibition of Eicosanoid Biosynthesis Modulates Basal Fluid Secretion in the Malpighian Tubules of the Yellow-Fever Mosquito (Aedes-Aegypti). Journal of Insect Physiology. 1992;38(1):1-8. doi: Doi 10.1016/0022-1910(92)90016-7. PubMed PMID: ISI:A1992HG54700001.

85. Burlandy FM, Ferreira DF, Rebello MA. Inhibition of vesicular stomatitis virus replication by prostaglandin A1 in Aedes albopictus cells. Z Naturforsch C. 2004;59(1-2):127-31. Epub 2004/03/17. PubMed PMID: 15018065.

86. Lin CK, Tseng CK, Wu YH, Liaw CC, Lin CY, Huang CH, et al. Cyclooxygenase-2 facilitates dengue virus replication and serves as a potential target for developing antiviral agents. Sci Rep. 2017;7:44701. Epub 2017/03/21. doi: 10.1038/srep44701
srep44701 [pii]. PubMed PMID: 28317866; PubMed Central PMCID: PMC5357798.

87. Wu WL, Ho LJ, Chang DM, Chen CH, Lai JH. Triggering of DC migration by dengue virus stimulation of COX-2-dependent signaling cascades in vitro highlights the significance of these cascades beyond inflammation. Eur J Immunol. 2009;39(12):3413-22. Epub 2009/10/29. doi: 10.1002/eji.200939306. PubMed PMID: 19862774.

88. Melo CF, de Oliveira DN, Lima EO, Guerreiro TM, Esteves CZ, Beck RM, et al. A Lipidomics Approach in the Characterization of Zika-Infected Mosquito Cells: Potential Targets for Breaking the Transmission Cycle. PLoS One. 2016;11(10):e0164377. Epub 2016/10/11. doi: 10.1371/journal.pone.0164377
PONE-D-16-28918 [pii]. PubMed PMID: 27723844; PubMed Central PMCID: PMC5056752.

89. Junjhon J, Pennington JG, Edwards TJ, Perera R, Lanman J, Kuhn RJ. Ultrastructural characterization and three-dimensional architecture of replication sites in dengue virus-infected mosquito cells. J Virol. 2014;88(9):4687-97. Epub 2014/02/14. doi: 10.1128/JVI.00118-14
JVI.00118-14 [pii]. PubMed PMID: 24522909; PubMed Central PMCID: PMC3993787.

90. Ishak R, Tovey DG, Howard CR. Morphogenesis of yellow fever virus 17D in infected cell cultures. J Gen Virol. 1988;69 (Pt 2):325-35. Epub 1988/02/01. doi: 10.1099/0022-1317-69-2-325. PubMed PMID: 3339329.

91. Ng ML. Ultrastructural studies of Kunjin virus-infected Aedes albopictus cells. J Gen Virol. 1987;68 (Pt 2):577-82. Epub 1987/02/01. doi: 10.1099/0022-1317-68-2-577. PubMed PMID: 3029292.

92. Girard YA, Schneider BS, McGee CE, Wen J, Han VC, Popov V, et al. Salivary gland morphology and virus transmission during long-term cytopathologic West Nile virus infection in Culex mosquitoes. Am J Trop Med Hyg. 2007;76(1):118-28. Epub 2007/01/27. doi: 76/1/118 [pii]. PubMed PMID: 17255239.

93. Miller S, Kastner S, Krijnse-Locker J, Buhler S, Bartenschlager R. The non-structural protein 4A of dengue virus is an integral membrane protein inducing membrane alterations in a 2K-regulated manner. J Biol Chem. 2007;282(12):8873-82. Epub 2007/02/06. doi: M609919200 [pii]
10.1074/jbc.M609919200. PubMed PMID: 17276984.

94. Roosendaal J, Westaway EG, Khromykh A, Mackenzie JM. Regulated cleavages at the West Nile virus NS4A-2K-NS4B junctions play a major role in rearranging cytoplasmic membranes and Golgi trafficking of the NS4A protein. J Virol. 2006;80(9):4623-32. Epub 2006/04/14. doi: 80/9/4623 [pii]
10.1128/JVI.80.9.4623-4632.2006. PubMed PMID: 16611922; PubMed Central PMCID: PMC1472005.

95. Mackenzie JM, Khromykh AA, Parton RG. Cholesterol manipulation by West Nile virus perturbs the cellular immune response. Cell Host Microbe. 2007;2(4):229-39. Epub 2007/11/17. doi: S1931-3128(07)00218-1 [pii]
10.1016/j.chom.2007.09.003. PubMed PMID: 18005741.

96. Rothwell C, Lebreton A, Young Ng C, Lim JY, Liu W, Vasudevan S, et al. Cholesterol biosynthesis modulation regulates dengue viral replication. Virology. 2009;389(1-2):8-19. Epub 2009/05/08. doi: 10.1016/j.virol.2009.03.025
S0042-6822(09)00202-5 [pii]. PubMed PMID: 19419745.

97. Carro AC, Damonte EB. Requirement of cholesterol in the viral envelope for dengue virus infection. Virus Res. 2013;174(1-2):78-87. Epub 2013/03/23. doi: 10.1016/j.virusres.2013.03.005
S0168-1702(13)00080-4 [pii]. PubMed PMID: 23517753.

98. Lee CJ, Lin HR, Liao CL, Lin YL. Cholesterol effectively blocks entry of flavivirus. J Virol. 2008;82(13):6470-80. Epub 2008/05/02. doi: 10.1128/JVI.00117-08
JVI.00117-08 [pii]. PubMed PMID: 18448543; PubMed Central PMCID: PMC2447114.

99. Clayton RB, Hinkle PC, Smith DA, Edwards AM. The Intestinal Absorption of Cholesterol, Its Esters and Some Related Sterols and Analogues in the Roac, Eurycotis Floridana. Comp Biochem Physiol. 1964;11:333-50. Epub 1964/04/01. PubMed PMID: 14167530.

100. Jupatanakul N, Sim S, Dimopoulos G. Aedes aegypti ML and Niemann-Pick type C family members are agonists of dengue virus infection. Dev Comp Immunol. 2014;43(1):1-9. Epub 2013/10/19. doi: 10.1016/j.dci.2013.10.002
S0145-305X(13)00293-0 [pii]. PubMed PMID: 24135719; PubMed Central PMCID: PMC3935818.

101. Nene V, Wortman JR, Lawson D, Haas B, Kodira C, Tu ZJ, et al. Genome sequence of Aedes aegypti, a major arbovirus vector. Science. 2007;316(5832):1718-23. Epub 2007/05/19. doi: 1138878 [pii]
10.1126/science.1138878. PubMed PMID: 17510324; PubMed Central PMCID: PMC2868357.

102. Geoghegan V, Stainton K, Rainey SM, Ant TH, Dowle AA, Larson T, et al. Perturbed cholesterol and vesicular trafficking associated with dengue blocking in Wolbachia-infected Aedes aegypti cells. Nat Commun. 2017;8(1):526. Epub 2017/09/15. doi: 10.1038/s41467-017-00610-8
10.1038/s41467-017-00610-8 [pii]. PubMed PMID: 28904344; PubMed Central PMCID: PMC5597582.

103. Liu B. Therapeutic potential of cyclodextrins in the treatment of Niemann-Pick type C disease. Clin Lipidol. 2012;7(3):289-301. doi: 10.2217/Clp.12.31. PubMed PMID: ISI:000306525100011.

104. Murphy DJ. The biogenesis and functions of lipid bodies in animals, plants and microorganisms. Prog Lipid Res. 2001;40(5):325-438. Epub 2001/07/27. doi: S0163-7827(01)00013-3 [pii]. PubMed PMID: 11470496.

105. Bozza PT, Magalhaes KG, Weller PF. Leukocyte lipid bodies - Biogenesis and functions in inflammation. Biochim Biophys Acta. 2009;1791(6):540-51. Epub 2009/05/07. doi: 10.1016/j.bbalip.2009.01.005
S1388-1981(09)00008-0 [pii]. PubMed PMID: 19416659; PubMed Central PMCID: PMC2693476.

106. Samsa MM, Mondotte JA, Iglesias NG, Assuncao-Miranda I, Barbosa-Lima G, Da Poian AT, et al. Dengue virus capsid protein usurps lipid droplets for viral particle formation. PLoS Pathog. 2009;5(10):e1000632. Epub 2009/10/24. doi: 10.1371/journal.ppat.1000632. PubMed PMID: 19851456; PubMed Central PMCID: PMC2760139.

107. Barletta AB, Alves LR, Silva MC, Sim S, Dimopoulos G, Liechocki S, et al. Emerging role of lipid droplets in Aedes aegypti immune response against bacteria and Dengue virus. Sci Rep. 2016;6:19928. Epub 2016/02/19. doi: 10.1038/srep19928
srep19928 [pii]. PubMed PMID: 26887863; PubMed Central PMCID: PMC4757862.

108. Heaton NS, Randall G. Dengue virus-induced autophagy regulates lipid metabolism. Cell Host Microbe. 2010;8(5):422-32. Epub 2010/11/16. doi: 10.1016/j.chom.2010.10.006
S1931-3128(10)00343-4 [pii]. PubMed PMID: 21075353; PubMed Central PMCID: PMC3026642.

109. Sim C, Denlinger DL. Transcription profiling and regulation of fat metabolism genes in diapausing adults of the mosquito Culex pipiens. Physiol Genomics. 2009;39(3):202-9. Epub 2009/08/27. doi: 10.1152/physiolgenomics.00095.2009
00095.2009 [pii]. PubMed PMID: 19706691; PubMed Central PMCID: PMC2789672.

110. Wang X, Hou Y, Saha TT, Pei G, Raikhel AS, Zou Z. Hormone and receptor interplay in the regulation of mosquito lipid metabolism. Proc Natl Acad Sci U S A. 2017;114(13):E2709-E18. Epub 2017/03/16. doi: 10.1073/pnas.1619326114
1619326114 [pii]. PubMed PMID: 28292900; PubMed Central PMCID: PMC5380040.

111. Heaton NS, Perera R, Berger KL, Khadka S, Lacount DJ, Kuhn RJ, et al. Dengue virus nonstructural protein 3 redistributes fatty acid synthase to sites of viral replication and increases cellular fatty acid synthesis. Proc Natl Acad Sci U S A. 2010;107(40):17345-50. Epub 2010/09/22. doi: 10.1073/pnas.1010811107
1010811107 [pii]. PubMed PMID: 20855599; PubMed Central PMCID: PMC2951450.

112. Jordan TX, Randall G. Dengue Virus Activates the AMP Kinase-mTOR Axis To Stimulate a Proviral Lipophagy. J Virol. 2017;91(11). Epub 2017/03/17. doi: e02020-16 [pii]
10.1128/JVI.02020-16
JVI.02020-16 [pii]. PubMed PMID: 28298606; PubMed Central PMCID: PMC5432877.

113. O'GOWER AK. The rate of digestion of human blood by certain species of mosquitoes. Australian Journal of Biological Sciences. 1955;9(1):125-9.

114. Perera R, Kuhn RJ. Host metabolism and its contribution in Flavivirus biogenesis. In: Arboviruses: Molecular Biology, Evolution and Control in press. Gubler D, Vasilakis N, editors2015, In press.

115. Zaitseva E, Yang ST, Melikov K, Pourmal S, Chernomordik LV. Dengue virus ensures its fusion in late endosomes using compartment-specific lipids. PLoS Pathog. 2010;6(10):e1001131. Epub 2010/10/16. doi: 10.1371/journal.ppat.1001131. PubMed PMID: 20949067; PubMed Central PMCID: PMC2951369.

116. Paul D, Bartenschlager R. Architecture and biogenesis of plus-strand RNA virus replication factories. World J Virol. 2013;2(2):32-48. Epub 2013/11/01. doi: 10.5501/wjv.v2.i2.32. PubMed PMID: 24175228; PubMed Central PMCID: PMC3785047.

117. Chatel-Chaix L, Bartenschlager R. Dengue virus- and hepatitis C virus-induced replication and assembly compartments: the enemy inside--caught in the web. J Virol. 2014;88(11):5907-11. Epub 2014/03/14. doi: 10.1128/JVI.03404-13
JVI.03404-13 [pii]. PubMed PMID: 24623440; PubMed Central PMCID: PMC4093888.

118. Romero-Brey I, Bartenschlager R. Membranous replication factories induced by plus-strand RNA viruses. Viruses. 2014;6(7):2826-57. Epub 2014/07/24. doi: 10.3390/v6072826
v6072826 [pii]. PubMed PMID: 25054883; PubMed Central PMCID: PMC4113795.

119. Deubel V, Kinney RM, Trent DW. Nucleotide sequence and deduced amino acid sequence of the structural proteins of dengue type 2 virus, Jamaica genotype. Virology. 1986;155(2):365-77. Epub 1986/12/01. PubMed PMID: 3024394.

120. Bennett KE, Olson KE, Munoz Mde L, Fernandez-Salas I, Farfan-Ale JA, Higgs S, et al. Variation in vector competence for dengue 2 virus among 24 collections of Aedes aegypti from Mexico and the United States. Am J Trop Med Hyg. 2002;67(1):85-92. Epub 2002/10/05. PubMed PMID: 12363070.

121. Richardson J, Molina-Cruz A, Salazar MI, Black Wt. Quantitative analysis of dengue-2 virus RNA during the extrinsic incubation period in individual Aedes aegypti. Am J Trop Med Hyg. 2006;74(1):132-41. Epub 2006/01/13. doi: 74/1/132 [pii]. PubMed PMID: 16407358.

122. Laue T, Emmerich P, Schmitz H. Detection of dengue virus RNA in patients after primary or secondary dengue infection by using the TaqMan automated amplification system. J Clin Microbiol. 1999;37(8):2543-7. Epub 1999/07/16. PubMed PMID: 10405398; PubMed Central PMCID: PMC85278.

123. Bligh EG, Dyer WJ. A rapid method of total lipid extraction and purification. Can J Biochem Physiol. 1959;37(8):911-7. Epub 1959/08/01. PubMed PMID: 13671378.

124. Team RC. R: A language and environment for statistical computing Vienna, Austria2015. Available from: http://www.R-project.org/.

125. Benton HP, Want EJ, Ebbels TM. Correction of mass calibration gaps in liquid chromatography-mass spectrometry metabolomics data. Bioinformatics. 2010;26(19):2488-9. Epub 2010/07/31. doi: 10.1093/bioinformatics/btq441
btq441 [pii]. PubMed PMID: 20671148.

126. Smith CA, Want EJ, O'Maille G, Abagyan R, Siuzdak G. XCMS: processing mass spectrometry data for metabolite profiling using nonlinear peak alignment, matching, and identification. Anal Chem. 2006;78(3):779-87. Epub 2006/02/02. doi: 10.1021/ac051437y. PubMed PMID: 16448051.

127. Tautenhahn R, Bottcher C, Neumann S. Highly sensitive feature detection for high resolution LC/MS. BMC Bioinformatics. 2008;9:504. Epub 2008/12/02. doi: 10.1186/1471-2105-9-504
1471-2105-9-504 [pii]. PubMed PMID: 19040729; PubMed Central PMCID: PMC2639432.

128. Prince JT, Marcotte EM. Chromatographic alignment of ESI-LC-MS proteomics data sets by ordered bijective interpolated warping. Anal Chem. 2006;78(17):6140-52. Epub 2006/09/02. doi: 10.1021/ac0605344. PubMed PMID: 16944896.

129. Wang W, Zhou H, Lin H, Roy S, Shaler TA, Hill LR, et al. Quantification of proteins and metabolites by mass spectrometry without isotopic labeling or spiked standards. Anal Chem. 2003;75(18):4818-26. Epub 2003/12/17. PubMed PMID: 14674459.

130. Ritchie ME, Phipson B, Wu D, Hu Y, Law CW, Shi W, et al. limma powers differential expression analyses for RNA-sequencing and microarray studies. Nucleic Acids Res. 2015;43(7):e47. Epub 2015/01/22. doi: 10.1093/nar/gkv007
gkv007 [pii]. PubMed PMID: 25605792; PubMed Central PMCID: PMC4402510.

131. Smyth GK. Linear models and empirical bayes methods for assessing differential expression in microarray experiments. Stat Appl Genet Mol Biol. 2004;3:Article3. Epub 2006/05/02. doi: 10.2202/1544-6115.1027. PubMed PMID: 16646809.

132. Benjamini Y, Hochberg Y. Controlling the false discovery rate: a practical and powerful approach to multiple testing. Journal of the Royal Statistical Society. 1995:289-300.

133. Kind T, Liu KH, Lee DY, DeFelice B, Meissen JK, Fiehn O. LipidBlast in silico tandem mass spectrometry database for lipid identification. Nat Methods. 2013;10(8):755-8. Epub 2013/07/03. doi: 10.1038/nmeth.2551
nmeth.2551 [pii]. PubMed PMID: 23817071; PubMed Central PMCID: PMC3731409.

134. MS PepSearch 2013. Available from: http://chemdata.nist.gov/dokuwiki/doku.php?id=peptidew:mspepsearch#restrictions_and_disclaimers.

135. Mass Spectrum Interpreter Ver. 3.

136. Fahy E, Subramaniam S, Murphy RC, Nishijima M, Raetz CR, Shimizu T, et al. Update of the LIPID MAPS comprehensive classification system for lipids. J Lipid Res. 2009;50 Suppl:S9-14. Epub 2008/12/23. doi: 10.1194/jlr.R800095-JLR200
R800095-JLR200 [pii]. PubMed PMID: 19098281; PubMed Central PMCID: PMC2674711.

137. van Meer G, Voelker DR, Feigenson GW. Membrane lipids: where they are and how they behave. Nat Rev Mol Cell Biol. 2008;9(2):112-24. Epub 2008/01/25. doi: 10.1038/nrm2330
nrm2330 [pii]. PubMed PMID: 18216768; PubMed Central PMCID: PMC2642958.

138. Dawaliby R, Trubbia C, Delporte C, Noyon C, Ruysschaert JM, Van Antwerpen P, et al. Phosphatidylethanolamine Is a Key Regulator of Membrane Fluidity in Eukaryotic Cells. J Biol Chem. 2016;291(7):3658-67. Epub 2015/12/15. doi: 10.1074/jbc.M115.706523
M115.706523 [pii]. PubMed PMID: 26663081; PubMed Central PMCID: PMC4751403.

139. Bohdanowicz M, Grinstein S. Role of phospholipids in endocytosis, phagocytosis, and macropinocytosis. Physiol Rev. 2013;93(1):69-106. Epub 2013/01/11. doi: 10.1152/physrev.00002.2012
93/1/69 [pii]. PubMed PMID: 23303906.

140. Sommer U, Molloy J, Viant M, Sinkins S. MTBLS210: Wolbachia modulation of lipid metabolism in Aedes albopictus mosquito cells 2015. Available from: http://www.ebi.ac.uk/metabolights/MTBLS210.

141. Molloy JC, Sommer U, Viant MR, Sinkins SP. Wolbachia Modulates Lipid Metabolism in Aedes albopictus Mosquito Cells. Appl Environ Microbiol. 2016;82(10):3109-20. Epub 2016/03/20. doi: 10.1128/AEM.00275-16
AEM.00275-16 [pii]. PubMed PMID: 26994075; PubMed Central PMCID: PMC4959074.

142. da Rocha Fernandes M, Martins R, Pessoa Costa E, Pacidonio EC, Araujo de Abreu L, da Silva Vaz I, Jr., et al. The modulation of the symbiont/host interaction between Wolbachia pipientis and Aedes fluviatilis embryos by glycogen metabolism. PLoS One. 2014;9(6):e98966. Epub 2014/06/14. doi: 10.1371/journal.pone.0098966
PONE-D-13-47807 [pii]. PubMed PMID: 24926801; PubMed Central PMCID: PMC4057193.

143. Caragata EP, Rances E, O'Neill SL, McGraw EA. Competition for amino acids between Wolbachia and the mosquito host, Aedes aegypti. Microb Ecol. 2014;67(1):205-18. Epub 2013/12/18. doi: 10.1007/s00248-013-0339-4. PubMed PMID: 24337107.

144. Canavoso LE, Frede S, Rubiolo ER. Metabolic pathways for dietary lipids in the midgut of hematophagous Panstrongylus megistus (Hemiptera: Reduviidae). Insect Biochem Mol Biol. 2004;34(8):845-54. Epub 2004/07/21. doi: 10.1016/j.ibmb.2004.05.008
S0965174804000840 [pii]. PubMed PMID: 15262288.

145. Arrese EL, Canavoso LE, Jouni ZE, Pennington JE, Tsuchida K, Wells MA. Lipid storage and mobilization in insects: current status and future directions. Insect Biochemistry and Molecular Biology. 2001;31(1):7-17. doi: Doi 10.1016/S0965-1748(00)00102-8. PubMed PMID: ISI:000166418400002.

146. Sarri E, Sicart A, Lazaro-Dieguez F, Egea G. Phospholipid synthesis participates in the regulation of diacylglycerol required for membrane trafficking at the Golgi complex. J Biol Chem. 2011;286(32):28632-43. Epub 2011/06/28. doi: 10.1074/jbc.M111.267534
M111.267534 [pii]. PubMed PMID: 21700701; PubMed Central PMCID: PMC3151104.

147. Lin YH, Chen YC, Kao TY, Lin YC, Hsu TE, Wu YC, et al. Diacylglycerol lipase regulates lifespan and oxidative stress response by inversely modulating TOR signaling in Drosophila and C. elegans. Aging Cell. 2014;13(4):755-64. Epub 2014/06/04. doi: 10.1111/acel.12232. PubMed PMID: 24889782; PubMed Central PMCID: PMC4116436.

148. Merida I, Avila-Flores A, Merino E. Diacylglycerol kinases: at the hub of cell signalling. Biochem J. 2008;409(1):1-18. Epub 2007/12/08. doi: BJ20071040 [pii]
10.1042/BJ20071040. PubMed PMID: 18062770.

149. Cheon HM, Shin SW, Bian G, Park JH, Raikhel AS. Regulation of lipid metabolism genes, lipid carrier protein lipophorin, and its receptor during immune challenge in the mosquito Aedes aegypti. J Biol Chem. 2006;281(13):8426-35. Epub 2006/02/02. doi: M510957200 [pii]
10.1074/jbc.M510957200. PubMed PMID: 16449228.

150. Martin-Acebes MA, Merino-Ramos T, Blazquez AB, Casas J, Escribano-Romero E, Sobrino F, et al. The composition of West Nile virus lipid envelope unveils a role of sphingolipid metabolism in flavivirus biogenesis. J Virol. 2014;88(20):12041-54. Epub 2014/08/15. doi: 10.1128/JVI.02061-14
JVI.02061-14 [pii]. PubMed PMID: 25122799; PubMed Central PMCID: PMC4178726.

151. Hannun YA, Obeid LM. Principles of bioactive lipid signalling: lessons from sphingolipids. Nat Rev Mol Cell Biol. 2008;9(2):139-50. Epub 2008/01/25. doi: 10.1038/nrm2329
nrm2329 [pii]. PubMed PMID: 18216770.

152. Hannun YA, Obeid LM. Sphingolipids and their metabolism in physiology and disease. Nat Rev Mol Cell Biol. 2018;19(3):175-91. Epub 2017/11/23. doi: 10.1038/nrm.2017.107
nrm.2017.107 [pii]. PubMed PMID: 29165427; PubMed Central PMCID: PMC5902181.

153. Jan JT, Chatterjee S, Griffin DE. Sindbis virus entry into cells triggers apoptosis by activating sphingomyelinase, leading to the release of ceramide. J Virol. 2000;74(14):6425-32. Epub 2000/06/23. PubMed PMID: 10864654; PubMed Central PMCID: PMC112150.

154. Schneider-Schaulies J, Schneider-Schaulies S. Viral infections and sphingolipids. Handb Exp Pharmacol. 2013;(216):321-40. Epub 2013/04/09. doi: 10.1007/978-3-7091-1511-4_16. PubMed PMID: 23563664.

155. Merrill AH, Jr. Sphingolipid and glycosphingolipid metabolic pathways in the era of sphingolipidomics. Chem Rev. 2011;111(10):6387-422. Epub 2011/09/29. doi: 10.1021/cr2002917. PubMed PMID: 21942574; PubMed Central PMCID: PMC3191729.

156. Hanada K. Serine palmitoyltransferase, a key enzyme of sphingolipid metabolism. Biochim Biophys Acta. 2003;1632(1-3):16-30. Epub 2003/06/05. doi: S1388198103000593 [pii]. PubMed PMID: 12782147.

157. Chen Y, Liu Y, Sullards MC, Merrill AH, Jr. An introduction to sphingolipid metabolism and analysis by new technologies. Neuromolecular Med. 2010;12(4):306-19. Epub 2010/08/04. doi: 10.1007/s12017-010-8132-8. PubMed PMID: 20680704; PubMed Central PMCID: PMC2982954.

158. Maceyka M, Sankala H, Hait NC, Le Stunff H, Liu H, Toman R, et al. SphK1 and SphK2, sphingosine kinase isoenzymes with opposing functions in sphingolipid metabolism. Journal of Biological Chemistry. 2005;280(44):37118-29. Epub 2005/08/25. doi: M502207200 [pii]
10.1074/jbc.M502207200. PubMed PMID: 16118219.

159. Maceyka M, Milstien S, Spiegel S. Sphingosine kinases, sphingosine-1-phosphate and sphingolipidomics. Prostaglandins Other Lipid Mediat. 2005;77(1-4):15-22. Epub 2005/08/16. doi: S1098-8823(04)00100-5 [pii]
10.1016/j.prostaglandins.2004.09.010. PubMed PMID: 16099387.

160. Vacaru AM, van den Dikkenberg J, Ternes P, Holthuis JC. Ceramide phosphoethanolamine biosynthesis in Drosophila is mediated by a unique ethanolamine phosphotransferase in the Golgi lumen. J Biol Chem. 2013;288(16):11520-30. Epub 2013/03/02. doi: 10.1074/jbc.M113.460972
M113.460972 [pii]. PubMed PMID: 23449981; PubMed Central PMCID: PMC3630839.

161. Liu YY, Hill RA, Li YT. Ceramide glycosylation catalyzed by glucosylceramide synthase and cancer drug resistance. Adv Cancer Res. 2013;117:59-89. Epub 2013/01/08. doi: 10.1016/B978-0-12-394274-6.00003-0
B978-0-12-394274-6.00003-0 [pii]. PubMed PMID: 23290777; PubMed Central PMCID: PMC4051614.

162. Horvath TD, Dagan S, Lorenzi PL, Hawke DH, Scaraffia PY. Positional stable isotope tracer analysis reveals carbon routes during ammonia metabolism of Aedes aegypti mosquitoes. FASEB J. 2017. Epub 2017/10/04. doi: fj.201700657R [pii]
10.1096/fj.201700657R. PubMed PMID: 28970248.

163. Canavoso LE, Jouni ZE, Karnas KJ, Pennington JE, Wells MA. Fat metabolism in insects. Annu Rev Nutr. 2001;21:23-46. Epub 2001/05/26. doi: 10.1146/annurev.nutr.21.1.23
21/1/23 [pii]. PubMed PMID: 11375428.

164. Brezinski ME, Serhan CN. Selective incorporation of (15S)-hydroxyeicosatetraenoic acid in phosphatidylinositol of human neutrophils: agonist-induced deacylation and transformation of stored hydroxyeicosanoids. Proc Natl Acad Sci U S A. 1990;87(16):6248-52. Epub 1990/08/01. PubMed PMID: 2117277; PubMed Central PMCID: PMC54510.

165. Funk CD, Powell WS. Metabolism of linoleic acid by prostaglandin endoperoxide synthase from adult and fetal blood vessels. Biochim Biophys Acta. 1983;754(1):57-71. Epub 1983/11/01. PubMed PMID: 6414520.

166. Tortoriello G, Rhodes BP, Takacs SM, Stuart JM, Basnet A, Raboune S, et al. Targeted Lipidomics in Drosophila melanogaster Identifies Novel 2-Monoacylglycerols and N-acyl Amides. Plos One. 2013;8(7). doi: UNSP e67865
DOI 10.1371/journal.pone.0067865. PubMed PMID: ISI:000322218800011.

167. Gregersen N, Kolvraa S, Rasmussen K, Christensen E, Brandt NJ, Ebbesen F, et al. Biochemical studies in a patient with defects in the metabolism of acyl-CoA and sarcosine: another possible case of glutaric aciduria type II. J Inherit Metab Dis. 1980;3(3):67-72. Epub 1980/01/01. PubMed PMID: 6158623.

168. Koves TR, Ussher JR, Noland RC, Slentz D, Mosedale M, Ilkayeva O, et al. Mitochondrial overload and incomplete fatty acid oxidation contribute to skeletal muscle insulin resistance. Cell Metab. 2008;7(1):45-56. Epub 2008/01/08. doi: 10.1016/j.cmet.2007.10.013
S1550-4131(07)00306-3 [pii]. PubMed PMID: 18177724.

169. Lasser NL, Edwards AM, Clayton RB. Distribution and dynamic state of sterols and steroids in the tissues of an insect, the roach Eurycotis floridana. J Lipid Res. 1966;7(3):403-12. Epub 1966/05/01. PubMed PMID: 5929356.

170. Lasser NL, Clayton RB. The intracellular distribution of sterols in Eurycotis floridana and its possible relation to subcellular membrane structures. J Lipid Res. 1966;7(3):413-21. Epub 1966/05/01. PubMed PMID: 5929357.

171. Rees HH. Ecdysteroid Biosynthesis and Inactivation in Relation to Function. European Journal of Entomology. 1995;92(1):9-39. PubMed PMID: ISI:A1995QN05500003.

172. Nchoutmboube JA, Viktorova EG, Scott AJ, Ford LA, Pei Z, Watkins PA, et al. Increased long chain acyl-Coa synthetase activity and fatty acid import is linked to membrane synthesis for development of picornavirus replication organelles. PLoS Pathog. 2013;9(6):e1003401. Epub 2013/06/14. doi: 10.1371/journal.ppat.1003401
PPATHOGENS-D-12-02884 [pii]. PubMed PMID: 23762027; PubMed Central PMCID: PMC3675155.

173. Mathews CK, Holde KEV, Appling DR, Anthony-Cahill SJ. Biochemistry. 4th ed. Toronto: Pearson Canada; 2013.

174. Ye YH, Woolfit M, Rances E, O'Neill SL, McGraw EA. Wolbachia-associated bacterial protection in the mosquito Aedes aegypti. PLoS Negl Trop Dis. 2013;7(8):e2362. Epub 2013/08/21. doi: 10.1371/journal.pntd.0002362
PNTD-D-13-00227 [pii]. PubMed PMID: 23951381; PubMed Central PMCID: PMC3738474.

175. Scaraffia PY, Zhang Q, Thorson K, Wysocki VH, Miesfeld RL. Differential ammonia metabolism in Aedes aegypti fat body and midgut tissues. J Insect Physiol. 2010;56(9):1040-9. Epub 2010/03/09. doi: 10.1016/j.jinsphys.2010.02.016
S0022-1910(10)00061-2 [pii]. PubMed PMID: 20206632; PubMed Central PMCID: PMC2910787.

176. Price DP, Nagarajan V, Churbanov A, Houde P, Milligan B, Drake LL, et al. The fat body transcriptomes of the yellow fever mosquito Aedes aegypti, pre- and post- blood meal. PLoS One. 2011;6(7):e22573. Epub 2011/08/06. doi: 10.1371/journal.pone.0022573
PONE-D-11-07310 [pii]. PubMed PMID: 21818341; PubMed Central PMCID: PMC3144915.

177. Koller CN, Raikhel AS. Initiation of Vitellogenin Uptake and Protein-Synthesis in the Mosquito (Aedes-Aegypti) Ovary in Response to a Blood Meal. Journal of Insect Physiology. 1991;37(9):703-11. doi: Doi 10.1016/0022-1910(91)90048-5. PubMed PMID: ISI:A1991GL93900009.

178. Brown DA, London E. Structure and function of sphingolipid- and cholesterol-rich membrane rafts. J Biol Chem. 2000;275(23):17221-4. Epub 2000/04/20. doi: 10.1074/jbc.R000005200
R000005200 [pii]. PubMed PMID: 10770957.

179. Kraut R. Roles of sphingolipids in Drosophila development and disease. J Neurochem. 2011;116(5):764-78. Epub 2011/01/11. doi: 10.1111/j.1471-4159.2010.07022.x. PubMed PMID: 21214556.

180. Fyrst H, Saba JD. Sphingosine-1-phosphate lyase in development and disease: sphingolipid metabolism takes flight. Biochim Biophys Acta. 2008;1781(9):448-58. Epub 2008/06/19. doi: 10.1016/j.bbalip.2008.05.005
S1388-1981(08)00102-9 [pii]. PubMed PMID: 18558101; PubMed Central PMCID: PMC2749932.

181. Yang TK, Means E, Anderson LE, Jenkin HM. Sphingophospholipids of species of Aedes and Culex mosquito cells cultivated in suspension culture from logarithmic and stationary phases of growth. Lipids. 1974;9(12):1009-13. Epub 1974/12/01. PubMed PMID: 4444421.

182. Aktepe TE, Pham H, Mackenzie JM. Differential utilisation of ceramide during replication of the flaviviruses West Nile and dengue virus. Virology. 2015;484:241-50. Epub 2015/07/01. doi: 10.1016/j.virol.2015.06.015
S0042-6822(15)00293-7 [pii]. PubMed PMID: 26122470.

183. Bremer J. The role of carnitine in intracellular metabolism. J Clin Chem Clin Biochem. 1990;28(5):297-301. Epub 1990/05/01. PubMed PMID: 2199593.

184. Lopaschuk GD, Ussher JR, Folmes CD, Jaswal JS, Stanley WC. Myocardial fatty acid metabolism in health and disease. Physiol Rev. 2010;90(1):207-58. Epub 2010/01/21. doi: 10.1152/physrev.00015.2009
90/1/207 [pii]. PubMed PMID: 20086077.

185. Schulz H. Oxidation of fatty acids in eukaryotes. In Biochemistry of Lipids, Lipoproteins and Membranes. 5th ed. Vance DE, Vance J, editors. Amsterdam: Elsevier; 2008.
186. Rutkowsky JM, Knotts TA, Ono-Moore KD, McCoin CS, Huang S, Schneider D, et al. Acylcarnitines activate proinflammatory signaling pathways. Am J Physiol Endocrinol Metab. 2014;306(12):E1378-87. Epub 2014/04/25. doi: 10.1152/ajpendo.00656.2013
ajpendo.00656.2013 [pii]. PubMed PMID: 24760988; PubMed Central PMCID: PMC4059985.

187. Knabb MT, Saffitz JE, Corr PB, Sobel BE. The dependence of electrophysiological derangements on accumulation of endogenous long-chain acyl carnitine in hypoxic neonatal rat myocytes. Circ Res. 1986;58(2):230-40. Epub 1986/02/01. PubMed PMID: 3948341.

188. Bakermans AJ, van Weeghel M, Denis S, Nicolay K, Prompers JJ, Houten SM. Carnitine supplementation attenuates myocardial lipid accumulation in long-chain acyl-CoA dehydrogenase knockout mice. J Inherit Metab Dis. 2013;36(6):973-81. Epub 2013/04/09. doi: 10.1007/s10545-013-9604-4. PubMed PMID: 23563854.

189. Kler RS, Jackson S, Bartlett K, Bindoff LA, Eaton S, Pourfarzam M, et al. Quantitation of acyl-CoA and acylcarnitine esters accumulated during abnormal mitochondrial fatty acid oxidation. J Biol Chem. 1991;266(34):22932-8. Epub 1991/12/05. PubMed PMID: 1744086.

190. El-Bacha T, Midlej V, Pereira da Silva AP, Silva da Costa L, Benchimol M, Galina A, et al. Mitochondrial and bioenergetic dysfunction in human hepatic cells infected with dengue 2 virus. Biochim Biophys Acta. 2007;1772(10):1158-66. Epub 2007/10/30. doi: S0925-4439(07)00184-6 [pii]
10.1016/j.bbadis.2007.08.003. PubMed PMID: 17964123.

191. Fontaine KA, Sanchez EL, Camarda R, Lagunoff M. Dengue virus induces and requires glycolysis for optimal replication. J Virol. 2015;89(4):2358-66. Epub 2014/12/17. doi: 10.1128/JVI.02309-14
JVI.02309-14 [pii]. PubMed PMID: 25505078; PubMed Central PMCID: PMC4338897.

192. Fullekrug J, Ehehalt R, Poppelreuther M. Outlook: membrane junctions enable the metabolic trapping of fatty acids by intracellular acyl-CoA synthetases. Front Physiol. 2012;3:401. Epub 2012/10/23. doi: 10.3389/fphys.2012.00401. PubMed PMID: 23087649; PubMed Central PMCID: PMC3467455.

193. Eyster KM. The membrane and lipids as integral participants in signal transduction: lipid signal transduction for the non-lipid biochemist. Adv Physiol Educ. 2007;31(1):5-16. Epub 2007/03/01. doi: 31/1/5 [pii]
10.1152/advan.00088.2006. PubMed PMID: 17327576.

194. Fernandis AZ, Wenk MR. Membrane lipids as signaling molecules. Curr Opin Lipidol. 2007;18(2):121-8. Epub 2007/03/14. doi: 10.1097/MOL.0b013e328082e4d5
00041433-200704000-00002 [pii]. PubMed PMID: 17353659.

195. Caragata EP, Rances E, Hedges LM, Gofton AW, Johnson KN, O'Neill SL, et al. Dietary cholesterol modulates pathogen blocking by Wolbachia. PLoS Pathog. 2013;9(6):e1003459. Epub 2013/07/05. doi: 10.1371/journal.ppat.1003459
PPATHOGENS-D-12-02513 [pii]. PubMed PMID: 23825950; PubMed Central PMCID: PMC3694857.

196. Matsumoto K. Dispensable nature of phosphatidylglycerol in Escherichia coli: dual roles of anionic phospholipids. Mol Microbiol. 2001;39(6):1427-33. Epub 2001/03/22. doi: mmi2320 [pii]. PubMed PMID: 11260460.

197. Liebscher S, Ambrose RL, Aktepe TE, Mikulasova A, Prier JE, Gillespie LK, et al. Phospholipase A2 activity during the replication cycle of the flavivirus West Nile virus. PLoS Pathog. 2018;14(4):e1007029. Epub 2018/05/01. doi: 10.1371/journal.ppat.1007029

PPATHOGENS-D-17-01303 [pii]. PubMed PMID: 29709018; PubMed Central PMCID: PMC5945048.

198. Ishii I, Fukushima N, Ye X, Chun J. Lysophospholipid receptors: signaling and biology. Annu Rev Biochem. 2004;73:321-54. Epub 2004/06/11. doi: 10.1146/annurev.biochem.73.011303.073731. PubMed PMID: 15189145.

199. Mishima K, Nakajima M, Ogihara T. Effects of lysophospholipids on membrane order of phosphatidylcholine. Colloids and Surfaces B-Biointerfaces. 2004;33(3-4):185-9. doi: 10.1016/j.colsurfb.2003.10.004. PubMed PMID: ISI:000189085900006.

200. Breslow DK, Weissman JS. Membranes in balance: mechanisms of sphingolipid homeostasis. Mol Cell. 2010;40(2):267-79. Epub 2010/10/23. doi: 10.1016/j.molcel.2010.10.005
S1097-2765(10)00781-1 [pii]. PubMed PMID: 20965421; PubMed Central PMCID: PMC2987644.

201. Lingwood D, Simons K. Lipid rafts as a membrane-organizing principle. Science. 2010;327(5961):46-50. Epub 2010/01/02. doi: 10.1126/science.1174621
327/5961/46 [pii]. PubMed PMID: 20044567.

202. Ewers H, Romer W, Smith AE, Bacia K, Dmitrieff S, Chai W, et al. GM1 structure determines SV40-induced membrane invagination and infection. Nat Cell Biol. 2010;12(1):11-8; sup pp 1-2. Epub 2009/12/22. doi: 10.1038/ncb1999
ncb1999 [pii]. PubMed PMID: 20023649.

203. Lippincott-Schwartz J, Phair RD. Lipids and cholesterol as regulators of traffic in the endomembrane system. Annu Rev Biophys. 2010;39:559-78. Epub 2010/03/03. doi: 10.1146/annurev.biophys.093008.131357. PubMed PMID: 20192772; PubMed Central PMCID: PMC3366628.

204. Lopez PH, Schnaar RL. Gangliosides in cell recognition and membrane protein regulation. Curr Opin Struct Biol. 2009;19(5):549-57. Epub 2009/07/18. doi: 10.1016/j.sbi.2009.06.001
S0959-440X(09)00092-X [pii]. PubMed PMID: 19608407; PubMed Central PMCID: PMC2763983.

205. Hayashi Y, Nemoto-Sasaki Y, Tanikawa T, Oka S, Tsuchiya K, Zama K, et al. Sphingomyelin synthase 2, but not sphingomyelin synthase 1, is involved in HIV-1 envelope-mediated membrane fusion. J Biol Chem. 2014;289(44):30842-56. Epub 2014/09/19. doi: 10.1074/jbc.M114.574285
M114.574285 [pii]. PubMed PMID: 25231990; PubMed Central PMCID: PMC4215260.

206. Carocci M, Hinshaw SM, Rodgers MA, Villareal VA, Burri DJ, Pilankatta R, et al. The bioactive lipid 4-hydroxyphenyl retinamide inhibits flavivirus replication. Antimicrob Agents Chemother. 2015;59(1):85-95. Epub 2014/10/15. doi: 10.1128/AAC.04177-14
AAC.04177-14 [pii]. PubMed PMID: 25313218; PubMed Central PMCID: PMC4291433.

207. Lorono-Pino MA, Farfan-Ale JA, Zapata-Peraza AL, Rosado-Paredes EP, Flores-Flores LF, Garcia-Rejon JE, et al. Introduction of the American/Asian genotype of dengue 2 virus into the Yucatan State of Mexico. Am J Trop Med Hyg. 2004;71(4):485-92. Epub 2004/11/02. doi: 71/4/485 [pii]. PubMed PMID: 15516647.

208. Merrill AH, Jr., Sullards MC, Allegood JC, Kelly S, Wang E. Sphingolipidomics: high-throughput, structure-specific, and quantitative analysis of sphingolipids by liquid chromatography tandem mass spectrometry. Methods. 2005;36(2):207-24. Epub 2005/05/17. doi: S1046-2023(05)00049-6 [pii]
10.1016/j.ymeth.2005.01.009. PubMed PMID: 15894491.

209. Schmittgen TD, Livak KJ. Analyzing real-time PCR data by the comparative C(T) method. Nat Protoc. 2008;3(6):1101-8. Epub 2008/06/13. PubMed PMID: 18546601.

210. Vera-Maloof FZ, Saavedra-Rodriguez K, Elizondo-Quiroga AE, Lozano-Fuentes S, Black Iv WC. Coevolution of the Ile1,016 and Cys1,534 Mutations in the Voltage Gated Sodium Channel Gene of Aedes aegypti in Mexico. PLoS Negl Trop Dis. 2015;9(12):e0004263. Epub 2015/12/15. doi: 10.1371/journal.pntd.0004263
PNTD-D-15-01137 [pii]. PubMed PMID: 26658798; PubMed Central PMCID: PMC4684211.

211. Mathur G, Sanchez-Vargas I, Alvarez D, Olson KE, Marinotti O, James AA. Transgene-mediated suppression of dengue viruses in the salivary glands of the yellow fever mosquito, Aedes aegypti. Insect Mol Biol. 2010;19(6):753-63. Epub 2010/08/27. doi: 10.1111/j.1365-2583.2010.01032.x
IMB1032 [pii]. PubMed PMID: 20738425; PubMed Central PMCID: PMC2976824.

212. Ruckert C, Weger-Lucarelli J, Garcia-Luna SM, Young MC, Byas AD, Murrieta RA, et al. Impact of simultaneous exposure to arboviruses on infection and transmission by Aedes aegypti mosquitoes. Nat Commun. 2017;8:15412. Epub 2017/05/20. doi: 10.1038/ncomms15412
ncomms15412 [pii]. PubMed PMID: 28524874; PubMed Central PMCID: PMC5454532.

213. Edsall LC, Van Brocklyn JR, Cuvillier O, Kleuser B, Spiegel S. N,N-Dimethylsphingosine is a potent competitive inhibitor of sphingosine kinase but not of protein kinase C: modulation of cellular levels of sphingosine 1-phosphate and ceramide. Biochemistry. 1998;37(37):12892-8. Epub 1998/09/16. doi: 10.1021/bi980744d
bi980744d [pii]. PubMed PMID: 9737868.

214. Chun J, Hartung HP. Mechanism of action of oral fingolimod (FTY720) in multiple sclerosis. Clin Neuropharmacol. 2010;33(2):91-101. Epub 2010/01/12. doi: 10.1097/WNF.0b013e3181cbf825. PubMed PMID: 20061941; PubMed Central PMCID: PMC2859693.

215. Pyne NJ, El Buri A, Adams DR, Pyne S. Sphingosine 1-phosphate and cancer. Adv Biol Regul. 2018;68:97-106. Epub 2017/09/25. doi: S2212-4926(17)30159-8 [pii]
10.1016/j.jbior.2017.09.006. PubMed PMID: 28942351.

216. Wang E, Norred WP, Bacon CW, Riley RT, Merrill AH, Jr. Inhibition of sphingolipid biosynthesis by fumonisins. Implications for diseases associated with Fusarium moniliforme. J Biol Chem. 1991;266(22):14486-90. Epub 1991/08/15. PubMed PMID: 1860857.

217. Pizzirani D, Bach A, Realini N, Armirotti A, Mengatto L, Bauer I, et al. Benzoxazolone carboxamides: potent and systemically active inhibitors of intracellular acid ceramidase. Angew Chem Int Ed Engl. 2015;54(2):485-9. Epub 2014/11/15. doi: 10.1002/anie.201409042. PubMed PMID: 25395373; PubMed Central PMCID: PMC4502975.

218. Francischetti IM, Ma D, Andersen JF, Ribeiro JM. Evidence for a lectin specific for sulfated glycans in the salivary gland of the malaria vector, Anopheles gambiae. PLoS One. 2014;9(9):e107295. Epub 2014/09/11. doi: 10.1371/journal.pone.0107295
PONE-D-14-21988 [pii]. PubMed PMID: 25207644; PubMed Central PMCID: PMC4160252.

219. Zheng W, Kollmeyer J, Symolon H, Momin A, Munter E, Wang E, et al. Ceramides and other bioactive sphingolipid backbones in health and disease: Lipidomic analysis, metabolism and roles in membrane structure, dynamics, signaling and autophagy. Bba-Biomembranes. 2006;1758(12):1864-84. doi: 10.1016/j.bbamem.2006.08.009. PubMed PMID: ISI:000243220800002.

220. Rodriguez-Cuenca S, Barbarroja N, Vidal-Puig A. Dihydroceramide desaturase 1, the gatekeeper of ceramide induced lipotoxicity. Biochim Biophys Acta. 2015;1851(1):40-50. Epub 2014/10/07. doi: 10.1016/j.bbalip.2014.09.021
S1388-1981(14)00207-8 [pii]. PubMed PMID: 25283058.

221. Narita T, Naganuma T, Sase Y, Kihara A. Long-chain bases of sphingolipids are transported into cells via the acyl-CoA synthetases. Sci Rep. 2016;6:25469. Epub 2016/05/04. doi: 10.1038/srep25469
srep25469 [pii]. PubMed PMID: 27136724; PubMed Central PMCID: PMC4853782.

222. Kono M, Dreier JL, Ellis JM, Allende ML, Kalkofen DN, Sanders KM, et al. Neutral ceramidase encoded by the Asah2 gene is essential for the intestinal degradation of sphingolipids. J Biol Chem. 2006;281(11):7324-31. Epub 2005/12/29. doi: M508382200 [pii]
10.1074/jbc.M508382200. PubMed PMID: 16380386.

223. Zhao Y, Kalari SK, Usatyuk PV, Gorshkova I, He D, Watkins T, et al. Intracellular generation of sphingosine 1-phosphate in human lung endothelial cells: role of lipid phosphate phosphatase-1 and sphingosine kinase 1. J Biol Chem. 2007;282(19):14165-77. Epub 2007/03/24. doi: M701279200 [pii]
10.1074/jbc.M701279200. PubMed PMID: 17379599; PubMed Central PMCID: PMC2659598.

224. Maier T, Leibundgut M, Ban N. The crystal structure of a mammalian fatty acid synthase. Science. 2008;321(5894):1315-22. Epub 2008/09/06. doi: 10.1126/science.1161269
321/5894/1315 [pii]. PubMed PMID: 18772430.

225. White SW, Zheng J, Zhang YM, Rock. The structural biology of type II fatty acid biosynthesis. Annu Rev Biochem. 2005;74:791-831. Epub 2005/06/15. doi: 10.1146/annurev.biochem.74.082803.133524. PubMed PMID: 15952903.

226. Jenni S, Leibundgut M, Boehringer D, Frick C, Mikolasek B, Ban N. Structure of fungal fatty acid synthase and implications for iterative substrate shuttling. Science. 2007;316(5822):254-61. Epub 2007/04/14. doi: 316/5822/254 [pii]
10.1126/science.1138248. PubMed PMID: 17431175.

227. Lomakin IB, Xiong Y, Steitz TA. The crystal structure of yeast fatty acid synthase, a cellular machine with eight active sites working together. Cell. 2007;129(2):319-32. Epub 2007/04/24. doi: S0092-8674(07)00329-7 [pii]
10.1016/j.cell.2007.03.013. PubMed PMID: 17448991.

228. Martín-Acebes M, Blázquez A, Oya NJd, Escribano-Romero E, Saiz J. West Nile virus replication requires fatty acid synthesis but is independent on phosphatidylinositol-4-phosphate lipids. Plos One. 2011;6(9).

229. Tongluan N, Ramphan S, Wintachai P, Jaresitthikunchai J, Khongwichit S, Wikan N, et al. Involvement of fatty acid synthase in dengue virus infection. Virol J. 2017;14(1):28. Epub 2017/02/15. doi: 10.1186/s12985-017-0685-9
10.1186/s12985-017-0685-9 [pii]. PubMed PMID: 28193229; PubMed Central PMCID: PMC5307738.

230. Camacho C, Coulouris G, Avagyan V, Ma N, Papadopoulos J, Bealer K, et al. BLAST+: architecture and applications. BMC Bioinformatics. 2009;10:421. Epub 2009/12/17. doi: 10.1186/1471-2105-10-421
1471-2105-10-421 [pii]. PubMed PMID: 20003500; PubMed Central PMCID: PMC2803857.

231. Larkin MA, Blackshields G, Brown NP, Chenna R, McGettigan PA, McWilliam H, et al. Clustal W and Clustal X version 2.0. Bioinformatics. 2007;23(21):2947-8. Epub 2007/09/12. doi: btm404 [pii]
10.1093/bioinformatics/btm404. PubMed PMID: 17846036.

232. Corpet F. Multiple sequence alignment with hierarchical clustering. Nucleic Acids Res. 1988;16(22):10881-90. Epub 1988/11/25. PubMed PMID: 2849754; PubMed Central PMCID: PMC338945.

233. Sievers F, Wilm A, Dineen D, Gibson TJ, Karplus K, Li W, et al. Fast, scalable generation of high-quality protein multiple sequence alignments using Clustal Omega. Mol Syst Biol. 2011;7:539. Epub 2011/10/13. doi: 10.1038/msb.2011.75
msb201175 [pii]. PubMed PMID: 21988835; PubMed Central PMCID: PMC3261699.

234. Brown NP, Leroy C, Sander C. MView: a web-compatible database search or multiple alignment viewer. Bioinformatics. 1998;14(4):380-1. Epub 1998/06/20. doi: btb054 [pii]. PubMed PMID: 9632837.

235. Mistry J, Bateman A, Finn RD. Predicting active site residue annotations in the Pfam database. BMC Bioinformatics. 2007;8:298. Epub 2007/08/11. doi: 1471-2105-8-298 [pii]
10.1186/1471-2105-8-298. PubMed PMID: 17688688; PubMed Central PMCID: PMC2025603.

236. Chotiwan N, Brewster CD, Magalhaes T, Weger-Lucarelli J, Duggal NK, Ruckert C, et al. Rapid and specific detection of Asian- and African-lineage Zika viruses. Sci Transl Med. 2017;9(388). Epub 2017/05/05. doi: eaag0538 [pii]
10.1126/scitranslmed.aag0538
9/388/eaag0538 [pii]. PubMed PMID: 28469032; PubMed Central PMCID: PMC5654541.

237. Lanciotti RS, Kosoy OL, Laven JJ, Velez JO, Lambert AJ, Johnson AJ, et al. Genetic and serologic properties of Zika virus associated with an epidemic, Yap State, Micronesia, 2007. Emerg Infect Dis. 2008;14(8):1232-9. Epub 2008/08/06. doi: 10.3201/eid1408.080287. PubMed PMID: 18680646; PubMed Central PMCID: PMC2600394.

238. Lanciotti RS, Lambert AJ, Holodniy M, Saavedra S, Signor Ldel C. Phylogeny of Zika Virus in Western Hemisphere, 2015. Emerg Infect Dis. 2016;22(5):933-5. Epub 2016/04/19. doi: 10.3201/eid2205.160065. PubMed PMID: 27088323; PubMed Central PMCID: PMC4861537.

239. Lanciotti RS, Valadere AM. Transcontinental movement of Asian genotype chikungunya virus. Emerg Infect Dis. 2014;20(8):1400-2. Epub 2014/07/31. doi: 10.3201/eid2008.140268. PubMed PMID: 25076384; PubMed Central PMCID: PMC4111183.

240. VectorBase. AaegL5. 2017. Available from: https://www.vectorbase.org/organisms/aedes-aegypti/lvp_agwg/aaegl5

241. NCBI. NCBI Aedes aegypti Annotation Release 101. Available from: https://www.ncbi.nlm.nih.gov/assembly/GCF_002204515.2/

242. VectorBase. AaegL3 2014. Available from: https://pre.vectorbase.org/organisms/aedes-aegypti/liverpool/aaegl3.

243. Lee E, Helt GA, Reese JT, Munoz-Torres MC, Childers CP, Buels RM, et al. Web Apollo: a web-based genomic annotation editing platform. Genome Biol. 2013;14(8):R93. Epub 2013/09/05. doi: 10.1186/gb-2013-14-8-r93
gb-2013-14-8-r93 [pii]. PubMed PMID: 24000942; PubMed Central PMCID: PMC4053811.

244. Beedessee G, Hisata K, Roy MC, Satoh N, Shoguchi E. Multifunctional polyketide synthase genes identified by genomic survey of the symbiotic dinoflagellate, Symbiodinium minutum. BMC Genomics. 2015;16:941. Epub 2015/11/18. doi: 10.1186/s12864-015-2195-8
10.1186/s12864-015-2195-8 [pii]. PubMed PMID: 26573520; PubMed Central PMCID: PMC4647583.

245. Maier T, Jenni S, Ban N. Architecture of mammalian fatty acid synthase at 4.5 A resolution. Science. 2006;311(5765):1258-62. Epub 2006/03/04. doi: 311/5765/1258 [pii]
10.1126/science.1123248. PubMed PMID: 16513975.

246. Sanchez-Vargas I, Scott JC, Poole-Smith BK, Franz AW, Barbosa-Solomieu V, Wilusz J, et al. Dengue virus type 2 infections of Aedes aegypti are modulated by the mosquito's RNA interference pathway. PLoS Pathog. 2009;5(2):e1000299. Epub 2009/02/14. doi: 10.1371/journal.ppat.1000299. PubMed PMID: 19214215; PubMed Central PMCID: PMC2633610.

247. Tang WC, Lin RJ, Liao CL, Lin YL. Rab18 facilitates dengue virus infection by targeting fatty acid synthase to sites of viral replication. J Virol. 2014;88(12):6793-804. Epub 2014/04/04. doi: 10.1128/JVI.00045-14
JVI.00045-14 [pii]. PubMed PMID: 24696471; PubMed Central PMCID: PMC4054357.

248. Downer RGH, Matthews JR. Patterns of lipid distribution and utilisation in insect. American Zoologist. 1976;16(4):733-45.

249. Chau LM, Goodisman MAD. Gene duplication and the evolution of phenotypic diversity in insect societies. Evolution. 2017;71(12):2871-84. Epub 2017/09/07. doi: 10.1111/evo.13356. PubMed PMID: 28875541.

250. Helmkampf M, Cash E, Gadau J. Evolution of the insect desaturase gene family with an emphasis on social Hymenoptera. Mol Biol Evol. 2015;32(2):456-71. Epub 2014/11/27. doi: 10.1093/molbev/msu315
msu315 [pii]. PubMed PMID: 25425561; PubMed Central PMCID: PMC4298175.

251. Wahid I, Sunahara T, Mogi M. Maxillae and mandibles of male mosquitoes and female autogenous mosquitoes (Diptera: Culicidae). J Med Entomol. 2003;40(2):150-8. Epub 2003/04/16. PubMed PMID: 12693842.

252. Baker DA, Nolan T, Fischer B, Pinder A, Crisanti A, Russell S. A comprehensive gene expression atlas of sex- and tissue-specificity in the malaria vector, Anopheles gambiae. BMC Genomics. 2011;12:296. Epub 2011/06/09. doi: 10.1186/1471-2164-12-296
1471-2164-12-296 [pii]. PubMed PMID: 21649883; PubMed Central PMCID: PMC3129592.

253. Wilson MJ, Dearden PK. Evolution of the insect Sox genes. BMC Evol Biol. 2008;8:120. Epub 2008/04/29. doi: 10.1186/1471-2148-8-120
1471-2148-8-120 [pii]. PubMed PMID: 18439299; PubMed Central PMCID: PMC2386450.

254. Tan QQ, Liu W, Zhu F, Lei CL, Wang XP. Fatty acid synthase 2 contributes to diapause preparation in a beetle by regulating lipid accumulation and stress tolerance genes expression. Sci Rep. 2017;7:40509. Epub 2017/01/11. doi: 10.1038/srep40509
srep40509 [pii]. PubMed PMID: 28071706; PubMed Central PMCID: PMC5223116.

255. Areiza M, Nouzova M, Rivera-Perez C, Noriega FG. 20-Hydroxyecdysone stimulation of juvenile hormone biosynthesis by the mosquito corpora allata. Insect Biochem Mol Biol. 2015;64:100-5. Epub 2015/08/11. doi: 10.1016/j.ibmb.2015.08.001
S0965-1748(15)30034-5 [pii]. PubMed PMID: 26255691; PubMed Central PMCID: PMC4558257.

256. Ye YH, Carrasco AM, Frentiu FD, Chenoweth SF, Beebe NW, van den Hurk AF, et al. Wolbachia Reduces the Transmission Potential of Dengue-Infected Aedes aegypti. PLoS Negl Trop Dis. 2015;9(6):e0003894. Epub 2015/06/27. doi: 10.1371/journal.pntd.0003894
PNTD-D-14-01758 [pii]. PubMed PMID: 26115104; PubMed Central PMCID: PMC4482661.

257. Macdonald G. The Epidemology and control of malaria Oxford University Press, London; 1957.

258. Carrington LB, Tran BCN, Le NTH, Luong TTH, Nguyen TT, Nguyen PT, et al. Field- and clinically derived estimates of Wolbachia-mediated blocking of dengue virus transmission potential in Aedes aegypti mosquitoes. Proc Natl Acad Sci U S A. 2018;115(2):361-6. Epub 2017/12/28. doi: 10.1073/pnas.1715788115
1715788115 [pii]. PubMed PMID: 29279375; PubMed Central PMCID: PMC5777059.

259. Schmidt TL, Barton NH, Rasic G, Turley AP, Montgomery BL, Iturbe-Ormaetxe I, et al. Local introduction and heterogeneous spatial spread of dengue-suppressing Wolbachia through an urban population of Aedes aegypti. PLoS Biol. 2017;15(5):e2001894. Epub 2017/05/31. doi: 10.1371/journal.pbio.2001894
pbio.2001894 [pii]. PubMed PMID: 28557993; PubMed Central PMCID: PMC5448718.

260. Nguyen TH, Nguyen HL, Nguyen TY, Vu SN, Tran ND, Le TN, et al. Field evaluation of the establishment potential of wMelPop Wolbachia in Australia and Vietnam for dengue control. Parasit Vectors. 2015;8:563. Epub 2015/10/30. doi: 10.1186/s13071-015-1174-x
10.1186/s13071-015-1174-x [pii]. PubMed PMID: 26510523; PubMed Central PMCID: PMC4625535.

261. Sumner LW, Amberg A, Barrett D, Beale MH, Beger R, Daykin CA, et al. Proposed minimum reporting standards for chemical analysis Chemical Analysis Working Group (CAWG) Metabolomics Standards Initiative (MSI). Metabolomics. 2007;3(3):211-21. Epub 2007/09/01. doi: 10.1007/s11306-007-0082-2. PubMed PMID: 24039616; PubMed Central PMCID: PMC3772505.

Table S1. List of identifiable molecules with changed abundance during DENV2 infection of the *Ae. aegypti* midgut. Select metabolites from mosquito midguts that show differential abundance following DENV2 infection are listed. Abundance of metabolites detected in DENV2-infected and uninfected midguts was compared. The following information is provided for each feature: m/z_{Avg}, average mass to charge ratio detected (averaged between the two biological replicate pools); RT_{Avg}, average retention time detected for each metabolite (averaged between the two biological replicate pools); Detection mode, both polar and nonpolar extracts were detected in both negative and positive ionization modes; Name, identification for each lipid; Lipid classes, classification of each lipid according to LIPID MAPS comprehensive classification system [136]; Formula, chemical component of the molecules at their neutral mass; Adducts, protonated or deprotonated molecular ions, [M+H]+, [M+Na]+, [M+NH4]+ and [M-H]-; PPM Error, difference between experimental mass and exact mass; Match ID, accession number for each metabolite; Database, database of the putative identification: LIPID MAPS, Human Metabolome Database or Metlin, Numbers of alternative IDs, other putative names that are isomers of the chosen name with this chemical formula; Log_2 FC, log_2 fold change of abundance compared between DENV2-infected and uninfected samples; p-value, adjusted p-value. MS/MS database, database used for searching tandem MS fragmentation; MSI level, Metabolomics Standard Initiative level of identification [261].

Number	M/Z_{Avg}	RT_{Avg}	Detection mode		Name	Lipid classes	Formula
			Phase	Ionization mode			
1	107.048563	5.37	Non-polar	Positive	Benzaldehyde	Other organic compounds	C7H6O
2	107.0696948	2.36	Non-polar	Positive	butanetriol	Other organic compounds	C4H10O3
3	116.0701149	4.98	Non-polar	Positive	Proline	Amino acids and peptides	C5H9NO2
4	130.0858	2.35	Non-polar	Positive	Pipecolic acid	Fatty acyls	C6H11NO2
5	135.0799962	5.36	Non-polar	Positive	Phenylpropanal	Other organic compounds	C9H10O
6	137.0452235	1.14	Polar	Positive	Ethyl propyl disulfide	Other organic compounds	C5H12S2
7	145.1219	2.32	Non-polar	Positive	Hydroxyphenylpentanoic acid	Fatty acyls	C11H14O3
8	157.1222	11.38	Non-polar	Positive	Hydroxynonenal	Fatty acyls	C9H16O2
9	157.1222	15.46	Non-polar	Positive	Nonanedione*	Fatty acyls	C9H16O2
10	157.1222	10.16	Non-polar	Positive	Nonanedione*	Fatty acyls	C9H16O2
11	159.1030	22.55	Polar	Negative	Hydroxyoctanoic acid	Fatty acyls	C8H16O3
12	167.1272791	2.35	Non-polar	Positive	N6-methylagmatine	Other organic compounds	C6H16N4
13	175.1329	10.19	Non-polar	Positive	Hydroxy pelargonic acid	Fatty acyls	C9H18O3
14	179.0850081	35.43	Polar	Positive	tetradecadienetetrayne	Other organic compounds	C14H10
15	187.1326	23.54	Polar	Positive	Oxodecanoic acid	Fatty acyls	C10H18O3
16	187.1344	28.36	Polar	Negative	Dimethyloctenetriol	Fatty acyls	C10H20O3
17	188.1277	39.27	Polar	Positive	N-heptanoylglycine	Fatty acyls	C9H17NO3
18	191.142765	8.22	Non-polar	Positive	Beta-damascenone	Other organic compounds	C13H18O
19	195.0665172	26.73	Polar	Negative	Dihydroferulic acid	polyketide	C10H12O4
20	195.1014	4.16	Non-polar	Positive	Hydroxyphenylpentanoic acid	Fatty acyls	C11H14O3
21	196.06908	27.58	Polar	Positive	Alpha-keto-delta-guanidinovaleric acid	Amino acids and peptides	C6H11N3O3
22	196.104865	4.15	Non-polar	Positive	apo-[3-Methylcrotonoyl-coa:carbon-dioxide ligase (ADP-forming)]	Amino acids and peptides	C7H15N3O2
23	198.1235112	13.89	Polar	Positive	Histidine trimethylbetaine	Amino acids and peptides	C9H15N3O2
24	201.0887	2.27	Non-polar	Positive	Phenylvaleric acid	Fatty acyls	C11H14O2
25	207.1028937	32.13	Polar	Negative	Asaron	Other organic compounds	C12H16O3
26	209.1168863	29.74	Polar	Positive	Methoxybenzyl butanoate	Other organic compounds	C12H16O3
27	211.0980	21.47	Polar	Negative	Dimethylidenenonanedioic acid	Fatty acyls	C11H16O4
28	213.1672	22.73	Polar	Positive	Dimethylidenenonanedioic acid	Fatty acyls	C11H16O4
29	214.1547107	3.63	Polar	Positive	Hydroxyphenylbenzoic acid	Other organic compounds	C13H10O3
30	215.1639	25.69	Polar	Positive	Oxododecanoic acid	Fatty acyls	C12H22O3

Number	Adducts	PPM error	Match ID	Database	Number of alternate IDs	DENV vs Mock Day 3		DENV vs Mock Day 7		DENV vs Mock Day 11		MS/MS database	MSI level
						Log_2 FC	p-value	Log_2 FC	p-value	Log_2 FC	p-value		
1	$[M+H]^+$	-5.451	HMDB0006115	HMDB	0	**2.589**	**0.003**	1.094	0.052	**3.270**	**0.002**		3
2	$[M+H]^+$	-5.423	HMDB0061944	HMDB	0	0.510	0.194	**-1.165**	**0.019**	-0.403	0.461		3
3	$[M+H]^+$	-4.259	HMDB0003411	HMDB	7	0.120	0.821	**-5.535**	**0.000**	-0.161	0.826		3
4	$[M+H]^+$	-3.182	HMDB0000070	HMDB	22	0.575	0.186	**-1.664**	**0.006**	-0.243	0.712		3
5	$[M+H]^+$	-3.318	HMDB0031626	HMDB	17	**2.410**	**0.010**	1.155	0.104	**3.391**	**0.004**		3
6	$[M+H]^+$	-0.690	HMDB0033053	HMDB	2	**-5.635**	**0.004**	**-3.609**	**0.035**	**-3.883**	**0.017**		3
7	$[M+Na]^+$	0.831	HMDB0031517	HMDB	30	0.620	0.146	**-1.579**	**0.006**	0.010	1.000		3
8	$[M+H]^+$	-0.865	HMDB0004362	HMDB	30	**1.479**	**0.031**	-0.143	0.901	0.049	0.982	NIST	2
9	$[M+H]^+$	-0.865	HMDB0031263	HMDB	30	**1.539**	**0.035**	-0.149	0.912	0.042	0.991		3
10	$[M+H]^+$	-0.865	HMDB0031263	HMDB	30	**2.238**	**0.039**	-0.248	0.896	-0.003	1.000		3
11	$[M-H]^-$	2.325	HMDB0000486	HMDB	8	**3.492**	**0.010**	**2.721**	**0.041**	**3.149**	**0.012**		3
12	$[M+Na]^+$	3.914	HMDB0039252	HMDB	1	0.525	0.192	**-1.349**	**0.010**	-0.055	0.971		3
13	$[M+H]^+$	1.723	LMFA01050024	LIPID MAPS	2	**1.416**	**0.036**	-0.065	0.985	-0.359	0.640		3
14	$[M+H]^+$	-2.892	HMDB0033187	HMDB	0	-0.686	0.581	0.576	0.653	**-2.359**	**0.045**		3
15	$[M+H]^+$	-1.561	HMDB0010724	HMDB	10	0.313	0.796	0.148	0.938	**3.224**	**0.005**		3
16	$[M-H]^-$	2.518	HMDB0038186	HMDB	9	**2.746**	**0.011**	2.015	0.062	**2.910**	**0.009**		3
17	$[M+H]^+$	-2.116	HMDB0013010	HMDB	2	**-2.833**	**0.013**	-1.983	0.075	-0.574	0.625		3
18	$[M+H]^+$	-1.452	HMDB0013804	HMDB	5	**1.608**	**0.030**	0.365	0.639	0.772	0.365		3
19	$[M-H]^-$	1.194	HMDB0062121	HMDB	0	5.215	0.307	**14.681**	**0.020**	**10.741**	**0.045**		3
20	$[M+H]^+$	-0.723	HMDB0031517	HMDB	19	-2.132	0.060	**-2.855**	**0.018**	-0.247	0.894		3
21	$[M+Na]^+$	-1.034	HMDB0004225	HMDB	0	0.616	0.522	0.961	0.344	**2.162**	**0.027**		3
22	$[M+Na]^+$	-4.506	HMDB0059607	HMDB	0	-0.079	0.889	**2.370**	**0.003**	-0.076	0.966		3
23	$[M+H]^+$	-0.968	HMDB0029422	HMDB	0	-0.410	0.699	1.507	0.112	**1.784**	**0.048**		3
24	$[M+Na]^+$	0.295	HMDB0002043	HMDB	16	0.288	0.591	**1.790**	**0.010**	-0.766	0.347		3
25	$[M-H]^-$	1.085	HMDB0031469	HMDB	0	**11.731**	**0.011**	7.898	0.085	**13.536**	**0.009**		3
26	$[M+H]^+$	-1.596	HMDB0034991	HMDB	14	**2.580**	**0.006**	1.571	0.064	**2.039**	**0.015**		3
27	$[M-H]^-$	1.999	HMDB0059744	HMDB	1	**18.399**	**0.005**	8.872	0.132	7.567	0.153		3
28	$[M+H]^+$	-0.677	HMDB0059744	HMDB	0	2.191	0.072	1.471	0.250	2.386	0.050		3
29	$[M+H]^+$	-2.263	HMDB0032583	HMDB	3	**-7.404**	**0.001**	0.525	0.801	1.544	0.274		3
30	$[M+H]^+$	-1.078	HMDB0010727	HMDB	2	**3.690**	**0.004**	**2.305**	**0.043**	**4.185**	**0.002**		3

Number	M/Z_{Avg}	RT_{Avg}	Detection mode		Name	Lipid classes	Formula
			Phase	Ionization mode			
31	216.1959	4.33	Non-polar	Positive	Dodecenoic acid	Fatty acyls	C12H22O2
32	217.0837	4.14	Non-polar	Positive	Hydroxyphenyl-valeric acid	Fatty acyls	C11H14O3
33	219.1743911	5.66	Non-polar	Positive	Solavetivone*	prenol	C15H22O
34	219.1743911	4.97	Non-polar	Positive	Solavetivone*	prenol	C15H22O
35	219.1759584	7.54	Non-polar	Negative	ditransFarnesal	prenol	C15H24O
36	221.1171153	29.11	Polar	Positive	Hexenyl salicylate	Other organic compounds	C13H16O3
37	221.1547838	29.38	Polar	Negative	hydroxynoreremophilenone	prenol	C14H22O2
38	222.2061	2.41	Non-polar	Positive	Octylglycerol	Glycerolipids	C11H24O3
39	225.1121179	21.98	Polar	Positive	Vanillin butylene glycol acetal	Other organic compounds	C12H16O4
40	226.1799782	6.06	Non-polar	Positive	diepoxymegastigmene	Other organic compounds	C13H20O2
41	227.1255	3.98	Non-polar	Positive	Dimethyloctenetetrol	Fatty acyls	C10H20O4
42	230.1381	21.27	Polar	Positive	Butenylcarnitine	Acylcarnitine	C11H19NO4
43	230.1750	2.71	Non-polar	Positive	Cucurbic acid	Fatty acyls	C12H20O3
44	230.1750	22.80	Polar	Positive	N-decanoylglycine	Fatty acyls	C12H23NO3
45	231.1955	10.18	Non-polar	Positive	Hydroxytridecanoic acid*	Fatty acyls	C13H26O3
46	231.1955	11.39	Non-polar	Positive	Hydroxytridecanoic acid*	Fatty acyls	C13H26O3
47	234.1123878	2.36	Non-polar	Positive	methylenedioxyphenylhexadienone	Other organic compounds	C13H12O3
48	237.1117378	29.75	Polar	Positive	Ethyl vanillin isobutyrate	Other organic compounds	C13H16O4
49	239.1271434	32.84	Polar	Positive	Tetramethyl(oxopropyl)cyclohexanetrione	prenol	C13H18O4
50	243.1603	28.48	Polar	Negative	Undecanedicarboxylic acid	Fatty acyls	C13H24O4
51	244.1555	19.42	Polar	Negative	Methylbutyroylcarnitine	Acylcarnitine	C12H23NO4
52	244.1901	45.54	Polar	Positive	N-undecanoylglycine	Fatty acyls	C13H25NO3
53	244.1909	6.05	Non-polar	Positive	N-undecanoylglycine	Fatty acyls	C13H25NO3
54	245.1747	28.18	Polar	Positive	Undecanedicarboxylic acid*	Fatty acyls	C13H24O4
55	245.1747	24.75	Polar	Positive	Undecanedicarboxylic acid*	Fatty acyls	C13H24O4
56	246.1697	19.27	Polar	Positive	methylbutyroylcarnitine	Acylcarnitine	C12H23NO4
57	253.1022735	2.31	Non-polar	Positive	Cycasin	Other organic compounds	C8H16N2O7
58	255.12211	29.74	Polar	Positive	Methyldihydroxymethylbutyl hydroxybenzoate	Other organic compounds	C13H18O5
59	256.1542704	2.02	Non-polar	Positive	Tetramethyl(oxopropyl)cyclohexanetrione	prenol	C13H18O4
60	256.162014	27.58	Polar	Positive	Hypusine*	Amino acids and peptides	C10H23N3O3

Number	Adducts	PPM error	Match ID	Database	Number of alternate IDs	DENV vs Mock Day 3		DENV vs Mock Day 7		DENV vs Mock Day 11		MS/MS database	MSI level
						Log_2 FC	p-value	Log_2 FC	p-value	Log_2 FC	p-value		
31	$[M+NH_4]^+$	0.696	HMDB0000529	HMDB	28	**1.102**	**0.027**	0.237	0.648	0.189	0.740		3
32	$[M+Na]^+$	0.831	HMDB0041666	HMDB	17	1.194	0.146	**4.708**	**0.001**	0.299	0.805		3
33	$[M+H]^+$	0.458	LMPR0103650001	LIPID MAPS	36	1.509	0.162	**3.754**	**0.008**	1.817	0.240		3
34	$[M+H]^+$	0.458	LMPR0103650001	LIPID MAPS	0	**2.182**	**0.014**	**2.785**	**0.003**	0.550	0.523		3
35	$[M-H]^-$	-2.359	HMDB60356	HMDB	0	**-4.601**	**0.045**	-2.387	0.156	**-5.823**	**0.009**		3
36	$[M+H]^+$	-0.474	HMDB0061942	HMDB	4	0.455	0.568	0.206	0.858	**1.534**	**0.045**		3
37	$[M-H]^-$	0.359	HMDB0037605	HMDB	0	0.980	0.089	0.199	0.799	**1.666**	**0.012**		3
38	$[M+NH_4]^+$	1.469	LMGL01020030	LIPID MAPS	1	0.038	0.931	**-1.192**	**0.019**	-0.165	0.798		3
39	$[M+H]^+$	-0.076	HMDB0032552	HMDB	6	**2.096**	**0.030**	1.390	0.141	**2.423**	**0.015**		3
40	$[M+NH_4]^+$	-0.840	HMDB0038529	HMDB	11	1.062	0.135	**2.222**	**0.011**	0.483	0.614		3
41	$[M+Na]^+$	0.358	HMDB0035133	HMDB	5	0.284	0.457	**1.971**	**0.002**	0.039	0.982		3
42	$[M+H]^+$	-2.528	HMDB0013126	HMDB	0	**13.663**	**0.033**	11.204	0.089	9.490	0.094		3
43	$[M+NH_4]^+$	-0.160	HMDB0029388	HMDB	7	**2.273**	**0.010**	-0.410	0.603	**2.944**	**0.005**		3
44	$[M+H]^+$	-0.156	HMDB0013267	HMDB	0	2.262	0.056	1.609	0.184	**2.479**	**0.037**		3
45	$[M+H]^+$	0.052	HMDB0061655	HMDB	2	**1.356**	**0.032**	-0.082	0.964	-0.056	0.980		3
46	$[M+H]^+$	0.052	HMDB0061655	HMDB	2	**1.484**	**0.029**	-0.106	0.950	0.017	1.000		3
47	$[M+NH_4]^+$	-0.367	HMDB0032035	HMDB	5	1.106	0.777	**-13.828**	**0.005**	-1.585	0.777		3
48	$[M+H]^+$	-1.675	HMDB0037683	HMDB	0	**3.222**	**0.003**	1.582	0.084	**2.364**	**0.011**		3
49	$[M+H]^+$	-2.683	HMDB0033191	HMDB	1	0.958	0.172	0.758	0.332	**2.090**	**0.010**		3
50	$[M-H]^-$	0.466	HMDB0002327	HMDB	2	**1.614**	**0.019**	0.965	0.176	**2.513**	**0.004**		3
51	$[M-H]^-$	0.310	HMDB0000378	HMDB	3	**7.810**	**0.049**	2.443	0.626	4.610	0.273		3
52	$[M+H]^+$	-2.412	HMDB0013286	HMDB	0	**-3.498**	**0.008**	-0.083	0.981	0.360	0.897		3
53	$[M+H]^+$	0.542	HMDB0013286	HMDB	3	**3.074**	**0.014**	**3.388**	**0.006**	1.496	0.238		3
54	$[M+H]^+$	-0.029	HMDB0002327	HMDB	0	1.255	0.256	1.020	0.395	**2.281**	**0.046**		3
55	$[M+H]^+$	-0.029	HMDB0002327	HMDB	0	**3.438**	**0.013**	2.458	0.069	0.318	0.953		3
56	$[M+H]^+$	-1.280	HMDB0000378	HMDB	4	**2.439**	**0.015**	1.573	0.104	**3.422**	**0.003**		3
57	$[M+H]^+$	-2.989	HMDB0038850	HMDB	1	**2.617**	**0.014**	0.696	0.479	1.034	0.365		3
58	$[M+H]^+$	-2.313	HMDB0032796	HMDB	0	**2.888**	**0.003**	**1.797**	**0.031**	**2.858**	**0.003**		3
59	$[M+NH_4]^+$	-0.259	HMDB0033191	HMDB	1	**3.052**	**0.012**	-0.140	0.964	2.037	0.088		3
60	$[M+Na]^+$	-4.915	HMDB0011140	HMDB	0	1.628	0.066	1.208	0.189	**2.646**	**0.009**		3

Number	M/Z_{Avg}	RT_{Avg}	Detection mode		Name	Lipid classes	Formula
			Phase	Ionization mode			
61	256.162014	28.92	Polar	Positive	Hypusine*	Amino acids and peptides	C10H23N3O3
62	256.1924662	26.91	Polar	Negative	N-lauroylglycine	Amino acids and peptides	C14H27NO3
63	258.1717	21.53	Polar	Negative	Hexanoylcarnitine	Acylcarnitine	C13H25NO4
64	260.1852	21.27	Polar	Positive	Hexanoylcarnitine	Acylcarnitine	C13H25NO4
65	261.1343	18.74	Polar	Negative	Phaseolic acid	Fatty acyls	C12H22O6
66	266.1723	24.74	Polar	Positive	N-undecanoylglycine	Fatty acyls	C13H25NO3
67	267.0735287	1.18	Polar	Negative	Inosine	nucleoside	C10H12N4O5
68	270.3153	30.65	Polar	Positive	Octadecylamine	Fatty acyls	C18H39N
69	271.2267	11.63	Non-polar	Positive	Oxohexadecanoic acid	Fatty acyls	C16H30O3
70	272.1866	23.41	Polar	Negative	Heptanoylcarnitine	Acylcarnitine	C14H27NO4
71	272.2581	24.64	Polar	Positive	C16 Sphingosine	Sphingolipids	C16H33NO2
72	273.1708	26.62	Polar	Negative	Hydroxytetradecanedioic acid	Fatty acyls	C14H26O5
73	274.2013	17.01	Polar	Positive	Heptanoylcarnitine*	Acylcarnitine	C14H27NO4
74	274.2013	23.10	Polar	Positive	Heptanoylcarnitine*	Acylcarnitine	C14H27NO4
75	277.1798	29.10	Polar	Positive	Ginsenoyne c	Fatty acyls	C17H24O3
76	278.2479	4.28	Non-polar	Positive	Obscuraminol A	Sphingolipids	C18H31NO
77	284.0448476	45.65	Polar	Positive	Tolfenamic acid	Other organic compounds	C14H12ClNO2
78	284.0991066	1.11	Polar	Positive	Guanosine	nucleoside	C10H13N5O5
79	284.1316695	7.67	Non-polar	Positive	Arginyl-serine	Amino acids and peptides	C9H19N5O4
80	286.2009	15.10	Polar	Positive	Octenoylcarnitine	Acylcarnitine	C15H27NO4
81	287.2226	29.74	Polar	Negative	Dihydroxypalmitic acid	Fatty acyls	C16H32O4
82	288.1440	20.97	Polar	Positive	hexenedioylcarnitine	Acylcarnitine	C13H21NO6
83	288.2170	19.21	Polar	Positive	Octanoylcarnitine	Acylcarnitine	C15H29NO4
84	289.1415167	3.42	Non-polar	Positive	dihydroabscisic acid	prenol	C15H22O4
85	289.1619477	14.04	Polar	Positive	Asparaginyl-arginine	Amino acids and peptides	C10H20N6O4
86	295.1552514	31.69	Polar	Negative	tocopheronic acid	Other organic compounds	C16H24O5
87	295.1830358	29.35	Polar	Negative	Hydrocinchonine	Other organic compounds	C19H24N2O
88	297.1116083	18.74	Polar	Negative	7c-aglycone	prenol	C18H18O4
89	297.2536987	5.84	Non-polar	Positive	Tetramethylhexadecatetraene	prenol	C20H34
90	300.2184	21.15	Polar	Negative	Dimethylheptanoyl carnitine	Acylcarnitine	C16H31NO4

Number	Adducts	PPM error	Match ID	Database	Number of alternate IDs	DENV vs Mock Day 3		DENV vs Mock Day 7		DENV vs Mock Day 11		MS/MS database	MSI level
						Log_2 FC	p-value	Log_2 FC	p-value	Log_2 FC	p-value		
61	$[M+Na]^+$	-4.915	HMDB0011140	HMDB	0	1.537	0.069	0.743	0.400	**2.467**	**0.010**		3
62	$[M-H]^-$	2.520	HMDB0013272	HMDB	0	**1.953**	**0.041**	1.712	0.113	1.910	0.051		3
63	$[M-H]^-$	2.203	HMDB0000705	HMDB	1	**12.786**	**0.000**	**3.634**	**0.016**	**4.684**	**0.004**		3
64	$[M+H]^+$	-1.671	HMDB0000705	HMDB	0	**3.519**	**0.004**	**2.347**	**0.031**	**3.723**	**0.003**		3
65	$[M-H]^-$	-0.319	HMDB0031897	HMDB	0	**2.879**	**0.019**	2.424	0.066	2.071	0.080		3
66	$[M+Na]^+$	-1.545	HMDB0013286	HMDB	0	0.384	0.834	2.685	0.069	**3.164**	**0.024**		3
67	$[M-H]^-$	0.129	HMDB0000195	HMDB	2	**-9.314**	**0.012**	-3.122	0.403	-3.662	0.297		3
68	$[M+H]^+$	-0.781	HMDB0029586	HMDB	0	**-10.828**	**0.000**	-0.055	0.982	0.017	0.999		3
69	$[M+H]^+$	-0.207	HMDB0010733	HMDB	2	**2.147**	**0.034**	-0.390	0.745	0.310	0.802		3
70	$[M-H]^-$	-0.624	HMDB0013238	HMDB	0	**11.760**	**0.015**	5.928	0.228	4.103	0.416		3
71	$[M+H]^+$	1.102	LMSP01040008	LIPID MAPS	0	**12.060**	**0.042**	4.496	0.430	**17.312**	**0.009**		3
72	$[M-H]^-$	0.233	HMDB0000394	HMDB	0	**14.766**	**0.003**	0.898	0.857	**12.712**	**0.006**		3
73	$[M+H]^+$	0.072	HMDB0013238	HMDB	0	**2.703**	**0.008**	1.592	0.091	**3.201**	**0.004**		3
74	$[M+H]^+$	0.072	HMDB0013238	HMDB	0	**5.734**	**0.006**	**4.709**	**0.020**	**5.265**	**0.008**		3
75	$[M+H]^+$	-0.194	HMDB0038994	HMDB	5	0.415	0.646	0.160	0.913	**1.845**	**0.028**		3
76	$[M+H]^+$	0.361	LMSP01080035	LIPID MAPS	3	**2.361**	**0.009**	**4.362**	**0.000**	-0.227	0.802		3
77	$[M+Na]^+$	-0.101	HMDB0042043	HMDB	0	-1.319	0.813	**-13.291**	**0.011**	0.272	0.999		3
78	$[M+H]^+$	0.569	HMDB0000133	HMDB	1	**-5.173**	**0.002**	**-3.816**	**0.012**	**-3.981**	**0.007**		3
79	$[M+Na]^+$	-4.796	HMDB0028718	HMDB	1	-5.052	0.115	-2.970	0.437	**-16.440**	**0.004**		3
80	$[M+H]^+$	-1.436	HMDB0013324	HMDB	0	4.569	0.302	**13.416**	**0.017**	**10.827**	**0.026**		3
81	$[M-H]^-$	-0.504	HMDB0037798	HMDB	4	**2.144**	**0.005**	**1.327**	**0.048**	**1.858**	**0.009**		3
82	$[M+H]^+$	0.694	LMFA07070013	LIPID MAPS	0	3.863	0.646	14.632	0.080	**15.235**	**0.045**		3
83	$[M+H]^+$	0.107	HMDB0000791	HMDB	0	**7.915**	**0.000**	**5.006**	**0.002**	**5.779**	**0.001**		3
84	$[M+Na]^+$	1.840	HMDB0039516	HMDB	23	1.161	0.154	**2.228**	**0.024**	-0.918	0.417		3
85	$[M+H]^+$	0.238	HMDB0028725	HMDB	0	0.162	0.990	0.719	0.946	**13.276**	**0.016**		3
86	$[M-H]^-$	0.338	LMPR02020062	LIPID MAPS	3	**10.358**	**0.000**	1.619	0.097	**2.917**	**0.009**		3
87	$[M-H]^-$	4.891	HMDB0030283	HMDB	2	0.945	0.056	-0.007	1.000	**1.409**	**0.012**		3
88	$[M-H]^-$	-5.450	HMDB0004808	HMDB	10	**3.180**	**0.015**	2.504	0.066	1.761	0.153		3
89	$[M+Na]^+$	-5.725	HMDB0035152	HMDB	1	**13.579**	**0.010**	3.029	0.510	**13.749**	**0.015**		3
90	$[M-H]^-$	1.197	HMDB0006320	HMDB	1	**22.212**	**0.000**	**16.288**	**0.004**	**20.436**	**0.001**		3

Number	M/Z_{Avg}	RT_{Avg}	Detection mode		Name	Lipid classes	Formula
			Phase	Ionization mode			
91	300.2901	11.82	Non-polar	Positive	Sphingosine	Sphingolipids	C18H37NO2
92	302.2328	20.98	Polar	Positive	Nonanoylcarnitine	Acylcarnitine	C16H31NO4
93	303.1777563	3.65	Non-polar	Positive	Glutaminyl-arginine	Amino acids and peptides	C11H22N6O4
94	303.2645	6.05	Non-polar	Positive	Myristoylglycine	Fatty acyls	C16H31NO3
95	304.2634781	6.06	Non-polar	Positive	Vitamin a	prenol	C20H30O
96	307.0938801	3.50	Non-polar	Positive	Dihydroxydimethylflavanone	polyketide	C17H16O4
97	309.1712472	30.63	Polar	Negative	Valdiate	prenol	C17H26O5
98	309.2283	2.80	Non-polar	Positive	Tris(ethoxyethoxy)propane	Glycerolipids	C15H32O6
99	310.2012	4.16	Non-polar	Positive	Decatrienoylcarnitine	Acylcarnitine	C17H27NO4
100	311.1848479	29.76	Polar	Positive	Botrydial	prenol	C17H26O5
101	311.1848479	8.30	Non-polar	Positive	Botrydial	prenol	C17H26O5
102	313.1621	3.64	Non-polar	Positive	Octenyl glucoside	Fatty acyls	C14H26O6
103	314.2115	5.97	Non-polar	Positive	Methoxydiphenylheptanone	Sterol	C20H24O2
104	314.2325	27.54	Polar	Positive	Decenoylcarnitine	Acylcarnitine	C17H31NO4
105	314.2325	6.95	Non-polar	Positive	Decenoylcarnitine	Acylcarnitine	C17H31NO4
106	314.2344	22.87	Polar	Negative	Decanoylcarnitine	Acylcarnitine	C17H33NO4
107	315.1784	2.78	Non-polar	Positive	Octanol glucoside	Fatty acyls	C14H28O6
108	315.1952787	11.06	Non-polar	Positive	oxo-retinoic acid	prenol	C20H26O3
109	316.2474	22.56	Polar	Positive	Decanoylcarnitine	Acylcarnitine	C17H33NO4
110	318.2797	8.12	Non-polar	Positive	N-methyl arachidonoyl amine	Fatty acyls	C21H35NO
111	319.2266	12.04	Non-polar	Positive	HEPE	Fatty acyls	C20H30O3
112	326.2178	3.24	Non-polar	Positive	Glucopyranosyloctanediol	Fatty acyls	C14H28O7
113	326.2534	2.49	Non-polar	Positive	Tris(ethoxyethoxy)propane	Glycerolipids	C15H32O6
114	326.3057	12.70	Non-polar	Positive	Eicosadienoic acid	Fatty acyls	C20H36O2
115	328.2482	7.72	Non-polar	Positive	HpOTrE	Fatty acyls	C18H30O4
116	328.2496	24.39	Polar	Negative	Dimethylnonanoyl carnitine	Acylcarnitine	C18H35NO4
117	328.3212	13.61	Non-polar	Positive	N,n-dimethylsphingosine*	Sphingolipids	C20H41NO2
118	328.3212	12.95	Non-polar	Positive	N,n-dimethylsphingosine*	Sphingolipids	C20H41NO2
119	329.1526	29.38	Polar	Negative	TriHOME	Fatty acyls	C18H34O5
120	330.2636	24.09	Polar	Positive	Undecanoylcarnitine	Acylcarnitine	C18H35NO4

Number	Adducts	PPM error	Match ID	Database	Number of alternate IDs	DENV vs Mock Day 3		DENV vs Mock Day 7		DENV vs Mock Day 11		MS/MS database	MSI level
						Log_2 FC	p-value	Log_2 FC	p-value	Log_2 FC	p-value		
91	$[M+H]^+$	1.339	HMDB0000252	HMDB	17	**7.006**	**0.001**	**4.408**	**0.003**	2.440	0.087		3
92	$[M+H]^+$	0.575	HMDB0013288	HMDB	1	**7.599**	**0.002**	3.607	0.073	3.438	0.054		3
93	$[M+H]^+$	0.752	HMDB0029143	HMDB	2	1.503	0.069	**2.023**	**0.022**	-0.862	0.405		3
94	$[M+NH_4]^+$	1.061	HMDB0013250	HMDB	1	**3.334**	**0.004**	**3.699**	**0.001**	1.862	0.053		3
95	$[M+NH_4]^+$	-0.038	HMDB0000305	HMDB	18	**4.692**	**0.041**	3.017	0.157	3.382	0.206		3
96	$[M+Na]^+$	-0.693	HMDB0030694	HMDB	16	**18.721**	**0.000**	0.000	1.000	**16.024**	**0.000**		3
97	$[M-H]^-$	1.609	HMDB0040980	HMDB	0	**2.450**	**0.003**	0.898	0.163	**2.606**	**0.003**		3
98	$[M+H]^+$	3.686	HMDB0037162	HMDB	0	0.155	0.799	**-3.074**	**0.001**	-1.232	0.113		3
99	$[M+H]^+$	0.323	LMFA07070016	LIPID MAPS	9	1.673	0.054	**1.885**	**0.031**	-0.534	0.599		3
100	$[M+H]^+$	1.285	LMPR0103640001	LIPID MAPS	2	**4.377**	**0.000**	**2.550**	**0.010**	**3.633**	**0.001**		3
101	$[M+H]^+$	1.290	LMPR0103640001	LIPID MAPS	3	**4.120**	**0.003**	**3.321**	**0.003**	**2.933**	**0.014**		3
102	$[M+Na]^+$	-0.142	HMDB0032959	HMDB	0	1.172	0.087	**2.193**	**0.008**	0.277	0.772		3
103	$[M+NH_4]^+$	0.054	HMDB0033293	HMDB	5	0.501	0.221	**3.127**	**0.000**	-0.219	0.730		3
104	$[M+H]^+$	-0.236	HMDB0013205	HMDB	0	1.274	0.166	0.792	0.411	**1.909**	**0.045**		3
105	$[M+H]^+$	-0.237	HMDB0013205	HMDB	5	0.409	0.351	**1.222**	**0.027**	0.366	0.566		3
106	$[M-H]^-$	2.221	HMDB0000651	HMDB	0	**20.015**	**0.001**	**15.754**	**0.004**	**20.098**	**0.001**		3
107	$[M+Na]^+$	1.921	HMDB0032958	HMDB	2	**1.813**	**0.034**	0.422	0.649	-0.259	0.802		3
108	$[M+H]^+$	-0.612	HMDB0006285	HMDB	8	**1.801**	**0.023**	-0.221	0.833	-0.136	0.909		3
109	$[M+H]^+$	-2.513	HMDB0000651	HMDB	0	**7.945**	**0.000**	**4.802**	**0.001**	**5.873**	**0.000**		3
110	$[M+H]^+$	1.576	LMFA08020007	LIPID MAPS	5	0.729	0.391	**3.514**	**0.005**	0.063	0.991		3
111	$[M+H]^+$	-0.425	HMDB0010209	HMDB	26	**2.119**	**0.016**	-0.462	0.592	0.612	0.483		3
112	$[M+NH_4]^+$	1.588	HMDB0029362	HMDB	0	0.381	0.556	-0.746	0.352	**-2.314**	**0.022**		3
113	$[M+NH_4]^+$	-0.916	HMDB0037162	HMDB	0	0.086	0.866	**-14.341**	**0.000**	-0.179	0.799		3
114	$[M+NH_4]^+$	1.284	HMDB0061864	HMDB	4	**7.026**	**0.000**	**4.322**	**0.001**	**2.614**	**0.013**		3
115	$[M+NH_4]^+$	0.000	LMFA02000109	LIPID MAPS	5	**1.560**	**0.044**	**2.000**	**0.013**	0.311	0.743		3
116	$[M-H]^-$	0.890	HMDB0006202	HMDB	1	**18.134**	**0.004**	**15.667**	**0.012**	**19.747**	**0.004**		3
117	$[M+H]^+$	0.647	HMDB0013645	HMDB	1	**7.924**	**0.001**	**6.260**	**0.002**	**6.914**	**0.004**		3
118	$[M+H]^+$	0.647	HMDB0013645	HMDB	1	**4.960**	**0.000**	**2.461**	**0.004**	1.598	0.055		3
119	$[M-H]^-$	1.489	HMDB0004708	HMDB	0	0.671	0.200	-0.004	1.000	**1.159**	**0.036**		3
120	$[M+H]^+$	-0.938	HMDB0013321	HMDB	0	**6.953**	**0.000**	**3.464**	**0.005**	**5.142**	**0.001**		3

Number	M/Z_{Avg}	RT_{Avg}	Detection mode		Name	Lipid classes	Formula
			Phase	Ionization mode			
121	331.1495508	29.39	Polar	Negative	Spectinomycin	Other organic compounds	C14H24N2O7
122	331.1723	3.23	Non-polar	Positive	Glucopyranosyloctanediol	Fatty acyls	C14H28O7
123	331.2475	15.47	Non-polar	Positive	TriHOME	Fatty acyls	C18H34O5
124	332.2427	19.74	Polar	Positive	Hydroxydecanoyl carnitine	Acylcarnitine	C17H33NO5
125	332.2781	3.42	Non-polar	Positive	DHOME	Fatty acyls	C18H34O4
126	333.1665113	29.74	Polar	Positive	Valdiate	prenol	C17H26O5
127	333.2538	5.37	Non-polar	Positive	Dimethylmethylidene(propanyl)tetracycloheptadecadiene	Sterol	C23H34
128	336.2173188	4.16	Non-polar	Positive	methylpropanoyloxygermacratrienolide	prenol	C19H26O4
129	339.1814	29.38	Polar	Negative	Dehydrodinor-TXB2	Fatty acyls	C18H26O6
130	339.2488	2.42	Non-polar	Positive	Dihydroxyoctadecanoic acid	Fatty acyls	C18H36O4
131	340.2839	24.69	Polar	Positive	Oleoyl glycine	Fatty acyls	C20H37NO3
132	341.2128	12.38	Non-polar	Negative	Epoxy-DHA	Fatty acyls	C22H28O3
133	342.3000	8.12	Non-polar	Positive	Cer(d20:1)	Sphingolipids	C20H39NO3
134	342.3000	27.46	Polar	Positive	Cer(d20:1)*	Sphingolipids	C20H39NO3
135	342.3000	28.76	Polar	Positive	Cer(d20:1)*	Sphingolipids	C20H39NO3
136	342.3000	29.53	Polar	Positive	Cer(d20:1)*	Sphingolipids	C20H39NO3
137	342.3000	28.14	Polar	Positive	Cer(d20:1)*	Sphingolipids	C20H39NO3
138	342.3000	28.42	Polar	Positive	Cer(d20:1)*	Sphingolipids	C20H39NO3
139	342.3000	27.84	Polar	Positive	Cer(d20:1)*	Sphingolipids	C20H39NO3
140	342.3371	13.44	Non-polar	Positive	N,N,N-trimethyl-sphingosine	Sphingolipids	C21H38O2
141	343.1893045	5.11	Non-polar	Positive	Hydroxymethoxyphenylmethoxyphenylheptanone	Other organic compounds	C21H26O4
142	344.2786	25.52	Polar	Positive	Dodecanoylcarnitine	Acylcarnitine	C19H37NO4
143	344.3160	10.60	Non-polar	Positive	Ethanolamine oleate*	Fatty acyls	C20H41NO3
144	344.3160	11.08	Non-polar	Positive	Ethanolamine oleate*	Fatty acyls	C20H41NO3
145	344.3160	10.07	Non-polar	Positive	Ethanolamine oleate*	Fatty acyls	C20H41NO3
146	344.3160	8.13	Non-polar	Positive	Ethanolamine oleate*	Fatty acyls	C20H41NO3
147	344.3160	11.82	Non-polar	Positive	Ethanolamine oleate*	Fatty acyls	C20H41NO3
148	345.1553275	18.41	Polar	Negative	dihydroxyfenchoneglucoside	prenol	C16H26O8
149	346.2586	21.36	Polar	Positive	Hydroxyundecanoyl carnitine	Acylcarnitine	C18H35NO5
150	348.2742	15.47	Non-polar	Positive	TriHOME	Fatty acyls	C18H34O5

Number	Adducts	PPM error	Match ID	Database	Number of alternate IDs	DENV vs Mock Day 3		DENV vs Mock Day 7		DENV vs Mock Day 11		MS/MS database	MSI level
						Log_2 FC	p-value	Log_2 FC	p-value	Log_2 FC	p-value		
121	$[M-H]^-$	-4.589	HMDB0015055	HMDB	0	0.653	0.241	0.154	0.857	**1.446**	**0.017**		3
122	$[M+Na]^+$	-1.220	HMDB0029362	HMDB	0	0.567	0.512	1.549	0.133	**-2.989**	**0.027**		3
123	$[M+H]^+$	-1.253	HMDB0004710	HMDB	1	**1.655**	**0.047**	-0.238	0.851	-0.165	0.904		3
124	$[M+H]^+$	-1.462	HMDB0061636	HMDB	0	**2.049**	**0.021**	0.119	0.946	0.584	0.472		3
125	$[M+NH_4]^+$	-4.481	HMDB0004705	HMDB	7	1.520	0.054	**4.124**	**0.001**	-0.277	0.792		3
126	$[M+Na]^+$	-2.356	HMDB0040980	HMDB	3	**3.289**	**0.004**	**2.606**	**0.017**	**3.930**	**0.002**		3
127	$[M+Na]^+$	-4.663	HMDB0060729	HMDB	0	-0.803	0.154	-0.771	0.233	**-2.756**	**0.006**		3
128	$[M+NH_4]^+$	1.216	HMDB0031373	HMDB	7	1.218	0.140	**4.013**	**0.002**	-0.058	0.991		3
129	$[M-H]^-$	0.294	LMFA03030013	LIPID MAPS	1	**1.776**	**0.040**	0.099	0.939	**1.774**	**0.046**		3
130	$[M+Na]^+$	-5.481	HMDB0059633	HMDB	3	0.563	0.237	**-20.795**	**0.000**	-0.740	0.316		3
131	$[M+H]^+$	-2.170	HMDB0013631	HMDB	1	**5.321**	**0.001**	0.757	0.487	**3.346**	**0.009**		3
132	$[M-H]^-$	1.753	LMFA04000014	LIPID MAPS	7	-0.955	1.000	**-4.207**	**0.045**	-2.630	0.234		3
133	$[M+H]^+$	0.586	LMSP02010014	LIPID MAPS	7	**6.139**	**0.016**	4.095	0.055	5.197	0.050		3
134	$[M+H]^+$	0.584	LMSP02010014	LIPID MAPS	2	**12.609**	**0.033**	4.346	0.442	5.881	0.263		3
135	$[M+H]^+$	0.584	LMSP02010014	LIPID MAPS	2	8.289	0.083	**11.163**	**0.042**	9.223	0.052		3
136	$[M+H]^+$	0.584	LMSP02010014	LIPID MAPS	2	**6.817**	**0.002**	2.045	0.211	**4.560**	**0.010**		3
137	$[M+H]^+$	0.584	LMSP02010014	LIPID MAPS	2	**8.311**	**0.000**	**3.617**	**0.027**	**12.954**	**0.000**		3
138	$[M+H]^+$	0.584	LMSP02010014	LIPID MAPS	2	**8.319**	**0.049**	7.144	0.105	5.379	0.158		3
139	$[M+H]^+$	0.584	LMSP02010014	LIPID MAPS	2	**12.319**	**0.015**	3.132	0.484	5.716	0.175		3
140	$[M+H]^+$	0.278	53957	Metlin	2	**8.042**	**0.001**	**7.024**	**0.001**	2.162	0.206		3
141	$[M+H]^+$	-3.158	HMDB0029525	HMDB	0	0.222	0.885	**-3.965**	**0.024**	-1.071	0.591		3
142	$[M+H]^+$	-2.614	HMDB0002250	HMDB	0	**15.275**	**0.000**	**12.992**	**0.001**	**20.503**	**0.000**		3
143	$[M+H]^+$	0.352	HMDB0015638	HMDB	2	**5.009**	**0.001**	**3.527**	**0.003**	**3.354**	**0.013**		3
144	$[M+H]^+$	0.352	HMDB0015638	HMDB	2	**5.942**	**0.001**	**2.697**	**0.008**	**2.664**	**0.021**		3
145	$[M+H]^+$	0.352	HMDB0015638	HMDB	2	**5.175**	**0.003**	**3.133**	**0.010**	**3.230**	**0.025**		3
146	$[M+H]^+$	0.352	HMDB0015638	HMDB	2	**5.093**	**0.006**	**3.212**	**0.021**	3.052	0.059		3
147	$[M+H]^+$	0.352	HMDB0015638	HMDB	0	**4.776**	**0.002**	**2.641**	**0.011**	2.155	0.064		3
148	$[M-H]^-$	-0.475	HMDB0033223	HMDB	0	**13.479**	**0.019**	**13.814**	**0.031**	**11.782**	**0.036**		3
149	$[M+H]^+$	-0.495	HMDB0061637	HMDB	0	**3.717**	**0.008**	0.829	0.474	1.532	0.158		3
150	$[M+NH_4]^+$	-0.858	HMDB0004708	HMDB	2	**1.656**	**0.032**	-0.395	0.629	-0.040	0.991		3

Number	M/Z_{Avg}	RT_{Avg}	Detection mode		Name	Lipid classes	Formula
			Phase	Ionization mode			
151	350.2690	7.49	Non-polar	Positive	Hydroxydione*	Sterol	C21H32O3
152	350.2690	6.01	Non-polar	Positive	Hydroxydione*	Sterol	C21H32O3
153	352.2110	25.73	Polar	Positive	Keto-decanoylcarnitine	Acylcarnitine	C17H31NO5
154	352.2485	5.44	Non-polar	Positive	Prostaglandin a2	Fatty acyls	C20H30O4
155	356.2200937	5.02	Non-polar	Positive	Pipercide	Other organic compounds	C22H29NO3
156	356.3522	38.73	Polar	Positive	Eicosanoyl-EA	Fatty acyls	C22H45NO2
157	359.2900	6.05	Non-polar	Positive	Trans-dodecenoylcarnitine	Acylcarnitine	C19H35NO4
158	361.2376	11.38	Non-polar	Positive	Resolvin d5	Fatty acyls	C22H32O4
159	366.2639	5.12	Non-polar	Positive	Trihydroxy-pregnenone	Sterol	C21H32O4
160	366.2851	3.49	Non-polar	Positive	Sativic acid	Fatty acyls	C18H36O6
161	367.2629367	46.61	Polar	Positive	nonadecapentaenyl)resorcinol	polyketide	C25H34O2
162	370.2589	8.29	Non-polar	Positive	Prostaglandin d2*	Fatty acyls	C20H32O5
163	370.2589	6.91	Non-polar	Positive	Prostaglandin d2*	Fatty acyls	C20H32O5
164	377.2142	2.54	Non-polar	Positive	Desoximetasone	Sterol	C22H29FO4
165	378.266688	7.19	Non-polar	Positive	Calycanthidine	Other organic compounds	C23H28N4
166	379.2957	5.04	Non-polar	Positive	N-arachidonoyl glycine	Fatty acyls	C22H35NO3
167	381.2959	8.77	Non-polar	Positive	MAG(18:0)	Glycerolipids	C21H42O4
168	384.3830	38.02	Polar	Positive	N-(Docosanoyl)-ethanolamine	Fatty acyls	C24H49NO2
169	387.2141	16.65	Polar	Positive	Dihydroxyoxopregnanal	Sterol	C21H32O5
170	390.1361203	29.10	Polar	Positive	fucopyranosylacetamidodeoxyglucopyranose	Other organic compounds	C14H25NO10
171	390.3108	5.63	Non-polar	Positive	Finasteride	Sterol	C23H36N2O2
172	392.2904	5.02	Non-polar	Positive	Hydroxy-N-(hydroxypropanyl)-dimethylazatetracyclo heptadecacarboximidic acid	Sterol	C22H34N2O3
173	395.0446694	28.36	Polar	Positive	Kaempferol 7,4'-dimethyl ether 3-O-sulfate	polyketide	C17H14O9S
174	397.1829	26.31	Polar	Positive	Epiisocucurbic acid glucoside	Fatty acyls	C18H30O8
175	401.1777578	2.36	Non-polar	Positive	N-acetyllactosamine	Other organic compounds	C14H25NO11
176	409.2925	15.46	Non-polar	Positive	Trihydroxycholanoic acid*	Sterol	C24H40O5
177	409.2925	14.73	Non-polar	Positive	Trihydroxycholanoic acid*	Sterol	C24H40O5
178	411.1048871	29.69	Polar	Positive	hydroxyauranetin	polyketide	C20H20O8
179	411.1437778	11.66	Non-polar	Negative	Garcimangosone c	Other organic compounds	C23H24O7
180	412.3214206	11.04	Non-polar	Positive	dehydromicropteroxanthin	prenol	C27H38O2

Number	Adducts	PPM error	Match ID	Database	Number of alternate IDs	DENV vs Mock Day 3		DENV vs Mock Day 7		DENV vs Mock Day 11		MS/MS database	MSI level
						Log_2 FC	p-value	Log_2 FC	p-value	Log_2 FC	p-value		
151	$[M+NH_4]^+$	-0.015	HMDB0062609	HMDB	11	**3.252**	**0.004**	**2.198**	**0.010**	1.740	0.061		3
152	$[M+NH_4]^+$	-0.015	HMDB0062609	HMDB	6	**3.604**	**0.031**	2.006	0.178	0.364	0.880		3
153	$[M+Na]^+$	4.807	HMDB0013202	HMDB	1	2.316	0.078	1.109	0.411	**3.203**	**0.023**		3
154	$[M+NH_4]^+$	0.745	HMDB0002752	HMDB	22	**4.122**	**0.007**	**2.587**	**0.026**	1.789	0.199		3
155	$[M+H]^+$	-5.423	HMDB0033449	HMDB	0	0.761	0.181	**3.624**	**0.001**	0.052	0.982		3
156	$[M+H]^+$	0.281	LMFA08040038	LIPID MAPS	0	**10.852**	**0.014**	0.136	0.994	**12.136**	**0.008**		3
157	$[M+NH_4]^+$	-1.279	HMDB0013326	HMDB	0	**3.107**	**0.007**	**3.142**	**0.004**	2.010	0.055		3
158	$[M+H]^+$	0.828	HMDB0004038	HMDB	8	**3.323**	**0.014**	-0.576	0.656	0.176	0.933		3
159	$[M+NH_4]^+$	0.189	HMDB0000353	HMDB	8	0.603	0.406	**3.260**	**0.004**	-0.878	0.414		3
160	$[M+NH_4]^+$	0.287	LMFA02000148	LIPID MAPS	0	0.605	0.154	**-1.786**	**0.004**	-0.185	0.783		3
161	$[M+H]^+$	0.545	LMPK15030034	LIPID MAPS	1	-0.021	0.990	0.084	0.962	**7.583**	**0.000**		3
162	$[M+NH_4]^+$	0.283	HMDB0001403	HMDB	18	**2.033**	**0.015**	1.230	0.072	0.888	0.320		3
163	$[M+NH_4]^+$	0.283	HMDB0001403	HMDB	15	0.925	0.055	**1.514**	**0.007**	0.308	0.587		3
164	$[M+H]^+$	5.197	HMDB0014687	HMDB	0	0.809	0.137	**-1.246**	**0.044**	-0.373	0.610		3
165	$[M+NH_4]^+$	4.075	HMDB0030281	HMDB	0	**2.047**	**0.022**	-0.182	0.900	-0.422	0.655		3
166	$[M+NH_4]^+$	0.401	HMDB0005096	HMDB	2	0.837	0.853	**9.457**	**0.045**	3.543	0.523		3
167	$[M+Na]^+$	-4.482	HMDB0011535	HMDB	0	**1.360**	**0.038**	-0.440	0.523	-0.460	0.529		3
168	$[M+H]^+$	1.561	LMFA08040052	LIPID MAPS	1	**-12.588**	**0.014**	3.153	0.483	1.329	0.922		3
169	$[M+Na]^+$	-0.386	HMDB0006754	HMDB	11	-0.829	0.469	**-2.598**	**0.045**	1.282	0.223		3
170	$[M+Na]^+$	-2.570	HMDB0006700	HMDB	5	0.569	0.426	0.080	0.956	**1.596**	**0.029**		3
171	$[M+NH_4]^+$	-1.789	HMDB0001984	HMDB	0	0.915	0.280	**3.988**	**0.003**	1.673	0.189		3
172	$[M+NH_4]^+$	-1.091	HMDB0061030	HMDB	1	1.087	0.201	**2.508**	**0.019**	1.894	0.125		3
173	$[M+H]^+$	3.797	LMPK12112596	LIPID MAPS	0	-0.392	0.623	-0.811	0.296	**2.130**	**0.010**		3
174	$[M+Na]^+$	-0.958	HMDB0029782	HMDB	1	0.638	0.880	2.446	0.410	**6.933**	**0.023**		3
175	$[M+NH_4]^+$	3.064	HMDB0001542	HMDB	3	1.189	0.094	**-2.395**	**0.006**	-0.929	0.339		3
176	$[M+H]^+$	-5.748	HMDB0000364	HMDB	18	**1.849**	**0.031**	-0.289	0.789	0.067	0.982		3
177	$[M+H]^+$	-5.748	HMDB0000364	HMDB	3	**1.504**	**0.041**	-0.231	0.822	0.035	0.993		3
178	$[M+Na]^+$	-0.384	HMDB0033275	HMDB	27	**16.853**	**0.003**	**11.135**	**0.026**	**16.347**	**0.003**		3
179	$[M-H]^-$	2.788	HMDB36984	HMDB	4	0.000	1.000	**7.619**	**0.000**	2.212	0.139		3
180	$[M+NH_4]^+$	1.059	HMDB0038506	HMDB	2	1.015	0.392	**4.377**	**0.008**	-0.300	0.904		3

Number	M/Z_{Avg}	RT_{Avg}	Detection mode		Name	Lipid classes	Formula
			Phase	Ionization mode			
181	421.3169	7.21	Non-polar	Positive	Nb-palmitoyltryptamine	Fatty acyls	C26H42N2O
182	422.2904	6.59	Non-polar	Positive	Dihydroxyoxocholenoic acid	Sterol	C24H36O5
183	426.2851	29.75	Polar	Positive	PGD2-dihydroxypropanylamine	Fatty acyls	C23H39NO6
184	431.1623746	29.10	Polar	Positive	Tamsulosin	Other organic compounds	C20H28N2O5S
185	433.2430174	26.55	Polar	Positive	Glucosyl dihydroxyfarnesadienoate	prenol	C21H36O9
186	434.8588	7.24	Non-polar	Positive	Hydroxydiiodophenyllactic acid	Fatty acyls	C9H8I2O4
187	435.3336	7.22	Non-polar	Positive	Glycerol acetate N-octadecanoate	Glycerolipids	C23H46O7
188	437.3392	7.22	Non-polar	Positive	Trimethyl(methylheptenyl) - dodecahydrocyclopentaphenanthrenediol	Sterol	C28H46O2
189	441.2624854	5.15	Non-polar	Positive	Cavipetin D*	prenol	C25H38O5
190	441.2624854	5.73	Non-polar	Positive	Cavipetin D*	prenol	C25H38O5
191	441.3022	17.15	Non-polar	Negative	Hydroxy (hydroxymethylpentynyloxy)-pentanorvitamin D3	Sterol	C28H42O4
192	443.4203	13.65	Non-polar	Positive	Tetracosanoylglycine	Fatty acyls	C26H51NO3
193	446.3838	14.73	Non-polar	Positive	DAG (22:0)	Glycerolipids	C25H48O5
194	448.2331771	6.79	Non-polar	Positive	Armillarilin	prenol	C24H30O7
195	449.1433036	21.94	Polar	Positive	Puddumin a	polyketide	C22H24O10
196	449.3483	7.22	Non-polar	Positive	N-stearoyl arginine	Fatty acyls	C23H46N4O3
197	450.2630	32.31	Polar	Negative	LysoPE(16:1)	Glycerophospholipids	C21H42NO7P
198	451.3284	4.67	Non-polar	Positive	C17 sphingosine-1-phosphocholine	Sphingolipids	C22H47N2O5P
199	452.2771	12.68	Non-polar	Positive	LysoPE(16:1)	Glycerophospholipids	C21H42NO7P
200	452.2795	14.10	Non-polar	Negative	LysoPE(16:0)	Glycerophospholipids	C21H44NO7P
201	453.3026176	16.47	Non-polar	Negative	Ubiquinone-4	prenol	C29H42O4
202	454.2912	34.15	Polar	Positive	LysoPE(16:0)	Glycerophospholipids	C21H44NO7P
203	454.2931	14.22	Non-polar	Positive	LysoPE(16:0)	Glycerophospholipids	C21H44NO7P
204	455.2126	27.42	Polar	Positive	Butylhydroxybutyrate arabinosylglucoside	Fatty acyls	C19H34O12
205	457.2722	10.87	Non-polar	Positive	Leukotriene e4	Fatty acyls	C23H37NO5S
206	461.1718	5.40	Non-polar	Positive	Punaglandin 7	Fatty acyls	C23H31O6Cl
207	470.3257	8.19	Non-polar	Positive	Norselic acid A	Sterol	C29H40O4
208	474.4659413	41.37	Polar	Positive	Longamide	Other organic compounds	C30H61NO
209	476.3729	17.60	Non-polar	Positive	Docosatetraenoylcarnitine	Acylcarnitine	C29H49NO4
210	479.3482	4.98	Non-polar	Positive	Butyldihydroxydidehydronorvitamin D3	Sterol	C30H48O3

Number	Adducts	PPM error	Match ID	Database	Number of alternate IDs	DENV vs Mock Day 3		DENV vs Mock Day 7		DENV vs Mock Day 11		MS/MS database	MSI level
						Log_2 FC	p-value	Log_2 FC	p-value	Log_2 FC	p-value		
181	$[M+Na]^+$	-5.153	HMDB0040815	HMDB	0	**1.603**	**0.022**	-0.568	0.367	-0.225	0.785		3
182	$[M+NH_4]^+$	0.833	HMDB0000447	HMDB	2	0.988	0.206	**3.133**	**0.005**	-0.076	0.982		3
183	$[M+H]^+$	0.235	LMFA03010191	LIPID MAPS	1	**3.442**	**0.006**	**2.291**	**0.047**	**4.255**	**0.002**		3
184	$[M+Na]^+$	3.096	HMDB0014844	HMDB	0	0.652	0.536	0.100	0.965	**2.312**	**0.029**		3
185	$[M+H]^+$	-0.442	HMDB0037823	HMDB	1	**3.235**	**0.049**	2.025	0.216	1.660	0.261		3
186	$[M+H]^+$	0.719	HMDB0059636	HMDB	0	**2.200**	**0.022**	-0.312	0.786	-0.219	0.853		3
187	$[M+H]^+$	4.560	HMDB0032157	HMDB	0	**1.405**	**0.025**	0.043	0.990	-0.181	0.802		3
188	$[M+Na]^+$	0.396	HMDB0034329	HMDB	17	-0.624	0.698	**-5.201**	**0.009**	-1.394	0.499		3
189	$[M+Na]^+$	3.212	HMDB0030365	HMDB	1	-0.886	0.427	**-4.456**	**0.006**	-1.486	0.390		3
190	$[M+Na]^+$	3.212	HMDB0030365	HMDB	0	0.938	0.103	**-3.051**	**0.001**	0.033	0.991		3
191	$[M-H]^-$	2.487	LMST03020591	LIPID MAPS	4	**3.122**	**0.045**	-0.411	0.774	-0.249	0.779		3
192	$[M+NH_4]^+$	-1.029	HMDB0013310	HMDB	0	6.572	0.080	**11.759**	**0.008**	6.622	0.167		3
193	$[M+NH_4]^+$	-0.477	ECMDB23242	ECMDB	2	**1.516**	**0.042**	-0.470	0.557	0.004	1.000		3
194	$[M+NH_4]^+$	0.467	HMDB0031673	HMDB	2	1.060	0.066	**2.322**	**0.003**	0.000	1.000		3
195	$[M+H]^+$	-2.047	HMDB0033741	HMDB	19	0.694	0.702	**3.589**	**0.042**	2.485	0.088		3
196	$[M+Na]^+$	4.925	LMFA08020136	LIPID MAPS	0	**1.307**	**0.039**	0.050	0.988	-0.164	0.842		3
197	$[M-H]^-$	0.910	HMDB0011504	HMDB	1	**-18.085**	**0.024**	-3.155	0.743	-7.003	0.428	Lipidblast	2
198	$[M+H]^+$	2.443	LMSP01060003	LIPID MAPS	0	**1.677**	**0.049**	0.506	0.597	0.589	0.542		3
199	$[M+H]^+$	-0.171	HMDB0011504	HMDB	3	-1.112	0.276	**-2.497**	**0.046**	-1.798	0.239	Lipidblast	2
200	$[M-H]^-$	-2.764	HMDB11503	HMDB	2	-3.345	0.063	-2.318	0.114	**-3.801**	**0.032**	NIST, Lipidblast	2
201	$[M-H]^-$	-3.486	HMDB06710	HMDB	4	**3.138**	**0.040**	-0.362	0.791	-0.531	0.466		3
202	$[M+H]^+$	-3.449	HMDB0011473	HMDB	1	**-3.720**	**0.008**	-0.854	0.454	**-4.134**	**0.005**	Lipidblast	2
203	$[M+H]^+$	0.578	HMDB0011473	HMDB	1	**-3.489**	**0.033**	-2.275	0.117	-2.480	0.175	NIST, Lipidblast	2
204	$[M+H]^+$	0.565	HMDB0039214	HMDB	0	**12.696**	**0.009**	**14.034**	**0.010**	**18.560**	**0.002**		3
205	$[M+NH_4]^+$	-1.886	HMDB0002200	HMDB	2	-0.017	0.986	**-2.563**	**0.007**	0.892	0.386		3
206	$[M+Na]^+$	3.651	LMFA03120044	LIPID MAPS	0	1.021	0.131	**1.560**	**0.042**	-0.504	0.568		3
207	$[M+NH_4]^+$	1.769	LMST01040189	LIPID MAPS	4	0.307	0.566	**2.454**	**0.003**	0.144	0.888		3
208	$[M+Na]^+$	3.150	HMDB0038842	HMDB	0	-6.290	0.179	-6.592	0.186	**14.928**	**0.008**		3
209	$[M+H]^+$	1.052	LMFA07070022	LIPID MAPS	6	**2.850**	**0.013**	-0.481	0.656	0.515	0.652		3
210	$[M+Na]^+$	2.849	LMST03020584	LIPID MAPS	12	0.110	0.915	**2.542**	**0.031**	2.263	0.103		3

Number	M/Z_{Avg}	RT_{Avg}	Detection mode		Name	Lipid classes	Formula
			Phase	Ionization mode			
211	480.3071	34.42	Polar	Positive	LysoPE(18:1)	Glycerophospholipids	C23H46NO7P
212	484.24386	13.36	Polar	Positive	Caffeoylferuloylspermidine	polyketide	C26H33N3O6
213	485.2356	4.86	Non-polar	Positive	Plantaricin BN	Fatty acyls	C24H36O10
214	485.3486938	7.24	Non-polar	Positive	Tiropramide	Amino acids and peptides	C28H41N3O3
215	487.3014	7.10	Non-polar	Positive	Ecdysone	Sterol	C27H44O6
216	488.3209	7.11	Non-polar	Positive	Ceanothine c	Fatty acyls	C26H38N4O4
217	489.3437	7.21	Non-polar	Positive	Sphinganine-1-phosphocholine	Sphingolipids	C23H51N2O5P
218	492.1938972	5.02	Non-polar	Positive	arabinofuranosyl mannopyranosyl mannose	Other organic compounds	C17H30O15
219	494.3230	12.53	Non-polar	Positive	LysoPC(16:1)	Glycerophospholipids	C24H48NO7P
220	496.3386	14.03	Non-polar	Positive	LysoPC(16:0)	Glycerophospholipids	C24H50NO7P
221	497.168046	9.06	Non-polar	Negative	Musabalbisiane b	prenol	C23H30O12
222	501.3427067	7.20	Non-polar	Positive	Adouetine x	Amino acids and peptides	C28H44N4O4
223	505.3655	7.22	Non-polar	Positive	dihydroxydiethyl-tetradehydrohomovitamin D3	Sterol	C32H50O3
224	512.2983	13.88	Non-polar	Positive	LysoPS(17:0)	Glycerophospholipids	C23H46NO9P
225	517.3751255	7.21	Non-polar	Positive	Menthol propylene glycol carbonate	prenol	C28H52O8
226	520.3732	46.39	Polar	Positive	LysoPC(P-19:1)	Glycerophospholipids	C27H54NO6P
227	524.3600	11.73	Non-polar	Positive	Deoxy-hydroxyecdysone acetate	Sterol	C29H46O7
228	526.2908	12.31	Non-polar	Positive	LysoPE(20:3)	Glycerophospholipids	C25H46NO7P
229	526.3159	5.13	Non-polar	Positive	LysoPS(18:0)	Glycerophospholipids	C24H48NO9P
230	529.4934	13.62	Non-polar	Positive	Stearyl palmitoleate	Fatty acyls	C34H66O2
231	532.3748	4.97	Non-polar	Positive	LysoPC(O-18:0)	Glycerophospholipids	C26H56NO6P
232	534.2917	7.82	Non-polar	Positive	Eriojaposide b	Fatty acyls	C25H40O11
233	587.3589	29.37	Polar	Negative	Hydroxyvitamin glucuronide	Sterol	C34H52O8
234	591.4285	12.39	Non-polar	Positive	Saringosterol 3-glucoside	Sterol	C35H58O7
235	595.3819	12.44	Non-polar	Positive	IC202A	Fatty acyls	C27H52N6O7
236	603.4030	13.23	Non-polar	Positive	PA(29:2)	Glycerophospholipids	C32H59O8P
237	606.2912934	7.70	Non-polar	Positive	ethyl bis(acetyloxy)(furanyl)hydroxytetramethyl methylideneoxodioxatetracycloheptadecan]acetate	Other organic compounds	C31H40O11
238	608.3195	13.87	Non-polar	Negative	PS(22:0(3-OH))	Glycerophospholipids	C28H52NO11P
239	611.3560	12.37	Non-polar	Positive	Hydroxyvitamin-(beta-glucuronide)	Sterol	C34H52O8
240	616.4034	14.33	Non-polar	Positive	Kurilensoside G	Sterol	C32H54O10

Number	Adducts	PPM error	Match ID	Database	Number of alternate IDs	DENV vs Mock Day 3		DENV vs Mock Day 7		DENV vs Mock Day 11		MS/MS database	MSI level
						Log_2 FC	p-value	Log_2 FC	p-value	Log_2 FC	p-value		
211	$[M+H]^+$	-2.884	HMDB0011475	HMDB	1	**-7.029**	**0.033**	0.400	0.949	-4.167	0.151	NIST, Lipidblast	2
212	$[M+H]^+$	-0.727	HMDB0038843	HMDB	0	-2.096	0.050	-0.774	0.452	-1.576	0.106		3
213	$[M+H]^+$	-5.174	HMDB0038238	HMDB	0	1.508	0.606	**10.421**	**0.008**	0.000	1.000		3
214	$[M+NH_4]^+$	0.169	HMDB0042042	HMDB	0	**1.336**	**0.049**	0.277	0.744	-0.360	0.656		3
215	$[M+Na]^+$	3.446	LMST01010210	LIPID MAPS	6	**1.943**	**0.029**	-0.040	1.000	1.382	0.151		3
216	$[M+NH_4]^+$	-4.646	HMDB0029340	HMDB	0	**2.502**	**0.026**	0.267	0.876	1.518	0.211		3
217	$[M+Na]^+$	1.930	LMSP01060002	LIPID MAPS	0	**1.720**	**0.032**	-0.152	0.918	-0.308	0.742		3
218	$[M+NH_4]^+$	3.383	HMDB0039818	HMDB	0	3.531	0.367	**18.080**	**0.003**	-3.481	0.538		3
219	$[M+H]^+$	-2.182	HMDB0010383	HMDB	2	**-3.272**	**0.025**	**-2.653**	**0.040**	-2.067	0.189	Lipidblast	2
220	$[M+H]^+$	2.324	HMDB0010382	HMDB	2	**-4.472**	**0.012**	-2.444	0.082	-2.304	0.195	NIST	2
221	$[M-H]^-$	-3.204	HMDB38681	HMDB	0	-0.121	1.000	**20.090**	**0.027**	-1.217	0.852		3
222	$[M+H]^+$	-1.649	HMDB0034216	HMDB	0	**1.960**	**0.020**	-0.479	0.557	-0.052	0.988		3
223	$[M+Na]^+$	0.622	LMST03020513	LIPID MAPS	1	1.475	0.050	-0.201	0.872	-0.040	0.991		3
224	$[M+H]^+$	0.000	LMGP03050030	LIPID MAPS	1	-1.186	0.178	**-2.416**	**0.024**	-0.511	0.691		3
225	$[M+H]^+$	3.158	HMDB0039785	HMDB	0	**1.630**	**0.025**	-0.063	0.985	-0.199	0.812		3
226	$[M+H]^+$	5.573	LMGP01070010	LIPID MAPS	0	-2.273	0.410	**6.770**	**0.033**	-1.035	0.838		3
227	$[M+NH_4]^+$	3.555	LMST01010191	LIPID MAPS	0	1.581	0.149	**4.205**	**0.005**	1.946	0.209		3
228	$[M+Na]^+$	0.795	LMGP02050066	LIPID MAPS	0	**3.639**	**0.038**	2.671	0.094	0.687	0.742		3
229	$[M+H]^+$	3.617	LMGP03050006	LIPID MAPS	1	0.774	0.230	**-2.706**	**0.004**	-0.266	0.797		3
230	$[M+Na]^+$	4.146	LMFA07010022	LIPID MAPS	6	**11.766**	**0.012**	**17.139**	**0.002**	**12.287**	**0.016**		3
231	$[M+Na]^+$	2.159	LMGP01060014	LIPID MAPS	0	**9.916**	**0.000**	2.137	0.079	**10.345**	**0.000**		3
232	$[M+NH_4]^+$	1.616	HMDB0038029	HMDB	0	**1.315**	**0.049**	0.234	0.797	1.127	0.153		3
233	$[M-H]^-$	-0.062	HMDB0010342	HMDB	1	**2.918**	**0.005**	0.099	0.939	**3.257**	**0.004**		3
234	$[M+H]^+$	5.004	HMDB0029767	HMDB	2	0.972	0.262	**2.683**	**0.016**	1.178	0.381		3
235	$[M+Na]^+$	5.066	LMFA08020182	LIPID MAPS	0	0.910	0.180	**2.114**	**0.014**	0.793	0.410		3
236	$[M+H]^+$	1.660	LMGP10010050	LIPID MAPS	0	**2.223**	**0.036**	0.656	0.557	1.017	0.400		3
237	$[M+NH_4]^+$	0.694	HMDB0037555	HMDB	0	0.908	0.288	**9.179**	**0.000**	-0.160	0.938		3
238	$[M-H]^-$	1.658	ECMDB23567	ECMDB	0	-3.880	0.068	-1.829	0.263	**-4.655**	**0.033**		3
239	$[M+Na]^+$	0.850	LMST05010021	LIPID MAPS	0	0.853	0.221	**2.956**	**0.004**	0.933	0.381		3
240	$[M+NH_4]^+$	3.510	LMST05050016	LIPID MAPS	0	0.924	0.191	**4.796**	**0.001**	-0.187	0.889		3

Number	M/Z_{Avg}	RT_{Avg}	Detection mode		Name	Lipid classes	Formula
			Phase	Ionization mode			
241	617.4395	17.17	Non-polar	Positive	Squamone	Fatty acyls	C35H62O7
242	636.4574	12.30	Non-polar	Positive	PE(28:0)	Glycerophospholipids	C33H66NO8P
243	645.4608	46.25	Polar	Negative	PE-Cer(d32:2(2OH))	Sphingolipids	C34H65N2O7P
244	655.3811	12.35	Non-polar	Positive	LysoPI(22:1)	Glycerophospholipids	C31H59O12P
245	655.6347	13.60	Non-polar	Positive	Cer(d40:1(2OH))	Sphingolipids	C40H792O4
246	661.4921	20.86	Non-polar	Positive	PE-Cer(d33:2(2OH))	Sphingolipids	C35H69N2O7P
247	677.5135	21.51	Non-polar	Positive	PA(34:0)	Glycerophospholipids	C37H73O8P
248	679.6235	13.61	Non-polar	Positive	DAG(40:1)	Glycerolipids	C43H82O5
249	680.4844	12.27	Non-polar	Positive	PE(30:0(3-OH))	Glycerophospholipids	C35H70NO9P
250	683.3668	2.60	Polar	Positive	Evobioside	Sterol	C35H54O13
251	683.434326	12.27	Non-polar	Positive	Cyclopassifloside ii	prenol	C37H62O11
252	687.5432	23.50	Non-polar	Negative	PE-Cer(d36:1)	Sphingolipids	C38H77N2O6P
253	696.3782	14.03	Non-polar	Positive	Jubanine a	Fatty acyls	C40H49N5O6
254	699.4077	12.23	Non-polar	Positive	PI(24:0)	Glycerophospholipids	C33H63O13P
255	703.5379	22.66	Non-polar	Positive	PE-Cer(d36:2(2OH))	Sphingolipids	C38H75N2O7P
256	712.4401384	12.59	Non-polar	Positive	Lipid X	Other organic compounds	C34H67NO12P
257	716.5234	22.07	Non-polar	Positive	PE(34:2)	Glycerophospholipids	C39H74NO8P
258	722.4797	10.20	Non-polar	Positive	PE(35:6)	Glycerophospholipids	C40H68NO8P
259	722.5054	12.19	Non-polar	Positive	PE(O-34:3)	Glycerophospholipids	C39H74NO7P
260	723.5078	12.17	Non-polar	Positive	PE-Cer(d36:3(2OH))	Sphingolipids	C38H73N2O7P
261	724.5124	12.17	Non-polar	Positive	PG(31:1)	Glycerophospholipids	C37H71O10P
262	726.5240	22.64	Non-polar	Positive	PG(31:0)	Glycerophospholipids	C37H73O10P
263	730.5399	23.35	Non-polar	Negative	PC(32:1)	Glycerophospholipids	C40H78NO8P
264	730.5735	24.57	Non-polar	Negative	PE(O-36:1)	Glycerophospholipids	C41H82NO7P
265	744.4591	15.51	Non-polar	Positive	PE(35:6)	Glycerophospholipids	C40H68NO8P
266	744.5175	22.35	Non-polar	Negative	PS(O-34:2)	Glycerophospholipids	C40H76NO9P
267	746.6046	23.39	Non-polar	Positive	PC(O-34:1)	Glycerophospholipids	C42H84NO7P
268	749.6075	18.86	Non-polar	Positive	DAG(44:5)	Glycerolipids	C47H82O5
269	751.5106	7.20	Non-polar	Positive	PG(33:0cyc(3-OH))	Glycerophospholipids	C39H75O11P
270	755.5424317	19.91	Non-polar	Positive	Ternatin	Amino acids and peptides	C37H67N7O8

Number	Adducts	PPM error	Match ID	Database	Number of alternate IDs	DENV vs Mock Day 3		DENV vs Mock Day 7		DENV vs Mock Day 11		MS/MS database	MSI level
						Log_2 FC	p-value	Log_2 FC	p-value	Log_2 FC	p-value		
241	$[M+Na]^+$	1.346	LMFA0500069	LIPID MAPS	1	**4.785**	**0.006**	0.580	0.717	-0.102	0.982		3
242	$[M+H]^+$	-3.843	HMDB0008821	HMDB	2	1.006	0.237	**3.837**	**0.003**	1.957	0.116		3
243	$[M-H]^-$	0.773	LMSP03020067	LIPID MAPS	0	**-13.385**	**0.041**	3.215	0.692	3.671	0.739		3
244	$[M+H]^+$	0.917	LMGP06050022	LIPID MAPS	1	1.461	0.099	**2.842**	**0.008**	1.543	0.188		3
245	$[M+NH_4]^+$	0.157	LMSP02010073	LIPID MAPS	0	**23.423**	**0.001**	**20.395**	**0.001**	**20.112**	**0.003**		3
246	$[M+H]^+$	0.908	LMSP03020076	LIPID MAPS	0	-1.314	0.409	1.079	0.639	**-8.148**	**0.006**		3
247	$[M+H]^+$	2.809	LMGP10010849	LIPID MAPS	1	-1.216	0.821	**12.097**	**0.033**	12.642	0.062		3
248	$[M+H]^+$	0.012	HMDB0007174	HMDB	0	**19.085**	**0.007**	7.491	0.146	-0.276	0.991		3
249	$[M+H]^+$	2.502	LMGP03020002	LIPID MAPS	1	0.372	0.655	**2.717**	**0.010**	1.183	0.332		3
250	$[M+H]^+$	4.566	HMDB0038020	HMDB	3	1.017	0.148	**3.583**	**0.002**	**2.070**	**0.039**		3
251	$[M+H]^+$	-3.170	HMDB0038389	HMDB	0	**-2.668**	**0.049**	**-2.965**	**0.045**	**-3.415**	**0.017**		3
252	$[M-H]^-$	2.178	LMSP03020008	LIPID MAPS	1	-0.895	1.000	**14.465**	**0.001**	0.440	0.883		3
253	$[M+H]^+$	3.756	HMDB0030205	HMDB	0	1.020	0.799	**11.903**	**0.010**	-0.610	0.945		3
254	$[M+H]^+$	0.286	LMGP06010962	LIPID MAPS	0	1.191	0.148	**4.022**	**0.002**	**2.319**	**0.047**		3
255	$[M+H]^+$	0.712	LMSP03020089	LIPID MAPS	0	-0.925	0.891	**15.776**	**0.035**	4.490	0.609		3
256	$[M+H]^+$	0.843	LMSL01020001	LIPID MAPS	0	**-10.925**	**0.037**	3.695	0.495	**19.675**	**0.007**		3
257	$[M+H]^+$	1.341	HMDB0009283	HMDB	2	-2.140	0.487	**10.103**	**0.013**	2.087	0.652		3
258	$[M+H]^+$	5.821	LMGP02010405	LIPID MAPS	1	-0.210	0.980	**19.833**	**0.018**	8.547	0.390		3
259	$[M+Na]^+$	5.861	LMGP02020099	LIPID MAPS	2	1.221	0.150	**5.170**	**0.001**	**2.991**	**0.021**		3
260	$[M+Na]^+$	4.425	LMSP03020071	LIPID MAPS	0	1.416	0.126	**5.288**	**0.001**	**2.924**	**0.027**		3
261	$[M+NH_4]^+$	0.142	LMGP04010058	LIPID MAPS	0	1.299	0.188	**4.388**	**0.003**	**2.968**	**0.041**		3
262	$[M+NH_4]^+$	-5.591	ECMDB23666	ECMDB	0	-1.015	0.512	**7.111**	**0.003**	**-7.825**	**0.006**		3
263	$[M-H]^-$	-0.866	HMDB07873	HMDB	2	-1.036	1.000	**14.942**	**0.001**	2.946	0.353		3
264	$[M-H]^-$	2.876	HMDB11347	HMDB	3	-0.698	1.000	**17.287**	**0.001**	2.769	0.385		3
265	$[M+Na]^+$	2.356	LMGP02011133	LIPID MAPS	0	7.331	0.166	**18.055**	**0.009**	-7.556	0.346		3
266	$[M-H]^-$	1.341	LMGP03020079	LIPID MAPS	1	1.770	1.000	**14.555**	**0.001**	4.821	0.158		3
267	$[M+H]^+$	1.609	LMGP02020069	LIPID MAPS	3	-0.674	0.846	**19.295**	**0.001**	2.393	0.566	NIST	2
268	$[M+Na]^+$	2.831	HMDB0007586	HMDB	0	0.785	0.551	**13.128**	**0.000**	0.542	0.797		3
269	$[M+H]^+$	-1.880	ECMDB23679	ECMDB	2	**3.312**	**0.006**	-0.198	0.906	-0.321	0.785		3
270	$[M+NH_4]^+$	-0.577	HMDB0040991	HMDB	0	-1.489	0.305	**8.925**	**0.001**	0.662	0.785		3

Number	M/Z_{Avg}	RT_{Avg}	Detection mode		Name	Lipid classes	Formula
			Phase	Ionization mode			
271	756.4651	12.53	Non-polar	Positive	PI(27:1)	Glycerophospholipids	C36H67O13P
272	765.3531178	8.35	Non-polar	Positive	Hordatine b glucoside	polyketide	C35H50N8O10
273	767.5333	12.08	Non-polar	Positive	PC(34:6)	Glycerophospholipids	C42H72NO8P
274	768.5384	7.20	Non-polar	Positive	PG(33:0cyc(3-OH))	Glycerophospholipids	C39H75O11P
275	771.4885	12.09	Non-polar	Positive	PS(34:5)	Glycerophospholipids	C40H68NO10P
276	771.5493	7.18	Non-polar	Positive	PG(O-35:1)	Glycerophospholipids	C41H81O9P
277	772.4892	12.08	Non-polar	Positive	PPA(34:1)	Glycerophospholipids	C37H72O11P2
278	773.4918	7.22	Non-polar	Positive	PG(33:0cyc(3-OH))	Glycerophospholipids	C39H75O11P
279	773.4918	12.05	Non-polar	Positive	PG(33:0cyc(3-OH))	Glycerophospholipids	C39H75O11P
280	779.4688	19.98	Non-polar	Negative	PI(30:1)	Glycerophospholipids	C39H73O13P
281	780.5487	12.71	Non-polar	Positive	PC(34:2)	Glycerophospholipids	C42H80NO8P
282	781.5134	11.83	Non-polar	Positive	SQDAG(30:0)	Glycerolipids	C40H76O12S
283	781.5506	12.67	Non-polar	Positive	PE(38:6)	Glycerophospholipids	C43H74NO8P
284	786.5637	23.35	Non-polar	Negative	PS(O-37:2)	Glycerophospholipids	C43H82NO9P
285	788.5806	24.11	Non-polar	Negative	PS(O-37:1)	Glycerophospholipids	C43H84NO9P
286	788.5807	23.96	Non-polar	Negative	PS(O-37:1)	Glycerophospholipids	C43H84NO9P
287	789.4677	7.21	Non-polar	Positive	PG(36:6)	Glycerophospholipids	C42H71O10P
288	796.5707	7.21	Non-polar	Positive	DAGCC(36:5)	Glycerolipids	C46H79NO8
289	801.6137	22.11	Non-polar	Positive	PC(36:3)	Glycerophospholipids	C44H82NO8P
290	807.4150082	21.06	Polar	Positive	Licoricesaponin C2	prenol	C42H62O15
291	807.5580	12.09	Non-polar	Positive	PG(P-40:6)	Glycerophospholipids	C46H79O9P
292	809.5180	22.31	Non-polar	Negative	PI(32:0)	Glycerophospholipids	C41H79O13P
293	809.5643	7.22	Non-polar	Positive	PG(O-38:3)	Glycerophospholipids	C44H83O9P
294	809.5817	12.13	Non-polar	Positive	PE(40:6)	Glycerophospholipids	C45H78NO8P
295	810.5833	7.23	Non-polar	Positive	PI-Cer(d36:0)	Sphingolipids	C42H84NO11P
296	811.5606	12.00	Non-polar	Positive	PS(O-38:6)	Glycerophospholipids	C44H76O9P
297	811.5868	7.22	Non-polar	Positive	PG(O-40:5)	Glycerophospholipids	C46H83O9P
298	812.5659	12.10	Non-polar	Positive	PI(O-32:1)	Glycerophospholipids	C41H79O12P
299	813.5687	12.05	Non-polar	Positive	PG(39:4)	Glycerophospholipids	C45H81O10P
300	813.5950	7.19	Non-polar	Positive	PG(O-38:1)	Glycerophospholipids	C44H87O9P

Number	Adducts	PPM error	Match ID	Database	Number of alternate IDs	DENV vs Mock Day 3		DENV vs Mock Day 7		DENV vs Mock Day 11		MS/MS database	MSI level
						Log_2 FC	p-value	Log_2 FC	p-value	Log_2 FC	p-value		
271	$[M+NH_4]^+$	0.948	LMGP06010016	LIPID MAPS	0	2.196	0.632	4.908	0.370	**16.368**	**0.020**		3
272	$[M+Na]^+$	-1.469	HMDB0030460	HMDB	0	1.128	0.843	**13.052**	**0.027**	4.254	0.531		3
273	$[M+NH_4]^+$	-0.063	HMDB0007918	HMDB	2	1.824	0.060	**5.959**	**0.001**	**3.232**	**0.015**		3
274	$[M+NH_4]^+$	-0.174	ECMDB23679	ECMDB	0	**3.303**	**0.006**	-0.102	0.980	-0.367	0.743		3
275	$[M+NH_4]^+$	-4.462	HMDB0012350	HMDB	3	1.593	0.080	**4.698**	**0.001**	**3.034**	**0.017**		3
276	$[M+Na]^+$	2.405	LMGP04020011	LIPID MAPS	1	**3.435**	**0.006**	-0.230	0.882	-0.203	0.888		3
277	$[M+NH_4]^+$	0.530	LMGP11010001	LIPID MAPS	0	**2.139**	**0.046**	**5.470**	**0.001**	**3.497**	**0.014**		3
278	$[M+Na]^+$	-2.759	ECMDB23679	ECMDB	1	**15.793**	**0.003**	**9.274**	**0.013**	3.894	0.378		3
279	$[M+Na]^+$	-2.759	ECMDB23679	ECMDB	2	**1.573**	**0.038**	0.025	1.000	-0.547	0.516		3
280	$[M-H]^-$	3.716	LMGP06010217	LIPID MAPS	0	-0.953	1.000	**13.656**	**0.000**	2.106	0.338		3
281	$[M+Na]^+$	-3.495	HMDB0010565	HMDB	2	0.550	0.900	**9.802**	**0.043**	4.620	0.418		3
282	$[M+H]^+$	0.512	LMGL05010005	LIPID MAPS	0	-3.218	0.484	4.696	0.440	**18.954**	**0.014**		3
283	$[M+NH_4]^+$	2.033	HMDB0009682	HMDB	1	7.356	0.056	**16.705**	**0.002**	**18.532**	**0.004**		3
284	$[M-H]^-$	2.286	LMGP03020050	LIPID MAPS	2	0.493	1.000	**3.840**	**0.045**	3.000	0.126		3
285	$[M-H]^-$	0.633	LMGP03020033	LIPID MAPS	2	1.064	1.000	**16.188**	**0.000**	**17.555**	**0.000**		3
286	$[M-H]^-$	0.507	LMGP03020033	LIPID MAPS	2	1.029	1.000	**16.303**	**0.000**	**16.951**	**0.000**		3
287	$[M+Na]^+$	0.003	HMDB0010666	HMDB	0	**2.204**	**0.044**	1.056	0.331	-0.570	0.660		3
288	$[M+Na]^+$	1.163	LMGL00000129	LIPID MAPS	1	**2.150**	**0.012**	-0.466	0.542	-0.215	0.809		3
289	$[M+NH_4]^+$	2.697	HMDB0008105	HMDB	1	-2.215	0.112	**8.569**	**0.001**	0.257	0.930		3
290	$[M+H]^+$	-1.410	HMDB0038759	HMDB	1	**-15.548**	**0.019**	-1.758	0.841	-7.009	0.206		3
291	$[M+H]^+$	5.703	LMGP04030089	LIPID MAPS	0	3.684	0.381	**14.983**	**0.010**	**18.490**	**0.013**		3
292	$[M-H]^-$	0.742	HMDB09778	HMDB	0	-0.498	1.000	**14.887**	**0.001**	0.923	0.689		3
293	$[M+Na]^+$	3.051	LMGP04020036	LIPID MAPS	0	**1.847**	**0.015**	0.041	0.996	-0.475	0.524		3
294	$[M+NH_4]^+$	1.747	HMDB0009684	HMDB	1	**11.546**	**0.042**	**16.941**	**0.007**	**19.040**	**0.013**		3
295	$[M+H]^+$	2.594	LMSP03030031	LIPID MAPS	0	**1.953**	**0.012**	-0.359	0.621	-0.186	0.822		3
296	$[M+NH_4]^+$	1.260	LMGP03020088	LIPID MAPS	1	**2.517**	**0.031**	**6.613**	**0.000**	**3.563**	**0.014**		3
297	$[M+H]^+$	2.591	LMGP04020064	LIPID MAPS	1	**2.055**	**0.010**	-0.338	0.649	-0.123	0.910		3
298	$[M+NH_4]^+$	1.510	LMGP06020008	LIPID MAPS	1	**9.825**	**0.000**	**7.440**	**0.001**	**4.412**	**0.013**		3
299	$[M+H]^+$	5.784	LMGP04010247	LIPID MAPS	0	0.466	0.934	**20.731**	**0.005**	14.906	0.054		3
300	$[M+Na]^+$	3.795	LMGP04020015	LIPID MAPS	1	**2.069**	**0.013**	0.214	0.839	-0.336	0.699		3

Number	M/Z_{Avg}	RT_{Avg}	Detection mode		Name	Lipid classes	Formula
			Phase	Ionization mode			
301	816.6093	23.35	Non-polar	Negative	PS(P-39:0)	Glycerophospholipids	C45H88NO9P
302	817.5763	15.45	Non-polar	Positive	PS(38:0)	Glycerophospholipids	C46H83O8P
303	818.5923	23.08	Non-polar	Negative	PI(33:2)	Glycerophospholipids	C44H86NO10P
304	819.5003	20.67	Non-polar	Negative	PI(33:2)	Glycerophospholipids	C42H77O13P
305	819.5846	15.46	Non-polar	Positive	PS(37:1)	Glycerophospholipids	C43H80NO10P
306	823.5350	22.66	Non-polar	Negative	PI(33:0)	Glycerophospholipids	C42H81O13P
307	826.5466	21.08	Non-polar	Positive	PI(32:1)	Glycerophospholipids	C41H77O13P
308	827.4873	20.98	Non-polar	Negative	PGP(34:1)	Glycerophospholipids	C40H78O13P2
309	832.4895	12.03	Non-polar	Positive	PE(42:11)	Glycerophospholipids	C47H72NO8P
310	833.5658	7.20	Non-polar	Positive	PG(O-40:5)	Glycerophospholipids	C46H83O9P
311	839.5618	15.47	Non-polar	Positive	PI(34:0)	Glycerophospholipids	C43H83O13P
312	840.5643	15.46	Non-polar	Positive	PI(33:1)	Glycerophospholipids	C42H79O13P
313	849.5829	23.81	Non-polar	Negative	PI(O-36:1)	Glycerophospholipids	C45H87O12P
314	852.6046	12.02	Non-polar	Positive	PS(O-40:2)	Glycerophospholipids	C46H88NO9P
315	855.5889	11.96	Non-polar	Positive	PS(40:5)	Glycerophospholipids	C46H80NO10P
316	856.5919	11.92	Non-polar	Positive	PI(34:0)	Glycerophospholipids	C43H83O13P
317	857.5160	21.15	Non-polar	Positive	PI(34:2)	Glycerophospholipids	C43H79O13P
318	861.5474	12.06	Non-polar	Positive	PI(34:3)	Glycerophospholipids	C43H83O13P
319	866.6135	7.22	Non-polar	Positive	PI(O-36:2)	Glycerophospholipids	C45H85O12P
320	868.6167	7.21	Non-polar	Positive	PC(P-42:6)	Glycerophospholipids	C50H88NO7P
321	878.6096	7.22	Non-polar	Positive	PI(P-37:2)	Glycerophospholipids	C46H85O12P
322	879.6139	7.21	Non-polar	Positive	PG(44:6)	Glycerophospholipids	C50H87O10P
323	880.6200	7.20	Non-polar	Positive	(3'-sulfo)GalCer(d40:1(2OH))	Sphingolipids	C46H89NO12S
324	882.6075	23.09	Non-polar	Positive	PI(36:1)	Glycerophospholipids	C45H85O13P
325	889.5813	23.19	Non-polar	Negative	PI(38:2)	Glycerophospholipids	C47H87O13P
326	892.5917	20.13	Non-polar	Positive	PI(37:3)	Glycerophospholipids	C46H83O13P
327	892.6269	7.20	Non-polar	Positive	PI(O-38:3)	Glycerophospholipids	C47H87O12P
328	897.488858	17.84	Non-polar	Negative	Medicoside c	prenol	C46H74O17
329	897.6245438	7.21	Non-polar	Positive	alpha,alpha'-Trehalose dioleate	Other organic compounds	C48H90O13
330	897.6347	11.96	Non-polar	Positive	PE(2epoxy-3Me-42:4)	Glycerophospholipids	C49H86NO10P

Number	Adducts	PPM error	Match ID	Database	Number of alternate IDs	DENV vs Mock Day 3		DENV vs Mock Day 7		DENV vs Mock Day 11		MS/MS database	MSI level
						Log_2 FC	p-value	Log_2 FC	p-value	Log_2 FC	p-value		
301	$[M-H]^-$	3.791	LMGP03020058	LIPID MAPS	2	-0.718	1.000	**16.762**	**0.001**	4.209	0.277		3
302	$[M+Na]^+$	5.789	LMGP10010700	LIPID MAPS	1	**2.281**	**0.027**	-0.533	0.615	0.021	1.000		3
303	$[M-H]^-$	-0.732	HMDB10164	HMDB	0	-1.196	1.000	**14.627**	**0.000**	3.530	0.242		3
304	$[M-H]^-$	3.169	LMGP06010527	LIPID MAPS	0	-0.117	1.000	**13.125**	**0.000**	2.559	0.235		3
305	$[M+NH_4]^+$	-1.455	ECMDB23612	ECMDB	2	**3.035**	**0.012**	-0.418	0.739	-0.185	0.910		3
306	$[M-H]^-$	0.970	LMGP06010824	LIPID MAPS	0	-0.553	1.000	2.189	0.053	**11.932**	**0.000**		3
307	$[M+NH_4]^+$	3.191	HMDB0009779	HMDB	0	-1.122	0.844	**11.681**	**0.046**	12.933	0.065		3
308	$[M-H]^-$	-3.418	HMDB13475	HMDB	0	-1.484	0.233	0.000	1.000	**2.507**	**0.044**		3
309	$[M+Na]^+$	0.930	HMDB0009474	HMDB	0	**15.706**	**0.004**	**13.276**	**0.004**	8.158	0.065		3
310	$[M+Na]^+$	1.110	LMGP04020064	LIPID MAPS	1	**2.315**	**0.014**	-0.124	0.960	-0.419	0.666		3
311	$[M+H]^+$	-3.156	HMDB0009781	HMDB	0	**2.108**	**0.032**	-0.472	0.651	-0.093	0.978		3
312	$[M+NH_4]^+$	5.714	LMGP06010051	LIPID MAPS	0	**3.435**	**0.011**	-0.389	0.797	-0.114	0.978		3
313	$[M-H]^-$	3.997	LMGP06030063	LIPID MAPS	2	0.687	1.000	2.731	0.157	**15.524**	**0.000**		3
314	$[M+Na]^+$	5.183	LMGP03020039	LIPID MAPS	1	12.217	0.057	**17.899**	**0.011**	8.839	0.268		3
315	$[M+NH_4]^+$	3.688	HMDB0010166	HMDB	1	**3.160**	**0.026**	**7.195**	**0.001**	**3.780**	**0.021**		3
316	$[M+NH_4]^+$	1.111	HMDB0009781	HMDB	1	**14.227**	**0.006**	**7.276**	**0.046**	4.315	0.360		3
317	$[M+Na]^+$	1.144	HMDB0009784	HMDB	0	-0.704	0.587	0.000	1.000	**9.264**	**0.002**		3
318	$[M+Na]^+$	1.252	HMDB0009781	HMDB	1	**11.453**	**0.033**	**20.254**	**0.003**	**15.192**	**0.020**		3
319	$[M+NH_4]^+$	2.121	LMGP06020014	LIPID MAPS	1	**1.404**	**0.042**	0.012	1.000	-0.181	0.844		3
320	$[M+Na]^+$	2.838	LMGP01030104	LIPID MAPS	0	**1.505**	**0.043**	-0.104	0.963	-0.332	0.717		3
321	$[M+NH_4]^+$	2.440	LMGP06030067	LIPID MAPS	0	**2.355**	**0.006**	-0.416	0.533	-0.197	0.802		3
322	$[M+H]^+$	3.415	LMGP04010979	LIPID MAPS	0	**2.404**	**0.009**	-0.040	1.000	-0.313	0.732		3
323	$[M+H]^+$	2.501	LMSP06020000	LIPID MAPS	0	**2.493**	**0.006**	0.110	0.956	-0.197	0.822		3
324	$[M+NH_4]^+$	1.041	LMGP06010074	LIPID MAPS	0	-1.269	0.399	1.111	0.607	**8.762**	**0.004**		3
325	$[M-H]^-$	-0.206	HMDB09791	HMDB	0	-0.596	1.000	**11.951**	**0.000**	1.002	0.350		3
326	$[M+NH_4]^+$	0.800	LMGP06010157	LIPID MAPS	0	-1.649	0.397	**-7.385**	**0.008**	**8.105**	**0.014**		3
327	$[M+NH_4]^+$	0.457	LMGP06020037	LIPID MAPS	1	**2.484**	**0.010**	-0.077	0.985	-0.345	0.720		3
328	$[M-H]^-$	-3.932	HMDB34547	HMDB		-0.173	1.000	**13.569**	**0.000**	0.443	0.726		3
329	$[M+Na]^+$	3.201	LMSL03001273	LIPID MAPS	0	**2.312**	**0.024**	-0.024	1.000	-0.332	0.785		3
330	$[M+NH_4]^+$	2.212	HMDB0061473	HMDB	0	0.000	1.000	**20.259**	**0.000**	**18.482**	**0.000**		3

Number	M/Z_{Avg}	RT_{Avg}	Detection mode		Name	Lipid classes	Formula
			Phase	Ionization mode			
331	901.6202	11.94	Non-polar	Positive	PI(O-40:4)	Glycerophospholipids	C49H89O12P
332	903.5028	18.83	Non-polar	Negative	PI(40:9)	Glycerophospholipids	C49H77O13P
333	905.5704858	11.96	Non-polar	Positive	Sulfated Dihydromenaquinone-9	Other organic compounds	C56H82O6S
334	919.5398	11.89	Non-polar	Positive	Beta1-tomatidine	Sterol	C45H75NO17
335	920.5413	11.87	Non-polar	Positive	PGP(40:6)	Glycerophospholipids	C46H80O13P2
336	945.6473	11.88	Non-polar	Positive	PI(42:3)	Glycerophospholipids	C51H93O13P
337	947.7049	17.47	Non-polar	Positive	TAG(58:11)	Glycerolipids	C61H96O6
338	948.5926749	11.82	Non-polar	Positive	Vinaginsenoside r3	prenol	C48H82O17
339	987.5562446	22.66	Non-polar	Negative	Pseudoginsenoside rc1	prenol	C50H84O19
340	1020.5745	23.35	Non-polar	Negative	CDP-DAG(37:1)	Glycerolipids	C49H89N3O15P2
341	1032.6959	11.73	Non-polar	Positive	FMC-6(d40:1(2OH))	Sphingolipids	C56H99NO14

Number	Adducts	PPM error	Match ID	Database	Number of alternate IDs	DENV vs Mock Day 3		DENV vs Mock Day 7		DENV vs Mock Day 11		MS/MS database	MSI level
						Log_2 FC	p-value	Log_2 FC	p-value	Log_2 FC	p-value		
331	$[M+H]^+$	4.108	LMGP06020041	LIPID MAPS	0	0.000	1.000	**16.816**	**0.005**	**14.891**	**0.025**		3
332	$[M-H]^-$	0.111	LMGP06010800	LIPID MAPS	0	-1.079	0.621	0.000	1.000	**12.608**	**0.000**		3
333	$[M+Na]^+$	2.153	LMPR02010038	LIPID MAPS	0	0.000	1.000	**20.408**	**0.000**	**11.404**	**0.000**		3
334	$[M+NH_4]^+$	2.710	HMDB0029343	HMDB	0	11.230	0.068	**17.523**	**0.011**	8.593	0.269		3
335	$[M+NH_4]^+$	0.014	HMDB0013558	HMDB	0	**11.212**	**0.042**	**16.315**	**0.007**	**18.430**	**0.013**		3
336	$[M+H]^+$	4.870	LMGP06010523	LIPID MAPS	1	-7.199	0.217	**20.222**	**0.009**	10.148	0.238		3
337	$[M+Na]^+$	-5.457	HMDB0010533	HMDB	0	**17.022**	**0.045**	**18.654**	**0.027**	9.061	0.383		3
338	$[M+NH_4]^+$	3.923	HMDB0040493	HMDB	0	**17.984**	**0.013**	**17.695**	**0.008**	8.041	0.269		3
339	$[M-H]^-$	-2.872	HMDB40467	HMDB	2	-0.455	1.000	**13.426**	**0.000**	**13.526**	**0.000**		3
340	$[M-H]^-$	-4.753	ECMDB23389	ECMDB	0	-0.220	1.000	**13.570**	**0.000**	**14.984**	**0.000**		3
341	$[M+Na]^+$	0.099	LMSP05010038	LIPID MAPS	1	**16.975**	**0.011**	**17.866**	**0.005**	**15.047**	**0.027**		3

Bold indicates significantly different levels of abundance between DENV2-infected and uninfected samples (|log2 fold change| ≥ 1, $p < 0.05$)

* These molecules were detected in the same detection modes and identified as the same name. They were retained separately because of differences in fold change. We anticipate they resulted from a split MS peak.

Table S2. List of identifiable molecules with changed abundance during DENV2 infection of the *Ae. aegypti* salivary glands. Metabolites from mosquito salivary glands that showed differential abundance following DENV2 infection are listed. Abundance of metabolites detected in DENV2-infected and uninfected salivary glands was compared. The following information is provided for each feature: *m/z*Avg, average mass to charge ratio detected (averaged between two biological replicate pools); RTAvg, average retention time detected for each metabolite (averaged between two biological replicate pools); Detection mode, both polar and nonpolar extracts were detected in both negative and positive ionization modes; Name, identification for each lipid; lipid classes, classification of each lipid according to LIPID MAPS comprehensive classification system [136]; Formula, chemical components of the molecules at their neural mass; adducts, protonated or deprotonated molecular ions, [M+H]+, [M+Na]+, [M+NH4]+ and [M-H]-; PPM Error, difference between experimental mass and exact mass; Match ID, accession number for each metabolite; Database, database of the putative identification: LIPID MAPS, Human Metabolome Database or Metlin, numbers of alternative IDs, other putative names that are isomers of the chosen name with this chemical formula; $\log_2$ FC, $\log_2$ fold change of abundance compared between DENV2-infected and uninfected samples; p-value, adjusted p-value. MS/MS database, database used for searching tandem MS fragmentation; MSI level, Metabolomics Standard Initiative level of identification [261].

Number	M/Z_{Avg}	RT_{Avg}	Detection mode		Name	Lipid classes	Formula	Adducts	PPM error
			Phase	ıization mo					
1	523.232	9.74	Non-polar	Positive	Carpelastofuran	Polyketides	C30H34O8	$[M+H]^+$	-1.419885
2	288.29	10.74	Non-polar	Positive	C17 Sphinganine	Sphingolipids	C17H37NO2	$[M+H]^+$	-0.870224
3	327.181	2.25	Polar	Positive	PC(O-5:0)	Glycerophospholipids	C13H30NO6P	$[M+H]^+$	-0.341401
4	218.049	21.78	Polar	Positive	p-Chlorobenzhydrol	Other organic compounds	C13H11ClO	$[M+H]^+$	-3.926167

Number	Match ID	Database	Number of alternate IDs	DENV vs Mock Day 3		DENV vs Mock Day 7		DENV vs Mock Day 11		MS/MS database	MSI level
				Log_2 FC	p-value	Log_2 FC	p-value	Log_2 FC	p-value		
1	LMPK12111524	LIPIDMAPS	0	**-20.47**	**0.00**	NA	NA	NA	NA		3
2	41558	Metlin	0	NA	NA	**8.31**	**0.00**	**7.50**	**0.02**		3
3	LMGP01060020	LIPIDMAPS	0	NA	NA	NA	NA	**-7.13**	**0.00**		3
4	C14672	KEGG	0	NA	NA	NA	NA	**-1.75**	**0.03**		3

APPENDIX II: COPYRIGHT INFORMATION

Chapter 2 and 3's re-print license from Plos Pathogens

Gmail

Nunya Chotiwan <nunya.chotiwan@gmail.com>

Re: Request for reprinting a manuscript

1 message

PLOS Pathogens <plospathogens@plos.org> Mon, Jun 4, 2018 at 3:55 PM
To: "nunya.chotiwan@colostate.edu" <nunya.chotiwan@colostate.edu>
Cc: "rushika.perera@colostate.edu" <rushika.perera@colostate.edu>

Dear Dr. Chotiwan,

Thank you for your email. PLOS generally applies the Creative Commons Attribution (CC BY) license to works we publish. Under the CC BY license, authors retain ownership of the copyright for their article, but authors allow anyone to download, reuse, reprint, modify, distribute, and/or copy articles in PLOS journals, so long as the original authors and source are cited. No permission is required from the authors or the publishers.

For further details, see: http://www.plospathogens.org/static/license

Please don't hesitate to contact us if you have any further queries.

Best,
Sarah

PLOS | OPEN FOR DISCOVERY
Sarah Sarber | Publications Manager, PLOS Pathogens
1160 Battery Street, Suite 225, San Francisco, CA 94111
ssarber@plos.org | Main +1 415-624-1200 | +1 415-590-3589 | Fax +1 415-546-4090
plos.org | Facebook | Twitter | Blog

Case Number: 05787931

---------- Original Message ----------
From: Chotiwan,Nunya [nunya.chotiwan@colostate.edu]
Sent: 5/30/2018
To: plospathogens@plos.org
Subject: Request for reprinting a manuscript

Dear Plos Pathogens,

I would like a permission to reproduce the manuscript from the article "Dynamic Remodeling of Lipids Coincides with Dengue Virus Replication in the Midgut of Aedes aegypti Mosquitoes," (PPATHOGENS-D-16-00829R2) for my PhD dissertation at Colorado State University.

I would like to receive a written acknowledgement of the publisher's permission. An emailed letter of permission would be acceptable. Please feel free to contact me if any additional information is needed.

Sincerely,
Nunya Chotiwan